DOTTORATO DI RICERCA IN CHIMICA

Convenzione tra
UNIVERSITÀ DEGLI STUDI DI TRIESTE
e
UNIVERSITÀ CA' FOSCARI DI VENEZIA

CICLO XXX

STUDY OF CALCIUM ETHOXIDE AS NEW SOLUTION FOR THE CONSOLIDATION OF CARBONATE STONES

Settore scientifico-disciplinare: ____**CHIM/12**____

DOTTORANDO / A
MARTINA ZUENA

COORDINATORE
PROF. MAURO STENER

SUPERVISORE DI TESI
PROF. ELISABETTA ZENDRI

CO-SUPERVISORE DI TESI
Dr. PATRIZIA TOMASIN – Dr. LORETTA STORARO

ANNO ACCADEMICO 2016/2017

Table of Contents

AIM OF THE THESIS

The combined action of several physical, chemical and biological factors causes the weathering of carbonate stones widely employed in the field of Cultural Heritage, leading to deterioration processes, which cause an increase of porosity and loss of material cohesion. The knowledge acquired till today about the deterioration processes has promoted consolidation interventions to prevent or remedy the weathering of carbonate stones, to improve their cohesion and adhesion and to preserve buildings and decorative surfaces of architectural monuments. However, the consolidation of carbonate stones is still an open debate and to overcome the limitations of traditional products and to meet the requirements of the historical building substrates, conservation scientists are constantly involved in the research of compatible, efficient, stable and long-lasting consolidation treatments. Within this context, during the European collaborative project NANOMATCH (November 2011 - October 2014), different consolidating agents for carbonate supports, as calcium alkoxides, were synthesized and applied.

The present PhD thesis aims at studying the properties and, especially, the effectiveness and the compatibility of one of these products - calcium ethoxide - as consolidant for carbonate stone, which was the least investigated during the NANOMATCH project, because it presented some limitations. This product is considered a promising alternative to traditional treatments for the conservation of carbonate stones, since it meets one of the key requirements in the field of the conservation of Cultural Heritage, such as the chemical compatibility with the support. In fact, calcium ethoxide, dissolved in an organic solvent, penetrates within the porous substrate and, reacting with moisture and carbon dioxide of the atmosphere, forms a calcium carbonate coating on the pore walls.

This work involved a first characterization of calcium ethoxide diluted in different solvents, through a study of the carbonation process: its kinetics, reaction pathway and evaluation of mineralogical phases formed at the end of this process. The purpose was to understand how different solvents and environmental conditions could affect the final results.

Subsequently, the consolidant was applied on carbonate stones with different total open porosity value to test its performance - effectiveness and compatibility - as consolidating agent. The compatibility and the efficacy of the treatment was investigated with a multi-

technique approach and compared with results obtained with e reference product, based on nanolime.

This work has revealed important information regarding the influence of environmental conditions and used solvent on the carbonation process of calcium ethoxide and therefore, on its potential as consolidating treatment for carbonate supports.

CHAPTER 1

Stone decay and conservation

Summary

The purpose of this chapter is to provide a short introduction to the weathering processes that affect stone materials used in the field of Cultural Heritage and a panoramic view on several treatments applied or proposed for their conservation and restoration, with a focus on carbonate stones. Knowing the decay processes that involve stone materials is crucial to plan a proper conservative project and to improve physical, mechanical and chemical properties of the works of art without influencing their aesthetical and visual characteristics.

1.1 Weathering of stone material

The term *stone material* is referred both to natural and artificial stones. The first ones can be divided in minerals and rocks, while the second ones include lime, plasters, mortars and ceramic products [1].

According to their genesis, natural rocks can be divided into three classes: igneous, sedimentary and metamorphic. Igneous rocks derive from the cooling of magma and can be distinct in plutonic (intrusive), if the cooling process is slow and in abyssal condition, and extrusive (volcanic), if the magma solidifies quickly on the earth surface by moving from high temperature and pressure conditions to atmospheric ones. Sedimentary rocks are the result of a lithification process of particles of sediments transported by agents as wind and water in sedimentation basins. Metamorphic rocks are the product of the metamorphism process, a re-crystallization of a pre-existing rock type due to the effect of temperature or temperature and pressure together [2], [3]. Carbonate stones, rocks composed mainly by calcium carbonate, can derive from both sedimentary or metamorphic process and, according to the formation mechanism, other components such as skeletal fragments of shell, corals, algae, can be included to the main mineral.

Natural stones undergo a natural deterioration due to chemical, physical and biological processes, according to their morphological structure, composition and weatherability.

Stone materials employed in the field of Cultural Heritage - used for architectural and artistic artworks - are subjected to more degradation effects in addition to natural ones, starting from the damage caused by quarrying, manufacturing and implementation [4].
The deterioration processes are connected to several intrinsic characteristics of the stone - porosity, pore size distribution, pore shapes, chemical composition, texture, homogeneity, rate of swelling - and to the environmental conditions in which the work of art is placed [5]–[7].
Stone materials can show different degrees and types of alterations: these have been classified by the normative UNI 11182 "Materiali lapidei naturali ed artificiali: descrizione della forma di alterazione - Termini e definizioni" [1] and the ICOMOS-ISCS Illustrated Glossary on Stone Deterioration Patterns [8] which are useful to define the correct terms by which referring to decay pattern within the Italian and international stone community, respectively.
Particularly, the deterioration of carbonate stones is strictly connected to the reaction of carbonate minerals with the environment and it is due to several factors such as air pollution, water, presence of salts and biodeteriogens that cause mechanical, physical and chemical stresses.
Generally, the recognized mechanisms connected to the degradation of stone materials can be divided as follows:

- dissolution of constituent minerals caused by water or acid solutions;
- mechanical stress due to freeze-thaw cycles of water;
- dissolution/re-precipitation of salts in the pore network of the stone;
- growth of microorganisms with consequent aesthetical problems and physico-chemical decay.

In the following paragraphs, a brief description of the main causes which may lead to deterioration of stone and references of several works which discuss these topics are reported.

1.1.1 Atmospheric pollution

The effects of atmospheric pollution on stone weathering has become an important topic in conservation of Cultural Heritage since the 1970s. The worldwide development of industrial activities caused a massive introduction in the atmosphere of some substances otherwise present in low concentration or even absent. Polluted atmosphere causes the deterioration of stone material leading to structural and aesthetic problems [9]–[14]. The main forms of deterioration of stone associated with atmospheric pollution are surface erosion and loss of

details, soiling, blackening and formation of crusts [15].

The transfer of pollutants from the atmosphere to the stone surface could occur in two different ways: dry and wet depositions. The first one consists in the direct deposition of particulate, aerosol and, mostly, gaseous species, on the stone surface in the absence of rain; Wet deposition is due to the dissolution of atmospheric pollutants in rain or atmospheric moisture which, subsequently, deposit on the stone surface [16].

The most important pollutants present in an urban context that react directly with the calcium carbonate minerals by inducing the formation of acids in the presence of oxidizing agents and water (the so called acid rains) are: nitrogen oxides NO_x (NO and NO_2) and sulphur dioxide (SO_2) [17]–[20]. The sources of these gases are both natural and anthropic.

During daytime, nitrogen oxide is oxidized by ozone (O_3), to NO_2 according to this reaction:

$$NO + O_3 \rightarrow NO_2 + O_2$$

Nitrogen dioxide is further oxidized by $^{\bullet}OH$ radicals to nitric acid gas:

$$NO_2 + {}^{\bullet}OH \rightarrow HNO_3$$

Another possible reaction path for HNO_3 generation is a gas-phase reaction of N_2O_5 with water vapour [4], [17]:

$$N_2O_5 + H_2O \rightarrow 2HNO_3$$

The contact between nitric acid and carbonate stones leads to the dissolution of carbonate minerals and, therefore, the degradation of stone surface according to the following reaction [21]:

$$CaCO_3 + 2HNO_3 \rightarrow Ca(NO)_3 + H_2O + CO_2$$

The other compound, sulphur dioxide, is responsible for the formation of the well known black crusts, very compact deposits developing in urban environment on areas protected from direct rainfall or water runoff and strongly attached to the stone support [8], [22]–[24]. Sulphur dioxide is a stable gas at room temperature and in a clean air; however, in presence of humidity, some pollutants and solar radiation, it could be subject to a catalytic oxidation that can follow two ways:

$$SO_2 + H_2O \rightarrow H_2SO_3$$
$$H_2SO_3 + 1/2O_2 \rightarrow H_2SO_4$$

$$SO_2 + 1/2O_2 \rightarrow SO_3$$
$$SO_3 + H_2O \rightarrow H_2SO_4$$

Both ways are possible and they depend on the presence of catalysts in the atmosphere such as NO_x and O_3. Indeed, if a carbonate stone is located in an atmosphere rich in SO_2 and humidity, sulphuric acid is formed and reacts quickly with the calcium carbonate of the stone following this reaction [25], [26]:

$$CaCO_3 + H_2SO_4 + H_2O \rightarrow CaSO_4 \cdot 2H_2O + CO_2$$

The new formed gypsum can absorb airborne particles and dust from the atmosphere and all types of carbonaceous particulate matter coming from hydrocarbon materials, making the deposition black and leading to the formation of the so called black crusts (**Fig. 1.1**) [27]–[29].

Figure. 1.1 *- Black crust tracing the surface of a limestone sculpture, Saint-Denis -France* [8].

The black crust tends to thicken and to harden over time by accentuating the different mechanical and thermal behaviour respect to the stone below. In fact, as the black crusts lead to the darkening of the external surfaces of monuments, the different colour between the crusts and the surrounding stone material results in a different thermal behaviour. Finally, the formation of gypsum improves the concentration of salts inside the stone leading to mechanical stress [30]. The effect of black crusts is different according to the porosity of the stone: on less porous material the effect is an intercrystalline crumbling that leads to a detachment of calcite grains; while, on more porous material, there is a cracking followed by the loss of elements. On the new exposed surface, a black curst can start to form again and the process continues to happen.

Finally, also carbon dioxide, which can reach high concentrations in an industrial

environments, can have an aggressive effect on carbonate stone by combining with water in the atmosphere to produce carbonic acid that reduce the pH of rains. The weakly acid solution formed by dissolution of CO_2 in rainwater dissolves the calcium carbonates in limestone, marble, lime mortars and plasters because it forms calcium bicarbonates (1,1 g/L at 20 °C) which is much more soluble than calcium carbonate ($1{,}4 \cdot 10^{-2}$ g/L at 20 °C) [4].
Carbon dioxide could be considered as a minor culprit when direct effects are involved; but, it represents the primary cause of climate change, a factor that overcomes the direct effects of pollutants [31].

1.1.2 Water

Water from different sources is one of the most harmful agents for stone materials. It is involved in different weathering processes of the material: mechanical stress (a factor connected to the capillary structure of stone), soluble salts transportation and crystallization/recrystallization processes [4].
Water is defined as a wetting liquid for stone materials and when it goes in contact with them, penetrates into the capillaries with a force inversely proportional to their diameter [32]; in the case of water, the wettability of a porous material - defined as the "attractivity" between water and solid - is related to the contact angle that the liquid makes with the material surface. This angle is considered as a measure of hydrophobicity of the surface (contact angle <90° defines hydrophilic surfaces) and it is described by Young's equation:

$$\sigma_{ls} + \sigma_{lv} \cdot \cos\gamma = \sigma_{sv}$$

with σ_{ls}, σ_{lv} and σ_{sv} the interfacial tensions at the boundaries between the solid (s), the vapour phase (v) and the liquid (l) (**Fig. 1.2**) [33].

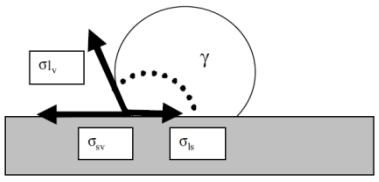

Figure 1.2 *- Definition of contact angle* [33].

When water is absorbed by a porous material, capillary pores are completely filled; while for the largest pores, the water wets the surfaces and the major part of the internal volume is filled

by air. Frost damage may occur when the conditions for ice crystallization are reached, but depends on the type of stone and in particular on pore size distribution. In fact, ice crystals begin to grow in the large pores because the bonds between water molecules and the solid wall are weak, therefore it is not difficult to move them in a new position to form a crystal seed. Only when the quantity of the available water around them becomes low, the water located in the capillaries - where the bond between the solid walls and the molecules is stronger - is used. The pores in stone building materials could have different shapes and dimensions and usually they are classified within two intervals: large pores (diameter > 10 μm) and microscopic or, better, capillary pores (1 μm < diameter < 0,1 μm). If the number of large pores is higher than that of capillary pores, ice crystals grow firstly in the large pores and when the water reserve is ended, the growth of ice crystals stops. In this condition, there is no stress for the material. On the contrary, when the number of large pores is lower than capillary ones, the space of large pores is insufficient for the ice crystal growth, therefore crystals tend to grow pushing against the pore's wall (**Fig. 1.3**). This situation will lead to a stress for the material [30].

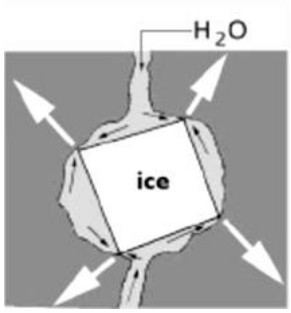

Figure 1.3 *- Frost pressure in a porous material* [30].

The damage due to the frost can vary widely and consists mainly of surface scaling, exfoliation and deep cracking. The temperature variation around the freezing point is more dangerous than continuous freezing for building materials. Hence, it is important to estimate the number of freeze-thaw cycles during a year to which a stone work of art is exposed. This calculation is not always easy to do, because not always there is a correspondence between the temperature in the stone and the thermal variation in the environment. In fact, more or less dark parts - which absorb solar infrared radiation in different way - can be present on the work of art due both to the use of different stone materials or to decay processes such as black crusts [4].
Furthermore, as reported in the previous paragraph, the water plays an important role in the weathering of stone connected to the presence of pollutants and in the transport of soluble salts in the porous structure of stone (paragraph 1.1.3).

1.1.3 Soluble salts

Salt damage in building stones is due to the growth of salt crystals within the pore space of the stone. A soluble salt can be originally present in the stone or it can derive from several external sources, such as atmosphere particles and soil and, sometimes by non-adequate conservation treatments.

The mechanisms responsible for the presence of soluble salts into porous material of a building are two: infiltration by rainwater and capillary rise of groundwater. The first involves salts resulting from marine aerosol or air pollution while the second regards deicing salts and those ones naturally present in the groundwater [34].

Once a soluble salt is in a porous stone, it can be transported through the material as aqueous solution and its movement is connected to ambient conditions, such as temperature and humidity, to the presence of other salts and to the morphological and textural characteristic of the stone material [35]. A mechanism similar to the formation of ice inside pores could be supposed to explain the effect produced by soluble salts crystallization. As in the case of crystallization of water, the capillaries can act as store of water and the growth of salt crystals may take place only inside the large pores. Thus, also in this case, a stone with a scarcity of large pores and rich of capillary pores is more subjected to deterioration.

The precipitation of salts could happen inside the stone or on the surface. When the migration of solution to the surface is higher than evaporation of water, the crystallization occurs on the surface and efflorescences are formed. On the contrary, if migration to the surface of the artwork is lower than evaporation of water, the crystallization of the salts occurs below the surface and sub-florescences are formed [25]. The exfoliation and the detachment observable on materials deteriorated by soluble salts are due to sub-efflorescence and to the connected concentration of pressure due to salt crystallization in layer below the surface. Efflorescences are less dangerous, most of all because they are visible and therefore can be removed, but they cause aesthetical damages such as the whitening of the surface. The environmental conditions surrounding a porous material influence the formation of sub-efflorescence/efflorescence; in fact low-moderate temperature, low air velocity and medium-high relative humidity, permit a slow evaporation of water and lead to the formation of efflorescence. On the contrary, warm, dry and windy conditions favour sub-efflorescence. Sub-efflorescence are responsible, mainly in sea environment, for the formation of deep alveolus on surface, a phenomenon called alveolization (**Fig. 1.4**).

Figure 1.4 *- Examples of alveolization on Noto stone (church of S. Francesco)* [36].

This phenomenon can eventually lead to the loss of the whole block of stone and it is due to combination of different factors such as high porosity of stone, high quantity of soluble salts and strong turbulence of air in contact with the material surface [6].

1.1.4 Biological colonization

The term biodeterioration is referred to any undesirable change in the properties of materials due to vital activity of organisms [37]. In fact, different biodeteriogens such as plants, algae, fungi, bacteria and lichens are often involved in stone deterioration. This process depends considerably upon the following factors: the type of involved organism, the environmental conditions of the site, the type of exposure and the chemical composition and the structure of the stone [38]–[42]. Stone could be considered an extreme environment from the biological point of view due to the lack of nutrients and the presence of variable moisture content [26]. Nevertheless, the biological colonization may occur anyway in all climate regions. The parameters that affect the development and growth of different microorganism are: sunlight, oxygen, carbon dioxide, water and some mineral salts. The effects due to the presence of microorganism can vary considerably and the biodeterioration of stone materials may occur through different types of mechanisms: physical and mechanical processes that lead to de-cohesion phenomena, rupture and crumbling, and chemical ones which are responsible for substrate's transformations and decompositions.

These processes include, in the first place, the aesthetical problem due to the staining of the stone surfaces by biogenic pigments (melanins, chlorophylls, carotenoids). These pigments can be connected to some cellular structure and therefore they are responsible for the colour of organisms, or be produced in the external environment [43]. Generally, in this case material loss or visible destruction are not involved and the alteration phenomenon is called biopatina

(**Fig. 1.5**). Secondly, a factor involved in stone mechanical stresses and alteration of the stone's pore size distribution is due to the presence of extracellular polymeric substances (EPS) produced by the organism to increase their resistance in cold conditions [44]. Finally, it has been studied that the presence of biofilms (bacterial cells and EPS) are responsible for clogging pores, increasing water uptake and retention within the stone; biofilms can block water diffusion and evaporation on exposed stone surfaces and might accelerate the accumulation of airborne particles [45].

Figure 1.5 *- Colonization of a statue with lichen, figures from the Calvary near Concarneau in Brittany* [26]**.**

The most important factor that allows microbial growth is the availability of water, despite some microorganism as fungi in dormant state can tolerate periods of complete dryness. Therefore, very humid and salty environments together with stones with higher porosity, able to retain a great quantity of water, are the combination for an easy biological colonization.
Stone microorganisms represent a complex ecosystem; they can inhabit the stone surface (epilithic) or penetrate into the stone, from several millimetres to some centimetres. In this latter case, they are divided into two groups: crypto-endolithic, when they penetrate inside the pore system and chasmo-endolithic, if they grow up in the stone fissures [37]. In particular, endolithic microorganism are responsible for a type of alteration called micro-pitting, characterized by the presence of cavities due to the previous solubilization of the stone [44].

1.1.5 Other factors

Other important factors that can contribute to the weathering of limestone are: the swelling of clay minerals, possibly present in the limestone, and the thermal cycles. Clay minerals are aluminium silicates with a layer structure. In the most common clay minerals, each layer is itself a stratified structure: the outer layers are formed by silica tetrahedrons and the central one by alumina octahedrons. When water enters in contact with these minerals, it penetrates

between the layers causing an increase of the distance and a weakening of the connection between them [30]. This process is called swelling and it generates damaging stresses (physical decay) especially during wetting and drying cycles [46]–[48].

Another important factor in the weathering of stone are the thermal cycles, both in the heating phase and in the cooling phase, which are responsible for the changes of dimensions stone materials. Limestone are particularly subjected to this type of weathering due to the anisotropic thermal expansion of calcite grains, the main constituents of limestone. In fact, upon heating it expands in one direction (usually the main axis) and, contracts along other ones (usually perpendicular to the main axis) [30], [49]. Therefore, thermal cycles lead to an inter-granular disjunction and a progressive weakening of the structure and the intensity of this phenomenon is strictly linked to the open porosity of the stone.

1.2 Stone conservation

The aim of conservation of stone Cultural Heritage - a complex topic that has been involving scientists and restores since the nineteenth century - is the preservation of the historic-artistic works of art for future generations. The first international documents that provide general directions for the restoration and maintenance of historic monuments is the Athens Charter for the Restoration of Historic Monuments, adopted at the First International Congress of Architects and Technicians of Historic Monuments (Athens 1931) [50]. Conservation of stone materials includes all the actions needed to prevent and remedy the deterioration of Cultural Heritage such as prevention, diagnosis, cleaning, consolidation, protection and maintenance. The first one involves all measures and actions aimed at preventing and/or minimizing future loss or deterioration [13]. Diagnosis is useful to understand the history of the work of art, the environmental conditions in which it is placed, the type and degree of decay processes and the factors affecting it; therefore, to have information about the state of conservation. Cleaning is crucial to remove dust deposition and weathering crusts from the stone surface; it involves chemical, mechanical or physical actions and it is useful not only for aesthetical reasons, but also for a better preservation of the stone. The aim of consolidation is to restore the lost adhesion/cohesion both on surface and in-depth and it is necessary to eliminate or, at least, to limit the mechanical difference between the in-depth part and the more external and deteriorated one, and to restore the structural characteristics of the material. Protection is the application of a protective layer that would act as a barrier against rainwater and atmospheric

pollutants. Finally, maintenance involves all the activities and appropriate strategies, able to maximize the results in terms of conservation, use and exploitation of Cultural Heritage.
Since the aim of this thesis regards the consolidation of stone, a more in depth overview about consolidation will be reported.

1.2.1 Consolidation

"*The ideal consolidant would be a product that is able to restore the strength as well as the other physical properties of the decayed stone layers to the level of the sound stone that existed before degradation and to achieve it without any harmful side effects*[1]"

A good consolidating agent should meet several performance requirements regarding effectiveness, compatibility, durability and re-treatability [51]–[54].
To be effective, a consolidant should have a homogeneous and good in depth penetration able to reach the unweathered stone and should improve mechanical resistance of the treated support [4], [55].
To be compatible, the used product must not have a negative effect on the original stone such as alteration of the original aesthetical aspect like darkening, yellowing and whitening [55], [56]. Furthermore, the consolidating product must not have an environmental impact leading to the formation of by-products dangerous for the stone or to the release of toxic compound harmful for human health or environment. Regarding the physical and micro-structural properties of the stone, a reduction in water sorptivity and open porosity is desirable; but, the clogging of pores and a great alteration of water transport properties inside the stone have to be avoided because, if the water vapour and liquid water are trapped behind the treated surface, some dangerous phenomena such as exfoliation of stone might occur [57]. Moreover, the thermal expansion coefficient of both consolidating product and treated stone should be similar, to prevent damages due to different thermal behaviour [4], [55].
Another important characteristic for a consolidant is durability. The consolidating product should remain on the treated support despite the exposure to environmental weathering and no harmful product, deriving from an ageing process of the consolidating product, should be formed.

[1] J. Delgado Rodrigues, "Consolidation of decayed stones. A delicate problem with few practical solutions," *Hist. Constr.*, pp. 3–14, 2001.

Finally, the term re-treatability has been recently introduced to overcome the concept of reversibility. In fact, the complete reversibility of a consolidant is not easily achieved; therefore the term re-treatability indicates that the used product should not impede or preclude further interventions in the future [54].
During the years, several inorganic and organic products have been developed to answer to different needs of restoration in terms of type of material and surrounding environment.
In the following paragraphs a description of the main inorganic and organic treatments used in the field of Cultural Heritage are reported.

1.2.1.1 Inorganic treatments

Inorganic consolidants improve the stone cohesion through the precipitation of water-soluble chemical precursors that lead to the formation of a crystal-texture of neo-formed insoluble products able to bond the detached grains and particles of a decayed stone through mechanisms of carbonation, hydrolysis and/or chemical interaction with the stone substrate [58], [59]. The chemical similarity between the decayed material and the bonding agent confers a high potential to this group of products.

Limewater
Limewater is one of the simplest and traditional consolidating products for carbonate stones, lime-based wall paintings and plasters and consists of a saturated solution of calcium hydroxide, $Ca(OH)_2$, a compound that forms new calcium carbonate - which is chemically identical to carbonate stone - inside the pores [60], [61].
It provides an improvement of the internal cohesion due to the precipitation of calcium carbonate, according to the following reaction:

$$Ca(OH)_2 + CO_2 \rightarrow CaCO_3 + H_2O$$

Unfortunately, the low solubility of $Ca(OH)_2$ (1.7 g/L at 20 °C) prevents the introduction into the treated material of an adequate amount of product for consolidating the porous system; the total amount of $CaCO_3$ formation is very low and repeated applications of the solution of limewater are necessary to obtain an appreciable deposition of portlandite [59].
There are some problems connected to the use if this product such as the dissolution and recrystallization of the substrate due to the physico-chemical action of water, clay-swelling, growth of microorganisms, mobilization or crystallization. Moreover, when used on wall

paintings, the high pH of the solution may influence pigments sensitive to an alkaline environment [62]. Therefore, despite its long history of use as stone consolidant, the effectiveness of the limewater is still open to debate.

Barium hydroxide

A basic concept similar to the limewater is the use of a barium hydroxide solution, formerly named baryta, for consolidation of plasters, stones and lime mortars since the end of the 19th century [63]–[65] This compound reacts with CO_2 from the air and forms barium carbonate, $BaCO_3$, a more stable and insoluble mineral [59]:

$$Ba(OH)_2 + CO_2 \rightarrow BaCO_3 + H_2O$$

The solubility of barium carbonate in water ($2.2 \cdot 10^{-2}$ g/L at 20 °C) is lower than that of calcium hydroxide (1.7 g/L at 20 °C) [66] and it is strongly dependent from the temperature. In theory, the applied solution of barium hydroxide contains a sufficient concentration to produce a strengthening effect of the treated substrate. But, in practice, the slow reaction with carbon dioxide will occur primarily on the surface which will be covered by grey-white deposits [26].

Also based on the presence of barium hydroxide, another important method, the so-called Ferroni-Dini, was proposed especially for wall paintings affected by the presence of gypsum.

It involves the application of ammonium carbonate and barium hydroxide aqueous solution though poultices, in a two-step procedure [67]:

$$(NH_4)_2CO_3 + CaSO_4 \cdot 2H_2O \rightarrow (NH_4)_2SO_4 + CaCO_3 + 2H_2O$$

$$(NH_4)_2SO_4 + Ba(OH)_2 \rightarrow BaSO_4 + 2NH_3 + 2H_2O$$

$$Ba(OH)_2 + CaCO_3 \rightarrow Ca(OH)_2 + BaCO_3$$

$$Ca(OH)_2 + CO_2 \rightarrow CaCO_3 + H_2O$$

$$Ba(OH)_2 + CO_2 \rightarrow BaCO_3 + H_2O$$

The procedure starts with a first application of a saturated solution of ammonium carbonate, $(NH_4)_2CO_3$, which reacting with gypsum leads to a desulfation of the treated surface and formation of calcium carbonate and ammonium sulphate which, being more soluble than gypsum, is mainly absorbed by poultices and removed from the treated surface.

The second step involves the application of barium hydroxide solution which converts the remaining ammonium sulphate into insoluble barium sulphate and reacts with calcium carbonate regenerating calcium hydroxide. The remaining barium hydroxide and the new formed calcium hydroxide react with carbon dioxide present in the atmosphere to form barium carbonate and calcium carbonate, respectively.

The consolidating action is obtained from the calcium carbonate, formed by the reaction between calcium hydroxide and CO_2, that acts as a binder improving the crystalline network.

The main characteristics of this method are that the insoluble barium sulphate does not migrate within the porous matrix of the treated support, preventing the mobilization of salts. The Ferroni-Dini method is still widely employed in the restoration field with successful results for consolidation of deteriorated surfaces (**Fig. 1.6**).

Figure 1.6 *- Crucifixion by Beato Angelico (15th century, Florence)* [68].

However, there are some limitations when copper pigments and some organic bindings are present on the treated surface. They do not tolerate water from the poultice and could undergo cleavage reactions due to strongly alkaline conditions. In addition, barium compounds are toxic for human health [69].

Nanolime

To overcome the limitation connected to limewater (low solubility of calcium hydroxide), in the last two decades a novel consolidating treatment based on nanostructured materials was proposed, the so-called nanolime. It is based on the use of $Ca(OH)_2$ nanoparticles, spherical or hexagonal with a size ranging from 50 to 600 nm, dispersed in alcohol medium; it is used particularly for restoration of mural paintings (**Fig. 1.7**) due to its consolidating properties and physico-chemical compatibility with calcareous supports [70]–[72].

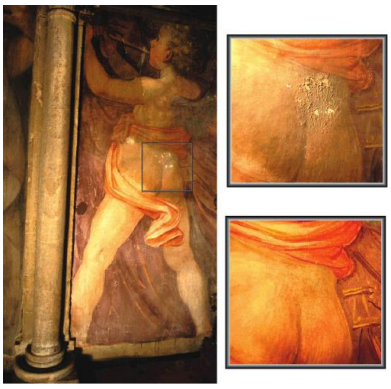

Figure 1.7 *- Example of application of nanolime during restoration of the wall paintings by Santi di Tito (16th century), Gli Angeli Musicanti on the Counterfaçade of the Santa Maria del Fiore Cathedral in Florence* [73].

The consolidating effect is obtained through the carbonation process of calcium hydroxide which, once penetrated inside the treated porous material, reacts with carbon dioxide. Respect to limewater, the presence of a short-chain alcohol dispersion leads to several advantages as higher colloidal stability and reduction of water amount introduced into the treated material [74] .

Different factors influence the effectiveness of nanolime as a consolidating agent: nanolime characteristics (particle size, morphology, specific surface area, concentration and type of solvent), characteristics of the substrate (both physical and mechanical), external factors (available CO_2, temperature, RH) and type of application.

Unfortunately, nanolimes show a weak result when mass consolidation is required, such as for plasters and lithotypes [75]. In fact, during drying process, lime nanoparticles may partially migrate back up to the surface, leading to a poor in depth consolidation [53].

Nanolime can be considered one of the most promising materials for the consolidation of carbonate stones due to its compatibility and reduced side effects. However, it appears to be an effective consolidant only for the superficial layer, while when in-depth consolidation is required, the results can change considerably depending to the material treated and the environmental conditions. Nanolime is very popular in the field of restoration and future research will contribute to improve its current limitations.

Fluosilicates

Another type of stone consolidant is the group of fluosilicates, salts of the fluosilicic acid H_2SiF_6, firstly synthesized in 1883 by Kessler [76]. Depending on the cations (Zn, Al, Mg, Pb), several salts can be formed. The consolidating effect is obtained by the formation of

amorphous silica gel deriving from the reaction between fluosilicates and calcium or other alkalis. When applied on carbonate stones, they react preferentially with $CaCO_3$ following this reaction:

$$2CaCO_3 + MgSiF_6 \rightarrow 2CaF_2 + MgF_2 + SiO_2 gel + 2CO_2$$

Silica gel is the product that leads to a consolidating effect. Fluosilicates show several advantages, the fluoride of magnesium is insoluble in cold water and they can prevent microbiological colonization by algae and fungi. But, due to the fast hydrolysis, the silica gel cannot precipitates in depth and the consolidating effect is reached only in the first two millimetres from the surface [26], [77]. Furthermore, it has been evaluated that, on vertical wall surface, fluosilicates show more harmful than beneficial effects; in fact in this case only the water penetrates by capillary action while the fluosilicate's particles remain on the surface [4].

Hydroxyapatite

Recently, a novel inorganic treatment based on the formation of hydroxyapatite (HAP) inside pores and micro-cracks, has been proposed [57], [78]–[80]. Hydroxyapatite is a naturally occurring mineral form of calcium apatite with the formula $Ca_{10}(PO_4)_6(OH)_2$. This compound is obtained from the reaction between phosphate ions (PO_4^{3-}), deriving from an aqueous solution of diammonium hydrogenphosphate $(NH_4)_2HPO_4$, also called DAP, and calcium ions Ca^{2+} from the calcite of the substrate. The formed calcium hydroxy phosphate, HAP, is able to physically and chemically bind the deteriorated substrates [81]:

$$10Ca^{2+} + 6PO_4^{3-} + 2OH^- \rightarrow Ca_{10}(PO_{4,})_6(OH)_2$$

The obtained HAP contains carbonate ions, and before its precipitation, several intermediate metastable precursors can form, according to different reaction conditions. Through a dissolution and re-precipitation process, this precursor phases transform into HAP. Regarding the compatibility between calcite and HAP, this last can be an effective consolidant for carbonate stones because: with respect to calcite it has a lower solubility, (about 18 times less), a similar crystal structure and a lower dissolution rate [79]. In addition, this treatment presents other important positive effects such as the non-toxic nature of the used products, a chemical compatibility with the support and no chromatic alteration.

Ammonium oxalate

This type of consolidating treatment has been applied over the past 30 years on different carbonate materials such as lithotypes [82]–[84] and wall paintings [85]–[87]. It involves the application of an aqueous ammonium oxalate solution which induces the transformation of calcium carbonate to calcium oxalate (whewellite). This compound has a lower solubility in water than calcium carbonate and it is more resistant to acid attack; thus, it is an ideal passivating agent for limestones in urban acidic atmosphere [88] and, furthermore, leads to an improvement in surface cohesion [89].

Calcium oxalate is formed according to the following reaction [90], [91]:

$$CaCO_3 + (NH_4)_2C_2O_4 \rightarrow CaC_2O_4 + 2NH_3 + H_2O + CO_2$$

Usually, a solution of ammonium oxalate (5 -7% with pH 7) is dispersed in a cellulose paste and applied on the surface to be treated. The time interval can vary between several hours and a few days in accordance to empirical experience. Experimental results show that the reaction takes place in the upper 2 mm of the treated surface.

This treatment does not affect the appearance of the treated stone; the only exception is due to the presence of gypsum in the surface layer which could lead to a chalky appearance. Respect to untreated stone, the water-absorption rate is reduced between 60% and 85% and the hydrophilic properties of the surface are maintained [59]. This treatment was applied also as a protective agent on marble sculptures and mural façades as well as on mural paintings [92]–[95].

However, this treatment presents some drawbacks: discolouration by iron ions mobilization, observed on few treated stone surfaces and alteration of Cu-based pigments when applied on wall paintings [82], [88].

Calcium acetoacetate

In very recent years, a new consolidating agent for carbonate materials based on a water solution of calcium acetoacetate $Ca(OOCCH_2COCH_3)_2$, also called CWF, has been developed during the HEROMAT FP7 project [96]. This product leads to the formation of calcium carbonate according to the following reaction:

$$Ca(OOCCH_2COCH_3)_2 + H_2O \rightarrow CaCO_3 + CO_2 + 2CH_3COCH_3$$

The used solution contains a high concentration of calcium acetoacetate (up to 100 g/L at 20°C), therefore a good consolidating effect may be reached with a low number of applications. Other important advantages are the lack of the whitening of the treated surface and its environmental compatibility due to the use of water as solvent.

Studies regarding the application of this product on wall painting indicate that it improves the mechanical properties of the stone; in fact, results from ultrasound velocity, drilling resistance and surface hardness confirm a higher penetration and a greater filling of porous substrate respect to other inorganic consolidants [97].

Biomineralization

Finally, a consolidating treatment developed in recent years, exploits the capacity of a certain type of bacteria to induce calcium carbonate precipitation with binding properties through their metabolic activity. The type of carbonate precipitation depends on the types of bacteria, nutrients and environmental factors and it is strictly correlated to the calcium concentration, availability of nucleation sites, pH and concentration of dissolved inorganic carbon [98].

The mechanism of calcium carbonate production through urea hydrolysis is the easiest controlled one: the urease catalyzes the hydrolysis of urea to dissolved inorganic carbonate (DIC) and ammonia (AMM), leading to an increase, in the bacterial environment, of carbonate concentration and pH. When adequate supersaturation is reached, crystals of calcium carbonate precipitate on bacterial cell walls [99], [100]. **Fig. 1.8** shows a synthetic scheme of the bacterial calcium metabolism and the relative carbonate precipitation.

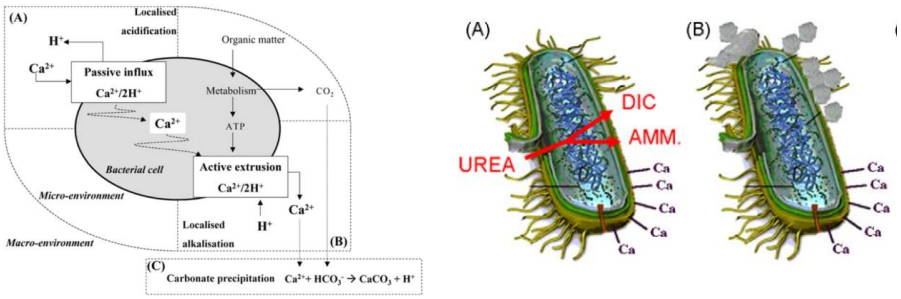

Figure 1.8 *- Scheme of bacterial calcium metabolism under high Ca^{2+} and pH extracellular conditions: a) Consumption of carbonate source, urea, by the bacterium and secretion of dissolved inorganic carbon (DIC) and ammonia (AMM) into the extracellular space, b) calcium ions in the microenvironment of the bacterium react with carbonate ions* [98], [101].

The biomineralization applied for the consolidation of carbonate stones can be performed following two different ways: by inoculating the bacterium strain on the stone surface and feeding it with the liquid culture media [102], [103], or by the application, directly on the

substrate to be consolidate, of a culture medium able to activate those bacteria capable to produce calcium carbonate, among the bacterial community of the stone [104], [105]. In the first case, the treatment showed good results in terms of effectiveness, but it reached a low penetration depth. In the second case, the calcium carbonate production is more intense but slower than the previous method.

The biomineralization as consolidating treatment can be considered as an environmentally friendly alternative respect to the other treatments and follows the concept of compatibility by forming calcium carbonate, the same component of carbonate stones [101]. Nevertheless, it is a complex treatment because the application of new microorganisms on stone surface can modify the fauna naturally present; furthermore, the microbial activity depends on several environmental factors not always controllable such as pH, temperature and concentrations and diffusion rates of nutrients and metabolites.

Silica-based consolidant

Among the inorganic consolidants based on silica, the most preferably employed for stone consolidation are ethyl silicate and a colloidal nano-suspension of silicon dioxide made of particles with an average diameter of 10-20 nm.

Concerning healthy risks for end users, these latter type of treatment represents a valid alternative to the traditional solvent-based products because are applied as an aqueous dispersion [106].

Ethyl silicate, the tetra ethyl ester of the orthosilicic acid, $Si(OC_2H_5)_4$, also called TEOS (tetraethoxysilane), has become very important in the field of stone conservation. It derives from an industrial process, the reaction between silicon tetrachloride ($SiCl_4$) and ethyl alcohol (C_2H_5OH) (**Fig. 1.9**).

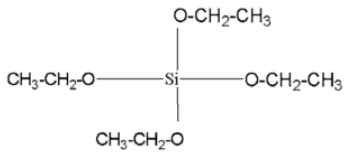

Figure 1.9 *- Ethyl silicate* [26].

The product used for consolidation is the amorphous silica gel obtained from TEOS through a two step process (**Fig. 1.10**).

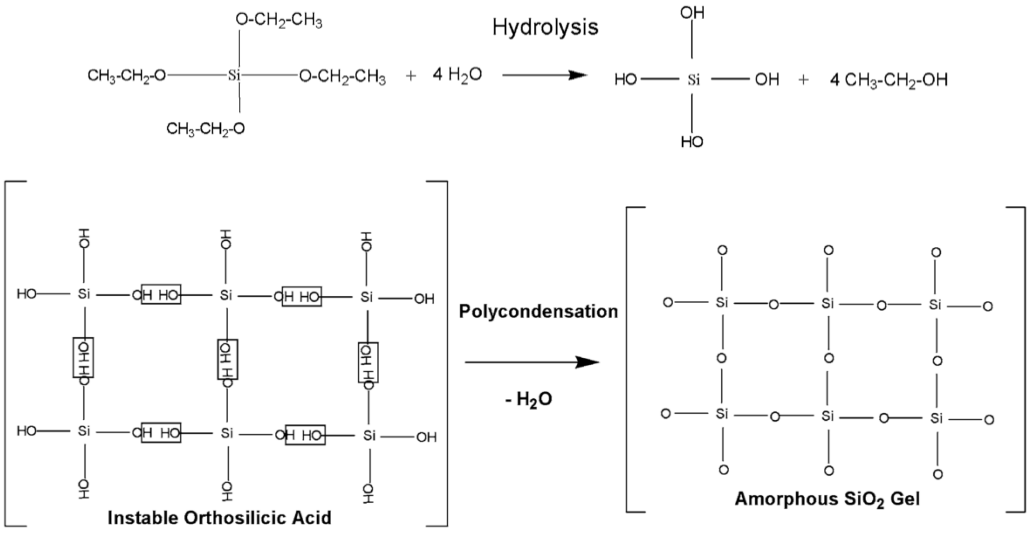

Figure 1.10 *- Hydrolysis and condensation of TEOS to silica gel* [26].

During the first step, the presence of water and a catalyst leads to the hydrolysis of ethoxy groups, forming ethyl alcohol (C_2H_5OH). The second step regards the condensation of the new product, called tetra-hydroxysilane, to amorphous silica gel composed by Si-O-Si. A good property of ethyl silicate is its low viscosity that allows an easy penetration into fissures and pores. Furthermore, ethyl alcohol, formed as the secondary product of the reaction, evaporates and does not cause problems.

However, a problem arises because ethyl silicate is rather volatile and if the hydrolysis is too slow, it may evaporate before reacting, leading to a scarce consolidation effect. To solve this problem, two solutions are possible: adding a catalyst to accelerate hydrolysis of ethyl silicate or obtaining an oligomer of ethyl silicate before the application of the product on decayed surface. The oligomer is obtained by combining, through a partial condensation process, a small number of molecules; in this way the oligomer does not evaporate and the use of a catalyst is not necessary [30]. This type of treatment is mostly used to consolidate sandstone because in this case the deposited silica gel can link covalently with silanol group that cover the grain surfaces [107], [108], while in carbonate stones there is only a physical bonding between grains and silica gel [109], [110]. To overcome this problem some authors have proposed to introduce some coupling agents characterized by the presence of an hydroxyl group on one end that bonds to silica gel and an anchor group on the other end to bond calcitic grains [111], [112]. However, this treatment can cause chromatic modifications and leads to a significant changes in the hydric behaviour [113].

Aqueous colloidal dispersion of nano-sized silica are preferred in some situation, where ethyl silicate is not convenient, such as presence of high relative humidity values, free water or damp surfaces or when little time is available, [114]. Also in this case, the consolidation effect is due to a network of silica gel formed among pore structure of stone and the effectiveness of the treatment is strongly dependent by the humidity conditions [115].

1.2.1.2 Organic treatments

The other group of products used to restore deteriorated stone materials includes a great variety of organic compounds. Both natural and synthetic polymeric materials, such as rubbers, waxes, acrylic resins, vinyl polymers, have been used as conservation materials. Their consolidating action is based on the introduction inside the porous material of macromolecules which solidify when solvent evaporates (thermoplastic polymers) or when a hardener agents cross-link the resin (thermosetting polymers). They are easy to apply and have good adhesion to the substrate. These types of polymer are widely used because, together with a consolidating effect, they make the treated surface water repellent. However, the polymeric compounds present several negative effects such as physico-chemical modification by action of ultraviolet rays (leading to yellowing and scarce compatibility with the stone surface) and possible biodeterioration due to fungal and bacterial growth [116], [117].
Nowadays, the most used organic consolidants belong to the family of acrylates, therefore a more in depth description of these compounds will be reported.

Acrylates

Acrylic resins have been used in the restoration field since 1960s. Chemically, all acrylic compounds are obtained from the esterification of acrylic acids with different alcohols. As shown in **Fig 1.11**, the polymerization process derives from the breaking of C=C double bond and the formation of long C-C single bond chains.

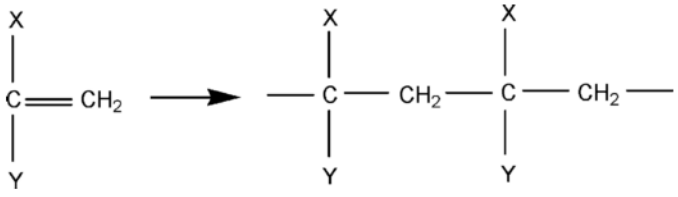

Figure 1.11 *- Reaction scheme of the formation of an acrylic polymer* [26].

According to the degree of polymerization, the acrylic polymers can be viscous or hard materials. The most frequently used acrylate is Paraloid B72, a copolymer (70/30) of EMA (ethyl methacrylate $CH_2=C(CH_3)COOC_2H_5$) and MA (methyl acrylate $CH_2=CH\text{-}COOCH_3$). Its diffusion in the restoration field is due to its good solubility in several solvents, its good adhesive power, transparency and, low rigidity at room temperature [118]. It is usually used in concentrations between 2-10% by weight in several types of organic solvents such as toluene, butyl acetate and acetone. According to the volatility of the solvent, areas of different size are consolidated. In fact, a deeper penetration is obtained when the solvent has a lower volatility. The consolidation effect is obtained with the formation of a polymer layer inside the material that brings together the de-coherent grains. Paraloid B72 was used also in combination with methyl-trimethoxy silane and diluted with a mixture of solvents, in a mixture called Bologna cocktail - firstly developed and tested in Bologna by Italian restorers. Problems connected to the use of this polymer coating are due to the used solvent (possibly harmful), to the yellowing process and, as the reached depth is not so high, to the delamination of the treated surface, most of all if the thickness of the decayed part is higher [26]. Furthermore, if submitted to an artificial weathering, it can form new products and strongly cross-linked structures, which limit the eventual removability of the polymer by reducing the solubility of the fraction [117].
To overcome some drawbacks, as those ones connected to the use organic solvent based formulation, water based polymer micro-emulsions have been recently proposed [119]–[123].

Taking into account the state of art regarding stone consolidation, this work aims at studying a new consolidating agent, calcium ethoxide, as an alternative to traditional treatments. The core idea is that, starting from this new product, stone can be consolidated thanks to the formation of calcium carbonate between grains, pores and micro-cracks. The product has been characterized and its compatibility with the stone support and efficacy as consolidating agent have been tested on several carbonate stones used in the Italian Cultural Heritage field.

1.3 Bibliography

[1] "UNI 11182 Materiali lapidei naturali ed artificiali Descrizione della forma di alterazione - Termini e definizioni," 2006.

[2] G. Negretti, *Fondamenti di petrografia*. Università La sapienza, Roma: Mc Graw Hill, ISBN 88-386-6182-0, 2003.

[3] H. Blatt, R. Tracy, and B. Owens, *Petrology: Igneous, Sedimentary, and Metamorphic*, 3rd ed. ISBN 13: 9780716737438: W. H. Freeman, 2005.

[4] G. G. Amoroso and V. Fassina, *Stone decay and conservation*, Elsevier. Amsterdam, New York, 1983.

[5] E. Doehne and C. A. Price, *Stone conservation: an overview on current research*, 2nd ed. Los Angeles: The getty conservation institute, 2010.

[6] I. Aalil, K. Beck, X. Brunetaud, K. Cherkaoui, A. Chaaba, and M. Al-Mukhtar, "Deterioration analysis of building calcarenite stone in the House of Venus in the archaeological site of Volubilis (Morocco)," *Constr. Build. Mater.*, vol. 125, pp. 1127–1141, 2016.

[7] A. Moropoulou, K. Bisbikou, R. Van Grieken, K. Torfs, and K. Polikreti, "Correlation between aerosols, deposits and weathering crusts on ancient marbles," *Environ. Technol.*, vol. 22, no. 6, pp. 607–618, 2001.

[8] *ICOMOS-ISCS: llustrated glossary on stone deterioration patterns, glossaire illustré sur les formes d'altération de la pierre*, Eng-Fr. Monuments & Sites, Paris, 2008.

[9] P. Brimblecombe, "History of air pollution and damage to the cultural heritage of European cities," in *Science, Technology and European Cultural Heritage. Butterworth-Heinemann, Oxford,* Baer N.S., Sabbioni C., Sors A.I., 1991, pp. 51–66.

[10] D. Camuffo, "Aspetti meteorologici e micro-climatici nel degrado dei materiali lapidei," in *Conservazione del Patrimonio Culturale. Accademia Nazionale dei Lincei, Contributi del Centro Linceo Interdisciplinare "Beniamino Segre", No. 88, Roma*, 1994, pp. 9–27.

[11] M. F. Striegel, E. B. Guin, K. Hallett, D. Sandoval, R. Swingle, K. Knox, F. Best, and S. Fornea, "Air pollution, coatings, and cultural resources," *Prog. Org. Coatings*, vol. 48, pp. 281–288, 2003.

[12] M. Ivaskova, P. Kotes, and M. Brodnan, "Air pollution as an important factor in

construction materials deterioration in Slovak Republic," *Procedia Eng.*, vol. 108, pp. 131–138, 2015.

[13] F. Di Turo, C. Proietti, A. Screpanti, M. F. Fornasier, I. Cionni, G. Favero, and A. De Marco, "Impacts of air pollution on cultural heritage corrosion at European level: What has been achieved and what are the future scenarios," *Environ. Pollut.*, vol. 218, pp. 586–594, 2016.

[14] M. F. La Russa, P. Fermo, V. Comite, C. M. Belfiore, D. Barca, A. Cerioni, M. De Santis, F. L. Barbagallo, M. Ricca, and S. A. Ruffolo, "The Oceanus statue of the Fontana di Trevi (Rome): The analysis of black crust as a tool to investigate the urban air pollution and its impact on the stone degradation," *Sci. Total Environ. J.*, vol. 594, pp. 297–309, 2017.

[15] J. Watt, J. Tiblad, V. Kucera, and R. Hamilton, *The Effects of Air Pollution on Cultural Heritage*. Springer, 2009.

[16] J. B. Johnson, S. J. Haneef, B. J. Hepburn, A. J. Hutchinson, G. E. Thompson, and G. C. Wood, "Laboratory exposure systems to simulate atmospheric degradation of building stone under dry and wet deposition conditions," *Atmos. Environ. Part A, Gen. Top.*, vol. 24, no. 10, pp. 2585–2592, 1990.

[17] S. W. Massey, "The effects of ozone and NO_x on the deterioration of calcareous stone," *Sci. Total Environ.*, vol. 227, pp. 109–121, 1999.

[18] A. J. Lewry, D. J. Bigland, and R. N. Butlin, "The effects of sulfur dioxide on calcareous stone: a chamber study," *Constr. Build. Mater.*, vol. 8, no. 4, pp. 261–265, 1994.

[19] M. M. Reddy, "Acid rain damage to carbonate stone: a quantitative assessment based on the aqueous geochemistry of rainfall runoff from stone," *Earth Surf. Process. Landforms*, vol. 13, no. 4, pp. 335–354, 1988.

[20] A. E. Charola and R. Ware, "Acid deposition and the deterioration of stone: a brief review of a broad topic," *Geol. Soc. London, Spec. Publ.*, vol. 205, no. 1, pp. 393–406, 2002.

[21] A. L. Goodman, G. M. Underwood, and V. H. Grassian, "A laboratory study of the heterogeneous reaction of nitric acid on calcium carbonate particles," *J. Geophys. Res.*, vol. 105, no. D23, pp. 29053–29064, 2000.

[22] C. Sabbioni, "Contribution of atmospheric deposition to the formation of damage layers," *Sci. Total Environ.*, vol. 167, pp. 49–55, 1995.

[23] G. Fronteau, C. Schneider-Thomachot, E. Chopin, V. Barbin, D. Mouze, and A. Pascal, "Black-crust growth and interaction with underlying limestone microfacies," *Geol. Soc. London, Spec. Publ.*, vol. 333, pp. 25–34, 2010.

[24] C. M. Belfiore, D. Barca, A. Bonazza, V. Comite, M. F. la Russa, A. Pezzino, S. A. Ruffolo, and C. Sabbioni, "Application of spectrometric analysis to the identification of pollution sources causing cultural heritage damage," *Environ. Sci. Pollut. Res.*, vol. 20, no. 12, pp. 8848–8859, 2013.

[25] L. Lazzarini and M. Laurenzi Tabasso, *Il restauro della pietra*. 2010.

[26] S. Snethlage and R. Siegesmund, *Stone in Architecture: Properties, Durability*. Springer, 2011.

[27] M. del Monte, C. Sabbioni, and O. Vittori, "Urban stone sulphation and oil-fired carbonaceous particles," *Sci. Total Environ.*, vol. 36, pp. 369–376, 1984.

[28] M. A. El-Gohary, "Investigations on limestone weathering of El-Tuba minaret El Mehalla, Egypt: a case study," *Mediterr. Archaeol. Archaeom.*, vol. 10, no. 1, pp. 61–79, 2015.

[29] S. A. Ruffolo, V. Comite, M. F. La Russa, C. M. Belfiore, D. Barca, A. Bonazza, G. M. Crisci, A. Pezzino, and C. Sabbioni, "An analysis of the black crusts from the Seville Cathedral: A challenge to deepen the understanding of the relationships among microstructure, microchemical features and pollution sources," *Sci. Total Environ.*, vol. 502, pp. 157–166, 2015.

[30] G. Torraca, *Lectures on Materials Science for Architectural Conservation*. Los Angeles: The getty conservation institute, 2009.

[31] A. Bonazza, P. Messina, C. Sabbioni, C. M. Grossi, and P. Brimblecombe, "Mapping the impact of climate change on surface recession of carbonate buildings in Europe," *Sci. Total Environ.*, vol. 407, no. 6, pp. 2039–2050, 2009.

[32] E. Rirsch and Z. Zhang, "Rising damp in masonry walls and the importance of mortar properties," *Constr. Build. Mater.*, vol. 24, no. 10, pp. 1815–1820, 2010.

[33] G. Houvenaghel and J. Carmeliet, "Dynamic contact angles, wettability and capillary suction of hydrophobic porous materials," *Hydrophobe III third Int. Conf. Surf. Technol.*

with water Repel. agents, vol. 200, pp. 191–200, 2001.

[34] A. E. Charola, "Salts in the deterioration of porous materials: an overview," *jAIC*, vol. 39, pp. 327–343, 2000.

[35] C. Alves, C. Figueiredo, A. Maurício, M. A. Sequeira Braga, and L. Aires-Barros, "Limestones under salt decay tests: assessment of pore network-dependent durability predictors," *Env. Earth Sci*, vol. 63, pp. 1511–1527, 2011.

[36] M. F. La Russa, G. Barone, C. M. Belfiore, P. Mazzoleni, and A. Pezzino, "Application of protective products to Noto calcarenite (south-eastern Sicily): a case study for the conservation of stone materials," *Env. Earth Sci*, vol. 62, pp. 1263–1272, 2011.

[37] G. Caneva, M. P. Nugari, and O. Salvadori, *La Biologia Vegetale per i Beni Culturali. Vol I: Biodeterioramento e conservazione*, Nardini Ed. 2007.

[38] S. G. Paine, F. V. Linggood, F. Schimmer, and T. C. Thrupp, *The Relationship of micro-organisms to the decay of stone. Philosophical Transactions of the Royal Society. London*, vol. CCXXII-B48. 1933.

[39] J. Pochon and C. Jaton, "Biological factors in the alteration of stone," in *Biodeterioration of Materials*, Elsevier., C. C. Wolters, A.H., Elphick, Ed. 1968, pp. 258–268.

[40] G. Caneva and O. Salvadori, "Biodeterioration of stone," in *The Deterioration and Conservation of Stone. UNESCO, Paris, Larraini, L., Pieper, R. (Eds.)*, 1989, pp. 182–234.

[41] C. E. Urzi, W. E. Krumbein, and T. Warscheid, "On the question of biogenic colour changes of mediterranean monuments (coating-crust-microstromatoloite-patina-scialbatura-skin-rock varnish)," in *Proceedings of the Second International Symposium on: The Conservation of Monuments in the Mediterranean Basins, Geneva*, 1992, pp. 397–420.

[42] T. Warscheid, T. Becker, J. Braams, S. Bruggerhoff, C. Gehrmann, W. E. Krumbein, and K. Petersen, "Studies on the temporal development of microbial infection of different types of sedimentary rocks and its effect on the alteration of the physico-chemical properties in building materials," in *Thiel, M.-J. (Ed.), Conservation of Stone and Other Materials, London,* vol. 1, 1993, pp. 303–310.

[43] C. E. Urzi and W. E. Krumbein, "Microbiological Impacts on the Cultural Heritage," in *Durability and Change*, C. Wiley, Ed. 1994, pp. 107–135.

[44] T. Warscheid and J. Braams, "Biodeterioration of stone: a review," *Int. Biodeterior.*

Biodegradation, vol. 46, pp. 343–368, 2000.

[45] M. Steiger, F. Wolf, and W. Dannecker, "Deposition and enrichment of atmospheric pollutants on building stones as determined by field exposure experiments," in *Conservation of Stone and Other Materials*, vol. 1 E&FN Spo, M.-J. Thiel, Ed. London, 1993, pp. 35–42.

[46] I. Jiménez-González and G. W. Scherer, "Evaluating the Potential Damage To Stones From Wetting and Drying Cycles," in *Konsta-Gdoutos MS, editor. Measuring, monitoring and modeling concrete properties. Netherlands: Springer*, 2006, pp. 685–693.

[47] C. Rodriguez-Navarro, E. Sebastian, E. Doehne, and W. S. Ginel, "The Role of Clays in the Decay of Ancient Egyptian Limestone Sculptures," *Clays Clay Miner.*, vol. 46, no. 4, pp. 414–422, 1998.

[48] J. Berthonneau, P. Bromblet, F. Cherblanc, E. Ferrage, J. M. Vallet, and O. Grauby, "The spalling decay of building bioclastic limestones of Provence (South East of France): From clay minerals swelling to hydric dilation," *J. Cult. Herit.*, vol. 17, pp. 53–60, 2015.

[49] S. Siegesmund, K. Ullemeyer, T. Weiss, and E. K. Tschegg, "Physical weathering of marbles caused by anisotropic thermal expansion," *Int. J. Earth Sci.*, vol. 89, no. 1, pp. 170–182, 2000.

[50] ICOMOS, "The Athens Charter for the Restoration of Historic Monuments. Adopted at the First Congress of Architects and Technicians of Historic Monuments. Athens, 1931." 1996.

[51] J. M. Teutonico, A. E. Charola, E. De Witte, G. Grassegger, R. J. Koestler, M. Tabasso Laurenzi, H. R. Sasse, and R. Snethlage, "Group report: how can we ensure the responsible and effective use of treatments (cleaning, consolidation, protection)?," in *Saving Our Architectural Heritage, the Conservation of Historic Stone Structures, Wiley, York*, 1997.

[52] V. Cnudde, J. P. Cnudde, C. Dupuis, and P. J. S. Jacobs, "X-ray micro-CT used for the localization of water repellents and consolidants inside natural building stones," *Mater. Charact.*, vol. 53, pp. 259–271, 2004.

[53] G. Borsoi, B. Lubelli, R. Van Hees, R. Veiga, and A. S. Silva, "Evaluation of the effectiveness and compatibility of nanolime consolidants with improved properties,"

Constr. Build. Mater., vol. 142, pp. 385–394, 2017.

[54] K. Van Balen, I. Papayianni, R. Van Hees, L. Binda, and A. Waldum, "Introduction to requirements for and functions and properties of repair mortars," *Mater. Struct.*, vol. 38, no. 282, pp. 781–785, 2005.

[55] "Italian Recommendation NORMAL 20/85, Conservazione dei materiali lapidei: Manutenzione ordinaria e straordinaria," *Istituto Centrale del Restauro (ICR), Rome*. 1985.

[56] J. Delgado Rodrigues and A. Grossi, "Indicators and ratings for the compatibility assessment of conservation actions," *J. Cult. Herit.*, vol. 8, no. 1, pp. 32–43, 2007.

[57] E. Sassoni, G. Graziani, and E. Franzoni, "An innovative phosphate-based consolidant for limestone. Part 1: Effectiveness and compatibility in comparison with ethyl silicate," *Constr. Build. Mater.*, vol. 102, pp. 918–930, 2016.

[58] J. Delgado Rodrigues, "Consolidation of decayed stones. A delicate problem with few practical solutions," *Hist. Constr.*, pp. 3–14, 2001.

[59] E. Hansen, E. Doehne, and C. Price, "A review of selected inorganic consolidants and protective treatments for porous calcareous materials," *Rev. Conserv.*, vol. 4, 2003.

[60] I. Brajer and N. Kalsbeek, "Limewater Absorption and Calcite Crystal Formation on a Limewater-Impregnated Secco Wall Painting," *Stud. Conserv.*, vol. 44, no. 3, pp. 145–156, 2017.

[61] M. Drdácky' and Z. Slízkova, "Calcium hydroxide based consolidation of lime mortars and stone," in *Proceedings of 1st Historical Mortars Conference HMC08 – Characterization, Diagnosis, Conservation, Repair and Compatibility*, 2008, pp. 299–308.

[62] C. Rodriguez-Navarro, A. Suzuki, and E. Ruiz-Agudo, "Alcohol Dispersions of Calcium Hydroxide Nanoparticles for Stone Conservation," *Langmuir*, vol. 29, pp. 11457–11470, 2013.

[63] M. Matteini, "In review: an assessment of Florentine methods of wall painting conservation based on the use of mineral treatments," in *Proc. Int. Symp. The Conservation of Wall Paintings,* 1991, pp. 137–148.

[64] J. Delgado Rodrigues and A. P. Ferreira Pinto, "Laboratory and onsite study of barium hydroxide as a consolidant for high porosity limestones," *J. Cult. Herit.*, vol. 19, pp. 467–476, 2016.

[65] Z. Slížková, M. Drdácký, and A. Viani, "Consolidation of weak lime mortars by means of saturated solution of calcium hydroxide or barium hydroxide," *J. Cult. Herit.*, vol. 16, no. 4, pp. 452–460, 2015.

[66] R. C. Weast, Ed., *Handbook of Chemistry and Physics. A ready-reference Book of Chemical and Physical Data*, 57th editi. CRC Press.

[67] D. Chelazzi, G. Poggi, Y. Jaidar, N. Toccafondi, R. Giorgi, and P. Baglioni, "Hydroxide nanoparticles for cultural heritage: Consolidation and protection of wall paintings and carbonate materials," *J. Colloid Interface Sci.*, vol. 392, pp. 42–49, 2013.

[68] P. Baglioni and R. Giorgi, "Soft and hard nanomaterials for restoration and conservation of cultural heritage," *Soft Matter*, vol. 2, p. 293, 2006.

[69] E. May and M. Jones, *Conservation science Heritage materials*. RCS Publishing, 2006.

[70] R. Giorgi, L. Dei, and P. Baglioni, "A New Method for Consolidating Wall Paintings Based on Dispersions of Lime in Alcohol," *Stud. Conserv.*, vol. 45, no. 3, pp. 154–161, 2000.

[71] L. Dei and B. Salvadori, "Nanotechnology in cultural heritage conservation: nanometric slaked lime saves architectonic and artistic surfaces from decay," *J. Cult. Herit.*, vol. 7, no. 2, pp. 110–115, 2006.

[72] P. Baglioni, D. Chelazzi, R. Giorgi, and G. Poggi, "Colloid and Materials Science for the Conservation of Cultural Heritage: Cleaning, Consolidation, and Deacidification," *Langmuir*, vol. 29, no. 17, pp. 5110–5122, 2013.

[73] M. Ambrosi, L. Dei, R. Giorgi, C. Neto, and P. Baglioni, "Colloidal Particles of Ca(OH) 2 : Properties and Applications to Restoration of Frescoes," *Langmuir*, vol. 17, no. 8, pp. 4251–4255, 2001.

[74] J. Otero, A. E. Charola, C. A. Grissom, and V. Starinieri, "An overview of nanolime as a consolidation method for calcareous substrates," *Ge-conservación*, vol. 1, no. 11, pp. 71–78, 2017.

[75] J. Delgado Rodrigues and D. Costa, "Consolidation of a porous limestone with nanolime," in *12th International Congress on the Deterioration and Conservation of Stone*, 2012, pp. 1–11.

[76] L. Kessler, "A Process for Hardening Soft Limestone by Means of the Fluosilicates of

Insoluble Oxides," *Comptes Rendus*, vol. 96, pp. 1317–1319, 1883.

[77] M. Sgobbi, E. Zendri, M. Melchiorre Di Crescenzo, F. C. Izzo, and G. Biscontin, "La prevenzione del degrado a Venezia nel XIX-XX secolo: studio delle superfici di Ca' Rezzonico," in *Scienza e Beni Culturali XXV*, 2010, vol. XXVI, pp. 803–812.

[78] E. Sassoni, G. Graziani, and E. Franzoni, "An innovative phosphate-based consolidant for limestone. Part 2: Durability in comparison with ethyl silicate," *Constr. Build. Mater.*, vol. 102, pp. 931–942, 2016.

[79] E. Sassoni, S. Naidu, and G. W. Scherer, "The use of hydroxyapatite as a new inorganic consolidant for damaged carbonate stones," *J. Cult. Herit.*, vol. 12, no. 4, pp. 346–355, 2011.

[80] S. Naidu, C. Liu, and G. W. Scherer, "Hydroxyapatite-based consolidant and the acceleration of hydrolysis of silicate-based consolidants," *J. Cult. Herit.*, vol. 16, no. 1, pp. 94–101, 2015.

[81] M. Ni and B. D. Ratner, "Nacre surface transformation to hydroxyapatite in a phosphate buffer solution," *Biomaterials*, vol. 24, no. 23, pp. 4323–4331, 2003.

[82] T. M. Cezar, "Calcium oxalate: a surface treatment for limestone," *J. Conserv. Museum Stud.*, vol. 4, no. May, pp. 1–17, 1998.

[83] G. S. M. Ambrosi, P. Baglioni, P.R. David, L. Dei, R. Giorgi, C. Lalli, G. Lanterna, A. Mairani, M. Matteini, M. Rizzi, "Inorganic consolidants and protectives for architectonic surfaces: experimental tests on Santa Prisca church apse in Rome," in *2nd international congress on Science and technology of the safeguard of cultural heritage in the mediterranean basin, Amsterdam*, 2000, pp. 873–877.

[84] S. Rescic, M. Matteini, and F. Fratini, "Carbonate lithotypes passivated with the ammonium oxalate treatment: colorimetric and morphological study of treated surfaces," *Sci. Technol. Cult. Herit.*, vol. 16, pp. 93–99, 2007.

[85] M. Realini, C. Colombo, C. Conti, R. Negrotti, T. Poli, S. Baldis, R. Grazioli, and M. Lanfranchi, "Il consolidamento della facciata del palazzo del Museo di Piazza della Cittadella a Bergamo: monitoraggio delle applicazioni di ossalato di ammonio sulle superfici dipinte," in *Scienza e Beni Culturali XXIII, Bressanone*, 2007, pp. 477–486.

[86] M. Realini, M. Matteini, C. Colombo, C. Birrozzi, and B. Ferriani, "Monitoraggio di

superfici policrome trattate con ossalato di ammonio," in *National Congress IGIIC, Genova,* 2004, pp. 330–338.

[87] M. Matteini, M. Camaiti, C. Colombo, F. Fratini, L. Pellegrino, and M. Realini, "Verifiche sperimentali dei trattamenti programmati per il recupero conservativo ed estetico dei mosaici pavimentali e degli intonaci dipinti," in *Progetto di recupero e conservazione della Villa Romana del Casale di Piazza Armerina, I grandi restauri N 12/1*, 2007, pp. 219–222.

[88] C. Conti, C. Colombo, D. Dellasega, M. Matteini, M. Realini, and G. Zerbi, "Ammonium oxalate treatment: evaluation by μ-Raman mapping of the penetration depth in different plasters," *J. Cult. Herit.*, vol. 12, no. 4, pp. 372–379, 2011.

[89] T. Dreyfuss and JoAnn Cassar, "Ammonium oxalate treatment application in the presence of soluble salts: laboratory results on soft limestone," in *Built Heritage: Monitoring Conservation Management*, 2015, pp. 335–346.

[90] M. Matteini, "Inorganic treatment for the consolidation and protection of stone artefacts and mural paintings," *Conserv. sceince Cult. Herit.*, vol. 8, pp. 13–27, 2008.

[91] M. Matteini, S. Rescic, F. Fratini, and G. Botticelli, "Ammonium Phosphates as Consolidating Agents for Carbonatic Stone Materials Used in Architecture and Cultural Heritage: Preliminary Research," *Int. J. Archit. Herit.*, vol. 5, no. 6, pp. 717–736, 2011.

[92] M. Matteini, A. Moles, and S. Giovannoni, "Calcium Oxalates as a Protective Mineral System for Wall Paintings: Methodology and Analyses," in *3rd International Symposium on the Conservation of Monuments in the Mediterranean Basin, Venezia, S.B.A.S.*, 1994, pp. 155–161.

[93] M. Matteini, A. Moles, G. Lanterna, and M. R. Nipoti, "Preliminary Monitoring on Painted Plasters and Marble Surfaces of a Mineral Protective Treatment Based on Artificially Formed Calcium Oxalate," in *II International Symposium, The Oxalate Films in the Conservation of Works of Art, Milan*, 1996, pp. 423–440.

[94] M. Matteini and S. Giovannoni, "The Protective effect of ammonium oxalate treatment on the surface of wall paintings," in *Painted Facades. Proceedings of the Eurocare Project, Vienna*, 1996, pp. 95–101.

[95] B. Doherty, M. Pamplona, C. Miliani, M. Matteini, A. Sgamellotti, and B. Brunetti, "Durability of the artificial calcium oxalate protective on two Florentine monuments,"

J. Cult. Herit., vol. 8, no. 2, pp. 186–192, 2007.

[96] L. Skrelp, A. Pondelak, and A. S. Skapin, "Method for reinforcing porous construction materials and use calcium acetoacetate solution to this aim: EP 3004028 (B1), European Patent Office (EPO)." Munich, 2017.

[97] A. Pondelak, S. Kramar, M. L. Kikelj, and A. S. Skapin, "In-situ study of the consolidation of wall paintings using commercial and newly developed consolidants," *J. Cult. Herit.*, vol. 28, pp. 1–8, 2017.

[98] V. Achal, A. Mukherjee, D. Kumari, and Q. Zhang, "Biomineralization for sustainable construction – A review of processes and applications," *Earth Sci. Rev.*, vol. 148, pp. 1–17, 2015.

[99] N. K. Dhami, M. Sudhakara Reddy, and A. Mukherjee, "Application of calcifying bacteria for remediation of stones and cultural heritage," *Front. Microbiol.*, vol. 5, 2014.

[100] W. De Muynck, D. Debrouwer, N. De Belie, and W. Verstraete, "Bacterial carbonate precipitation improves the durability of cementitious materials," *Cem. Concr. Res.*, vol. 38, pp. 1005–1014, 2008.

[101] W. De Muynck, N. De Belie, and W. Verstraete, "Microbial carbonate precipitation in construction materials: A review," *Ecol. Eng.*, vol. 36, pp. 118–136, 2010.

[102] C. Rodriguez-Navarro, M. Rodriguez-Gallego, K. Ben Chekroun, and M. T. Gonzalez-Muñoz, "Conservation of Ornamental Stone by Myxococcus xanthus-Induced Carbonate Biomineralization," *Appl. Environ. Microbiol.*, vol. 69, no. 4, p. 2182, 2003.

[103] F. M. Helmi, H. R. Elmitwalli, S. M. Elnagdy, and A. F. El-Hagrassy, "Calcium carbonate precipitation induced by ureolytic bacteria Bacillus licheniformis," *Ecol. Eng.*, vol. 90, pp. 367–371, 2016.

[104] F. Jroundi, P. Gómez-Suaga, C. Jimenez-Lopez, M. T. González-Muñoz, and M. A. Fernandez-Vivas, "Stone-isolated carbonatogenic bacteria as inoculants in bioconsolidation treatments for historical limestone," *Sci. Total Environ.*, vol. 425, pp. 89–98, 2012.

[105] C. Jimenez-Lopez, F. Jroundi, C. Pascolini, C. Rodriguez-Navarro, G. Piñar-Larrubia, M. Rodriguez-Gallego, and M. T. González-Muñoz, "Consolidation of quarry calcarenite by calcium carbonate precipitation induced by bacteria activated among the

microbiota inhabiting the stone," *Int. Biodeterior. Biodegrad.*, vol. 62, pp. 352–363, 2008.

[106] E. Zendri, G. Biscontin, I. Nardini, and S. Riato, "Characterization and reactivity of silicatic consolidants," *Constr. Build. Mater.*, vol. 21, pp. 1098–1106, 2007.

[107] C. Miliani, M. L. Velo-Simpson, and G. W. Scherer, "Particle-modified consolidants: A study on the effect of particles on sol-gel properties and consolidation effectiveness," *J. Cult. Herit.*, vol. 8, no. 1, pp. 1–6, 2007.

[108] M. A. Al-Dosari, S. Darwish, M. A. El-Hafez, N. Elmarzugi, N. Al-Mouallimi, and S. Mansour, "Effects of Adding Nanosilica on Performance of Ethylsilicat (TEOS) as Consolidation and Protection Materials for Highly Porous Artistic Stone," *J. Mater. Sci. Eng. A*, vol. 6, no. 4, pp. 192–204, 2016.

[109] A. Calia, M. Masieri, G. Baldi, and C. Mazzotta, "The evaluation of nanosilica performance for consolidation treatment of an highly porous calcarenite," in *12th International Congress on the Deterioration and Conservation of Stone Columbia University, New York*, 2012, pp. 1–10.

[110] A. Zornoza-Indart, P. Lopez-Arce, N. Leal, J. Simão, and K. Zoghlami, "Consolidation of a Tunisian bioclastic calcarenite: From conventional ethyl silicate products to nanostructured and nanoparticle based consolidants," *Constr. Build. Mater.*, vol. 116, pp. 188–202, 2016.

[111] A. P. Ferreira Pinto and J. Delgado Rodrigues, "Hydroxylating conversion treatment and alkoxysilane coupling agent as pre-treatment for the consolidation of limestones with ethyl silicate," in *Stone Consolidation in Cultural Heritage: Research and Practice; Proceedings of the International Symposium, Lisbon,* 2008, pp. 141–140.

[112] A. P. Ferreira Pinto, J. Delgado Rodrigues, S. Bracci, and B. Sacchi, "The action of APTES as coupling agent of ethylsilicate for limestone and marble consolidation," in *Stone Consolidation in Cultural Heritage: Research and Practice; Proceedings of the International Symposium*, 2008, pp. 71–80.

[113] A. Zornoza-Indart, P. López-Arce, and L. López-Polín, "Durability of traditional and new nanoparticle based consolidating products for the treatment of archaeological stone tools: chert artifacts from Atapuerca sites (Burgos, Spain)," *J. Cult. Herit.*, vol. 24, pp. 9–21, 2017.

[114] C. T. S. Europe, "Un consolidante atipico Nano Estel. Nuovi Prodotti, in: Bollettino

C.T.S. Europe, no 27.1, C.T.S., Europe, 2011." .

[115] A. Zornoza-Indart and P. Lopez-Arce, "Silica nanoparticles (SiO_2): Influence of relative humidity in stone consolidation," *J. Cult. Herit.*, vol. 18, pp. 258–270, 2016.

[116] F. Cappitelli, P. Principi, R. Pedrazzani, L. Toniolo, and C. Sorlini, "Bacterial and fungal deterioration of the Milan Cathedral marble treated with protective synthetic resins," *Sci. Total Environ.*, vol. 385, pp. 172–181, 2007.

[117] M. Favaro, R. Mendichi, F. Ossola, U. Russo, S. Simon, P. Tomasin, and P. A. Vigato, "Evaluation of polymers for conservation treatments of outdoor exposed stone monuments. Part I: Photo-oxidative weathering," *Polym. Degrad. Stab.*, vol. 91, pp. 3083–3096, 2006.

[118] M. K. Khallaf, A. A. El-midany, and S. E. El-mofty, "Influence of acrylic coatings on the interfacial , physical , and mechanical properties of stone-based monuments," *Prog. Org. Coatings*, vol. 72, no. 3, pp. 592–598, 2011.

[119] J. V. Grafía Sales, X. M. Barberà, E. P. Marín, and L.-B. Roig, "Ideología Y Metodología En Los Procesos De Intervención En Las Esculturas Y Ornamentos Del Espacio Central Y Acceso Sur De La Basílica," in *Arché. Publicación del instituto universitario de restauración del patrimonio de la UPV*, 2008, pp. 127–136.

[120] C. Guinamard, "Techniques de restauration de la polychromie du choeur de la cathédrale de Chartres. Restaurations récentes et nouvelles recherches," *Bull. Monum.*, vol. 169, pp. 23–26, 2011.

[121] M. Camaiti, L. Borgioli, and L. Rosi, "Photostability of innovative formulations for artworks restoration," *La Chim. e l'industria*, pp. 100–105, 2011.

[122] J. L. Regidor Ros, P. Soriano Sancho, M. A. Zalbidea Muñoz, A. Iaccarino Ildeson, and P. Roig Picazo, "Puesta en práctica de soluciones propuestas para las pinturas arracadas de Palomino en la Iglesia de Los Santos Juanes de Valencia," in *XVIII Congreso International Conservación y Restauración de Bienes Bulturales*, 2011, pp. 524–527.

[123] A. Sansonetti, "Il cantiere della 'Ca' Granda'. La lettura dell'esperto scientifico," in *Istituto Lombardo (Rend. Scienze)*, vol. 146, 2012, pp. 93–112.

CHAPTER 2

Materials and Methods

Summary

This chapter gives a summary of materials and investigation techniques employed in this research project. The starting materials involved: a new product for consolidation of stone materials - calcium ethoxide nanosuspension diluted in three types of organic solvents - and mock-ups of four different carbonate stones, widely employed in the field of Italian Cultural Heritage, to be treated to understand the effect of the consolidating treatment. Several investigation techniques were used for the study of calcium ethoxide and the characterization of carbonate stones, while others were carried out to evaluate the effectiveness and the compatibility of the applied product, according to European and Italian standards.

2.1 Evaluation strategy

This research project was carried out in collaboration with different national and international institutions, such as Consiglio Nazionale delle Ricerche in Padua, University of Palermo and Labóratorio National de Engenharia Civil in Lisbon.

The investigation started with the characterization of the consolidating treatment, calcium ethoxide $Ca(OEt)_2$, a product developed during the European NANOMATCH project. The ethoxide nanosuspension was diluted in three organic solvents and, therefore, three different products to be tested were obtained. The consolidating effect of calcium ethoxide is due to a carbonation reaction which leads to the formation of calcium carbonate; therefore, the first part of the project regarded the characterization of the three obtained products through:

- the study of the kinetic and the reaction pathway of the carbonation process to understand how the three different solvents could affect the carbonation reaction; during this analysis, the products were kept at laboratory relative humidity and temperature conditions;

- the evaluation of mineralogical phases formed from the reaction of the products with air, by analyzing products' coatings deposited on glass surface and maintained at different relative humidity condition (RH%) and controlled room temperature for two weeks, one months and three months, to investigate the effects of solvents and different relative humidity conditions on carbonate phase formation. The chosen values of RH% were 50% and 90% to simulate a dry and a very humid environment, respectively.

The analyses performed in this first part were: micro Fourier Transform-Infrared Spectroscopy (μFT-IR) and X-ray Diffraction (XRD) which allow to discriminate the three mineralogical phases of calcium carbonate (calcite, aragonite and vaterite).

The second part of the project regarded the application of three products on mock-ups of four carbonate stones characterized by a different total open porosity value and widely used in the field of Italian Cultural Heritage. Before the application of the consolidating products on laboratory samples, the involved carbonate stones were chemically characterized by Fourier Transform Infrared Spectroscopy (FT-IR) and Differential Scanning Calorimetry/Thermogravimetric Analysis (TG- DSC) and, then, subjected to an artificial to simulate the deterioration of materials. The effect of the ageing was studied by analyzing samples with Mercury Intrusion Porosimetry (MIP) before and after this process. Subsequently, several types of analyses and techniques were used, before and after the application of the consolidating treatments, to understand their performance. These techniques involved the observation of the following characteristics:

- variation of cumulative volume and pore size distribution with Mercury Intrusion Porosimetry (MIP) and Nuclear Magnetic Resonance Relaxometry (NMR);
- variation of water transport properties by evaluating absorption coefficient through capillarity, drying behaviour and water vapour permeability;
- morphological and aesthetical variation of the surface with Scanning Electron Microscopy (SEM) and spectrophotometric measurements according to CIEL*a*b* system, respectively;
- the consolidating effect and the penetration reached by the products by using Ultrasonic Pulse Velocity (UPV) and Drilling Resistance Measurement System (DRMS).

The obtained results were compared with those reached with the application of a reference

commercial product, CaLoSil E50 - calcium hydroxide nanoparticles dispersed in ethanol.

2.2 Starting material

In this section a brief description of the applied consolidating products, the reference one and the carbonate supports is given.

2.2.1 Metal alkoxides

The study of chemistry of metal alkoxides began more than 150 years ago, but recently it has received new attention due their intriguing structural chemistry, interesting catalytic properties and great potential for industrial applications, for example, as molecular precursors in the synthesis of materials of modern technology based on complex or simple oxides - such as the sol-gel technology [1], [2].

In 1846 the first derivatives of metal alkoxide has been described but, only starting from the half of nineteen century, progresses led to the investigation of the chemistry of alkoxides of the whole periodic table [1].

The general formula of a metal alkoxides is $M(OR)_x$ where M is a metal of valency x, and R is a simple or substituted alkyl, aryl or alkenyl group. They derive from the replacement of the hydroxylic hydrogen of an alcohol ROH by a metal cation [3].

The physical properties of metal alkoxides are influenced by several factors such as shape and size of the R group and metal's properties (valency, atomic radius, coordination number of the metal and stereochemistry). The high electronegativity of oxygen should confer a ionic character to the M-OR bonds (in alkoxides of metallic elements). However, most of these alcohols exhibit a low degree of volatility and solubility in common organic solvents, which can be considered as a characteristic of covalent compounds. It was postulated that the factors to explain the attenuation of M-O bond polarity are: the inductive effect of alkyl groups at the oxygen atom, which increases with the branching of the alkyl chain, and the formation of oligomeric species through alkoxo bridges, according to the following geometry (**Fig. 2.1**):

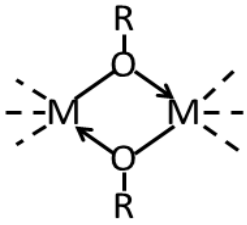

Figure 2.1 *- Oligomeric structure of an alkoxide* [1].

Alkoxides show a high tendency to oligomerization, unless it is inhibited by steric and electronic factors. The degree of aggregation of these compounds can be reduced by varying some characteristics of alkoxy group, in particular by increasing the size of the substituents and/or with the presence of coordinating donor atoms in the group. Studying the steric and electronic factors, the degree of aggregation depends by the following factors: (i) aggregation increases as the metal atom becomes more electron deficient, (ii) the larger size of the metal atom, the greater the tendency to increase degree of association (n) by forming alkoxo bridged system, (iii) the steric effect of the alkyl substituent which, by increasing steric demand, inhibits aggregation and it has been found to be of greater importance than the electronic nature of the substituents in determining the ultimate extent of aggregation and (iv) presence of donor atoms (O, N) in the substituents, capable to coordinate the metal, preventing further coordination with another molecule.

From a chemical point of view, metallic alkoxides are a highly reactive class of metallorganic compounds and they can be subjected to three different groups of reactions: complex formation with donor ligands or alkoxides of other metals, complete or partial substitution for the OR-groups and several degradation reactions - such as hydrolysis and oxidation - which lead to formation of oxoligands [2].

The alcoholic reactions in which the metal alkoxides are involved consist in an exchange reactions with an alcohol to achieve the following equilibrium:

$$M(OR)_x + yR'OH \rightarrow M(OR)_{x-y}(OR')_y + yROH$$

This process is influenced by several factors: solubility of metallic alkoxide, steric size of both ligands and alcohol, relative strength of alkoxides' bonds and presence of terminal alkoxide groups, strictly bounded or easily substitutable [1].

During hydrolysis process, including that caused by environmental humidity, they react with a wide variety of hydroxyl reagents such as water, alcohol and carboxylic acids. During this process, the alkoxy groups are replaced by OH groups and O^{2-} groups. This reaction is influenced by several factors, such as: nature of the R group, nature of the solvent, the concentration of the species present in the solution and the temperature.

Furthermore, alkoxides tend to undergo oxidation processes in the presence of oxygen traces in the atmosphere and solvents. The primary products of this reaction consist of radical groups such as -OOR and -OOH, which decompose through a radical process by providing water, hydroxyl and carboxylic groups. This process is followed by the appearance of a brown-

yellow colour, probably due to the presence of free radical as traces. All these physico-chemical properties result in a broad spectrum of properties ranging from insoluble and non-volatile polymer solids to volatile monomeric liquids [2].

The main alkoxide of alkaline earth metals are colourless solids, generally insoluble, non-volatile and very sensitive to moisture and carbon dioxide [2]. The properties of these compounds seem to be dominated by their ionic character and the preference to reach a metal coordination number greater than six, thus leading to the formation of rather large associated species [1].

2.2.1.1 Calcium alkoxides as stone consolidants

Calcium alkoxides have been proposed in recent years as a new conservation product to consolidate carbonate stones and wall paintings. In fact, these compounds, dissolved in a proper organic solvent, penetrate inside the stone and react with humidity and atmospheric carbon dioxide to form calcium carbonate through a carbonation process releasing the starting alcohol, which evaporates. This behaviour makes them suitable for consolidation of carbonate supports, such as wall paintings, plasters and building stone materials [4], [5].

Calcium alkoxides as well as other alkaline earth alkoxides, have been synthesized and studied during the EU-NANOMATCH Project (Nano-systems for the conservation of immoveable and moveable polymaterial Cultural Heritage in a changing environment FP7/2007-2013, Grant Agreement No 283182) with the aim of consolidate carbonate through their penetration inside the porous material and formation of calcium carbonate able to restore the lost cohesion of the treated supports [6], [7].

Previous studies [8]–[10] showed that the carbonation process can follow two different pathways: insertion of a CO_2 molecule within the Ca-O bond with a formation of an intermediate alkylcarbonate followed by hydrolysis and alcohol elimination, and a second type of reaction involving a first hydrolysis of the alkoxide with the formation of calcium hydroxide as intermediate, which subsequently carbonates (**Fig. 2.2**).

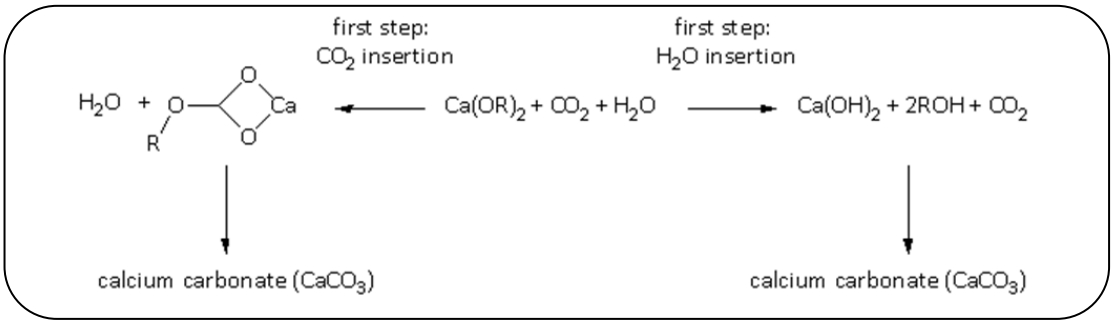

Figure 2.2 *- Possible carbonation pathways of calcium alkoxides: insertion of CO_2 can either precede or follow the hydrolysis* [6].

Synthesis of metal alkoxides has been studied by different researches for more than a century. A large variety of synthetic techniques and protocols aimed at the preparation of different distinct derivatives have been proposed [2], [3].

During the EU-NANOMATCH project calcium alkoxide were synthesized with five different protocols and, therefore, several types of products have been obtained [9], [10]; in order to avoid the presence of oxygen and moisture all the methods were performed in a nitrogen filled glove-box.

The first type of synthesis involves a direct reaction between metallic calcium and alcohol: powdered metallic calcium is deeply stirred - with or without reflux - in an excess of anhydrous alcohol, another solvent could be possibly used together. After a certain time, the metal totally disappears from the solution and the obtained product is recovered by precipitation or crystallization. During this type of synthesis, an oligomeric form of calcium alkoxide is often obtained.

A second type of synthesis regards an alcoholysis reaction between one alkoxide (such as calcium ethoxide chosen for its solubility, easy synthesis and reactivity) and a second alcohol. This represents a simple methodology to obtain another calcium alkoxide.

A third type of synthesis is called Rieke synthesis and it starts with an initial formation of the Rieke calcium which, having a high surface area, can easily react with the proper alcohol. Rieke calcium derives from the reduction of a THF suspension of an anhydrous metal halide with an alkali metal.

The fourth type of synthesis starts from $Ca(OH)_2$, the cheapest source of calcium, which can lead to the formation of calcium carbonate: in this case the reaction is forced by removing the forming water with a Dean Stark apparatus.

Finally, the fifth type of synthesis is the so called "ammonia method" and it is based on the use of liquid ammonia that can dissolve and activate the metals. Under inert atmosphere,

freshly anhydrous distilled solvent containing metallic calcium is cooled from -45 to -60°C and gaseous ammonia is bubbled inside. Once the metal has dissolved, a solution of the desired alcohol in the suitable solvent is inserted, and the temperature cautiously made to reach room temperature [9], [10].

Among more than twenty different alkoxides synthesized during the project, calcium tetrahydrofurfuryloxide ($Ca(OTHF)_2$ - NANOMATCH1) and calcium ethoxide ($Ca(OEt)_2$ - NANOMATCH2) were selected according to their favourable features and their production was scaled up by ABCR labs (Spain) to produce about 3 kg of consolidants, which were then applied and tested [11].

The new treatments were evaluated on several carbonate substrates in terms of workability, effectiveness and compatibility, compared to a number of commercial products. The products were firstly tested on laboratory samples and then or real case study to understand their durability in situ conditions. Finally, the optimal processing parameters for industrial production were defined and an economical cost-benefit analysis of new products was performed.

Between calcium tetrahydrofurfuryloxide and calcium ethoxide, the latter presented some drawbacks and was the least investigated during the project; therefore, the aim of this research was to modify some characteristics of the base product, as the carrier solvent, to understand if these changes could influence its effectiveness and compatibility as consolidating agent. Moreover, the new obtained product was applied on carbonate stones with different porosity to understand its ability to reach different penetration level according to the chosen support.

2.2.1.2 Calcium ethoxide

This product is a nanosuspension of $Ca(OEt)_2$ in a 1:3 solution (v/v %) of ethanol and tetrahydrofuran, with an initial calcium concentration of 46.5 g/L and average particles' dimension of 295 nm determined by DLS. Based on previous studies carried out during the NANOMATCH project, a calcium concentration of 20 g/L showed the best results [12]; in fact, different calcium concentration were studied and 20 g/L resulted the only one combining a good consolidation effect without cause a colour change of the surface.

Therefore, to reach a calcium concentration of 20 g/L, the initial product was diluted in three different solvents chosen for their different boiling point and because they are actually used in the restoration field: ethanol, 2-butanol and n-butylacetate (**Tab 2.1**). The solvent's boiling

point is an important value because it could influence the penetration of the product inside the porous materials [13].

Table 2.1 *- Physicochemical properties of the employed solvent. The term REL derives from the US legislation and means Recommended Exposure Limits, the concentration not to be exceed, mediated in a 40-hour working week* [14].

Solvent	Formula	Boiling point (°C)	REL (ppm)	Solubility in water (wt%)*
Ethanol	C_2H_6O	78.4	1000	∞
2-buthanol	$C_4H_{10}O$	100	100	44.1
n-butylacetate	$C_6H_{12}O_2$	127	150	1.86

** These values are reported in percentage and are expressed in weight (g/g): g of solvent in 100 g of water. The symbol ∞ indicates that the solvent is completely miscible* [14].

Therefore, three products to study were obtained:

- Calcium ethoxide nanosuspension diluted in ethanol - labelled as *ET*;
- Calcium ethoxide nanosuspension diluted in 2-butanol - labelled as *2BUT*;
- Calcium ethoxide nanosuspension diluted in n-butylacetate - labelled as *NBUT*.

The three prepared solutions based on $Ca(OEt)_2$ nanosuspension were firstly subjected to two different studies, both alone and mixed with the four different powdered carbonate supports:

- study of kinetic and reaction pathway of the carbonation process in atmosphere, to understand if the different solvents could affect the velocity of this process; during the analysis samples were maintained at laboratory relative humidity and temperature conditions;
- study of mineralogical phases formed leaving coating of three solutions at different relative humidity conditions (50% - 90%) and at controlled room temperature, to understand the possible influence of solvents and RH% conditions on the formation of the three polymorphs of calcium carbonate.

  The study of mineralogical phases is important because calcium carbonate presents at least six different phases: three anhydrous crystalline polymorphs (calcite, vaterite and aragonite) and three hydrated forms (monohydrocalcite $CaCO_3 \cdot H_2O$, ikaite $CaCO_3 \cdot 6H_2O$ and amorphous calcium carbonate ACC) [15]. From the thermodynamic point of view, calcite is more stable than aragonite and vaterite and the

physicochemical properties of these three polymorphs are different in terms of morphology, density and solubility (**Tab. 2.2**) [16]. In fact, the crystal structure of calcite is rhombohedral and appears often like cubes [17]. Aragonite presents an orthorhombic cell [18] and particles are usually found as needles [19]. The unit cell of vaterite is hexagonal [20] and it appears often as spheres. Monohydricalcite is a trigonal mineral while ikaite crystallizes in the monoclinic crystal system. Several factors can influence the precipitation of these polymorphs as pH, conductibility, presence of impurities, relative humidity [16], temperature [21] and type of solvent [22]. Previous studies have shown that the transformation from vaterite and aragonite to calcite occurs through a process of dissolution of the metastable phase and recrystallization of the stable one [23], [24].

Table 2.2 *- Properties of crystalline polymorphs of calcium carbonate.*

Mineral	Crystalline system	Density (g/cm³)	Form
Calcite	Rhombohedral	2.7	anhydrous
Vaterite	Hexagonal	2.6	anhydrous
Aragonite	Orthorhombic	2.9	anhydrous
Monohydrocalcite	Trigonal	2.4	hydrated
Ikaite	Monoclinic	1.8	hydrated

2.2.2 CaLoSil E50

CaLoSil E50® was used as reference product in the consolidation of porous support due to its effectiveness in filling micro cracks and small voids [25]. It is composed of a stable colloidal $Ca(OH)_2$ nanoparticles (50-250 nm) dispersed in ethanol and it is produced by the IBZ-Salzchemie (GmbH & Co.KG, Germany). In this case, the calcium concentration is 26.3 g/L; therefore, to achieve a calcium concentration of 20 g/L - the same chosen for calcium ethoxide - it was diluted with ethanol. This product will be labelled in the text as *CAL*.

2.2.3 Carbonate stones

The selection of stones has been restricted to calcareous stones since calcium ethoxide used in this research project is mainly meant for the consolidation of calcite-based substrates. The chosen carbonate stones are widely used in the field of Italian Cultural Heritage both as

building materials and for works of art such as sculptures and architectural-decorative elements. They consist of both metamorphic - Carrara marble - and sedimentary rocks - Lecce stone, Noto stone and Vicenza Stone. These different carbonate stones have been chosen both for their different values of total open porosity % and because they are employed in different region of Italy.

2.2.3.1 Lecce stone

Lecce stone is a sedimentary rock, a biocalcarenite, whose name derives from the city of Lecce, in the south of Italy, but it is widely employed in the whole Salento region. It was used by sculptors and architects mostly during Baroque period, but also nowadays, for sculpture, decorative objects and to cover the façades of buildings [26]. Significant examples are the friezes, the capitals, the pinnacles and the rosettes which decorate many of the palaces and churches of Lecce, such as the Church of Santa Chiara, the Cathedral, the Church of Santa Croce and the Celestine Palace.

This biocalcarenite dates back to the Miocene period (between 12 and 20 million years ago); it presents a compact and fine grain and it is well known for its gold-yellow colour. This stone shows a quite homogeneous composition made mainly of calcium carbonate in the form of calcite cement and granules (fragments of fossils and microfossils of marine organism) together with other minerals such as quartz, various feldspars, glauconite and phosphates [27], [28]. According to the percentage of these clay minerals, sensitive variations could be registered also in the same quarry regarding the colour, the degree of hardness, porosity and compressive strength. This stone is extracted from open sky quarries and it is well known for its simple extraction - cubic parallelepipeds are obtained - and manufacturing. The main important quarries are in the Salento territory, particularly in the city of Lecce, Corigliano d'Otranto, Melpignano, Cursi and Maglie. Till the middle of the twentieth century, the extraction was performed completely by hand with the help of rudimentary instruments. This process followed the quarry bed, according to the natural sedimentation plans. From the 50's onwards, the extraction has taken place with the help of the machines.

The hardness and strength of the stone, when extracted, grow with the passing of time. The rock is compact with a fine grain and has an easy workability due to the presence of clay, which allows both the lathe and manual modelling.

2.2.3.2 Noto stone

The Noto stone is a calcarenite with a typical pale cream colour composed by calcium carbonate and several small bioclasts, including foraminifera, echinoids, plankton and bryozoa. It was mainly used during the Baroque period and it characterizes the whole architecture of the Noto Valley (Sicily). It was used both for construction and decorative elements due to its easy workability and proper physical and mechanical properties. An extremely high spread of this stone took place after the earthquake of 1693, which involved the entire eastern part of Sicily. In the Hyblean area, this material became the protagonist of the reconstruction, by characterizing and defining the urban planning and the architecture of the reconstructed cities with its yellow-golden coloration. The easy workability and the good physical and mechanical qualities determined its several use: both structural (arches, piers, walls, vaults) and decorative (stairs, balustrades, gargoyles, fountains and capitals) [29]. Geologically, it formed during lower Oligocene-Pliocene and belongs to Palazzolo Formation, which emerges in a long zone of seven kilometres between Palazzolo Acreide and Noto [30]. Quarries of the Palazzolo Formation are situated between the left side of the Tellaro River and Buscemi [31]. The extraction takes place in open-pit quarries and it proceeds to horizontal descending levels.

2.2.3.3 Vicenza stone

This sedimentary stone is an organogenic limestone characterized by the presence of micro and macro clastics of foraminifera, bryozoans, algae, and echinoderms [32]. It has a strongly heterogeneous structure and consists of calcium carbonate (80-90%) combined with small percentage of silicon oxide, aluminium and iron. From a physical point of view, it shows modest mechanical properties and, due to its strong compositional heterogeneity and low value of hardness, presents a good workability. Furthermore, according to its low value of tensile strength, flexion and compression, this stone does not respond very well to mechanical stress, so it was used mainly for sculpture and surface manufacturing. In fact, it is a soft stone and a great material to be molded. Its formation goes back to the Middle Eocene and the subsequent Oligocene (between 55 and 23 million years ago), and it belongs to the calcarenite family of Castelgomberto, one of the mainly constituents of the Berici hills, located to the south of Vicenza. This lithotype was formed by the accumulation of sand and skeletons of microorganisms at the bottom of a sea that anciently occupied the present area of the hills. Currently, the Vicenza stone quarries on the Berici Hills are about fifteen. Inside these quarries, there are different types of Vicenza stone, recognizable by colour, grain and

extraction site: yellow, white and grey [33]. In this case, the stone used for the project is the white Vicenza, extracted from Badia Quarries.

Regarding the extraction activity, at the beginning of the twentieth century, the processing techniques were essentially the same as five hundred years earlier. The extraction process began by practicing a square opening in the rock and it was worked till the complete isolation of the block. Today, the modern excavation machine, called "mole", is a gigantic mechanical saw, which works isolating the desired block.

2.2.3.4 Carrara marble

Carrara Marble is a metamorphic stone mainly composed of calcite crystals and it is considered the most prestigious marble in Italy. It is a metamorphic rock originated from pre-existing ones which, due to strong pressure and/or temperature changes, underwent a complete reorganization of the crystalline structure and transformed into entirely different rocks. It has a typical saccharoidal structure due to the re-crystallization process after the metamorphism. This stone is extracted from quarries in Tuscany and includes a wide variety of marble types with different chromatic and structural characteristics: the main varieties are seven and, according to small chromatic variations, they can be further divided into many other qualities. The seven main varieties are: *white, statuario, venato, arabescato, calacata, bardiglio and zerbino cipollino*. White marble was the one used in this project and its main feature is to contain only very small quantities of impurities which are insufficient to alter the natural colour of calcite. It has a homogenous white to grey ground colour, irregular grey veins and shining grains.

Marble quarries were probably already used during the Copper Age from inhabitants of the area to produce domestic and decorative objects, or for grave goods to be buried with the body of the deceased. Extraction flourished under the Roman time and in this period the marble was called Lunense marble, as the centre of extraction was identified in the city of Luni, a colony founded by the Romans; from Luni port ships loaded with this material used to sail to Rome. After the Romans and for many centuries there are no news about marble excavation: only at the end of the thirteenth century, under the Empire of Frederick I, there was the rebirth of the extraction activities in the Carrara basins. Even at that time the excavation technique was similar to that practiced by the Romans and it remained the same until the 1700 when the method with explosive was introduced. The use of this technique had the defect of destroying much of the marble and producing a large amount of waste material

[34]. Nowadays, marble is extracted with the combined action of helical wire and pulley.

2.3 Evaluation techniques

In accordance with the evaluation strategy, this part describes all the analytical techniques and material tests employed to investigate the calcium ethoxide for the consolidation of carbonate stones. Some techniques were used to characterize the three obtained products based on $Ca(OEt)_2$ nanosuspension: the kinetic and reaction pathway of carbonation process and the mineralogical phases formed in different RH% conditions; while others, were employed to assess the performance - effectiveness and compatibility - of the three products as consolidating agents by evaluating how some properties of stones' mock-ups change after their application. For each type of proof and treatment, the amount of product retained - evaluated by weighing samples before and one month after treatment application - is expressed as the weight of product per unit surface (kg/m^2) and this value is reported as the average value of three samples and the associated error expressed as standard deviation[1]. As it will be reported in chapter 3, differences among quantity of product retained for samples treated with the same product are probably due to the different shape of mock-ups (in accordance to the different analyses, mock-ups of different dimensions were necessary).
It is expected that the effectiveness of the treatment is linked to the amount of applied product, but technical data regarding consolidants do not provide a recommended amounts of product to be applied to achieve a good consolidating effect. Therefore, there are not many information about the right quantity of product to apply to reach a desirable consolidation effect [35].

2.3.1 Artificial ageing of stone

Since the main objective of consolidation is to increase the mechanical cohesion of weathered stone, to test the effectiveness of a consolidating product, it should be applied on a weathered substrates rather on fresh stones. As taking weathered samples in situ (art objects and/or monumental buildings) is generally not allowed in the field of conservation of Cultural Heritage, it is easier to reproduce weathered substrate in laboratory. Different types of weathering processes of stones have been tested during the years and the efficacy of the

[1] Standard deviation σ is given by the following formula: $\sigma = \sqrt{\frac{\sum (x - x_m)^2}{(n-1)}}$ where x_m is the mean value and n corresponds to the repeated measurements.

method is related to the type and microstructure of the stone [36]–[39].

In this project an artificial ageing based on thermal cycles (heating/cooling) was performed on the chosen stones substrate. The specimens were subjected to six daily heating - cooling cycles: 100°C for 6 hours, cooling to room temperature for 6 hours, chilling to -20°C for 6 hours and finally warming to room temperature for 6 hours [40]. To understand if the ageing was successful, Mercury Intrusion Porosimetry (MIP) was performed on samples before and after the process.

2.3.2 Fourier Transform InfraRed Spectroscopy (FT-IR)

FT-IR measurements were performed to characterize stone materials, to study the kinetic and the reaction pathway of carbonation process of $Ca(OEt)_2$ based products (through the variation of the signal) and finally to evaluate the mineralogical phases of calcium ethoxide coating kept at different RH%.

The characterization of carbonate stones was carried out at Ca' Foscari University of Venice by means of a FT-IR Nicolet Nexus 750 spectrometer in transmission configuration. Carbonate samples were powdered in an agate mortar, mixed with KBr (1:100-wt% sample/KBr) and compressed as pellets (10 tons pressure). Every spectrum was collected from 4000-400 cm^{-1} and was the average of 64 scans using a spectral resolution of 4 cm^{-1}.

The study of kinetic and pathway reaction of carbonation process and mineralogical phases formation of $Ca(OEt)_2$ based products coating were performed at CNR-ICMATE of Padua with a Nicolet microscope connected to a Nicolet 560 FT-IR system, equipped with an MCT (mercury-cadmium-telluride) detector working in a reflectance mode. The spectra were acquired within a range of 4000-650 cm^{-1}, with a resolution of 4 cm^{-1}, and 64 scans were collected each time. The analysed area consists of a square of 50 x 50 μm. All the collected spectra, shown in the transmittance mode, were firstly elaborated with Omnic 6.0 software including smoothing and normalization and, then, with OriginPro9 software.

For the kinetic measurements, a small drop of calcium ethoxide, diluted in the proper solvent, was laid down on a glass surface and FT-IR spectra were acquired at different times, from the beginning of the analysis till two weeks later. The analysed samples were kept at laboratory humidity and temperature conditions during the analysis.

Instead, the mineralogical phases were determined by analyzing the products previously deposited on a glass surface, left to dry and properly preserved at different RH%, 50% and 90%. The samples were preserved in two different driers maintained at controlled room

temperature (20-25 °C) and the two different RH% conditions were obtained by inserting a beaker with a saturated solution of a specific salt in a drier [41]; in particular, saturated solutions of $Ca(NO_3)_2$ - calcium nitrate - and KNO_3 - potassium nitrate - were prepared to create a 50% RH and a 90% RH environments, respectively. The control of relative humidity was performed with a RH sensor (Oregon Scientific ™ Wireless Weather Station BAR388HG).

To perform μFT-IR analysis, a small quantity of product was taken away from the deposit, rolled out on a glass surface and finally analysed. This analysis was performed after two weeks, one month and three months of air exposure. The coating composition was evaluated by observing the characteristic absorption peaks of calcium carbonate polymorphs.

2.3.3 X-Ray diffraction (XRD)

Crystalline phases of carbonate stones and mineralogical phases of $Ca(OEt)_2$ based products stored at different RH% conditions were determined by powdered X-ray Diffraction.

The stone samples were grinded in an agate mortar and analysed with Philips PW1050 diffractometer with a Bragg-Brentano geometry and an incident radiation of Cu kα (40 kV and 30 mA)[2].

The $Ca(OEt)_2$ based products coatings, previously analysed with μFT-IR, were investigated with a Philips X'Pert PW3710 diffractometer with a Bragg-Brentano geometry. The incident radiation of Cu X-ray tube is the same of the previous diffractometer[3]. Also in this case, the analysis was carried out after two weeks, one month and three months.

All the measurements were performed in continuous mode in the range $10° < 2\theta < 70°$, with a step size of 0.02° and an acquisition time of 4 s. The obtained graphic were elaborated with X'Pert Higscore software and then processed by OriginPro9 software.

2.3.4 Differential Scanning Calorimetry/Thermogravimetric Analysis (TG-DSC)

This type of analysis provides information about the type and the quantity of compounds present in a samples. The method consists in a continual recording of the mass variations of a

[2] Prof. Pietro Riello and his team, from the department of Molecular Science and Nanosystems of Ca' Foscari University of Venice, are kindly acknowledged for performing XRD measurements.

[3] Dr. Naida El Habra, from CNR-ICMATE, Istituto di Chimica della Materia Condensata e di Tecnologie per l'Energia, Padova, is kindly acknowledged, for performing XRD measurement.

sample as function of temperature, in a controlled atmosphere. The result of the analysis is expressed by a thermogram which reports the mass variation as function of the temperature [42]. In this study, this technique was carried out to evaluate the percentage of calcium carbonate inside the analysed carbonate stones. The measurement was carried out on powdered samples with a Netzsch STA 409/C instrument using platinum crucibles at 10°C/min heating rate, in N_2 atmosphere, from 30°C to 1000°C. The NETSCHTA3.5 software was used to elaborate the obtained data while, the final curve was processed by OriginPro9 software.

2.3.5 Mercury intrusion porosimetry

MIP technique provides information about the microstructure of materials through the evaluation of bulk density, total open porosity and pore size distribution (%). Mercury, being a non wettable liquid, with a contact angle with stone materials of 141.3° [43], cannot penetrate spontaneously inside small pores because of the capillary pressure. For this reason an external pressure has to be applied. The volume of mercury V (mm^3/g) intruded at a given pressure P (kg/cm^2) gives the pore volume value that can be accessed [44]. The intrusion pressure is related to the pore volume through the Washburn equation [45]:

$$P = \frac{2\gamma \cos\theta}{r}$$

where P is the intrusion pressure, γ is the mercury surface tension (486.5 mN/m^{-1}), θ is mercury/solid contact angle and r is the pore radius (μm).

The followed standard to perform this proof is NORMAL 4/80 [46]; dried samples were analysed with Pascal 140 and Pascal 240 Thermo Nicolet instrument for the individuation of macropores and mesopores [47], respectively. For each type of stone support, the results are reported as the average of three analysed samples and the associated error is expressed as standard deviation. The acquired data were processed with OriginPro 9 software.

2.3.6 Water absorption through capillarity

The water absorption measurements were performed to understand how the consolidating products can affect the water transport inside the stone support and shows the quantity of water which over time penetrates inside the stone through its pores driven by capillary processes. This method were carried out according to the normative UNI EN 10859:2000 [48]. The standard defines a method to determine the absorption of water by capillarity of

porous inorganic materials employed in the field of Cultural Heritage by putting in contact a fixed surface with water. For each type of stone, cubic samples of dimensions 3x3x3 cm, were firstly dried until constant mass in an oven (60 ± 2 °C) and then put in a drier for 3 h. Samples' surfaces were covered with an aluminium tape leaving only one surface free, that one on which the consolidating treatments will be applied. Each specimen was individually placed on a filter paper saturated with distilled water and then, at regular intervals, each sample was weighted. For each samples, the quantity of absorbed water for unit of surface was calculated as follow:

$$Q_i = \frac{(m_i - m_0)}{A} \cdot 1000$$

where m_i (g) is the specimen mass at time t_i, m_0 (g) is the mass of the dried specimens and A is the specimen's surface (cm^2).

This parameter was represented graphically as a function of the square root of time and the capillary water absorption coefficient, defined as the angular coefficient of this curve, was calculated by linear regression of the experimental data. The analyses were performed before and after treatments on the same set of specimens (three samples). During the analyses, samples were stored at laboratory temperature and relative humidity. The results are reported as the average of the analysed samples and the associated error is expressed as standard deviation.

2.3.7 Dry index

As for water absorption through capillarity, the measurement of dry index provides information about change in water transport inside the stone after the application of a consolidation treatment. The normative NORMAL 29/88 defines a method to calculate the drying rate of the specimen [49]. This protocol was performed directly after the capillary water absorption test. The samples were immersed in distilled water until constant mass was reached and then put in a drier on a rigid network of non-oxidizable material. The samples were regularly weighted till a constant weight was reached. The amount of water remained in the samples (Q_i) at time t_i was calculated as:

$$Q_i = \frac{m_i - m_{of}}{m_{of}} \cdot 100$$

where m_i (g) is the samples mass at time t_i (h) and m_{of} (g) is the sample mass dried at the end

of the proof.

The drying rate is an evaluation of water transport behaviour of the stone and with these experimental values it is possible to built a dry curve of values of Q_i in function of time. To study the evolution of the drying curve for the different supports, the rate at which the samples dry is needed.

The analyses were performed before and after treatments on the same set of specimens (three samples). During the analysis, the drier was stored at laboratory temperature and relative humidity conditions. The results are reported as the average of the analysed samples and the associated error is expressed as standard deviation.

2.3.8 Water vapour permeability

This type of analysis measures the behaviour of a material at humidity passage and allows to detect the resistance of the material to the diffusion of water vapour. The followed standard to perform the water vapour permeability test is DIN 52 615 [50]. It allows to calculate this factor trough similar parameters: water vapour permeability coefficient (g), water vapour resistance factor (μ), density of water vapour flow rate (WDD). In this project, the comparison of results between treated and untreated samples is reported as g value.

This proof was performed on regular samples with dimension of 5x5x1 cm and covered on the lateral surfaces, placed and fixed on open vessels half-filled with a saturated salt solution of sodium carbonate to reach an internal RH% of 93%. These vessel-sample systems were allocated in a room with constant air temperature (23°C) and RH% (50%) and they were weighted at specific time intervals. In fact, the mass loss allows to determine the quantity of water vapour diffused through the specimens. Weighing was repeated until the reaching of a steady state. The analyses were performed before and after treatments on the same set of specimens (three samples). During the analysis, samples were stored at room temperature and relative humidity conditions. The results are reported as the average of the analysed samples and the associated error expressed as standard deviation.

2.3.9 Nuclear magnetic resonance relaxometry (NMR)

NMR relaxometry is a technique used in the field of Cultural Heritage to characterize pore-space structure of high surface-to-volume ratio (S/V) systems and, in recent years, it has been increasingly applied to characterize and monitor works of art of Cultural Heritage interest [51]–[54]. Through the study of the return to equilibrium of the nuclear magnetization of

water ^{1}H nuclei - which fully saturate the porous system - after an appropriate sequence of radiofrequency pulse, it is possible to acquire qualitative information about pore size distribution [55], [56].

The process of the return back to equilibrium is called "relaxation" and it is characterized by a constant decay time named relaxation time. The transverse relaxation time T2 is the decay time related to the component xy of the nuclear spin magnetization in the xy plane, while the longitudinal relaxation time T1 is the decay connected to the z component of the nuclear spin magnetization [51]. Being non-destructive and non-invasive, it is possible to obtain both transverse (T2) and longitudinal (T1) relaxation time distributions of water protons, before and after the application of a consolidating treatment. NMR measurements were performed by a relaxometer mq-ProFiler equipped with single-sided magnet (Bruker Biospin ®, Italy) which works at a Larmor frequency of about 15 MHz (**Fig. 2.3**).

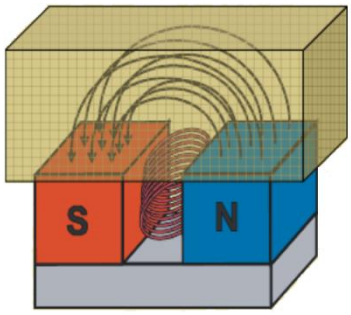

Figure 2.3 *- Schematic representation of NMR mouse* [57].

The sensitive volume xyz from which the resonant conditions were obtained is about 2x0,2x0,8 cm^3, where the x and y axes are parallel and perpendicular to the magnet surface, respectively; while, z coincides to the direction of the main magnetic field. The longitudinal relaxation time was acquired by the saturation recovery-spin echo sequence (echo time 44 μs) and, in this case, the relaxation trendlines of the NMR signal were obtained as function of the saturation time (T_S), which is the time between the first and the second 90° pulses. These trendlines are related to the recovery of the longitudinal magnetization after a first 90° pulse; they start from zero and tend to saturate to a maximum value. The acquisition was carried out for various values of recovery delay T_S, ranging from 0.1 ms and 8500 ms. The interpulse delay for spin-echo signals was 44 μs, the shortest possible delay. After each sequence, a recycle delay of 1.2 s was set to allow the longitudinal magnetization to fully recover before next pulse sequence. Each measurement was the average of 16 subsequent accumulations. Transverse relaxation decays were obtained performing the Carr-Purcell-Meiboom-Gill

(CPMG) pulse sequence. In this sequence the echo time to 44 μs was set and the total number of echo was chosen equal to 8000. After each sequence a recycle delay of 2 ms was set to allow the longitudinal magnetization to fully recover before next pulse sequence. The chosen samples with dimensions of 10x5x2 cm were previously dried in a oven and then saturated under vacuum with distilled water. Before the analysis, the samples were completely covered with a plastic film in order to avoid any leak of water during the measurements. All the analyses were carried out at room temperature and the same set of samples was analysed before and after the application of treatments. Experimental data, acquired through the Minispec software, were turned into pore-size distributions by the inversion of the relaxation decay data using the UPEN algorithm and then, processed by OriginPro9 software[4].

2.3.10 Colorimetric measurements

Colour measurements were performed to evaluate the aesthetic compatibility of $Ca(OEt)_2$ based treatments with stone supports.

The colour measurements were made in the CIEL*a*b* colour space where L* is the lightness, positive and negative values, while a* and b* are the chromaticity coordinates, the red-green direction and the yellow-blue direction, respectively (**Fig 2.4**).

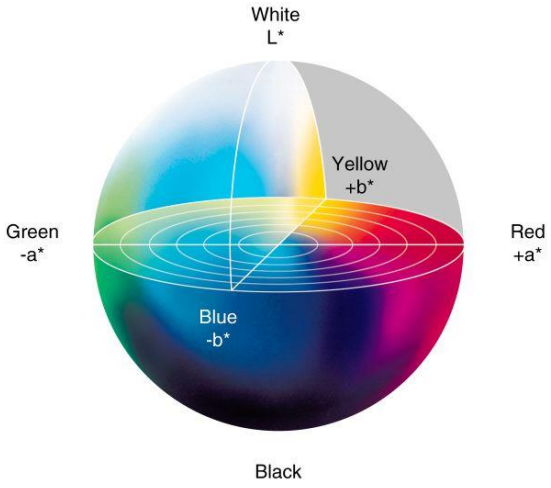

Figure 2.4 *– Representation of CIEL*a*b* space.*

The total colour difference (ΔE^*) was computed as:

$$\Delta E^* = \sqrt{\Delta L^{*2} + \Delta a^{*2} + \Delta b^{*2}}$$

[4] Prof. Maria Brai and her group, from the department of Physics and Chemistry of University of Palermo, are kindly acknowledged for their collaboration in NMR measurements.

According to the NORMAL 43/93 [58] colour data were acquired with a CM2600d Konica Minolta portable spectrophotometer with a D65 illuminant and 10° standard observer. This instrument has a 5 mm diameter measurement area and it is set to quantify the potential specular component included (SCI) colour variations due to the application of the consolidating treatments. This type of measurement was acquired on two different set of samples: a first set of prismatic samples of 5x10x2 cm on which the products were applied with one type of application procedure (brush till saturation) and a second one of 5x5x5 cm on which the products were applied with a second type of application procedures (absorption through capillarity); details about application procedures are reported in paragraph 2.4. For the first set of samples, in order to obtain a reproducible measurement, an average of 4 points with 3 scans each was considered for each specimen and the same set of samples was analysed before and after the application of treatments; data are reported as the average of three samples and the relative standard deviation. For the second set, data from treated and not treated material were acquired from the same sample on opposite surface and ten points with 3 scans each were considered from each side. In this case data are reported as the average of ten measurements.

The data were processed firstly with the Spectra Magic NX software and after with OriginPro9 software. The analyses were performed before and after treatments on the same set of specimens (three samples). The results are reported as the average of three analysed samples and the associated error is expressed as standard deviation.

2.3.11 Scanning electron microscopy (SEM)

SEM images were obtained in order to achieve information on the morphology changes induced by the applied products on the treated surface [42]. These analyses were performed using an FEI Quanta 200 FEG-ESEM and the observations were carried out in high vacuum condition - after metallization with carbon - and low vacuum condition with secondary electron detector (ETD and LFD detector, respectively) and different magnifications according to the information to be acquired [5].

[5] Dr. Patrizia Tomasin, from CNR-ICMATE, Istituto di Chimica della Materia Condensata e di Tecnologie per l'Energia, Padova, is kindly acknowledged for the acquisition of SEM images.

2.3.12 Ultrasonic pulse velocity (UPV)

Ultrasound pulse velocity is a non-destructive technique very useful to evaluate the effectiveness of consolidating treatment and the penetration depth reached by the product [59]–[61]. It is based on the propagation of ultrasonic pulse of p-waves through a material and the results are obtained by measuring the travel time t (s) of waves between two transducers. By knowing the distance d (m) between the transducers, it is possible to calculate the waves' velocity propagation v_p (m/s) [62]:

$$v_p = \frac{d}{t}$$

Generally speaking, a higher p-waves velocity propagation indicates a denser material; therefore, the porosity decrease of a treated material due to the effect of the consolidating agent, produces an increase in p-waves velocity with respect to untreated material. In this project the direct transmission method was used: the ultrasonic transmitter and receiver were placed opposite to each other on opposite sides as illustrated in **Fig. 2.5 (a)**. These measurements were done in profile using a particular set-up (**Fig. 2.5 (b)**), to evaluate the penetration depth of the consolidant. The measurement were acquired proceeding from the treated surface to the bottom. In each point, the equipment measured and recorded the travel time of p wave along the two transducers.

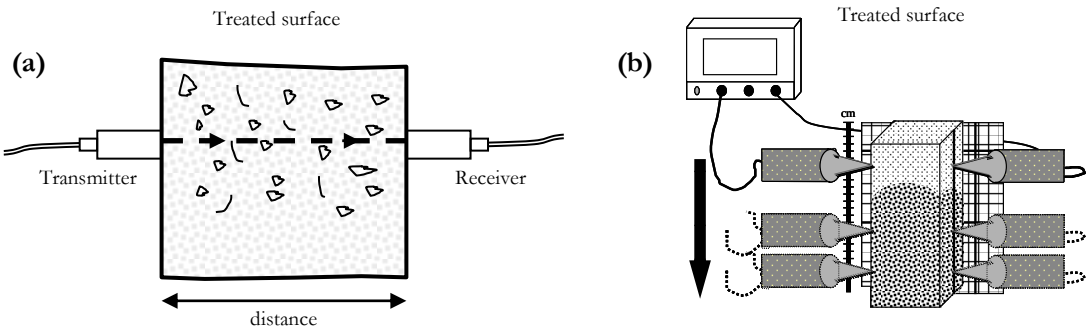

Figure 2.5 *- Ultrasonic pulse velocity (direct transmission mode):* ***(a)*** *transmission method and* ***(b)*** *set up of measurements.*

The equipment used is from Steinkamp (model BP-7) coupled to 45kHz exponential transducers, without contact material.

This measurement was carried out in laboratory on dried samples (with dimension 5x5x5x cm). The results are expressed as mean value of three measurements in each point, established

with 5 mm interval, from 5 to 45mm. The profiles were determined before and after treatment. The acquired data were elaborated with OriginPro 9 software [6].

2.3.13 Drilling Resistance measurement system (DRMS)

DRMS is a sensitive and micro-destructive technique that provides information about stone resistance. It allows to have information about the efficacy of a consolidating treatment and also the penetration depth reached by product [63]–[65]. It is based on the determination of the hardness of stone material, a parameter related to the drilling penetration force (in Newton) necessary to drill a hole under defined and controlled operative conditions such as: the rotational speed and the penetration rate. For comparative purpose, these conditions must be kept constant for both not-treated and treated material [63], [66]. The result is a graph showing the force, measured and recorded each 0,1 mm, versus depth. The mechanical device consists of a power drill able to keep a constant rotational speed and to maintain a predefined advancing rate.

To perform this test a 5 mm-diameter flat diamond was used and the operating conditions were the following: advancing rate of 10 mm/min, rotational speed of 300 rpm and penetration depth 10-15 cm, in accordance with the type of carbonate stone (**Fig. 2.6**).

The material test was carried out on dried cubic samples (5x5x5 cm); treated and not treated data were obtained from the same mock-ups, on opposite surfaces and expressed as the average of three holes. The acquired data have been elaborated with OriginPro 9 software [7].

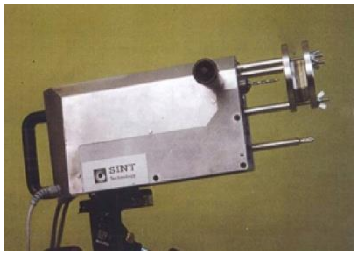

Figure 2.6 *- DRMS equipment.*

2.4 Consolidant application procedures

Consolidating treatments were applied on stone materials with three different application

[6] Dr. Doria Costa and her group, from Laboratório Nacional de Engenharia Civil, Lisbon, are kindly acknowledged for their collaboration in UPV measurements.

[7] Dr. Doria Costa and her group from Laboratório Nacional de Engenharia Civil, Lisbon, are kindly acknowledged for their collaboration in DRMS measurements.

procedures to assess how the absorption of products and the related consolidation effect are influenced by the application procedure:

a) by brush till saturation: treatments were applied till saturation of the surface was reached, intended as the condition when stone surface remains wet for 1 min. This procedures was used for all tested products (**Fig. 2.7 (a)**);

b) by brush with a pre-set number of brush strokes in order to avoid a colour change of the treated surface (**Fig. 2.7 (a)**). This latter type of application was considered only for calcium ethoxide diluted in ethanol and CaLoSil E50 because the purpose of this second application was only to the evaluate the compatibility between the products and the stone supports. To understand how many applications have to be applied before having a colour change of the surface, a colorimetric measurement was performed after each brush stroke of calcium ethoxide diluted in ethanol till the maximum value of $\Delta E^* < 5$ was reached. To better compare the results obtained with the reference product and to limit the number of variables, CaLoSil E50 was applied in the same number of brush strokes. This procedure was used only for $Ca(OEt)_2$ nanosuspension diluted in ethanol and CaLoSil E50.

c) by absorption through capillarity (**Fig. 2.7 (b)**): samples were allocated on glass rods in the base of a vessel containing the consolidating product and were left to absorb the product by capillarity contact for 90 minutes (a time interval decided on the base of previous tests). To avoid formation of superficial deposits, the surfaces left in contact with the product were cleaned with the same solvent used to prepare the consolidating treatment (ethanol, 2-butanol or n-butylacetate), immediately after the end of application. This procedure was used for all tested products.

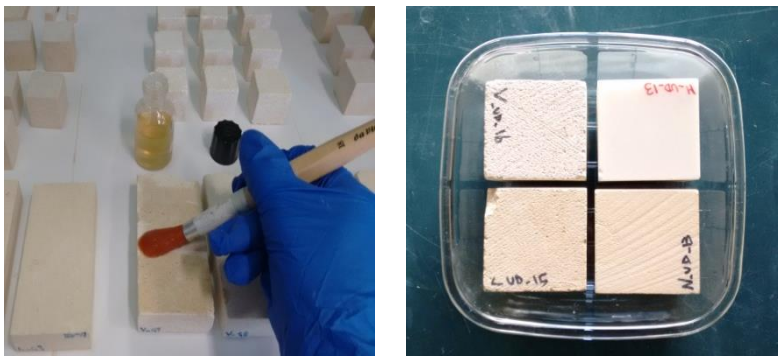

***Figure 2.7** - Application forms: **(a)** by brush and **(b)** by absorption through capillarity.*

The samples treated with the application *a)* were analysed with all the techniques listed in the previous paragraphs; those ones treated with application *b)* were analysed with all techniques except than UPV and DRMS; and, finally, samples treated with application *c)* were analysed only with UPV and DRMS. A summary of the techniques and tests applied for each type of application procedures and type of product is listed in **Tab. 2.3**.

Table 2.3 *- Techniques and material tests applied for each type of application procedure.*

PROCEDURE CODE	APPLIED PRODUCT CODE	STONE SUPPORT	TECNIQUES AND MATERIAL TESTS
a)	1. *ET* 2. *2BUT* 3. *NBUT* 4. *CAL*	ALL (UPV and DRMS were not performed on marble)	• Water absorption by capillarity • Determination of drying curve • Water vapour Permeability • NMR Relaxometry • Mercury Intrusion Porosimetry (MIP) • Surface observation with SEM • Colorimetric measurements • Ultrasonic pulse velocity • Drilling resistant measurement system
b)	1. *ET* 2. *CAL*	ALL (UPV and DRMS were not performed on marble)	• Water absorption by capillarity • Determination of drying curve • Water vapour Permeability • NMR Relaxometry • Mercury Intrusion Porosimetry • Surface observation with SEM • Colorimetric measurements
c)	1. *ET* 2. *2BUT* 3. *NBUT* 4. *CAL*	Lecce Noto Vicenza	• Ultrasonic pulse velocity • Drilling resistant measurement system • Colorimetric measurements

2.5 Bibliography

[1] D. C. Bradley, R. C. Mehrotra, I. P. Rothwell, and A. Singh, *Alkoxo and Aryloxo Derivatives of Metals*. Elsevier, 2001.

[2] N. Y. Turova, E. P. Turevskaya, V. G. Kessler, and M. I. Yanovskaya, *The chemisry of metal alkoxides*. New York, Boston, Dordrecht, London, Moscow Print: Kluwer Academic Publishers, 2002.

[3] D. C. Bradley, "Metal Alkoxides," in *Progress in Inorganic Chemisty*, vol. II, F. A. Cotton, Ed. 1960.

[4] F. Ossola, P. Tomasin, C. De Zorzi, N. El Habra, M. Chiurato, and M. Favaro, "New Calcium Alkoxides for Consolidation of Carbonate Rocks. Influence of Precursors' characteristics on morphology, crystalline phase and consolidation effects," *New J. Chem.*, vol. 36, pp. 2618–2624, 2012.

[5] S. Duchêne, V. Detalle, M. Favaro, R. Ossola, P. Tomasin, C. De Zorzi, and N. El Habra, "Nanomaterials for the consolidation of marble and wall paintings," in *12th International Congress on the Deterioration and Conservation of Stone Columbia University, New York, 2012 NANOMATERIALS*, 2012, pp. 1–9.

[6] I. Natali, P. Tomasin, F. Becherini, A. Bernardi, C. Ciantelli, M. Favaro, O. Favoni, V. J. F. Pérez, I. D. Olteanu, M. Dolores, R. Sanchez, A. Vivarelli, and A. Bonazza, "Innovative consolidating products for stone materials: field exposure tests as a valid approach for assessing durability," *Herit. Sci.*, vol. 3, no. 6, pp. 1–13, 2015.

[7] A. Bernardi, M. Favaro, F. Becherini, A. Bonazza, M. Chiurato, N. El Habra, F. Ossola, P. Tomasin, and A. Vivarelli, "Nanomaterials from Metal-alkoxides Precursors for Conservation of Building Materials: the EU Project NANOMATCH," in *NanotechItaly2012 - International showcase for Nanotechnologies*, 2012, pp. 81–82.

[8] M. Favaro, P. Tomasin, F. Ossola, and P. A. Vigato, "A novel approach to consolidation of historical limestone: the calcium alkoxides," *Appl.Organometal.Chem.*, vol. 22, pp. 698–704, 2008.

[9] M. Favaro, M. Chiurato, P. Tomasin, F. Ossola, E. Habra, I. Svensson, E. Beckers, and A. Bernardi, "Calcium and magnesium alkoxides for conservation treatment of stone and wood in built heritage," in *Built Heritage 2013 Monitoring Conservation Management*,

2013, pp. 1296–1303.

[10] M. Favaro, M. Chiurato, P. Tomasin, F. Ossola, E. Habra, N. Brianese, I. Svensson, E. Beckers, V. J. F. Perez, M. D. Romero Sánchez, G. Orial, E. Bourguignon, and A. Bernardi, "Alkaline earth alkoxides for conservation treatment of stone and wood in built heritage," in *3rd European Workshop on Cultural Heritage Preservation, EWCHP 2013*, 2013, pp. 105–111.

[11] M. Favaro, M. Chiurato, P. Tomasin, F. Ossola, and A. Bernardi, "Metodo per la preparazione di sospensioni di particelle di alcossidi di metalli alcalino- terrosi," patent n° 1426959, 2017.

[12] "Reserved NANOMATCH EU-project report," 2014.

[13] G. Borsoi, B. Lubelli, R. van Hees, R. Veiga, A. S. Silva, L. Colla, L. Fedele, and P. Tomasin, "Effect of solvent on nanolime transport within limestone: How to improve in-depth deposition," *Colloids Surfaces A Physicochem. Eng. Asp.*, vol. 497, pp. 171–181, 2016.

[14] P. Cremonesi, *L'uso di solventi organici nella pulitura di opere policrome*, Il Prato. Collana I talenti, 2004.

[15] R. M. Hazen, R. T. Downs, A. P. Jones, and L. Kah, "Carbon Mineralogy and Crystal Chemistry," *Rev. Mineral. Geochemistry*, vol. 75, no. 1, pp. 7–46, 2013.

[16] M. Kitamura, "Crystallization and Transformation Mechanism of Calcium Carbonate Polymorphs and the Effect of Magnesium Ion," *J. Colloid Interface Sci.*, vol. 236, no. 2, pp. 318–327, 2001.

[17] R. Beck and J. P. Andreassen, "The onset of spherulitic growth in crystallization of calcium carbonate," *J. Cryst. Growth*, vol. 312, no. 15, pp. 2226–2238, 2010.

[18] W. L. Bragg, "The structure of aragonite," *Proceeding R. Soc. London A*, vol. 105, pp. 16–39, 1924.

[19] L. Wang, I. Sondi, and E. Matijević, "Preparation of uniform needle-like aragonite particles by homogeneous precipitation," *J. Colloid Interface Sci.*, vol. 218, pp. 545–553, 1999.

[20] J. Nyvlt and J. Ulrich, "Admixtures in Crystallization," *Chemie Ing. Tech.*, vol. 68, pp. 851–852, 1995.

[21] S. P. Gopi and V. K. Subramanian, "Polymorphism in $CaCO_3$ - Effect of temperature under the influence of EDTA (di sodium salt)," *Desalination*, vol. 297, pp. 38–47, 2012.

[22] F. Manoli and E. Dalas, "Spontaneous precipitation of calcium carbonate in the presence of ethanol, isopropanol and diethylene glycol," *J. Cryst. Growth*, vol. 218, pp. 359–364, 2000.

[23] P. López-arce, L. S. Gómez-villalba, S. Martínez-ramírez, M. Alvarez de Buergo, and R. Fort, "Influence of relative humidity on the carbonation of calcium hydroxide nanoparticles and the formation of calcium carbonate polymorphs," *Powder Technol.*, vol. 205, pp. 263–269, 2011.

[24] T. Ogino, T. Suzuki, and K. Sawada, "The formation and transformation mechanism of calcium carbonate in water," *Geochim. Cosmochim. Acta*, vol. 51, no. 10, pp. 2757–2767, 1987.

[25] K. Niedoba, Z. Slízková, D. Frankeová, C. Lara Nunes, and I. Jandejsek, "Modifying the consolidation depth of nanolime on Maastricht limestone," *Constr. Build. Mater.*, vol. 133, pp. 51–56, 2017.

[26] M. Licchelli, M. Malagodi, M. Weththimuni, and C. Zanchi, "Anti-graffiti nanocomposite materials for surface protection of a very porous stone," *Appl. Phys. A*, vol. 116, pp. 1525–1539, 2014.

[27] D. Agostino, "Moisture dynamics in an historical masonry structure: The Cathedral of Lecce (South Italy)," *Build. Environ.*, vol. 63, pp. 122–133, 2013.

[28] C. De Giorgi, *Note e ricerche sui materiali edilizi adoperati nella provincia di Lecce*. Galatina, 1981.

[29] F. Rodolico, *Le pietre delle città d'Italia*. Le Monnier, 1952.

[30] M. F. La Russa, G. Barone, C. M. Belfiore, P. Mazzoleni, and A. Pezzino, "Application of protective products to Noto calcarenite (south-eastern Sicily): a case study for the conservation of stone materials," *Env. Earth Sci*, vol. 62, pp. 1263–1272, 2011.

[31] L. Anania, A. Badalà, G. Barone, C. M. Belfiore, C. Calabrò, M. La Russa, P. Mazzoleni, and A. Pezzino, "The stones in monumental masonry buildings of the 'Val di Noto' area: New data on the relationships between petrographic characters and physical-mechanical properties," *Constr. Build. Mater.*, pp. 122–132, 2012.

[32] S. Scrivano, L. Gaggero, and J. G. Aguilar, "Porosity characterization of fresh and altered stones by ultrasound velocity and mercury intrusion porosimetry," *Geophys. Res. Abstr.*, vol. 18, p. 9418, 2016.

[33] P. Ornale, P. Rosanò, E. Alberti, and A. Princivalle, *Le pietre tenere del vicentino: uso e restauro*. Vicenza: Associazione artigiani della provincia di Vicenza - Camera di commercio industria artigianato agricoltura - Amministrazione provinciale - Consorzio artigiani restauratori veneti, 1994.

[34] F. Bradley, *Le cave di marmo di Carrara*. Promorama, Guide al paesaggio d'Italia, 2008.

[35] A. P. Ferreira Pinto and J. Delgado Rodrigues, "Stone consolidation: The role of treatment procedures," *J. Cult. Herit.*, vol. 9, no. 1, pp. 38–53, 2008.

[36] E. Sassoni, E. Franzoni, B. Pigino, G. W. Scherer, and S. Naidu, "Consolidation of calcareous and siliceous sandstones by hydroxyapatite: Comparison with a TEOS-based consolidant," *J. Cult. Herit.*, vol. 14, no. 3, pp. e103–e108, 2013.

[37] E. Franzoni, E. Sassoni, G. W. Scherer, and S. Naidu, "Artificial weathering of stone by heating," *J. Cult. Herit.*, vol. 14, no. 3, pp. e85–e93, 2013.

[38] B. Lubelli, R. P. J. Van Hees, T. G. Nijland, and J. Bolhuis, "A new method for making artificially weathered stone specimens for testing of conservation treatments," *J. Cult. Herit.*, vol. 16, no. 5, pp. 698–704, 2015.

[39] E. Franzoni, E. Sassoni, and G. Graziani, "Brushing, poultice or immersion? The role of the application technique on the performance of a novel hydroxyapatite-based consolidating treatment for limestone," *J. Cult. Herit.*, vol. 16, no. 2, pp. 173–184, 2015.

[40] J. R. Gordillo and M. P. S. Pérez, "Comportamiento físico del mármol blanco de Macael (España) por oscilación térmica de bajo y medio rango Performance of Spanish white Macael marble exposed to narrow- and medium-range temperature cycling," *Mater. Constr.*, vol. 60, no. 297, pp. 127–141, 2010.

[41] L. Greenspan, "Humidity fixed points of binary saturated aqueous solutions," *J. Res. Natl. Bur. Stand. Sect. A Phys. Chem.*, vol. 81A, no. 1, p. 89, 1977.

[42] H. B. Stuart, *Analytical techniques in materials conservation*, Wiley edit. 2007.

[43] N. Fusi and J. Martinez-Martinez, "Mercury porosimetry as a tool for improving quality of micro-CT images in low porosity carbonate rocks," *Eng. Geol.*, vol. 166, pp. 272–282,

2013.

[44] C. Volzone and N. Zagorodny, "Applied Clay Science Mercury intrusion porosimetry (MIP) study of archaeological pottery from Hualfin Valley, Catamarca, Argentina," *Appl. Clay Sci.*, vol. 91–92, pp. 12–15, 2014.

[45] E. W. Washburn, "The Dynamics of Capillary Flow," *Phys. Rev.*, vol. 17, pp. 273–283, 1921.

[46] "NORMAL 4/80 Distribuzione del volume dei pori in funzione del loro diametro (italian normative on stone material- Distribution of pores volume vs their diameter). Commissione Beni Culturali UNI NORMAL."

[47] J. Rouquerol, D. Anvir, C. W. Fairbridge, D. H. Everett, J. . Haynes, N. Pernicone, J. D. . Ramsay, K. S. W. a Sing, and K. K. Unger, "Recommendations for the characterization of porous solids," *Pure Appl. Chem*, vol. 66, no. 8, pp. 1739–1758, 1994.

[48] "UNI EN 10859:2000 beni culturali. Materiali lapidei naturali ed artificiali: determinazione dell'assorbimento d'acqua per capillarità." .

[49] "NORMAL 29/88 Misura dell'indice di asciugamento (Italian normative on stone material - Dry index eveluation). Commissione Beni Culturali UNI NORMAL."

[50] "DIN 52 615 Testing of thermal insulating material; Determination of water vapour permeability of construction and insulating materials."

[51] N. Proietti, D. Capitani, and V. Di Tullio, "Applications of Nuclear Magnetic Resonance Sensors to Cultural Heritage," *Sensors*, vol. 14, pp. 6977–6997, 2014.

[52] C. Nunes, L. Pel, J. Kunecky, and Z. Slízková, "The influence of the pore structure on the moisture transport in lime plaster-brick systems as studied by NMR," *Constr. Build. Mater.*, vol. 142, pp. 395–409, 2017.

[53] T. Colinart and P. Glouannec, "Investigation of drying of building materials by single-sided NMR," *Energy Procedia*, vol. 78, pp. 1484–1489, 2015.

[54] R. Viola, A. Tucci, G. Timellini, and P. Fantazzini, "NMR techniques: A non-destructive analysis to follow microstructural changes induced in ceramics," *J. Eur. Ceram. Soc.*, vol. 26, pp. 3343–3349, 2006.

[55] M. Brai, C. Casieri, F. De Luca, P. Fantazzini, M. Gombia, and C. Terenzi, "Validity of NMR pore-size analysis of cultural heritage ancient building materials containing

magnetic impurities," *Solid State Nucl. Magn. Reson.*, vol. 32, pp. 129–135, 2007.

[56] M. Brai, M. Camaiti, C. Casieri, F. De Luca, and P. Fantazzini, "Nuclear magnetic resonance for cultural heritage," *Magn. Reson. Imaging*, vol. 25, pp. 461–465, 2007.

[57] B. Blümich, J. Perlo, and F. Casanova, "Mobile single-sided NMR," *Prog. Nucl. Magn. Reson. Spectrosc.*, vol. 52, no. 4, pp. 197–269, 2008.

[58] "NORMAL 43/93 Misure colorimetriche di superfici opache (Italian normative on stone material- colorimetric measurement of opaque surfaces). Commissione Beni Culturali UNI NORMAL."

[59] M. Favaro, R. Mendichi, F. Ossola, U. Russo, S. Simon, P. Tomasin, and P. A. Vigato, "Evaluation of polymers for conservation treatments of outdoor exposed stone monuments. Part I: Photo-oxidative weathering," *Polym. Degrad. Stab.*, vol. 91, pp. 3083–3096, 2006.

[60] M. J. Varas-muriel, E. M. Pérez-monserrat, C. Vázquez-calvo, and R. Fort, "Effect of conservation treatments on heritage stone. Characterisation of decay processes in a case study," *Constr. Build. Mater.*, vol. 95, pp. 611–622, 2015.

[61] E. Vasanelli, D. Colangiuli, A. Calia, M. Sileo, and M. Antonietta, "Ultrasonic pulse velocity for the evaluation of physical and mechanical properties of a highly porous building limestone," *Ultrasonics*, vol. 60, pp. 33–40, 2015.

[62] M. El Boudani, N. Wilkie-chancellier, L. Martinez, R. Hébert, S. Forst, V.-B. Véronique, and S. Serfaty, "Marble Characterization by ultrasonic methods," *Procedia Earth Planet. Sci.*, vol. 15, pp. 249–256, 2015.

[63] M. Al-Naddaf, F. Wakid, and Y. Abu Alhassan, "Micro-drilling resistance measurement: a new technique to estimate the porosity of a building stone," *Mediterr. Archeol. Archaeom.*, vol. 13, no. 1, pp. 225–233, 2013.

[64] P. Tiano, J. Delgado Rodrigues, E. De Witte, V. Verfès-Belmin, S. Massev, R. Snethlage, D. Costa, L. Cadot-Leroux, E. Garrod, and B. Singer, "The conservation of monuments: A new method to evaluate consolidating treatments," *J. Restor. Build. Monum.*, vol. 6, no. 2, pp. 133–150, 2000.

[65] P. Tiano, "The use of microdrilling techniques for the characterization of stone materials, in site control and non destructive evaluation of masonry structures and

materials.," in *In: L. Binda and R.C. de Vekey (Eds.) (Rilem PRO26, 2003): Proceedings of the RILEM TC177 MDT International Workshop, Mantova*, 2000, pp. 203–2014.

[66] J. Delgado Rodrigues, A. P. Ferreira Pinto, and D. Rodrigues da Costa, "Tracing of decay profiles and evaluation of stone treatments by means of microdrilling techniques," *J. Cult. Herit.*, vol. 3, no. 2, pp. 117–125, 2002.

CHAPTER 3

Results and Discussion

Summary

This chapter presents the results regarding the characterization of the three products obtained by diluting calcium ethoxide nanosuspension[1] *in three organic solvents (ethanol, 2-buthanol and n-butylacetate) and the study concerning their performance as consolidating agents for carbonate stones with different porosity. The first part, focused on the characterization of products, includes studies concerning the kinetic of the carbonation process, reaction pathway and individuation of mineralogical phases formed at different RH% conditions. The second part regards the characterization of carbonate supports, the application of new obtained products on laboratory mock-ups - compared with a reference product - and an efficacy evaluation of consolidating treatments, through the comparison between treated and untreated samples.*

3.1 Kinetic of carbonation process and reaction pathway

In this section the results about kinetic and reaction pathway of the carbonation process occurring between the products and the atmosphere are reported. The investigated products were those obtained by diluting calcium ethoxide nanosuspension in ethanol, 2-butanol and n-butylacetate to reach a calcium concentration of 20 g/L. All products were analysed both alone and mixed with the powdered stones, to understand if the presence of the substrate could affect the carbonation process. Both kinetic process and reaction pathway were monitored by collecting μFT-IR spectra at different times, from the beginning of the analysis - the laying of a drop of the product on a glass slide - till complete conversion of compounds to calcium carbonate.

Regarding the kinetic results, for each product, three graphs are reported:

[1] The term calcium ethoxide - $Ca(OEt)_2$ - is referred to the nanosuspension in a 1:3 solution (v/v %) of EtOH and THF, with an initial calcium concentration of 46.5 g/L.

- the first graph shows five different spectra (from the bottom to the top: the beginning of the analysis; first appearance of peaks related to calcium carbonate; the spectrum recorded after ten minutes; after six hours and finally after two weeks);
- the second graph focuses on the situation when calcium carbonate peaks start to emerge;
- the third graph is referred to the carbonation reaction almost completed.

The analysed products will be labelled in the text with the following acronyms:

- *ET*: $Ca(OEt)_2$ nanosuspension diluted in ethanol;
- *2BUT*: $Ca(OEt)_2$ nanosuspension diluted in 2-butanol;
- *NBUT*: $Ca(OEt)_2$ nanosuspension diluted in n-butylacetate;

3.1.1 Calcium ethoxide in ethanol

The **Fig. 3.1 (a)** reports the spectra collected at different times and, therefore, the evolution of calcium carbonate formation from the beginning of the reaction till two weeks later. After alcohol evaporation in the first instants, a broad vibrational band related to the presence of carbonate ion CO_3^{2-} in the region between 1400-1480 cm^{-1} (asymmetric stretching mode υ_3 of CO_3^{2-}) starts to be present after two minutes from the beginning of the reaction (**Fig 3.1 (b)**) [1]–[3].

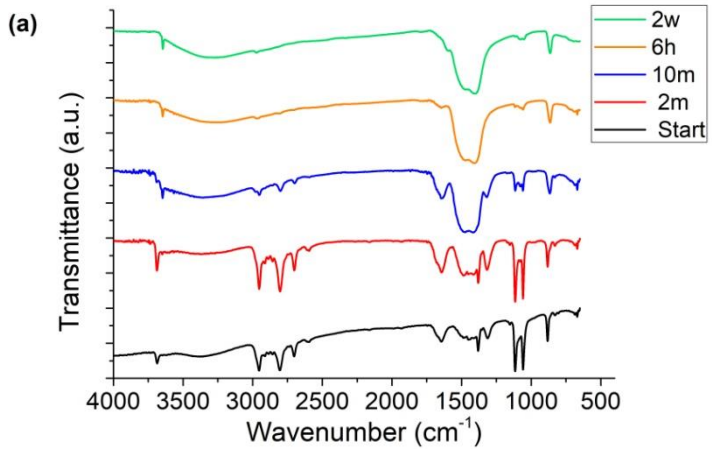

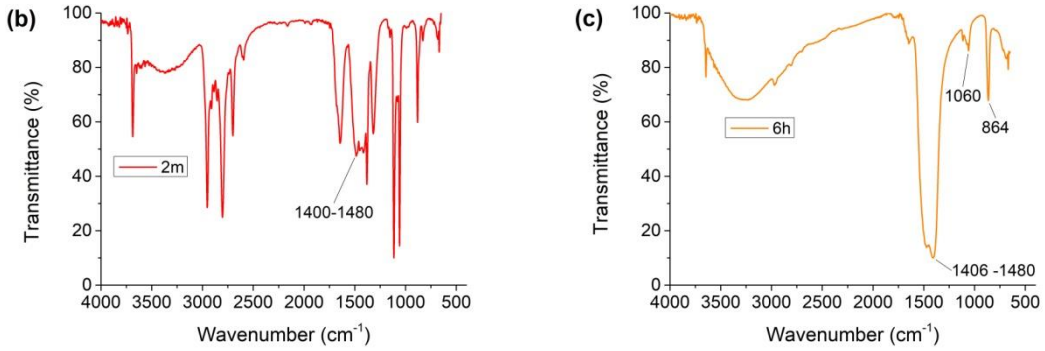

Figure 3.1 *- μFT-IR spectra showing kinetic process of ET:* ***(a)*** *entire process,* ***(b)*** *spectrum acquired after 2 minutes and* ***(c)*** *spectrum acquired after 6 hours. Time intervals: start, beginning of the reaction; 2m, two minutes; 10m, ten minutes; 6h, six hours; 2w, two weeks.*

After six hours (**Fig 3.1 (c)**), only peaks related to amorphous calcium carbonate (ACC) are present: 1406-1480 cm^{-1} (asymmetric stretching mode υ_3 of CO_3^{2-}), 1060 cm^{-1} (symmetric stretching mode υ_1 of CO_3^{2-}) and 864 cm^{-1} (out of plane bending mode υ_2 of CO_3^{2-}) [4]–[6]. Furthermore, the broad band between 2700 and 3600 cm^{-1} related to O-H stretching is present from the beginning till two weeks later and corresponds to structural water within ACC [7], [8]. After two weeks (green spectrum in **Fig. 3.1 (a)**), the results remain constant, showing the presence of ACC, confirmed by absorption peak at 864 cm^{-1}.

Regarding the reaction pathway, absorption peaks at 1650 and 1320 cm^{-1}, corresponding respectively to asymmetrical and symmetrical stretching of $CH_3CH_2OCO_2$, have been observed (**Fig. 3.2**) [9], [10]. These peaks are related to the insertion of CO_2 in the Ca-O bond of calcium ethoxide producing the corresponding calcium ethyl carbonate, which successively transforms into $CaCO_3$ by hydrolysis. In fact, this absorption peak decreases until it disappears in about 6 hours, being replaced by the characteristic signals of $CaCO_3$. However, the presence of an absorption peak at 3645 cm^{-1} related to O-H stretching [8], [11] suggests also a second kinetic pathway due to a hydrolysis process leading first to the formation of $Ca(OH)_2$, which successively undergoes a carbonation process through CO_2 insertion into the Ca–O bond of $Ca(OH)_2$. Small signals at 1470-1483 and 1380 -1410 cm^{-1} evidence the formation of various coordinated bicarbonate groups, as reported in [10], [12], which overlap $CaCO_3$ absorption bands.

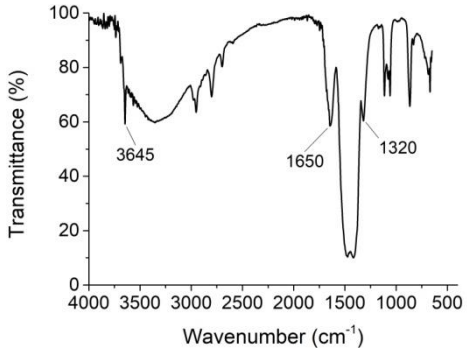

***Figure 3.2** - μFT-IR spectrum showing reaction pathway of ET.*

After two weeks, peak related to O-H stretching (3645 cm^{-1}) is still present - as shown by the green spectrum in **Fig 3.1 (a)** - evidence that the carbonation process is not concluded. The presence of powdered carbonate stones mixed with the analysed product does not affect the kinetic and the reaction pathway of *ET,* as observed in the spectra reported in **Fig A.1** in **Appendix A**.

3.1.2 Calcium ethoxide in 2-buthanol

The kinetic of carbonation process for this product is reported in **Fig. 3.3 (a)**. As for $Ca(OEt)_2$ nanosuspension diluted in ethanol, the formation of calcium carbonate starts after two minutes as shown by the presence of absorption peaks in the region between 1415-1460 cm^{-1} (**Fig. 3.3 (b)**). After six hours, only peaks related to calcium carbonate are evident: 1410-1480, 1074, 864 cm^{-1} (**Fig. 3.3 (c)**). After two weeks, only amorphous calcium carbonate is present with characteristic absorption peak at 864 cm^{-1} (green spectrum in **Fig. 3.3 (a)**).

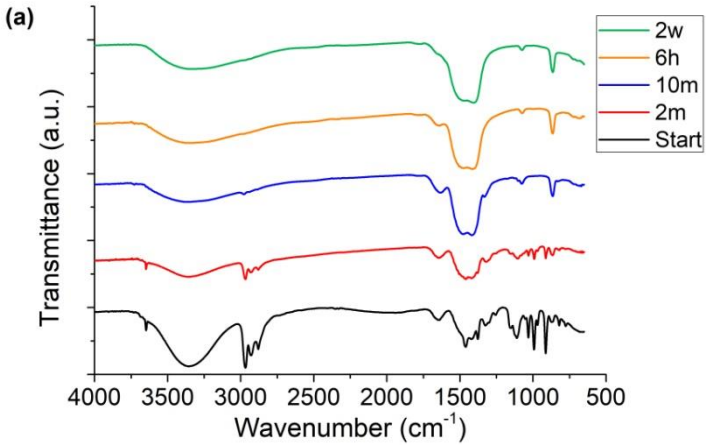

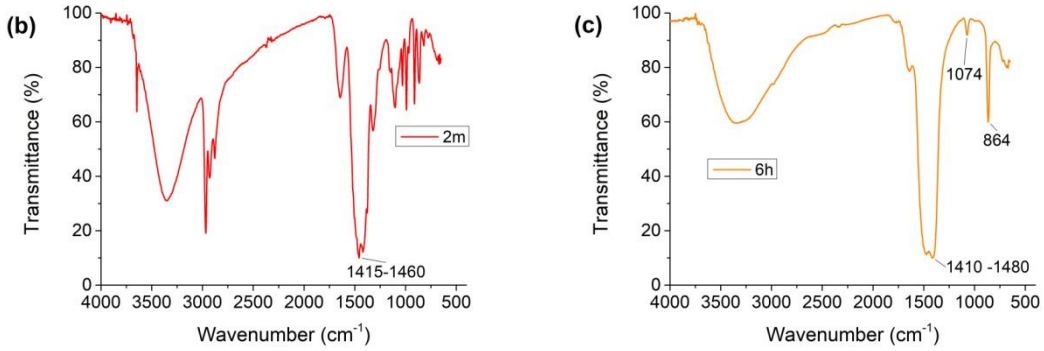

Figure 3.3 *- μFT-IR spectra showing kinetic process of 2BUT:* ***(a)*** *entire process,* ***(b)*** *spectrum acquired after 2 minutes and* ***(c)*** *spectrum acquired after 6 hours. Time intervals: start, beginning of the reaction; 2m, two minutes; 10m, ten minutes; 6h, six hours; 2w, two weeks.*

As for calcium ethoxide diluted in ethanol, the followed reaction pathway involves the insertion of CO_2 inside Ca-O bond as testified by the bands at 1640 and 1328 cm^{-1} which disappear in few minutes, attributed to asymmetrical and symmetrical stretching of $CH_3CH_2OCO_2$ groups, respectively (**Fig. 3.4**) [9], [10].

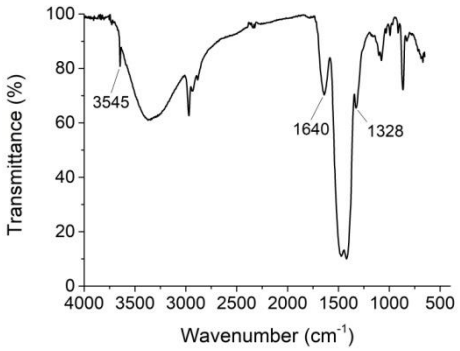

Figure 3.4 *- μFT-IR spectrum showing reaction pathway of 2BUT.*

Also in this case, a second reaction pathway occurs as shown by the peak at 3645 cm^{-1} associated to O-H stretching. This peak, looking at the orange spectrum in **Fig 3.3 (c)**, disappears after six hours, indicating a faster carbonation process compared to *ET*.

The kinetic and the reaction pathway of *2BUT* are not influenced by the presence of powdered carbonate stones, as observed in the spectra reported in **Fig. A.2** in **Appendix A**.

The difference between *ET* and *2BUT* are only related to the duration of the carbonation process; in fact, after two weeks, this process is still ongoing for *ET,* while it is completed for *2BUT*.

3.1.3 Calcium ethoxide in n-butylacetate

Fig. 3.5 (a) reports the kinetic process of calcium ethoxide nanosuspension diluted in n-butylacetate. Differently from the alcohols seen in the previous paragraphs, the presence of this solvent delays the beginning of the carbonation process. In fact, a first broad band in the region between 1410-1470 cm^{-1} starts to be present at six minutes from the beginning of the reaction (**Fig. 3.5 (b)**). After six hours (**Fig. 3.5 (c)**), peaks related to CO_3^{2-} are clearly present: 1420-1470, 1077, 864 cm^{-1}. Also in this case, the final calcium carbonate is amorphous with characteristic absorption peak at 864 cm^{-1} and the broad band between 2700 and 3600 cm^{-1} related to O-H stretching, corresponds to structural water within ACC. This delay in the beginning of the carbonation process may be explained with the low volatility of solvent. In fact, as reported in **Table 2.1** (chapter 2, paragraph 2.2.1.2), n-butylacetate has the higher boiling point respect to other used solvents.

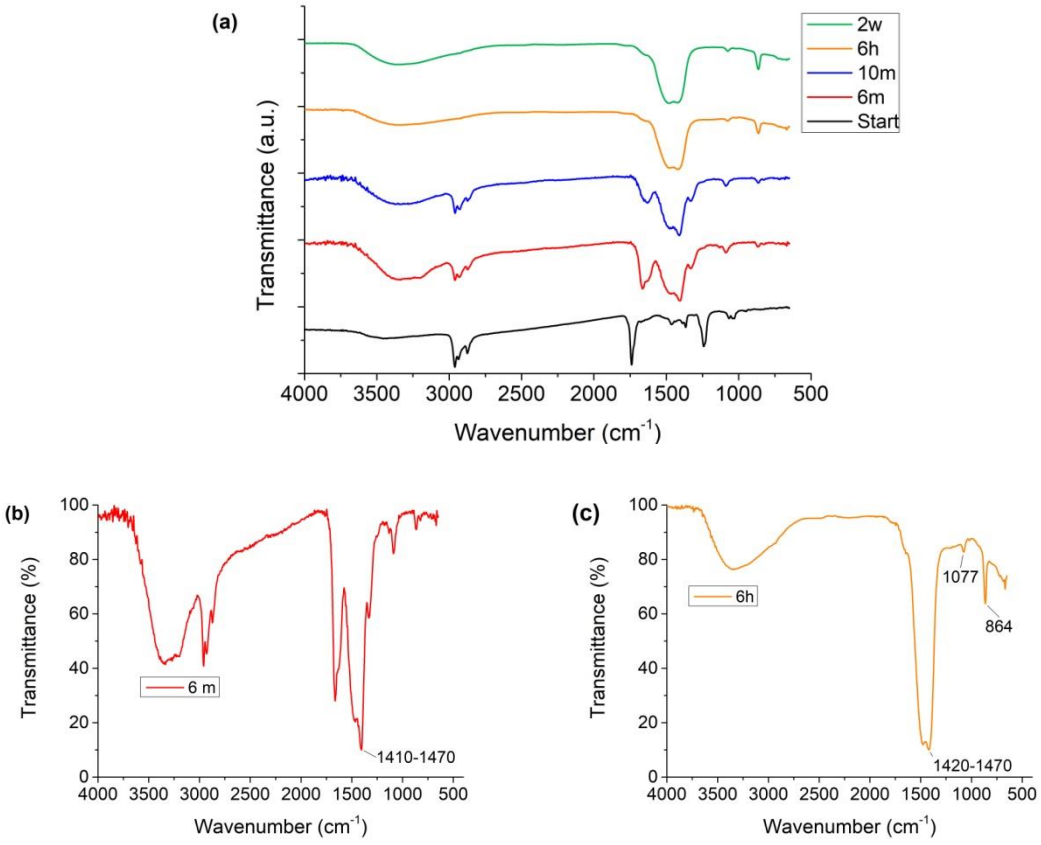

Figure 3.5 *- μFT-IR spectra showing kinetic process of NBUT:* ***(a)*** *entire process,* ***(b)*** *spectrum acquired after 6 minutes and* ***(c)*** *spectrum acquired after 6 hours. Time intervals: start, beginning of the reaction; 6m, six minutes; 10m, ten minutes; 6h, six hours; 2w, two weeks.*

Differently from the product diluted in alcohols, in this case only one reaction pathway occurs shown by the presence of vibrational peaks at 1634 and 1328 cm^{-1} and by the lack of peak at 3645 cm^{-1} related to the formation of $Ca(OH)_2$ (**Fig 3.6**).

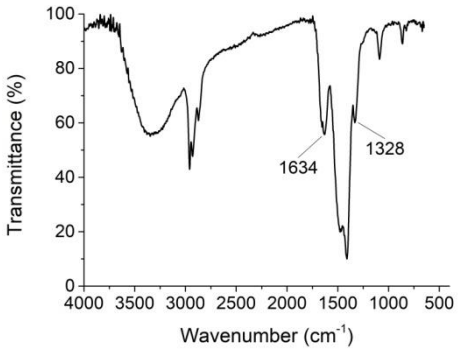

Figure 3.6 *- μFT-IR spectrum showing reaction pathway of NBUT.*

The presence of powdered carbonate stones does not affect the kinetic and the reaction pathway of *NBUT* as observed in the spectra reported in **Fig. A.3**, **Appendix A**.

3.1.4 Final remarks

Results regarding the kinetic pathway show how both alcohols - ethanol and 2-buthanol - lead to the formation of first peaks related to calcium carbonate after two minutes, while n-butylacetate, probably due to its higher boiling point, delays this process allowing the formation of characteristic calcium carbonate peaks after six minutes from the beginning of the reaction. All products lead to the formation of amorphous calcium carbonate - differently from what will be shown in the following paragraphs for coating analysis for which crystalline phases are always formed when laboratory temperature and relative humidity conditions are kept constant during the day and the weeks. Furthermore, a difference between two alcohols is evident regarding the kinetic of the carbonation process which after two weeks ends for *2BUT,* while for *ET* it is not concluded.

The study of reaction pathway highlights how only for the alcohols both carbonation pathways occur: 1) insertion of a CO_2 molecule within the Ca-O bond with a formation of an intermediate ethyl carbonate followed by hydrolysis and alcohol elimination, and 2) a first hydrolysis of the alkoxide with the formation of calcium hydroxide as intermediate, which subsequently carbonates. Instead, for calcium ethoxide diluted in n-butylacetate only the first reaction pathway takes place. This difference with alcohols may be related to the type of

solvent which reduces the quantity of water and therefore the presence of OH groups available.

3.2 Coating analysis

The phase identification of final products of deposits left in two different RH% conditions - 50% and 90% - was carried out by XRD and μFT-IR techniques. These measurements were performed on prepared samples left in constant RH% condition for two weeks, one month and three months.

XRD and μFT-IR analyses were also performed on CaLoSil E50, previously diluted in ethanol to reach a calcium concentration of 20 g/L.

The analysed coatings will be indicated with the following acronyms:

- *ET50* and *ET90* will be $Ca(OEt)_2$ diluted in ethanol preserved at 50% RH and 90% RH, respectively;
- *2BUT50* and *2BUT90* will be $Ca(OEt)_2$ diluted in 2-butanol preserved at 50% RH and 90% RH, respectively;
- *NBUT50* and *NBUT90* will be $Ca(OEt)_2$ diluted in n-butylacetate preserved at 50% RH and 90% RH, respectively;
- *CAL50* and *CAL90* will be CaLoSil E50 preserved at 50% RH and 90% RH, respectively.

3.2.1 Calcium ethoxide in ethanol

Results obtained after two weeks at 50% RH and 90% RH, for both XRD and μFT-IR analyses, are reported in **Fig 3.7** and **Fig 3.8**, respectively. At 50% RH, XRD results show the presence of portlandite with hexagonal structure and characteristic reflections at 2θ = 17.9°/34° (ICCD: 00-001-1079) together with a carbonatic phase also characterized by vaterite with hexagonal structure and main reflection at 2θ = 27° (ICCD: 00-001-1033) [13]–[16] (**Fig. 3.7 (a)**). μFT-IR spectrum confirms the presence of vaterite with characteristic absorption peak at 1088 cm^{-1} [6] and portlandite with absorption peak at 3645 cm^{-1} due to O-H stretching (**Fig 3.7 (b)**).

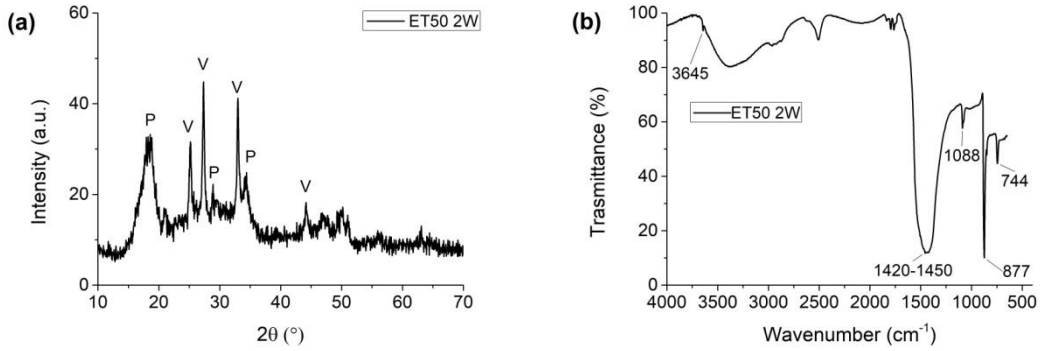

Figure 3.7 *- ET50 after two weeks:* ***(a)*** *XRD pattern and* ***(b)*** *μFT-IR spectrum. XRD peak assignments: P, portlandite; V, vaterite.*

At 90% RH, there is still portlandite with the same structure and a co-presence of carbonatic phases of vaterite and calcite. The latter has a rhombohedral structure and principal reflection at 2θ = 29° (ICCD: 01-072-1651) (**Fig. 3.8 (a)**) [17]. μFT-IR results are consistent with XRD; in fact at 90% RH there are vaterite, calcite (713 cm^{-1}) and portlandite (**Fig 3.8 (b)**). The presence of portlandite after two weeks proves that the carbonation process is not concluded, confirming the results shown in the paragraph 3.1.1 regarding kinetic measurements. But, differently from them, the final calcium carbonate is present in a crystalline phase, a difference probably due to the constant RH% condition which remain constant during all the analysed period.

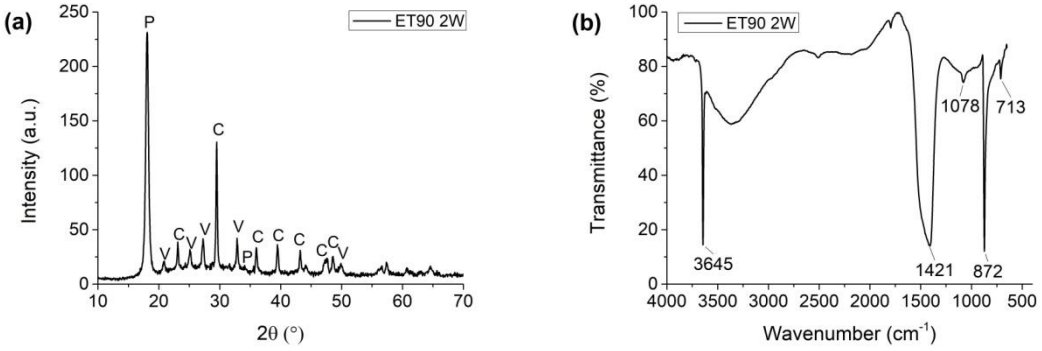

Figure 3.8 *- ET90 after two weeks:* ***(a)*** *XRD pattern and* ***(b)*** *μFT-IR spectrum. XRD peak assignments: P, portlandite; C, calcite; V, vaterite.*

XRD and μFT-IR measurements after one month at 50% RH show only the presence of vaterite, while peaks related to portlandite disappeared indicating that the carbonation process is ended (**Fig 3.9. (a)** - **(b)**).

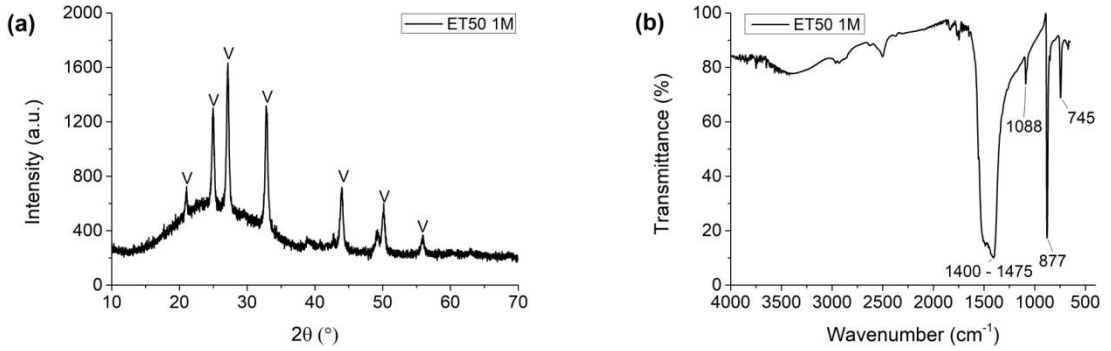

Figure 3.9 *- ET50 after one month:* ***(a)*** *XRD pattern and* ***(b)*** *μFT-IR spectrum. XRD peak assignments: V, vaterite.*

At 90% RH both the presence of vaterite (ICCD 00-033-0268) and calcite (ICCD 00-003-0612) are shown by XRD analysis while peaks related to portlandite are not detected (**Fig 3.10 (a)**); however, μFT-IR confirms only the presence of vaterite and the lack of calcite; this discordance is probably due to the fact that μFT-IR analysis is a punctual technique (**Fig 3.10 (b)**).

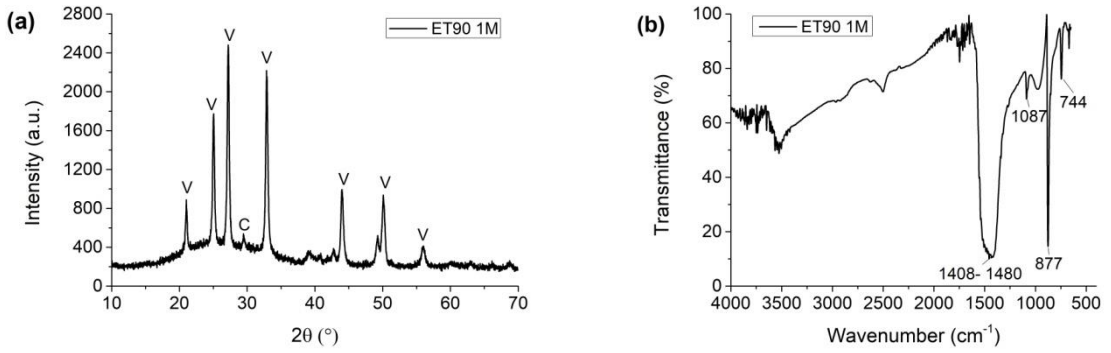

Figure 3.10 *- ET90 after one month:* ***(a)*** *XRD pattern and* ***(b)*** *μFT-IR spectrum. XRD peak assignments: C, calcite; V, vaterite.*

Finally, **Fig. 3.11** and **Fig. 3.12** report the results after three months and both the techniques confirm the presence of calcite only at 90% RH.

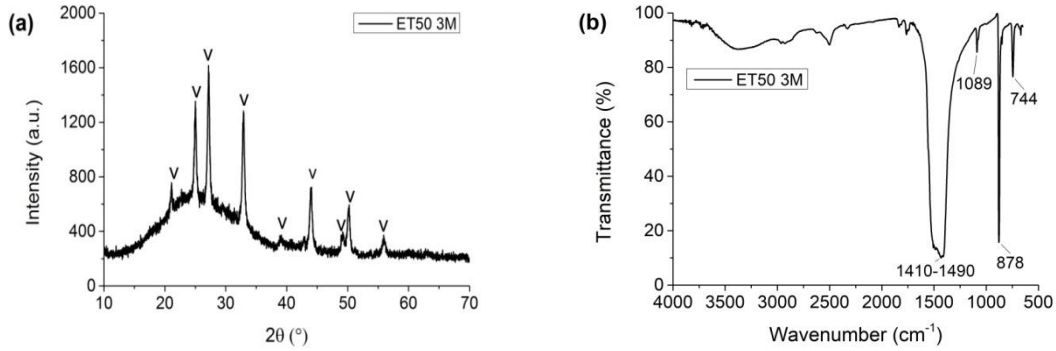

Figure 3.11 *- ET50 after three months:* ***(a)*** *XRD pattern and* ***(b)*** *μFT-IR spectrum. XRD peak assignments: V, vaterite.*

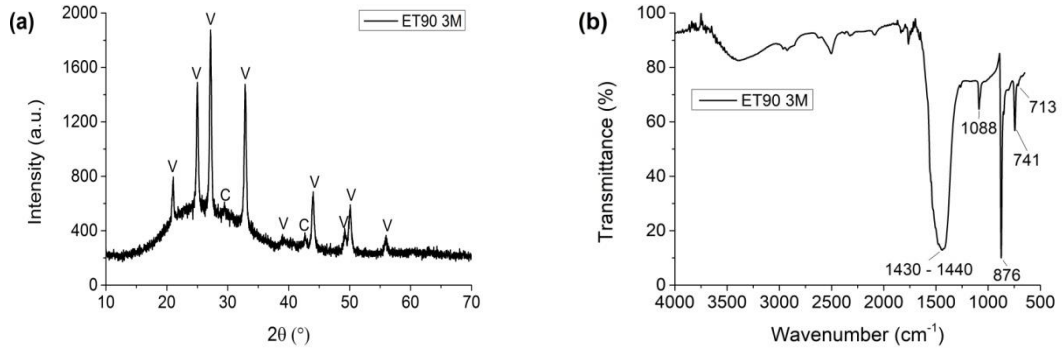

Figure 3.12 *- ET90 after three months:* ***(a)*** *XRD pattern and* ***(b)*** *μFT-IR spectrum. XRD peak assignments: C, calcite; V, vaterite.*

Tab 3.1 shows the results obtained from the coating analysis of $Ca(OEt)_2$ nanosuspension diluted in ethanol at different time intervals and for both relative humidity conditions.

Table 3.1 *- Summary of coating results of ET.*

Sample	XRD/μFT-IR analyses		
	portlandite	vaterite	calcite
ET50 2W	✓	✓	
ET90 2W	✓	✓	✓
ET50 1M		✓	
ET90 1M		✓	✓
ET50 3M		✓	
ET90 3M		✓	✓

Portlandite is present only after two weeks for both relative humidity conditions, result consistent with kinetic measurements discussed in paragraph 3.1.1, showing that the carbonation process is not completed within this time interval. After one month and three months, the absence of portlandite shows that the formation of calcium carbonate polymorph is completed. Vaterite is formed for both relative humidity conditions, while calcite forms only at 90% RH probably because the major presence of water allows the process of dissolution of vaterite and crystallization of calcite [7], [18], [19]. The prevalence of vaterite at 50% RH can be ascribed to the presence of ethanol which, as reported by Manoli et al. [20], influences the morphology of the vaterite precipitation crystals stabilizing this phase and preventing the transformation to the more thermodynamically stable calcite. Therefore, despite vaterite is the most thermodynamically unstable polymorph of calcium carbonate, in terms of crystallization it is kinetically the most favoured of the three polymorphs in all relative humidity conditions [21], [22], [23].

3.2.2 Calcium ethoxide in 2-butanol

XRD and μFT-IR results regarding $Ca(OEt)_2$ diluted in 2-butanol after two weeks obtained at 50% and 90% RH, are illustrated in **Fig. 3.13** and **Fig. 3.14**, respectively. As for $Ca(OEt)_2$ diluted in ethanol, XRD shows the formation of calcite (ICCD 01-072-1651) only for 90% RH value (**Fig. 3.14 (a)**), while vaterite (ICCD 00-001-1033) is present for both relative humidity conditions (**Fig 3.13 (a)** and **Fig 3.14 (a)**).

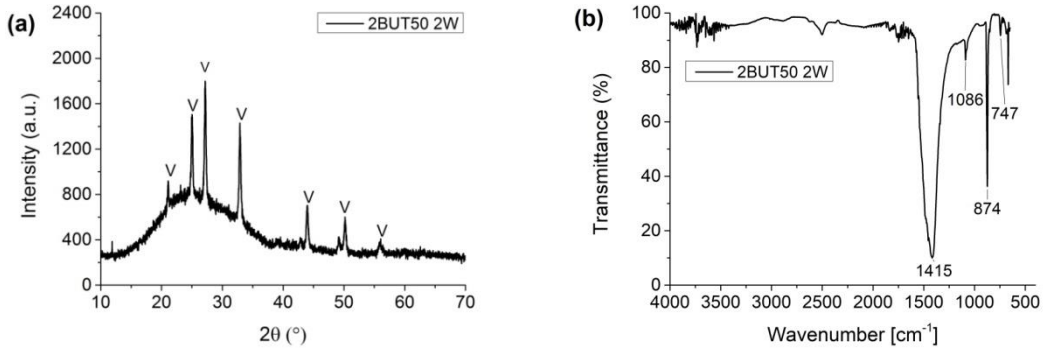

Figure 3.13 *- 2BUT50 after two weeks:* ***(a)*** *XRD pattern and* ***(b)*** *μFT-IR spectrum. XRD peak assignments: V, vaterite.*

μFT-IR measurements confirm this results showing the characteristic vibrational peaks of calcite at 876 and 712 cm^{-1} only at 90% RH (**Fig. 3.14 (b)**). Differently from *ET50* and *ET90*, in this case portlandite is not present, confirming the kinetic results reported in paragraph

3.1.2 and showing that the carbonation process is already concluded after two weeks. Also in this case, the final calcium carbonate phase is not amorphous.

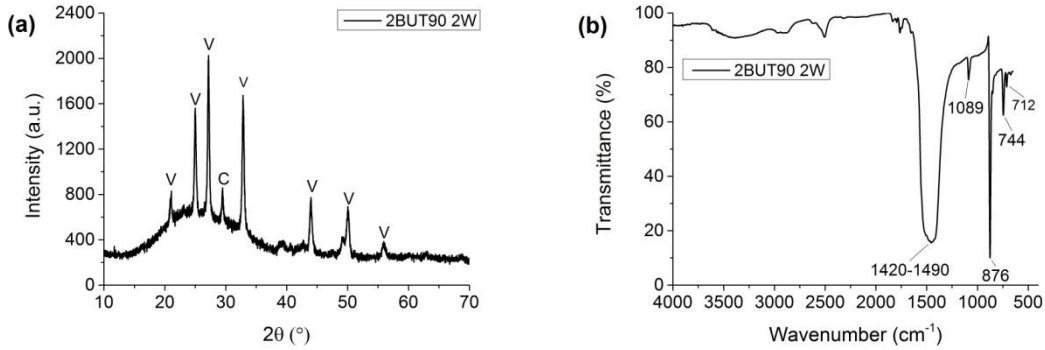

Figure 3.14 *- 2BUT90 after two weeks:* ***(a)*** *XRD pattern and* ***(b)*** *μFT-IR spectrum. XRD peak assignments: C, calcite; V, vaterite.*

XRD results after one month confirm the presence of vaterite (ICCD 00-004-0844) at 50% RH (**Fig. B.1 (a)** in **Appendix B**) and of both vaterite (ICCD 00-001-1033) and calcite with the typical reflection at 2θ = 29° (ICCD 01-072-1650) at a 90% RH (**Fig. B.2 (a)** in **Appendix B**). The characteristic vibrational peaks acquired by μFT-IR at both relative humidity conditions are consistent with XRD results (**Fig B.1 (b)** and **Fig. B.2 (b)** in **Appendix B**).

Finally, the results after three months (**Fig. B.3** and **Fig B.4** in **Appendix B**) totally match with those ones obtained after one month.

The **Tab 3.2** summarizes the results obtained from the coating analysis of $Ca(OEt)_2$ nanosuspension diluted in 2-butanol for the different time intervals and for all relative humidity conditions. Differently from *ET,* coating characterization shows that after two weeks the carbonation process ends, confirming the kinetic results; in fact, peaks related to portlandite are not detected by XRD and μFT-IR for both RH% conditions at this stage. While, after one month and three months both *ET* and *2BUT* show the same results, vaterite at 50% RH and vaterite and calcite at 90% RH. Also in this case, the presence of vaterite at 50% can be ascribed to the presence of alcohols, as explained before for $Ca(OEt)_2$ diluted in ethanol.

Table 3.2 *- Summary of coating results of 2BUT.*

Sample	XRD /μFT-IR analyses	
	vaterite	calcite
2BUT50 2W	✓	
2BUT90 2W	✓	✓
2BUT50 1M	✓	
2BUT90 1M	✓	✓
2BUT50 3M	✓	
2BUT90 3M	✓	✓

3.2.3 Calcium ethoxide in n-butylacetate

The use of n-butylacetate produced different results with respect to the alcohols. After two weeks at 50% RH, XRD shows the presence of an amorphous phase (**Fig 3.15 (a)**) in accordance with μFT-IR analysis where peaks related to amorphous calcium carbonate (1400-1490, 1070, 864cm^{-1}) are evident (**Fig 3.15 (b)**). Differently from *ET* and *2BUT,* for which a constant condition of RH% leads to the formation of a crystalline polymorph, the amorphous phase connected to the presence of n-butylacetate could be related to the higher boiling point of this solvent which delays the formation of crystalline calcium carbonate.

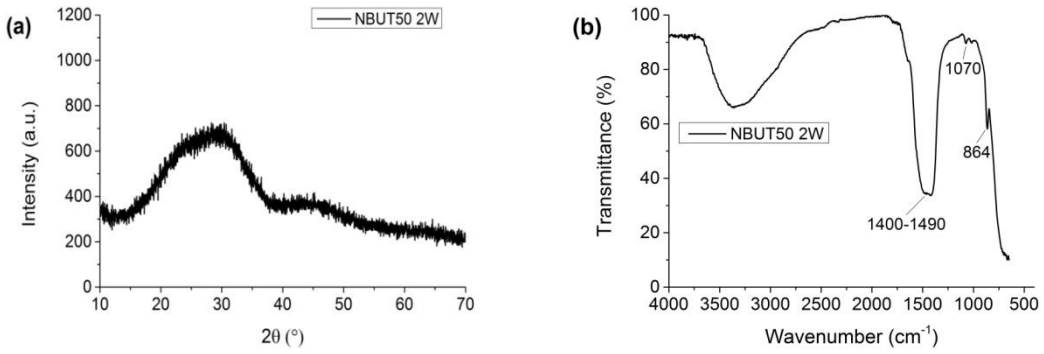

Figure 3.15 *- NBUT50 after two weeks:* ***(a)*** *XRD pattern and* ***(b)*** *μFT-IR spectrum.*

The diffractogram obtained at 90% RH (**Fig. 3.16 (a)**) shows a crystalline phase related to both vaterite (ICCD 00-001-1033) and calcite (ICCD 00-024-0027). These results are confirmed by μFT-IR analysis (**Fig. 3.16 (b)**).

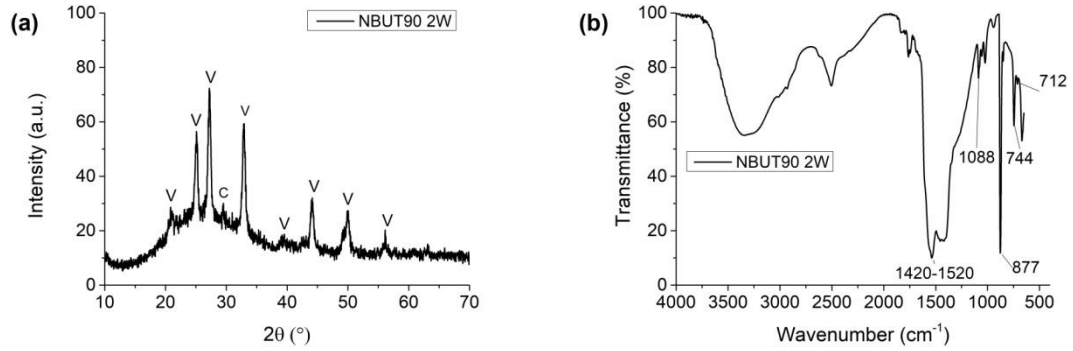

Figure 3.16 *- NBUT90 after two weeks:* ***(a)*** *XRD pattern and* ***(b)*** *μFT-IR spectrum. XRD peak assignments: C, calcite; V, vaterite.*

The results after one month show again an amorphous phase at 50% RH, as both XRD and μFT-IR analyses indicate (**Fig. 3.17**).

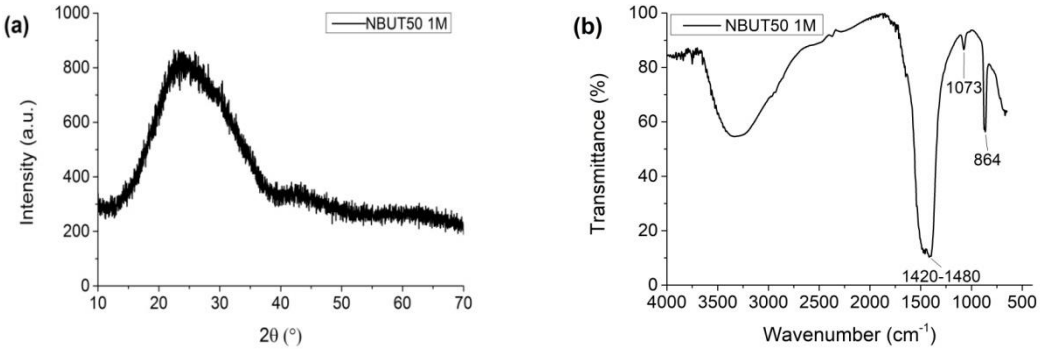

Figure 3.17 *- NBUT50 after one month:* ***(a)*** *XRD pattern and* ***(b)*** *μFT-IR spectrum.*

Differently from 50% RH, at 90% RH vaterite is present (ICCD 00-033-0268) (**Fig. 3.18 (a)**).

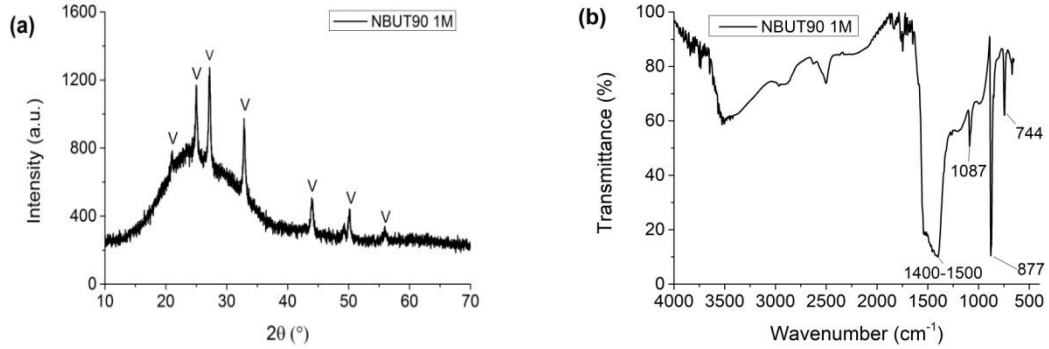

Figure 3.18 *- NBUT90 after one month:* ***(a)*** *XRD pattern and* ***(b)*** *μFT-IR spectrum. XRD peak assignments: V, vaterite.*

After three months a crystalline phase of vaterite (00-001-1033) is shown for an RH value of

50% (**Fig 3.19 (a)**) and confirmed by μFT-IR analysis, with the characteristic vibrational peak at 873 cm^{-1} (**Fig. 3.19 (b)**). The set of results points out that the formation of crystalline phases of calcium carbonate is possible when constant value of RH% are considered, but the crystallization process is slower when compared with the use of ethanol and 2-buthanol.
This effect might be related to the higher boiling point of n-butylacetate which delays the carbonation process.

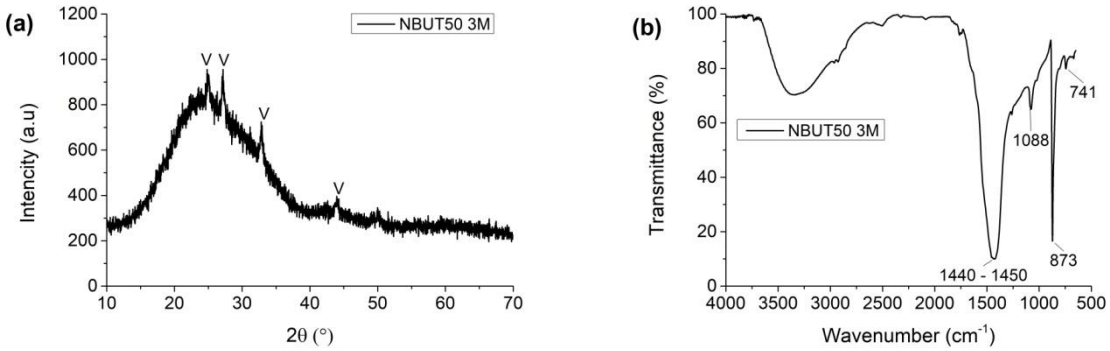

Figure 3.19 *- NBUT50 after 3 months:* ***(a)*** *XRD pattern and* ***(b)*** *μFT-IR spectrum. XRD peak assignments: V, vaterite.*

Results at 90% RH (**Fig 3.20 (a)** - **(b)**) after three months remain constant respect to those obtained after one month. In fact, only the presence of vaterite is confirmed by both XRD and μFT-IR analyses.

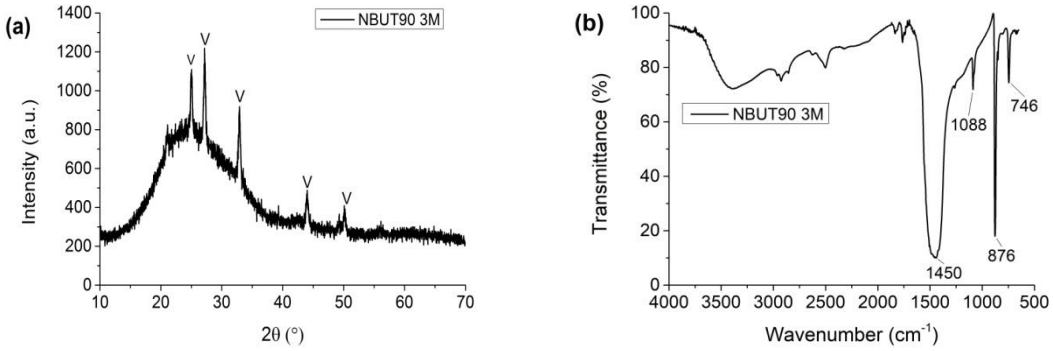

Figure 3.20 *- NBUT90 after 3 months:* ***(a)*** *XRD pattern and* ***(b)*** *μFT-IR spectrum. XRD peak assignments: V, vaterite.*

The **Tab 3.3** summarizes the results obtained from the coating analysis of $Ca(OEt)_2$ nanosuspension diluted in n-butylacetate at different time intervals and for all relative humidity conditions. As mentioned before, the presence of amorphous calcium carbonate at 50% RH after two weeks and one month, could be related to the higher boiling point of the

solvent which delay the formation of a crystalline phases despite a constant value of RH%. On the contrary, a higher value of RH% promotes the formation of a crystalline phase.

Table 3.3 *- Summary of coating results of NBUT. ACC - amorphous calcium carbonate.*

Sample	XRD /μFT-IR analyses		
	ACC	vaterite	calcite
NBUT50 2W	✓		
NBUT90 2W		✓	✓
NBUT50 1M	✓		
NBUT90 1M		✓	
NBUT50 3M		✓	
NBUT90 3M		✓	

3.2.4 CaLoSil E50

The carbonation process of CaLoSil E50 at different relative humidity conditions was also studied to compare its behaviour respect to the other three products based on calcium ethoxide. XRD results show that an RH value of 50% leads to the formation of the crystalline phase of aragonite (ICCD 00-001-0628) with typical reflections at 2θ = 26°/45.7° (**Fig. 3.21 (a)**) [17]. This result is different respect to those obtained from products based on calcium ethoxide in which aragonite has never been formed. The presence of aragonite is confirmed by μFT-IR where characteristic vibrational peak of aragonite at 855 cm^{-1} is shown (**Fig. 3.21 (b)**) [6], [24]. The presence of aragonite could be due to some internal modification of vaterite crystal [25].

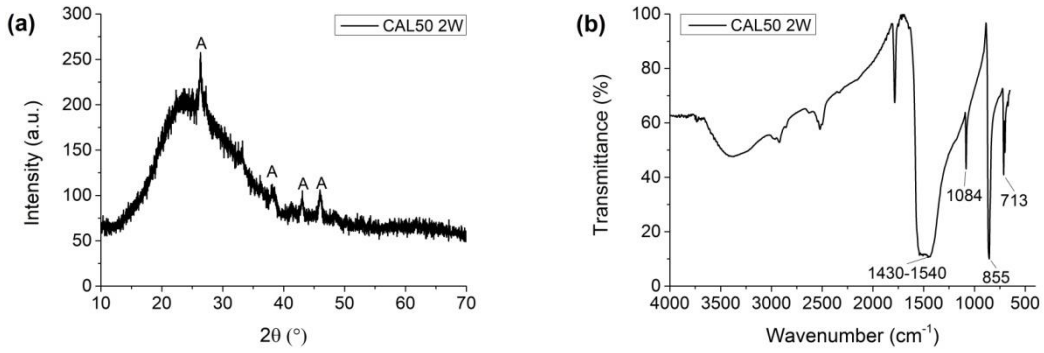

Figure 3.21 *- CAL50 after two weeks:* ***(a)*** *XRD pattern and* ***(b)*** *μFT-IR spectrum. XRD peak assignments: A, aragonite.*

On the contrary, a higher quantity of water at 90% RH leads to the formation of both vaterite (ICCD 00-001-1033) and calcite (ICCD: 01-072-1651) as shown by XRD pattern in **Fig 3.22 (a)**. These results are consistent with characteristic absorption peaks at 1085 and 745 cm^{-1} for vaterite and 713 $cm^{-1}$for calcite, shown by μFT-IR spectrum (**Fig. 3.22 (b)**).

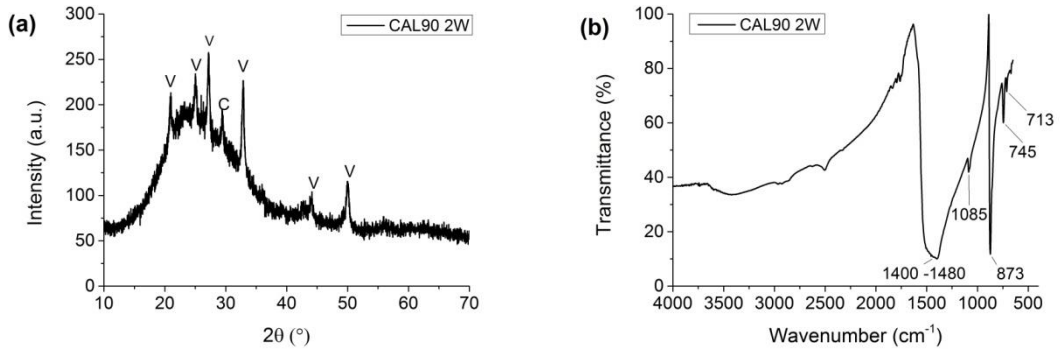

Figure 3.22 *- CAL90 after two weeks:* ***(a)*** *XRD pattern and* ***(b)*** *μFT-IR spectrum. XRD peak assignments: C, calcite; V, vaterite.*

After one month and three months the XRD and μFT-IR results remain constant, confirming the presence of aragonite at 50% RH and vaterite and calcite at 90% RH. The graphs are reported in **Appendix B** (**Fig. B.5**, **B.6**, **B.7**, **B.8**).

The **Tab 3.4** summarizes the results obtained from the coating analysis of CaLoSil for all time intervals and relative humidity conditions. Differently from another study [23], no portlandite has been detected at 50% RH; this result can be ascribed to a quick carbonation process.

Table 3.4 *- Summary of coating results of CAL.*

Sample	**XRD/μFT-IR analyses**		
	aragonite	vaterite	calcite
CAL50 2W	✓		
CAL90 2W		✓	✓
CAL50 1M	✓		
CAL90 1M		✓	✓
CAL50 3M	✓		
CAL90 3M		✓	✓

3.3 Characterization and analysis of treated samples

In the following paragraphs the results regarding the performance of the consolidating products on different carbonate stones are shown, divided on the basis of the three different application procedures:

- brush till saturation;
- brush with a pre-set number of brush strokes;
- absorption through capillarity.

For each type of stone support, the results involve:

- characterization of chemical composition of support, obtained by Thermogravimetric analysis/Differential Scanning Calorimetry (TG-DSC) and Fourier Transform Infrared Spectroscopy (FT-IR);
- results of the effect due to the ageing process performed for each type of stone support before the application of the consolidating products, evaluated with mercury intrusion porosimetry (MIP);
- results about the performance - effectiveness and compatibility - of the four consolidating products applied with different application procedures and evaluated with several techniques and material tests as listed in chapter 2, paragraph 2.4. For each type of analysis, data obtained from treated samples are analysed by comparing them with the respective untreated as references.

As for the study of carbonation process and coating analysis, the analysed products will be labelled with the following acronyms:

- *ET*: $Ca(OEt)_2$ nanosuspension diluted in ethanol;
- *2BUT*: $Ca(OEt)_2$ nanosuspension diluted in 2-butanol;
- *NBUT*: $Ca(OEt)_2$ nanosuspension diluted in n-butylacetate;
- *CAL*: CaLoSil E50 diluted in ethanol.

For each type of application procedure, samples will be labelled as follow:

- untreated samples, which refers to samples already subjected to the ageing process: Lecce stone (*L_NT*), Noto stone (*N_NT*), Vicenza stone (*V_NT*) and Carrara marble (*M_NT*);

- samples treated with $Ca(OEt)_2$ nanosuspension diluted in ethanol: *support initial letter_ET* (*L_ET*, *N_ET*, *V_ET*, *M_ET*);
- samples treated with $Ca(OEt)_2$ nanosuspension diluted in n-butylacetate: *support initial letter _NBUT* (*L_NBUT*, *N_ NBUT*, *V_ NBUT*, *M_ NBUT*);
- samples treated with $Ca(OEt)_2$ nanosuspension diluted 2-butanol: *support initial letter _2BUT* (*L_2BUT*, *N_ 2BUT*, *V_ 2BUT*, *M_ 2BUT*);
- samples treated with CaLoSil E50 diluted in ethanol: *support initial letter _CAL* (*L_CAL*, *N_ CAL*, *V_ CAL*, *M_ CAL*).

3.3.1 Lecce stone

Lecce stone was chemically characterized by TG-DSC and FT-IR analyses. The first one shows that this stone is mainly composed by 91.9%, of calcium carbonate, determined on the basis of the mass loss of 39.9% between 600-800 °C (**Fig. 3.23 (a)**) [3], [26]–[28]. FT-IR analysis confirms this result showing the characteristic vibrational bands of calcite at 1450 cm^{-1} (asymmetric stretching mode υ_3), 876 cm^{-1} (out of plane bending mode υ_2) and, finally at 713 cm^{-1} (υ_4 in plane bending mode) [6], [29]–[32]. The further peak at 1034 cm^{-1} is connected to the presence of silicate minerals. In fact bands in the region 1150-1000 cm^{-1} are associated to asymmetric stretching vibration of silicon-oxygen group (Si-O) [33]–[36].

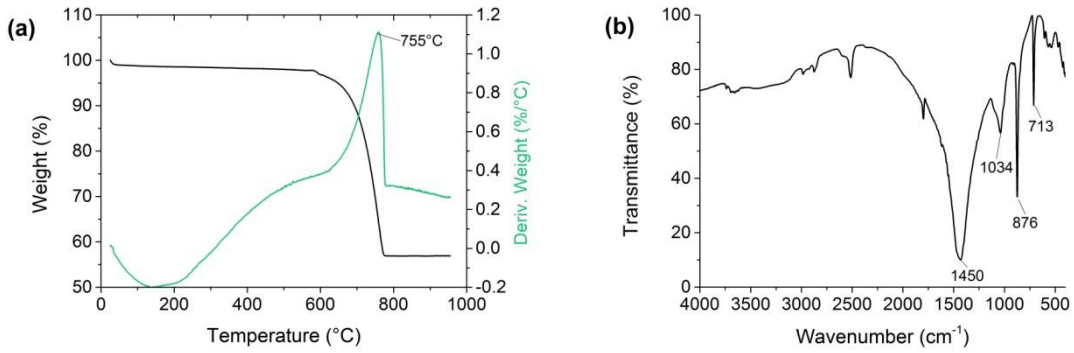

Figure 3.23 - *Chemical characterization of Lecce stone by* ***(a)*** *TG-DSC and* ***(b)*** *FT-IR analyses.*

The stone was subjected to an artificial ageing and mercury intrusion porosimetry measurements, performed before and after the ageing process (**Fig. 3.24 (a)** and **(b)**), highlight the increase of total open porosity value, from an initial value of 34.4 ± 0.5% to a final value of 37.6 ± 0.9%. This change of open porosity led to an increase of total cumulative volume from 201.8 ± 2.1 mm^3/g to 223.8 ± 1.3 mm^3/g and an increase of medium pore radius in the range 1-4 μm.

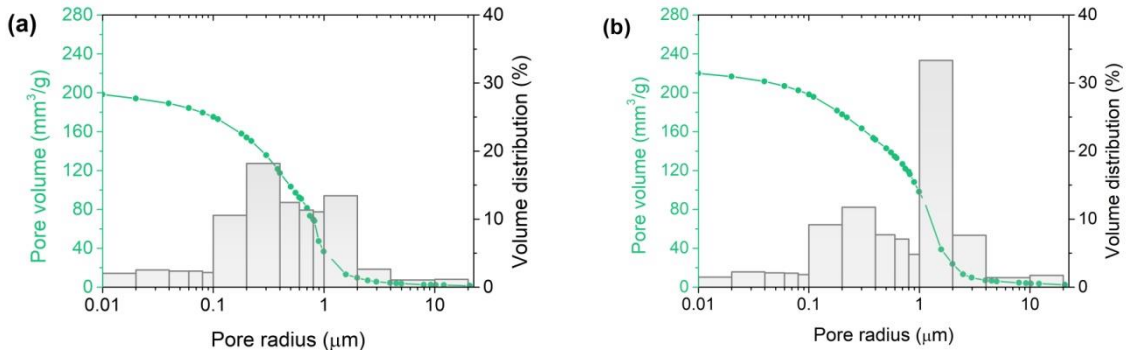

Figure 3.24 *- Cumulative pore volume and volume distribution versus pore radius of* ***(a)*** *not aged and* ***(b)*** *aged Lecce stone.*

In the following paragraphs, results concerning the efficacy of four different products as consolidating agents, applied on Lecce stone with three different application procedures, are reported.

3.3.1.1 Application procedure: by brush till saturation

In this section, results related to the application by brush till saturation of three products based on $Ca(OEt)_2$ nanosuspension and the reference one (CaLoSil E50) are discussed.

Tab. 3.5 presents data regarding the amount of consolidant retained after one month from the application. The results are reported as a range of value between the minimum and the maximum quantity for each type of product. Differences among quantity of product retained for samples treated with the same product are probably due to the different shape of mock-ups (in accordance to the different analyses, mock-ups of different dimensions were necessary). More details of product retained in relation to the different analyses are shown in **Tab. C.1** in **Appendix C**.

Table 3.5 *- Application by brush till saturation: range of amount of product retained after one month from the application.*

Product	Quantity of product retained (kg/m²)
ET	0.016 – 0.115
NBUT	0.012 – 0.108
2BUT	0.017 – 0.165
CAL	0.012 – 0.097

The change in water transport properties was studied through capillarity water absorption test, drying rate and water vapour permeability test. Each type of test was carried out according to

specific Italian and European standard as described in chapter 2; data are reported as the average of three samples.

Fig. 3.25 graphically reports the capillary water absorption for each type of product applied. Looking at the first 45 minutes of the analysis (≈50 $s^{1/2}$), the amount of water uptake, expressed as the amount of water absorbed Q (mg/cm^2) as a function of the square root of time ($s^{1/2}$), is lower for all treated samples, compared to untreated ones. The higher decrease of capillary water absorption is registered with *L_2BUT* (**Fig 3.25 (c)**). This result agrees with data reported in **Tab C.1**, which shows a higher amount of product when *2BUT* is applied.

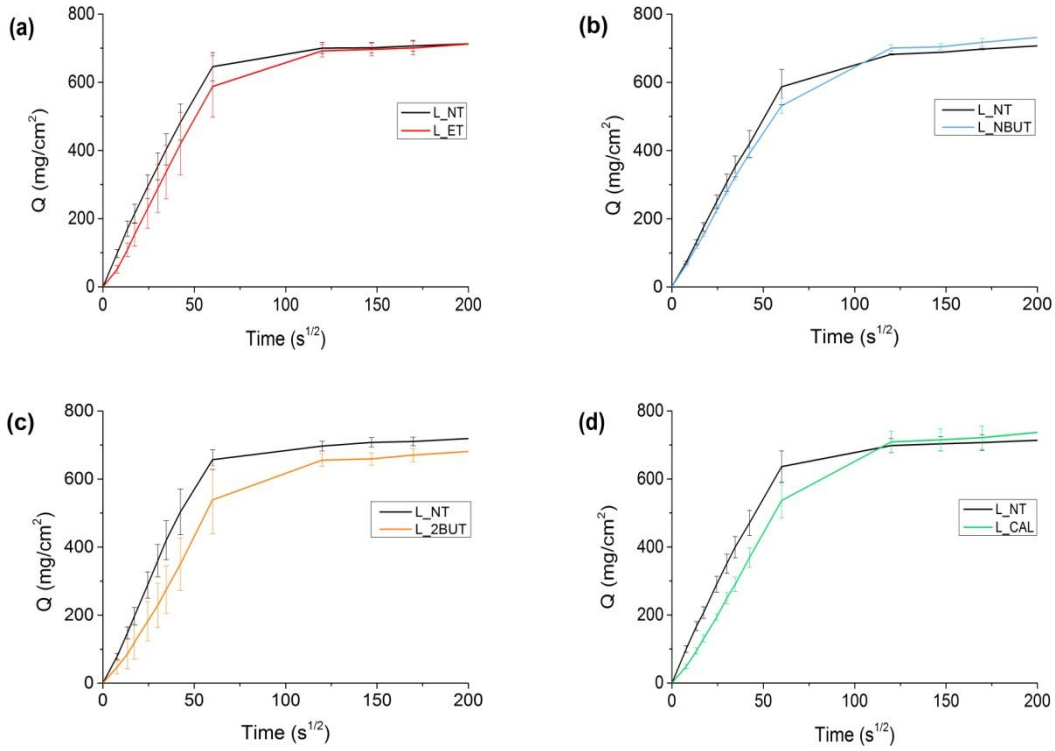

Figure 3.25 *- Quantity of water absorbed by capillarity, comparison before and after treatment:* ***(a)*** *L_ET,* ***(b)*** *L_NBUT,* ***(c)*** *L_2BUT and* ***(d)*** *L_CAL.*

The histogram in **Fig. 3.26** compares the difference of average capillary water absorption coefficient (CWAC) between treated and untreated samples. All treatments cause a reduction of absorption coefficient, but the main difference between treated and untreated samples is observed for *L_2BUT*, with a reduction (from 12.2 ± 1.7 $mg/cm^2 \cdot s^{1/2}$ to 9.2 ± 1.6 $mg/cm^2 \cdot s^{1/2}$) which remains in an acceptable limit to not alter the natural properties of the stone (< than 25% respect to the value of untreated samples [37]).

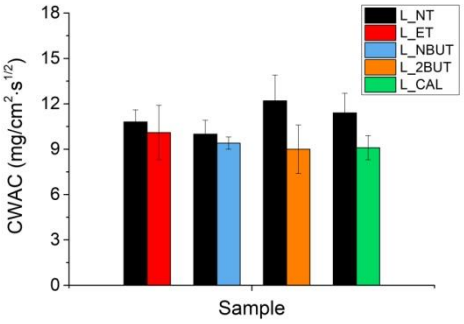

Figure 3.26 *- Comparison of capillary water absorption coefficient (CWAC) before and after treatment.*

Considering the drying rate, calculated as the time necessary to obtain the full drying of the samples, it does not give the absolute rate at which one sample dries with respect to another. Therefore, to obtain the rate at which the samples dry, the evolution of the drying curve must be studied. In this case, the behaviour of treated and untreated samples is quite similar; but, all treated samples take more hours to reach a drying state in comparison to untreated ones, especially samples *L_2BUT* and *L_NBUT* (**Fig. 3.27**). However, all treatments affect the natural behaviour of the stone in an acceptable way.

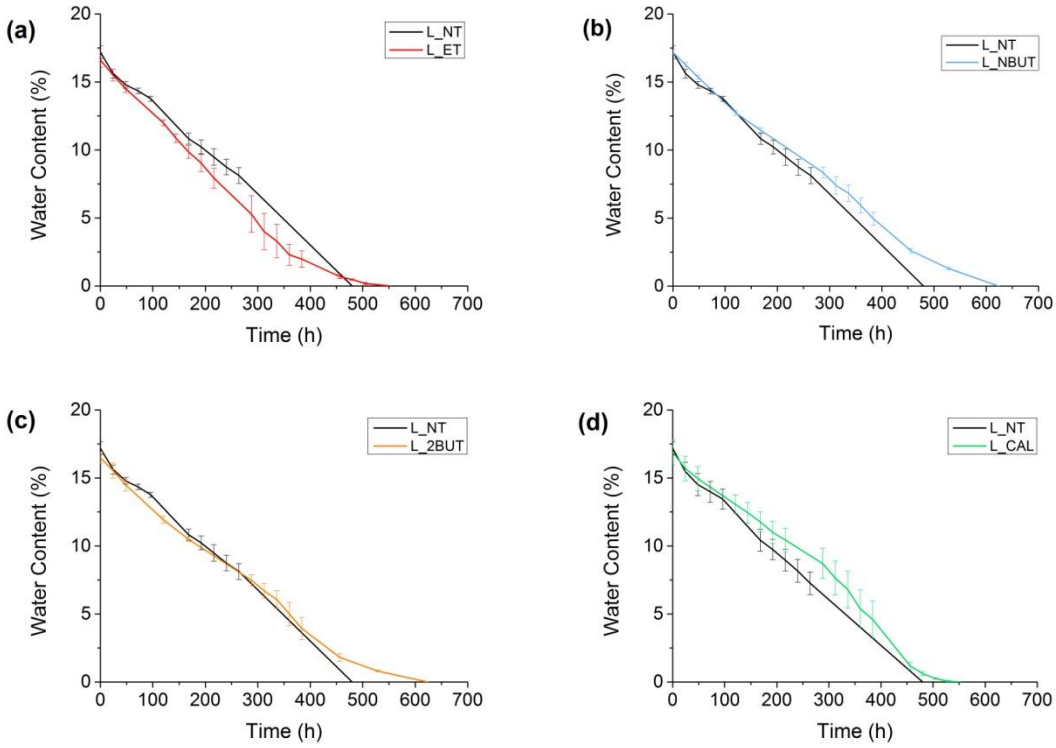

Figure 3.27 *- Comparison of drying curves before and after treatment:* ***(a)*** *L_ET,* ***(b)*** *L_NBUT,* ***(c)*** *L_2BUT and* ***(d)*** *L_CAL.*

The water vapour permeability of samples reported as the water vapour permeability coefficient (g), changes after the application of every type of treatment, except for samples treated with *ET* (**Fig. 3.28**). Samples treated with *2BUT* show a major decrease, in accordance with the capillary water absorption test for which the application of *2BUT* induced a lower absorption of water.

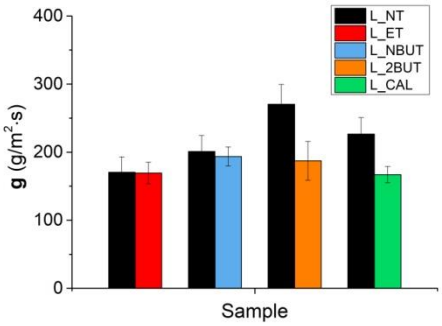

Figure 3.28 *- Water vapour permeability test results expressed as water vapour permeability coefficient (g) and reported as comparison before and after treatment.*

Changing in pores size distribution was measured with two different techniques: mercury intrusion porosimetry and nuclear magnetic resonance relaxometry (NMR). While the first gives a quantitative result, NMR is a qualitative analysis which provides information about the variation in the pore dimensions. Smaller relaxation times correspond to pores of smaller dimensions, while higher relaxation times refer to pores of bigger dimensions.

A summary of MIP data expressed as total open porosity of stone and total cumulative volume for each type of applied treatment is reported in **Tab. 3.6**.

Table 3.6 *- Porosity data obtained by MIP measurements, reported as comparison between treated and untreated samples.*

Sample code	Total open porosity (%)	Total cumulative volume (mm^3/g)
L_NT	37.6 ± 0.9	223.8 ± 1.3
L_ET	34.1 ± 0.6	190.3 ± 4.4
L_NBUT	34.7 ± 0.7	216.5 ± 7.2
L_2BUT	34.2 ± 0.3	205.5 ± 5.3
L_CAL	36.8 ± 0.6	216.7 ± 3.2

All the products based on $Ca(OEt)_2$ bring to a decrease of both total open porosity with better results respect to CaLoSil. In fact, *L_ET*, *L_NBUT* and *L_2BUT* show a reduction of total open porosity to the initial value of not aged stone (34.4 ± 0.5%) as reported in paragraph 3.1.1. **Fig 3.29** reports a comparison of pores size distribution between treated and untreated samples and shows that especially *NBUT* causes a reduction of macropores with radius > 1 μm respect to untreated stone. The curves related to other treatments are very similar among them.

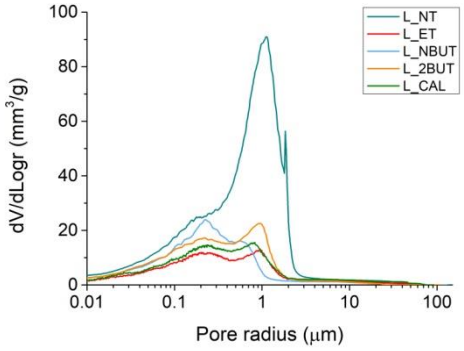

Figure 3.29 *- Pore size distribution curves expressed as log differential intruded volume versus pore radius of untreated and treated samples.*

Cumulative pore volume and volume distribution are reported as function of pore radius and graphically shown in **Fig. 3.30**. As reported in **Tab. 3.6**, all the treatments cause a change in the porosity and cumulative volume distribution. In particular, *NBUT* and *CAL* lead to a decrease of cumulative volume for pores with radius between 1-4 μm respect to untreated stone with a higher decrease for *NBUT;* furthermore, also an increase of pores with radius between 0.1- 1 μm is registered (**Fig. 3.30 (c)** and **(e)**); *ET* causes a reduction of pores with radius between 1-4 μm and a small increase for pores of smaller dimension (0.1-0.8 μm) (**Fig. 3.30 (b)**). Finally, *2BUT* leads to a small decrease of pore with radius in the range 2-4 μm.

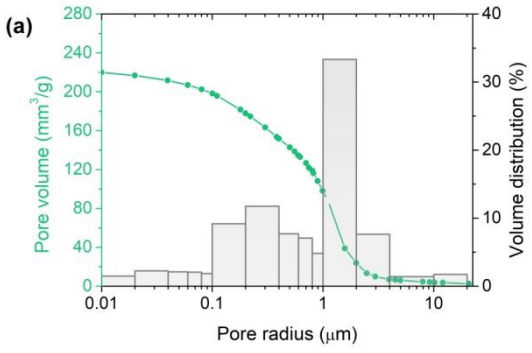

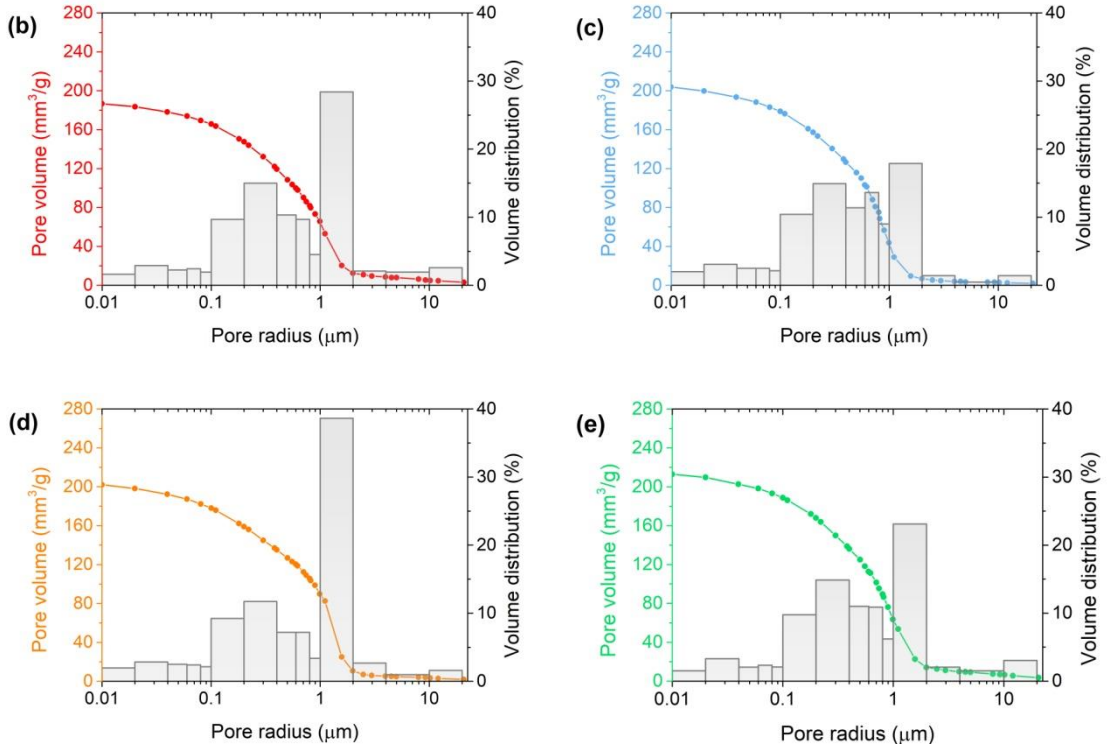

Figure 3.30 *- Cumulative pore volume and volume distribution versus pore radius:* ***(a)*** *L_NT,* ***(b)*** *L_ET,* ***(c)*** *L_NBUT,* ***(d)*** *L_2BUT and* ***(e)*** *L_CAL.*

Changes in pores size distribution due to application of treatments obtained with NMR analysis were evaluated through transverse relaxation time distributions (T2), more readable respect to longitudinal relaxation time (T1) (**Fig. 3.31**). This analysis allows to make a qualitative consideration about change in pore radius dimensions.

The results agree with MIP measurements for pores of bigger dimensions; in fact, changes in the curve for pores of bigger dimensions (T > 10 ms) are visible especially for treatment *ET*, *NBUT* and *CAL*, while for *2BUT* no important change are detectable. Regarding pores of smaller dimensions (T < 1 ms), small changes of the curves referred to treated samples *L_NBUT* and *L_CAL* agree with MIP measurement for which a small increase of pores of smaller dimensions was registered.

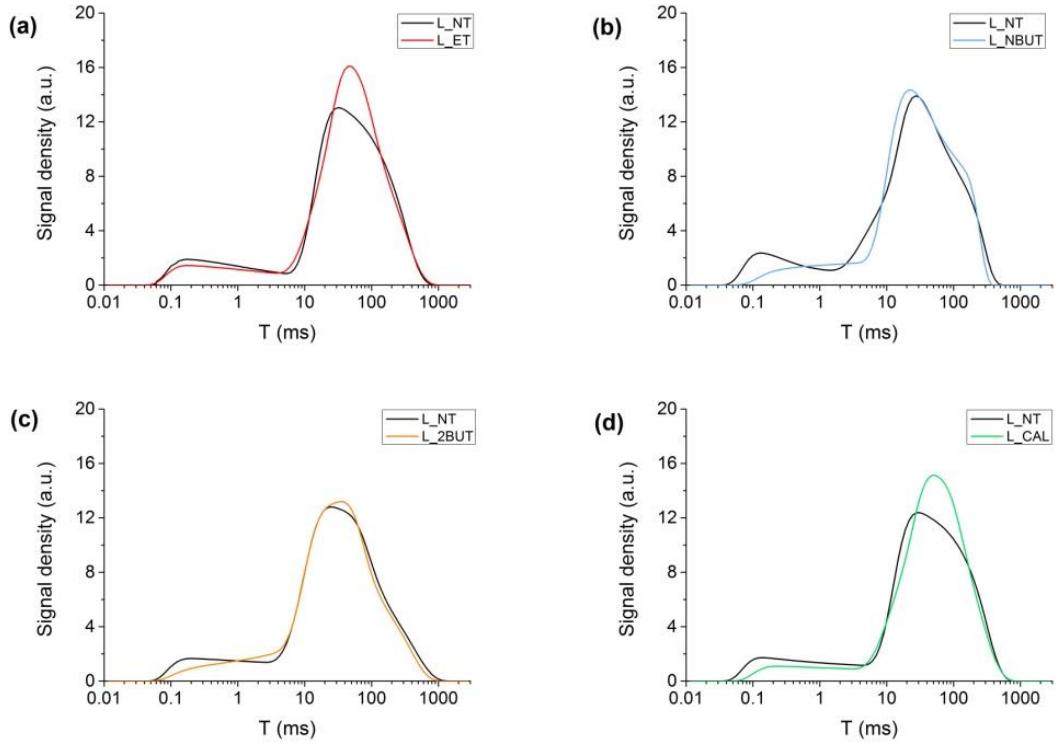

Figure 3.31 *- Comparison of T2 distribution functions before and after treatment:* ***(a)*** *L_ET,* ***(b)*** *L_NBUT,* ***(c)*** *L_2BUT and* ***(d)*** *L_CAL.*

To evaluate the colour changes induced by the treatments, the overall colour difference ΔE^* (before and after treatment) offers an index of the variation of all colour components. **Fig. 3.32** represents graphically the average values of ΔE^* for four different treatments. For this type of stone, all the treatments cause a colour variation > 5 - the limit value for an acceptable colour change of the surface [37], [38].

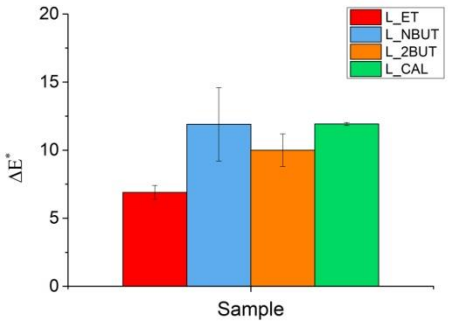

Figure 3.32 *- Colour variation ⊿E* generated by four consolidating products.*

Looking at SEM images of treated and untreated surfaces, it is visible how *CAL* forms a

superficial layer on the surface while, other treatments based on calcium ethoxide nanosuspension maintain a surface morphology similar to untreated sample (**Fig. 3.33**).

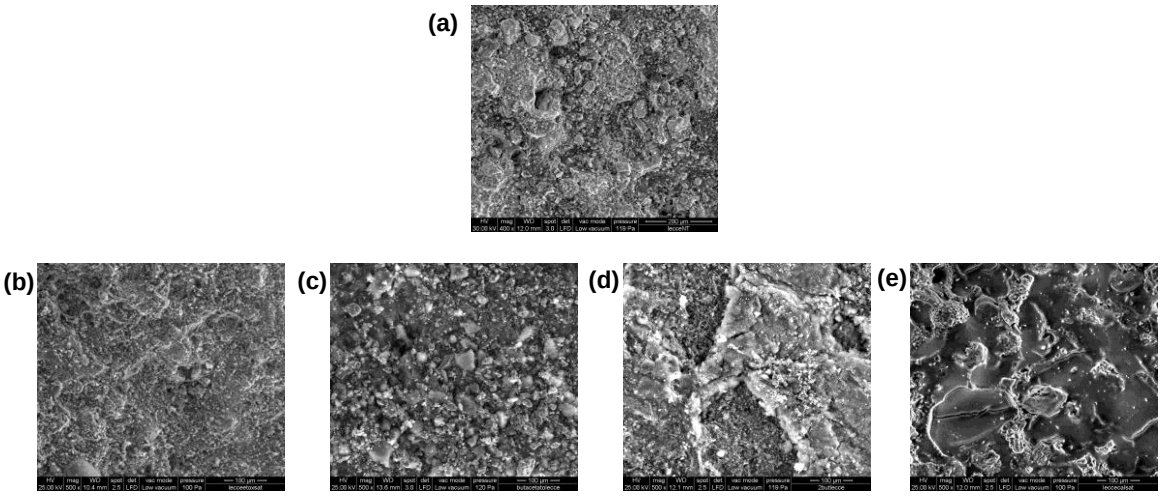

Figure 3.33 *- Surface observation with SEM:* ***(a)*** *L_NT,* ***(b)*** *L_ET,* ***(c)*** *L_NBUT* ***d)*** *L_2BUT and* ***(e)*** *L_CAL.*

Ultrasound pulse velocity investigates the changes in porous network due to the application of consolidating treatments. Higher UPV velocity may indicate a decrease of porosity due to the presence of the consolidant inside pores, facilitating the propagation of wave in the consolidated zone in comparison to the original rock material. The results are expressed as the average of three measurements performed on the same sample, before and after treatment. The graphs in **Fig. 3.34** reports the UPV profile from the treated surface (0 mm) to the top of the material (50 mm). Therefore, y axes show the increase of distance from the treated surface. While *ET* seems to not have a consolidating effect or the treatment penetrates less than 5 mm (**Fig. 3.34 (a)**), *NBUT* presents an increase of ultrasound velocity in the first mm from the treated surface (**Fig. 3.34 (b)**). The results obtained for *L_2BUT* and *L_CAL* are particular; in fact, in these cases there is a visible velocity increase only after 10 mm from the treated surface. This effect could be ascribable to the type of measurement, rather than an in-depth penetration of consolidating agents. More details about UPV values before and after treatment for all products are reported in **Tab. C.2** (**Appendix C**).

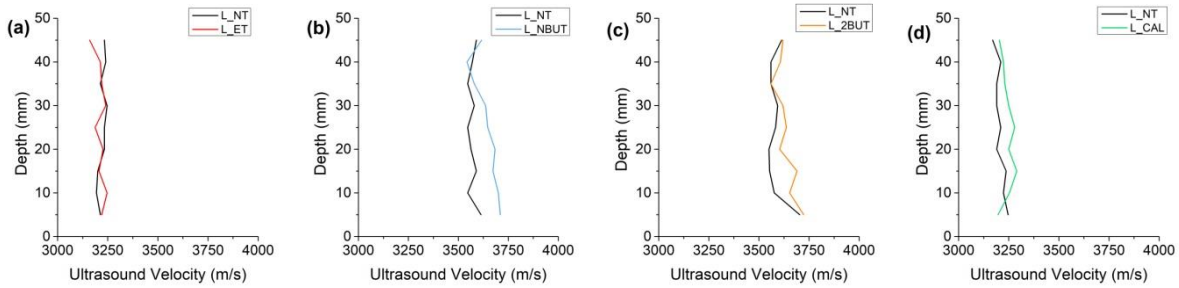

Figure 3.34 *- Ultrasonic profile before and after treatment:* ***(a)*** *L_ET,* ***(b)*** *L_NBUT,* ***(c)*** *L_2BUT and* ***(d)*** *L_CAL.*

Drilling tests were carried out on the same samples previously analysed with UPV, measured in profile; treated and untreated data are obtained from the same mock-ups, on opposite surfaces. The results are expressed as the average of three measurements performed on the same sample. By comparing the resistance profiles before and after treatments, data reported agree with UPV analysis. In fact, only *NBUT* induces an increasing of stone resistance from a medium value of 8.3 N for untreated part to 9.4 N for treated part, for a penetration of 9 mm (**Fig. 3.35 (b)**) while, *ET*, *2BUT* and *CAL* do not produce a visible increase of stone resistance after treatment.

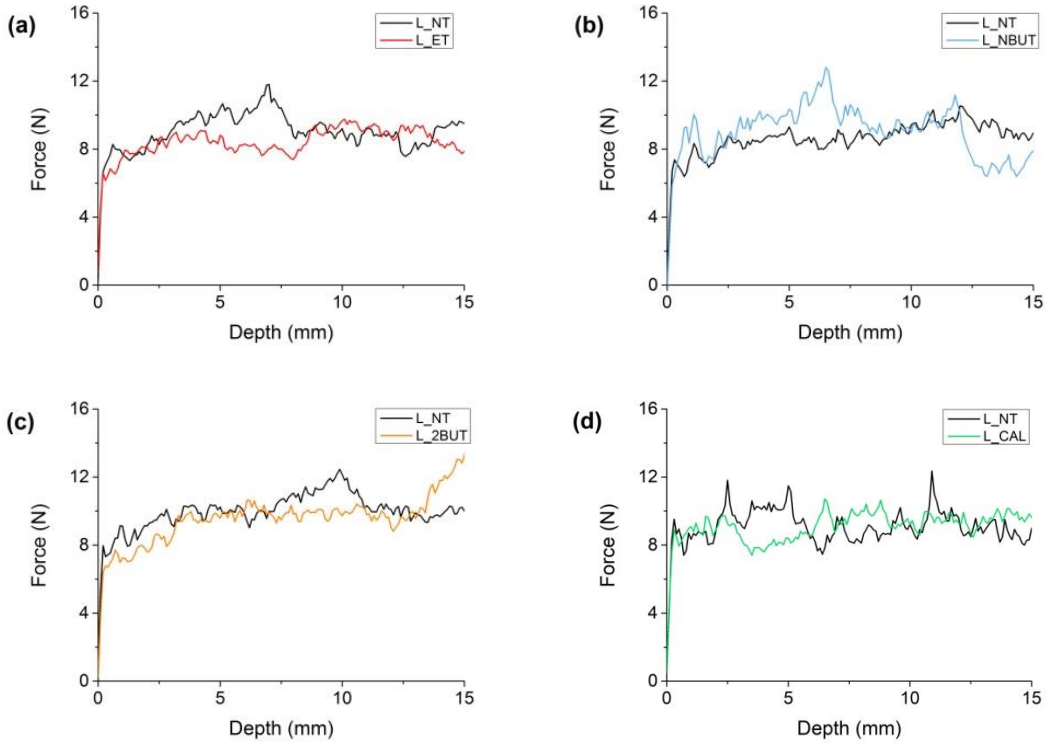

Figure 3.35 *- Drilling profiles before and after treatment:* ***(a)*** *L_ET,* ***(b)*** *L_NBUT,* ***(c)*** *L_2BUT and* ***(d)*** *L_CAL.*

By comparing the overall results obtained with the different analyses and material tests, treatments based on $Ca(OEt)_2$ nanosuspension and the reference product show a similar behaviour regarding the modification of water transport properties inside the material, leading to an acceptable change of this value with a higher change, however acceptable, for *L_2BUT*. Nevertheless, a compatibility in water transport behaviour does not correspond to an acceptable chromatic variations, being the value of calculated ΔE^* always higher than 5.

Regarding the consolidation effect, all products, except the reference one, induce a decrease of stone porosity measured by MIP, but the only treatment which can reach a good penetration, as shown by both UPV and DRMS measurements is *NBUT*. These results may be related to the boiling point of the solvent, in fact, as reported by the study of carbonation process kinetic, the highest boiling point of this solvent allows to reach a greater penetration of the product by delaying the carbonation process. This result agrees with a study reported by Borsoi et al. [39] for which solvents having a higher boiling point improve the deposition of lime nanoparticles in depth.

3.1.1.1 Application procedure: by brush with pre-set number of brush strokes

This type of application procedure was performed only for calcium ethoxide diluted in ethanol and the reference product, CaLoSil. The maximum number of applications of $Ca(OEt)_2$ nanosuspension diluted in ethanol for Lecce stone was decided in order to avoid a colour change of the surface ($\Delta E^* > 5$) [37]. Colour measurements were performed after each brush stroke and the number of 7 brush strokes was indicated as the maximum possible to avoid a significant colour change of the surface. ΔE^* result for *L_ET* after 7 brush strokes was 4.8 ± 0.8 while for *L_CAL* was 3.2 ± 0.8.

Tab. 3.7 reports data regarding the quantity of product retained after one month from the application. The results are reported as a range of value between the minimum and the maximum quantity for each type of product. As for the previous application procedure, differences among quantity of product retained for samples treated with the same product are probably due to the different shape of mock-ups (in accordance to the different analyses, mock-ups of different dimensions were necessary). More details of product retained in relation to the different analyses are shown in **Tab. C.3** in **Appendix C**.

Looking at the results, this type of application procedure, compared to brush till saturation, led to a similar quantity of product retained for *L_ET,* and a lower quantity for *L_CAL*.

***Table 3.7** - Application by brush with pre-set number of brush strokes: range of amount of product retained after one month from the application.*

Product	Quantity of product retained (kg/m²)
ET	0.019 – 0.114
CAL	0.010 – 0.022

As for the application by brush till saturation, water transport properties were estimated by capillarity water absorption, drying rate evaluation and water vapour permeability test. **Fig 3.36** shows data regarding the water absorption through capillarity test which illustrate how both treatments cause a reduction of the quantity of water absorbed in the first 45 minutes, with a higher reduction for *L_ET* compared to *L_CAL*.

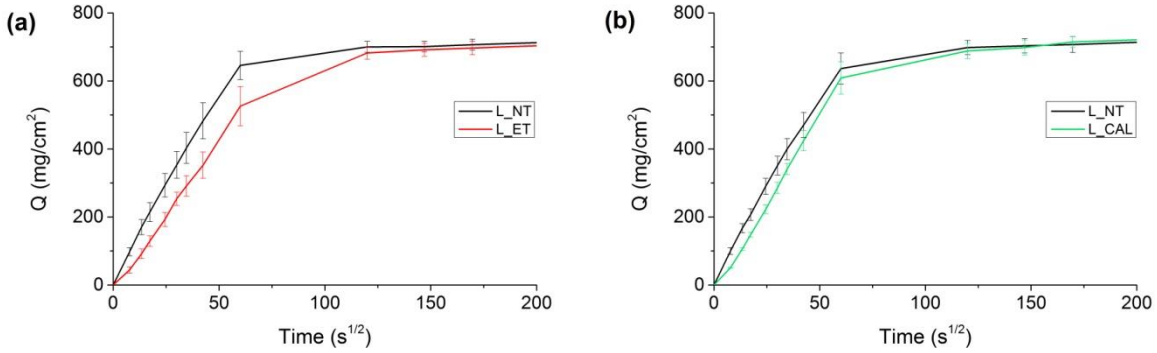

***Figure 3.36** - Quantity of water absorbed by capillarity, comparison before and after treatment: **(a)** L_ET and **(b)** L_CAL.*

The value of capillary water absorption coefficient (CWAC) agrees with this behaviour showing a higher decrease of this coefficient for *L_ET* (from 10.8 ± 0.8 mg/cm²·s$^{1/2}$ to 8.9 ± 0.9 mg/cm²·s$^{1/2}$) compared to *L_CAL* (from 11.4 ± 1.3 mg/cm²·s$^{1/2}$ to 10.5± 0.8 mg/cm²·s$^{1/2}$) in accordance with the major amount of product retained (**Fig. 3.37**).

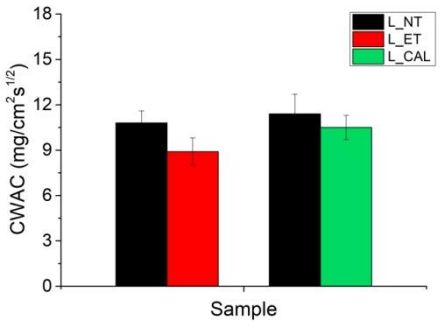

***Figure 3.37** - Comparison of capillary water absorption coefficient (CWAC) before and after treatment.*

Regarding the drying rate (**Fig 3.38**), the behaviour between treated and untreated samples is quite similar. However, treated samples reach the drying state slower than untreated samples and both trend starts from a content of water lower than untreated samples, showing a reduction of quantity of water absorbed.

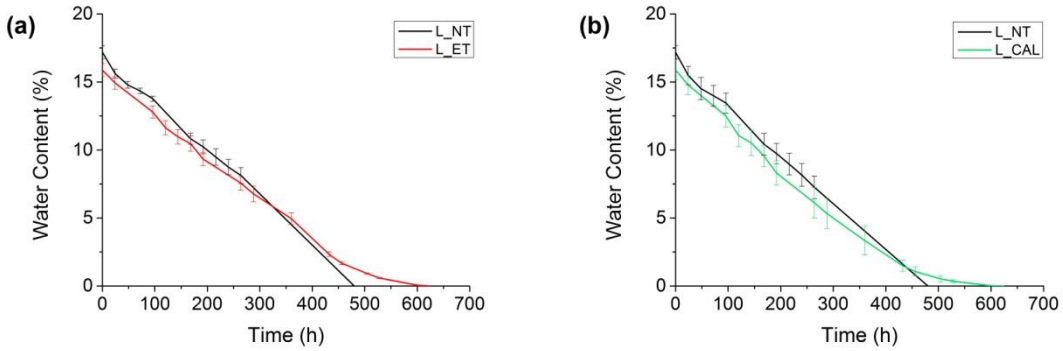

Figure 3.38 *- Comparison of drying curves before and after treatment:* ***(a)*** *L_ET and* ***(b)*** *L_CAL.*

Water vapour permeability test (**Fig. 3.39**) confirms the water absorption test with a higher decrease of water vapour permeability for *L_ET* (from 151.41 ± 9.88 g/m^2·s to 94.39 ± 0.41 g/m^2·s) compared to *L_CAL* (from 226.66 ± 24.25 g/m^2·s to 167.3 ± 36.7 g/m^2·s), probably due to the higher quantity of product retained. In this case, the variation of g value respect to untreated stone due to *ET* is higher than 25%.

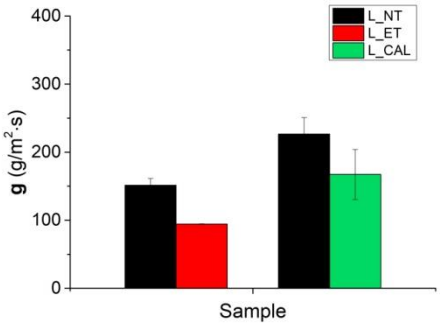

Figure 3.39 *- Water vapour permeability test results expressed as water vapour permeability coefficient (g) and reported as comparison before and after treatment.*

The variation in pore size distribution was evaluated with MIP and NMR. Changes in total open porosity, cumulative volume and pores size distribution, evaluated by MIP before and after treatments, are reported in **Tab 3.8** and **Fig. 3.40**.

Table 3.8 *- Porosity data obtained by MIP measurements, reported as comparison between treated and untreated samples.*

Sample code	Total open porosity (%)	Total cumulative volume (mm^3/g)
L_NT	37.6 ± 0.9	223.8 ± 1.3
L_ET	34.5 ± 0.9	201.6 ± 1.8
L_CAL	34.1 ± 0.3	211.3 ± 3.4

The results show how both treatments lead to a porosity value similar to natural stone (not aged stone as reported in paragraph 3.3.1). However, *CAL* preserves a pore radius distribution more similar to untreated support respect to *ET*; in fact, while *ET* reduces pores with radius between 1-4 μm, leading to an increase of pores of smaller dimensions, *CAL* reduces only pores with radius between 2-4 μm (**Fig. 3.40** and **Fig. 3.41)**.

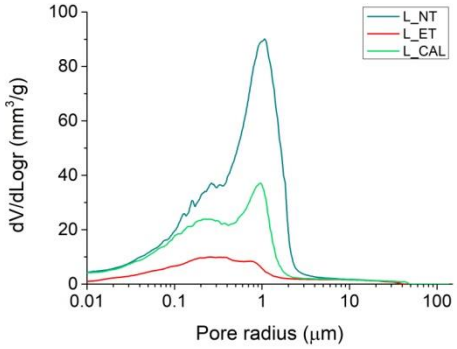

Figure 3.40 *- Pore size distribution curves expressed as log differential intruded volume vs. pore radius of untreated and treated samples.*

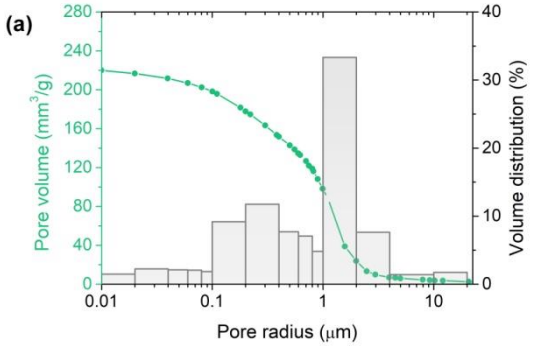

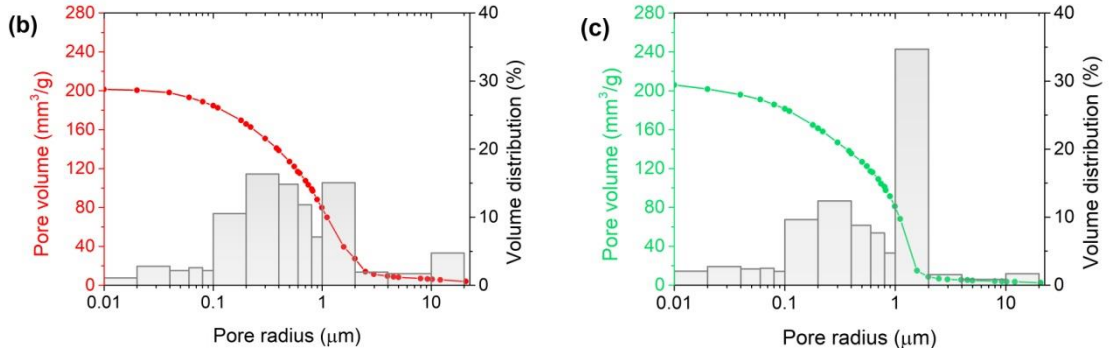

Figure 3.41 *- Cumulative pore volume and volume distribution versus pore radius:* ***(a)*** *L_NT,* ***(b)*** *L_ET and* ***(c)*** *L_CAL.*

NMR results are consistent with MIP analysis; *ET* causes a higher qualitative variation of pore size distribution respect to *CAL* especially for pores of higher dimensions (T > 10 ms), while *L_CAL* maintains a pore distribution more similar to untreated stone (**Fig. 3.42**).

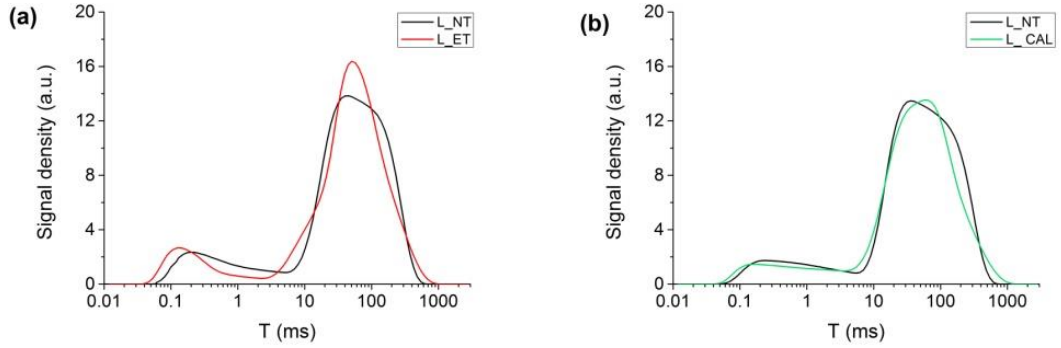

Figure 3.42 *– Comparison of T2 distribution functions before and after treatment:* ***(a)*** *L_ET and* ***(b)*** *L_CAL.*

As in the case of the application by brush till saturation, looking at the treated surface with SEM, a difference between the two consolidating treatments can be seen; in fact, differently from *L_ET*, surface treated with *CAL* shows the formation of a superficial layer rather than an homogeneous one respect to the support (**Fig. 3.43**).

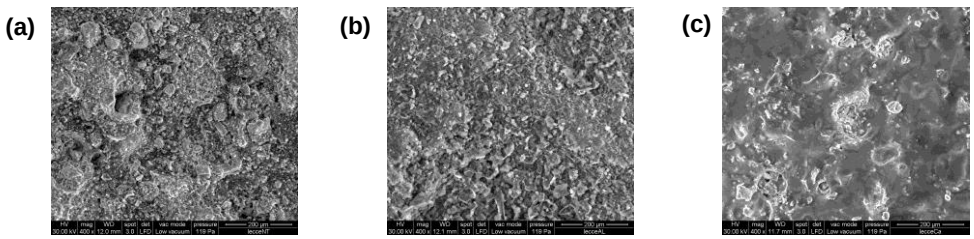

Figure 3.43 *- Surface observation with SEM:* ***(a)*** *L_NT,* ***(b)*** *L_ET and* ***(c)*** *L_CAL.*

For this type of application procedure, results about ultrasonic pulse velocity and drilling resistance measurement system were not performed.

All the obtained data show how both *ET* and *CAL* applied with controlled number of brush strokes to avoid a colour change of the surface, cause a change in water transport properties inside the stone; these changes range within acceptable limits for *L_CAL*, while the change of water vapour permeability due to *L_ET* is greater than 25% respect to untreated stone. Both treatments induce a reduction of porosity value measured by MIP. However, information concerning the ability of treatments to penetrate inside the stone is crucial to have a complete view regarding their effectiveness as consolidating products with this type of application procedure.

3.3.1.2 Application procedure: by absorption through capillarity

Treated and untreated samples were analysed with ultrasonic pulse velocity and drilling resistance measurement system to study a possible different penetration of products. Colorimetric measurements were performed to evaluate the possible change of colour surface due to this type of application procedure. **Tab. 3.9** reports data regarding the quantity of product retained after one month from the application; it shows how for *NBUT* and *CAL*, this quantity is higher respect to application by brush till saturation, while for *2BUT* is lower and for *ET* is similar.

Table 3.9 *- Application by absorption through capillarity: amount of product retained after one month from the application.*

Product	Quantity of product retained (kg/m²)
ET	0.067
NBUT	0.097
2BUT	0.034
CAL	0.086

For this type of application procedure, it was possible to measure the fringe reached by the product during the proof and the results are reported in **Tab. C.4** in **Appendix C**.

Results concerning treated and untreated samples, acquired by ultrasonic pulse velocity, were obtained from the same samples and expressed as the average of three measurements. Data show that there are no consistent variation between treated and untreated samples for *L_2BUT* and *L_CAL*; while, *ET* seems to increase UPV velocity in the first 25 mm and only

NBUT causes a small increase of UPV between 5 and 10 mm from the treated surface (**Fig. 3.44 (b)**). In fact, *NBUT* is the product which penetrates mostly as reported in **Tab. C.4** in **Appendix C**. The increase of UPV for *L_NBUT* after 20 mm from the treated surface can be ascribed to water inside the material, rather than a consolidating effect. More details about UPV values before and after treatments for all products are reported in **Tab. C.5** (**Appendix C**).

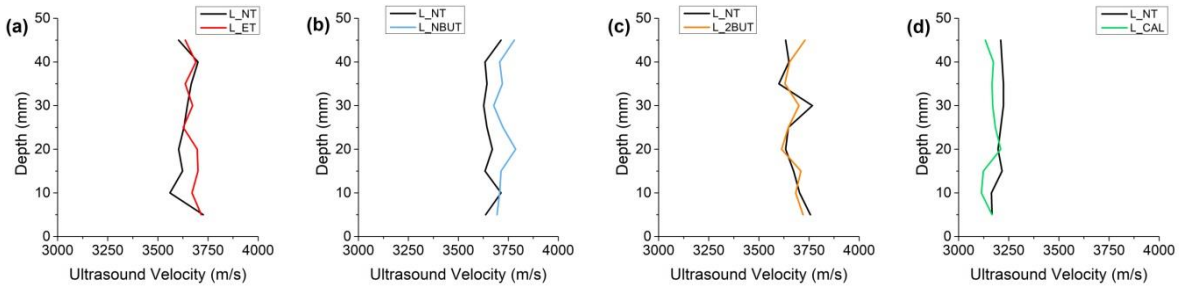

Figure 3.44 *- Ultrasonic profile before and after treatment:* ***(a)*** *L_ET,* ***(b)*** *L_NBUT,* ***(c)*** *L_2BUT and* ***(d)*** *L_CAL.*

The consolidating effect due to *NBUT* is confirmed by DRMS which shows how this treatment causes an increase of stone resistance from 6.6 N to 7.4 N in the first 10 mm from the treated surface (**Fig. 3.45 (b)**).

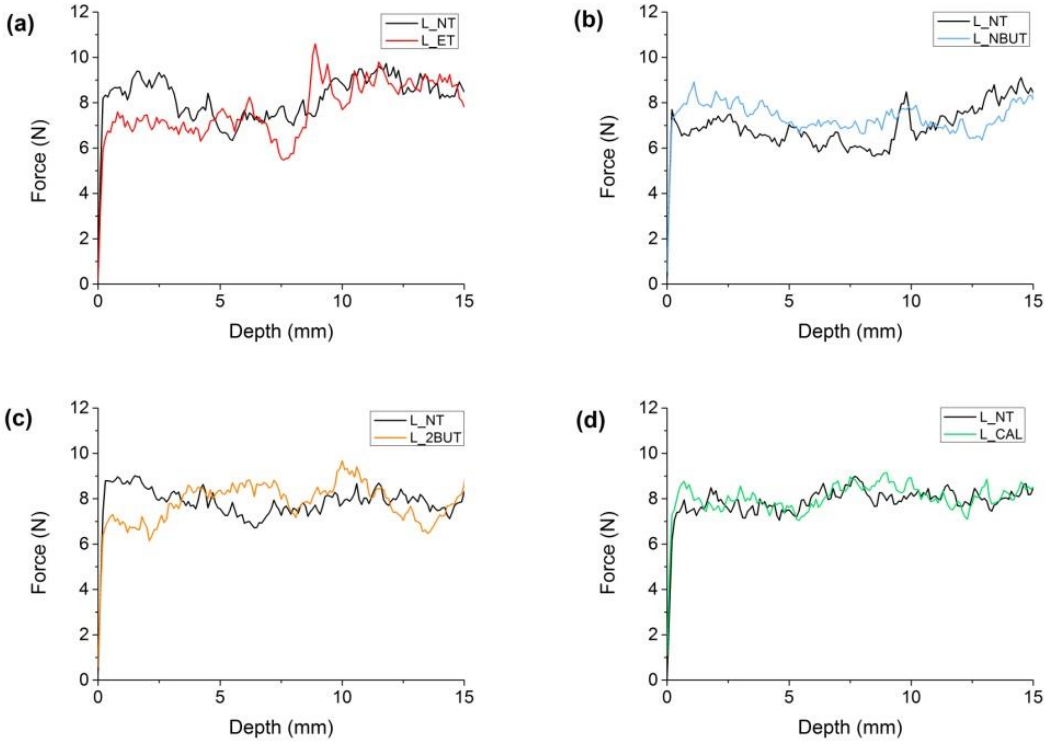

Figure 3.45 *- Drilling profiles before and after treatment:* ***(a)*** *L_ET,* ***(b)*** *L_NBUT,* ***(c)*** *L_2BUT and* ***(d)*** *L_CAL.*

Instead, a consolidation effect due to *ET* is not confirmed by this technique. This different result could be related to heterogeneous treated and untreated parts.

Colorimetric data were obtained by analysing ten points from both treated and untreated parts. As for the application by brush till saturation, the procedure by absorption through capillarity led to a higher change of surface colour for all type of applied treatments (**Fig. 3.46**). However, in this case the most important change are due to *ET* and *2BUT*, differently from the application by brush where the higher colour variation are registered for *NBUT* and *CAL*.

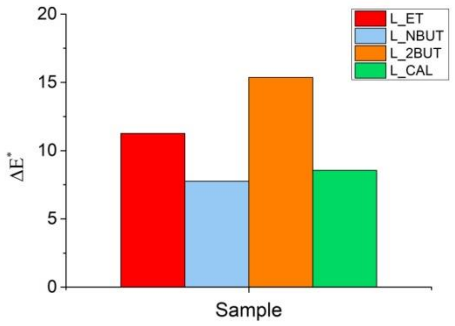

Figure 3.46 *- Colour variation ⊿E* generated by four consolidating products.*

Making a comparison between applications by brush till saturation and absorption through capillarity, it can be seen that even if the quantity of product retained for *L_NBUT* and *L_CAL* is a little bit higher in the last case, the results regarding consolidating efficacy are similar. In fact, the only product which can penetrate more deeply inside this variety of stone is *NBUT*.

3.3.2 Noto stone

TG-DSC analysis performed on Noto Stone, shows that this limestone is composed by calcium carbonate for a percentage of 96,2%, determined from the mass loss of 41.8% between 600-800 °C (**Fig. 3.47 (a)**). FT-IR analysis confirms the presence of calcium carbonate in the form of calcite with characteristic peaks at 1430, 875 and 713 cm^{-1}; a silicate component is also present, as evidenced by the absorption peak at 1036 cm^{-1}(**Fig. 3.47 (b)**).

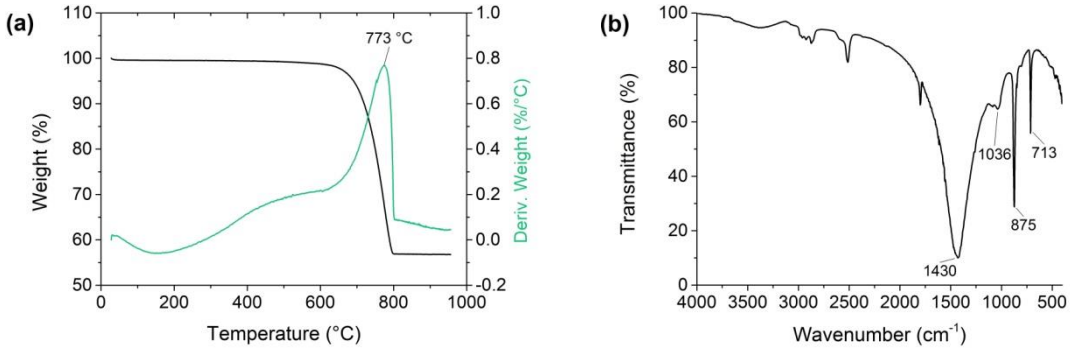

Figure 3.47 *- Chemical characterization of Noto stone by* ***(a)*** *TG-DSC and* ***(b)*** *FT-IR analyses.*

The ageing process was successful also for this stone leading to an increase of porosity from 30.3 ± 0.9% to 34.5 ± 0.6% and cumulative volume from 155.9 ± 2.4 mm^3/g to 172.1 ± 0.9 mm^3/g (**Fig. 3.48**). Furthermore, it is visible an increase of pores with radius > 2 μm.

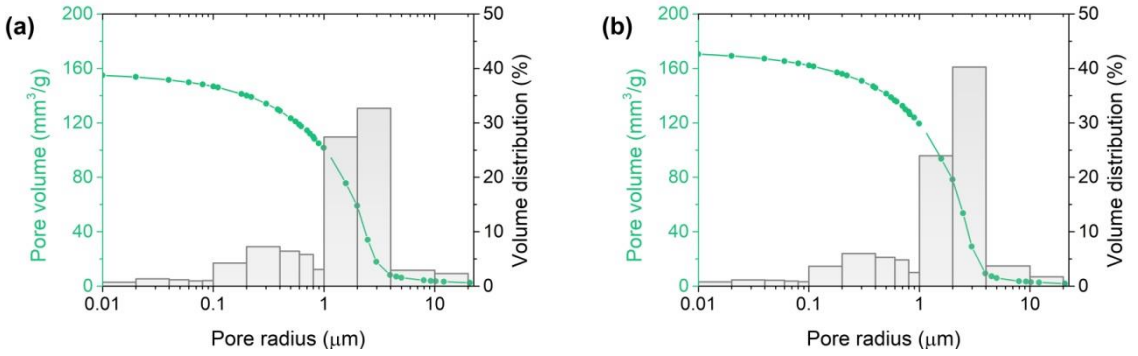

Figure 3.48 *- Cumulative pore volume and volume distribution versus pore radius of* ***(a)*** *not aged and* ***(b)*** *aged Noto stone.*

In the following section, results concerning the efficacy of four products as consolidating agent for Noto stone, applied with different procedures, will be examined.

3.3.2.1 Application procedure: by brush till saturation

In this section, results regarding the different analyses performed to understand the efficacy of four products applied by brush till saturation are reported. **Tab. 3.10** presents data regarding the quantity of product retained after one month from the application for each type of product, reported as a range of value between the minimum and the maximum quantity. Differences among quantity of product retained for samples treated with the same product are probably due to the different shape of mock-ups (in accordance to the different analyses,

mock-ups of different dimensions were necessary). More details of product retained in relation to the different analyses are shown in **Tab. C.6** in **Appendix C**.

Table 3.10 *- Application by brush till saturation: range of amount of product retained after one month from the application.*

Product	Quantity of product retained (kg/m²)
ET	0.028 – 0.208
NBUT	0.010 – 0.077
2BUT	0.019 – 0.113
CAL	0.017 – 0.122

Starting with water transport properties, **Fig. 3.49** shows the results about water absorption through capillarity for the different consolidating products. All treatments lead to a decrease of water absorbed in the first 45 minutes with a higher reduction for products based on calcium ethoxide rather than the reference one (**Fig. 3.49 (a), (b), (c)**).

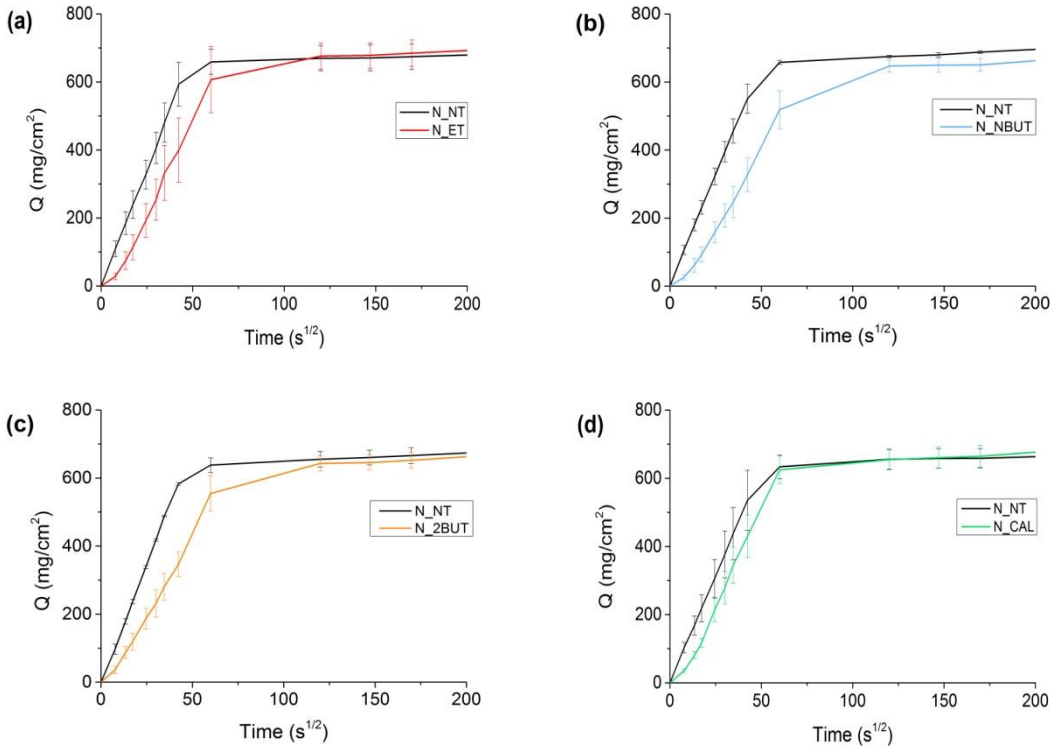

Figure 3.49 *- Quantity of water absorbed by capillarity, comparison before and after treatment:* ***(a)*** *N_ET,* ***(b)*** *N_NBUT,* ***(c)*** *N_2BUT and* ***(d)*** *N_CAL.*

This different behaviour among calcium ethoxide based products and CaLoSil is confirmed by the average of capillary water absorption coefficient (CWAC) (**Fig 3.50**); the values confirm

that *N_ET*, *N_NBUT* and *N_2BUT* show a higher decrease of water absorption, maintaining the variation within an acceptable limit [37].

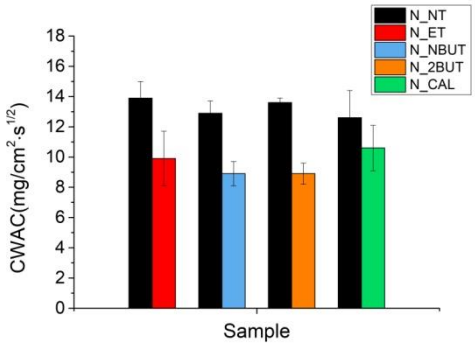

Figure 3.50 *- Comparison of capillary water absorption coefficient (CWAC) before and after treatment.*

Regarding the drying test (**Fig. 3.51**), treated and untreated samples show a different behaviour in reaching a drying state, except for *N_ET* which presents a similar trend respect to untreated stone. In particular, *N_ NBUT* and *N_CAL* retain a major quantity of water during the test.

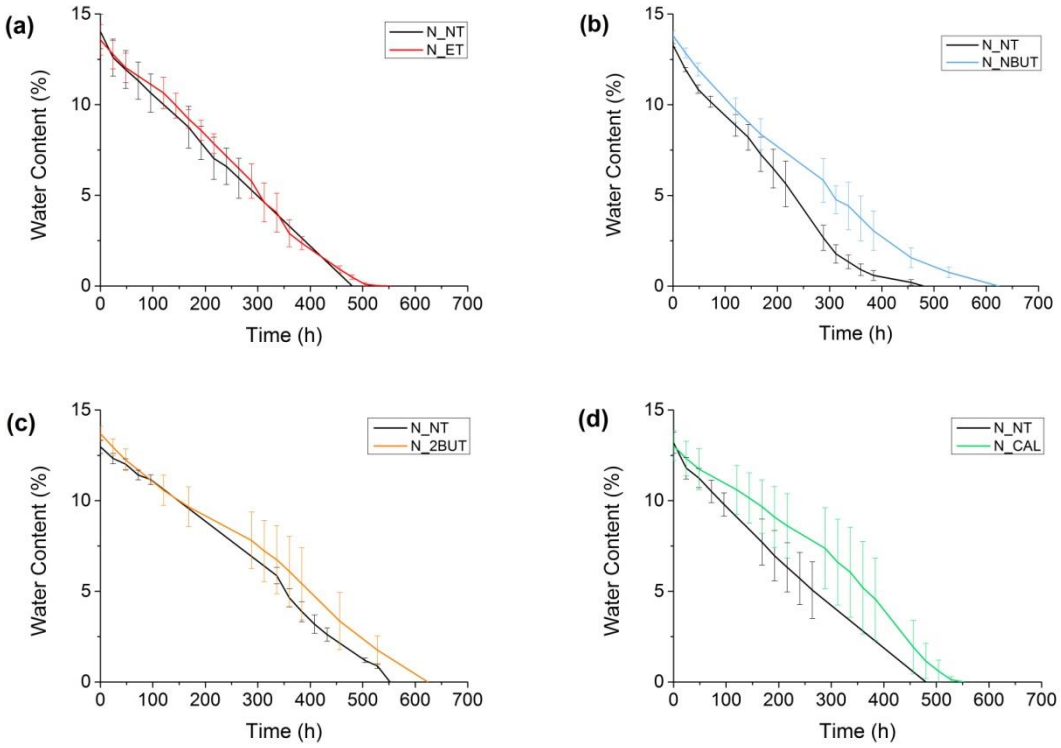

Figure 3.51 *- Comparison of drying curves before and after treatment:* ***(a)*** *N_ET,* ***(b)*** *N_NBUT,* ***(c)*** *N_2BUT and* ***(d)*** *N_CAL.*

The water vapour permeability test (**Fig. 3.52**) indicates that all treatments lead to a decrease of water vapour permeability compared to untreated samples.

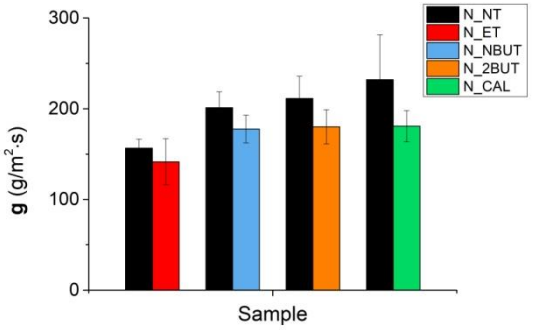

Figure 3.52 *- Water vapour permeability test results expressed as water vapour permeability coefficient (g) and reported as comparison before and after treatment.*

Results obtained with mercury intrusion porosimetry (**Tab. 3.11**) show that all the products based on calcium ethoxide and the reference one (CaLoSil), are successful in reducing the total open porosity of stone leading to a porosity value similar to not aged stone (30.3 ± 0.9%), considering the value reported in paragraph 3.3.2.

Table 3.11 *- Porosity data obtained by MIP measurements, reported as comparison between treated and untreated samples.*

Sample code	Total open porosity (%)	Total cumulative volume (mm^3/g)
N_NT	34.5 ± 2.6	172.1 ± 0.9
N_ET	29.6 ± 0.2	156.1 ± 3.1
N_NBUT	29.6 ± 0.6	166.7 ± 2.7
N_2BUT	29.6 ± 0.6	154.1 ± 15.1
N_CAL	29.2 ± 0.8	153.3 ± 4.9

Fig. 3.53 reports a comparison among the pores medium dimension of treated and untreated samples and shows that all treatments, included the reference one, lead to a decrease of pores radius dimension respect to untreated stone.

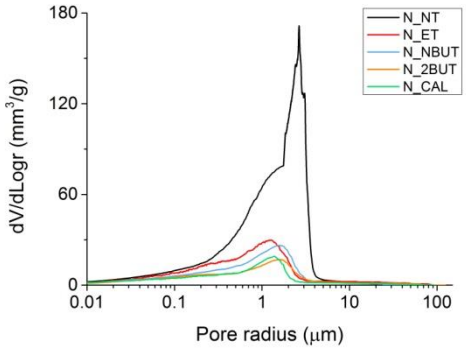

Figure 3.53 *- Pore size distribution curves expressed as log differential intruded volume vs. pore radius of untreated and treated samples.*

Fig. 3.54 shows cumulative pore volume and volume distribution for each treatment. The most evident change in the cumulative volume distribution is referred to pore with radius greater than 1 μm. In fact, all treatments show a decrease of pores with radius between 2-10 μm, mostly for *N_ET* and *N_CAL;* while, *N_NBUT* and *N_2BUT* present also a small decrease of pore radius between 1-2 μm.

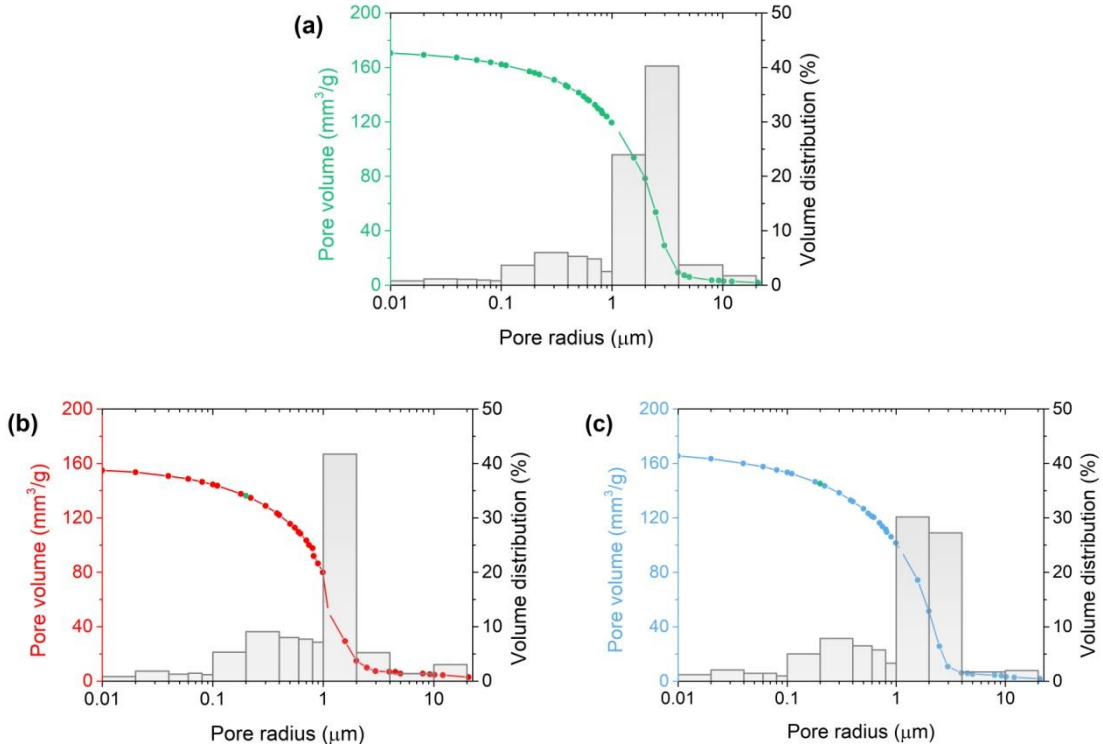

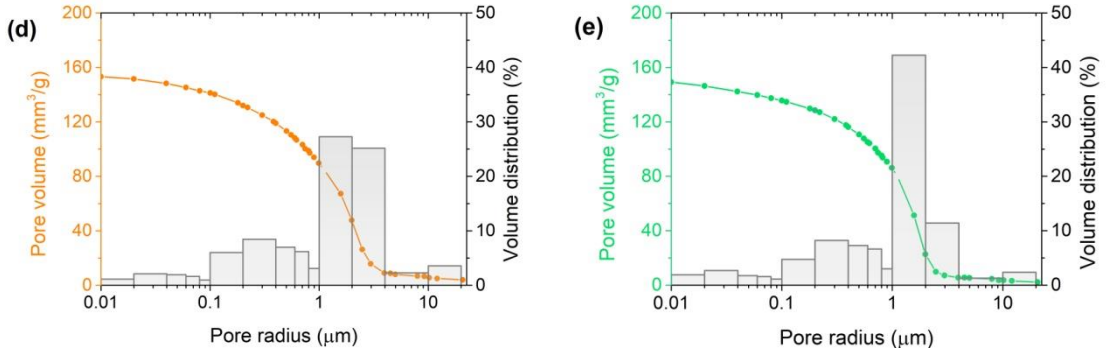

Figure 3.54 *- Cumulative pore volume and volume distribution versus pore radius:* ***(a)*** *N_NT,* ***(b)*** *N_ET,* ***(c)*** *N_NBUT,* ***(d)*** *N_2BUT and* ***(e)*** *N_CAL.*

NMR analysis reports T2 distribution functions for both treated and untreated samples; as reported by MIP results, all treatments are able in reducing pores of bigger dimension (T>10 ms), with better results for *ET* and *CAL* (**Fig 3.55**). Furthermore, **Fig 3.56 (c)** shows that *N_2BUT* presents a variation also in the part of curve related to pores of smaller dimension (T< 1 ms), an effect not visible for MIP measurement.

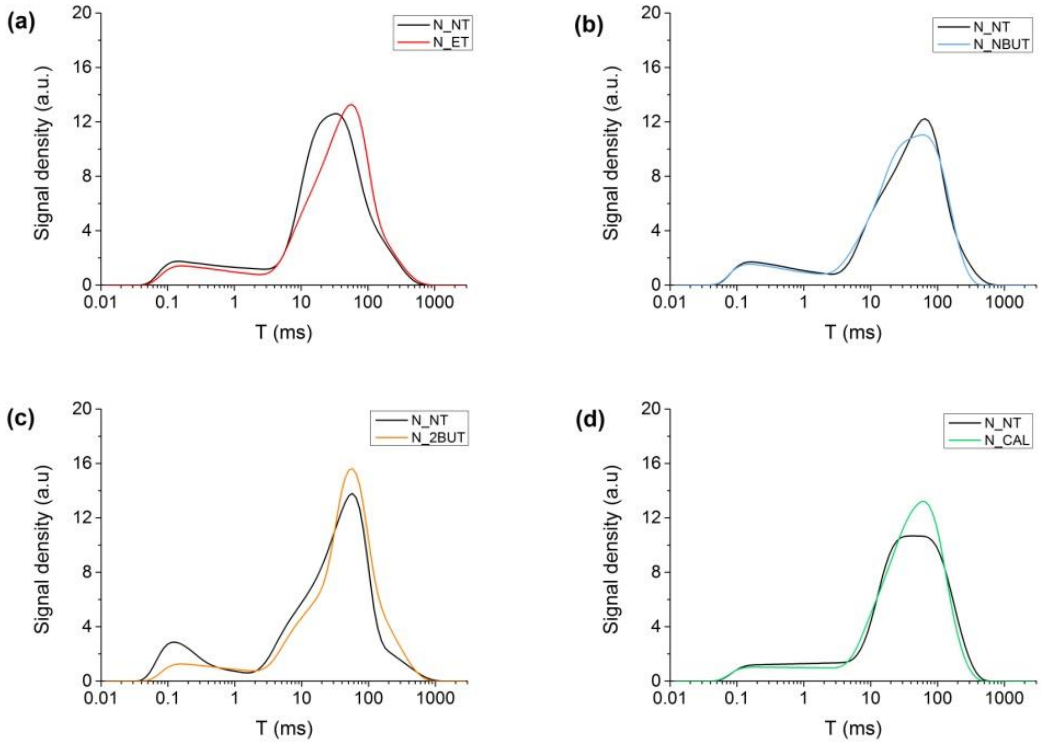

Figure 3.55 *- Comparison of T2 distribution functions before and after treatment:* ***(a)*** *N_ET,* ***(b)*** *N_NBUT,* ***(c)*** *N_2BUT and* ***(d)*** *N_CAL.*

To evaluate the colour change due to the application of products, ΔE^* was evaluated before and after treatments. All products lead to a colour change > 5 with the higher change for *N_2BUT* (**Fig. 3.56**).

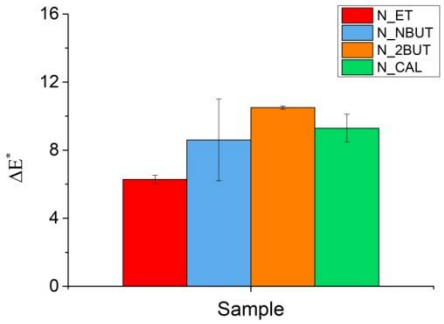

Figure 3.56 *- Colour variation ⊿E* generated by four consolidating products.*

By considering morphological variation, observations with SEM show how treatments based on calcium ethoxide maintain a surface morphology similar to untreated stone, differently from *CAL* (**Fig 3.57**).

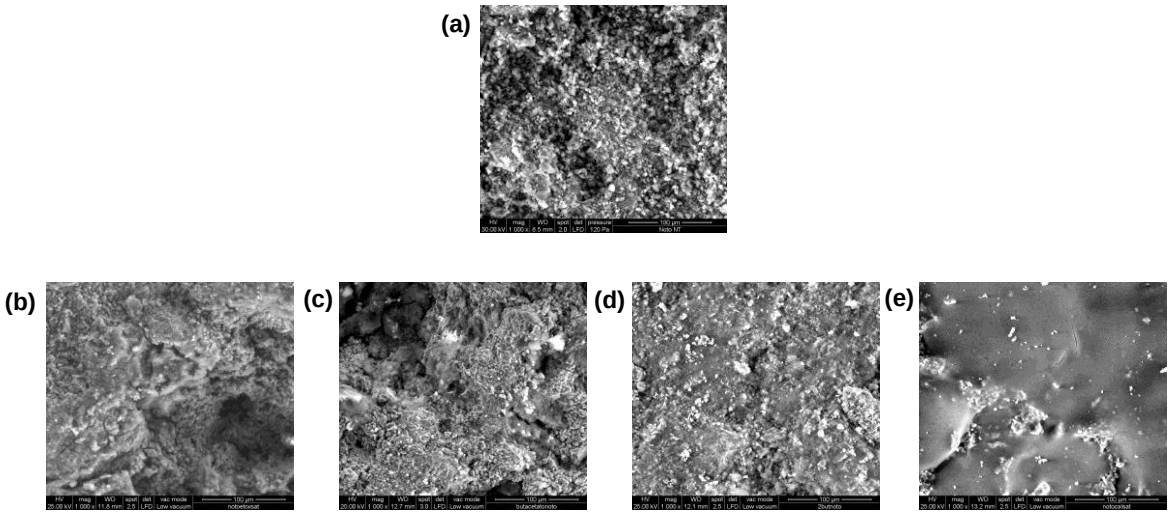

Figure 3.57 *- Surface observation with SEM:* ***(a)*** *N_NT,* ***(b)*** *N_ET,* ***(c)*** *N_NBUT* ***d)*** *N_2BUT and* ***(e)*** *N_CAL.*

Looking at UPV measurements - obtained and reported as for Lecce stone - only *NBUT* and *2BUT* cause an increase of UPV value several mm below the treated surface (**Fig 3.58**). More details about UPV values before and after treatments for all products are reported in **Tab. C.7** (**Appendix C**).

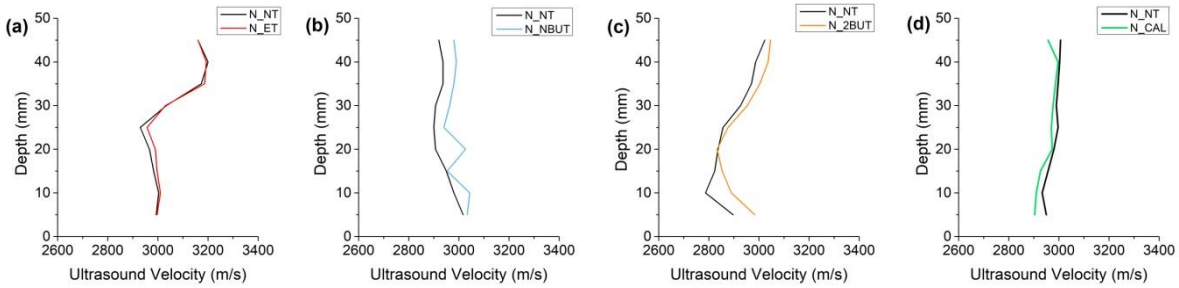

Figure 3.58 *- Ultrasonic profile before and after treatment:* ***(a)*** *N_ET,* ***(b)*** *N_NBUT* ***(c)*** *N_2BUT and* ***(d)*** *N_CAL.*

UPV results are confirmed by DRMS only for *NBUT* which seems to penetrates several mm inside the stone leading to a change of stone resistance from 2 N to 3 N (**Fig 3.59 (b)**) in the first 15 mm. *CAL* does not cause an increase of stone resistance while a different datum regards *N_ET*; in fact, UPV shows no variation before and after treatment (**Fig. 3.58 (a)**), but highlights two zones with different ultrasound pulse velocities: 5-25 mm with a lower velocity and 25-45 mm with a higher velocity. This difference is confirmed by DRMS which presents a higher stone resistance for untreated stone, the part with higher ultrasound pulse velocity. Therefore, the difference between treated and not treated parts registered with DRMS are due to a non homogeneous mock-up, characteristic of natural stones.

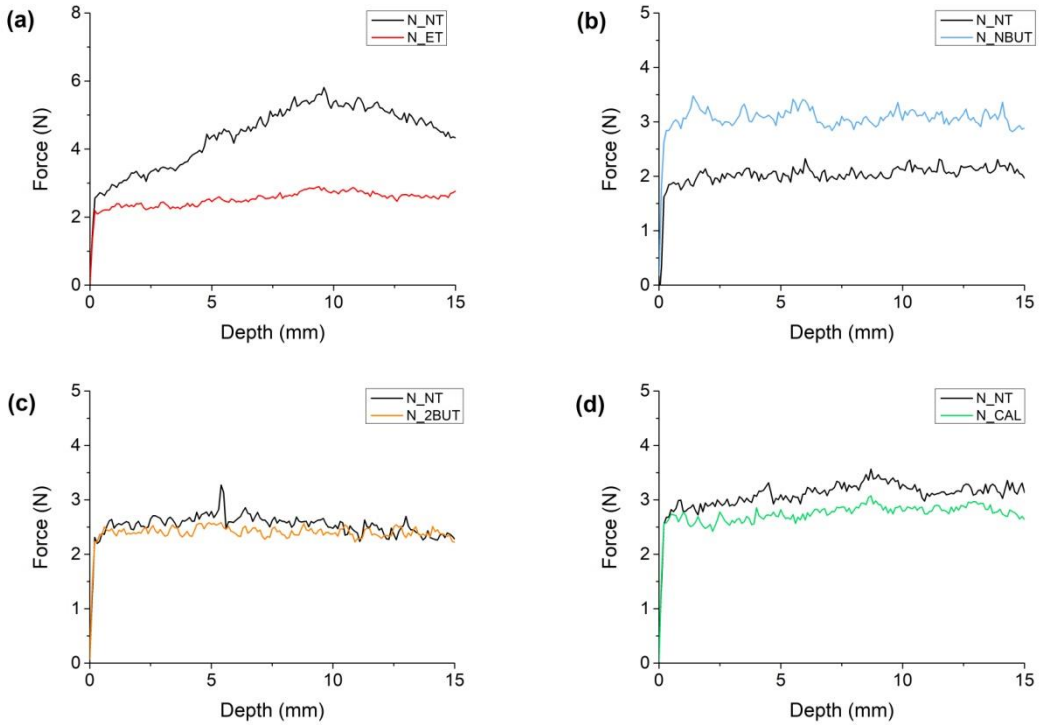

Figure 3.59 *- Drilling profiles before and after treatment:* ***(a)*** *N_ET,* ***(b)*** *N_NBUT* ***(c)*** *N_2BUT and* ***(d)*** *N_CAL.*

Looking at the overall results regarding application by brush till saturation, all tested consolidating agents change water transport properties of stone by reducing water absorption through capillarity and water vapour permeability in a tolerable way; therefore, they are compatible with this stone support. MIP measurement shows that all products are able to reduce stone open porosity; but, in accordance with SEM images, the reference product seems to form a superficial layer on the treated surface.
However, this compatible behaviour does not correspond to aesthetical requirement, in fact all products lead to a ΔE^* value higher than 5. Furthermore, among all consolidating agents, the only product which can penetrate more in depth is *NBUT*.

3.3.2.2 Application procedure: by brush with pre-set number of brush strokes

This application procedure was performed only for calcium ethoxide nanosuspension diluted in ethanol and the reference product. The maximum number of brush strokes for Noto stone to avoid a colour change of the surface ($\Delta E^* > 5$) was 8. ΔE^* results calculated after 8 applications were: 4.5 ± 0.4 for *N_ET* and 2.1 ± 0.8 for *N_CAL*.
Data regarding the quantity of product retained after one month from the application are presented in **Tab. 3.12**. The results are reported as a range of value between the minimum and the maximum quantity for each type of product. As for the application by brush till saturation, differences among quantity of product retained for samples treated with the same product are probably due to the different shape of mock-ups (in accordance to the different analyses, mock-ups of different dimensions were necessary). More details of product retained in relation to the different analyses are shown in **Tab. C.8** in **Appendix C**.
By comparing these results with those obtained after application by brush till saturation, it can be seen that in this case the amount of product retained is a bit lower respect to the previous application procedure.

Table 3.12 *- Application by brush with pre-set number of brush strokes: range of amount of product retained after one month from the application.*

Product	Quantity of product retained (kg/m²)
ET	0.017 – 0.051
CAL	0.010 – 0.025

Information concerning water transport inside the material was obtained with capillary water absorption test, drying behaviour and water vapour permeability test. For each test, data are reported as the average of three samples. The quantity of water absorbed in the first 45 minutes (**Fig. 3.60)**, decrease for treated samples respect to untreated ones.

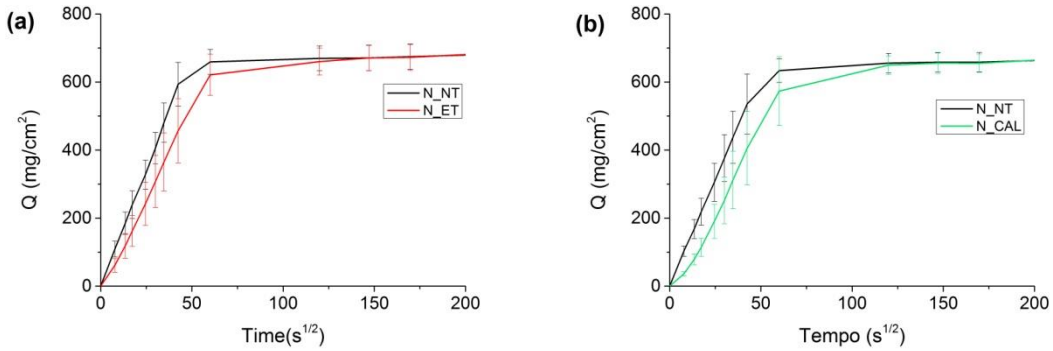

Figure 3.60 *- Quantity of water absorbed by capillarity, comparison before and after treatment:* ***(a)*** *N_ET and* ***(b)*** *N_CAL.*

Also the capillary water absorption coefficient (**Fig. 3.61**) shows a major reduction for *N_ET* (from 13.9 ± 1.1 mg/cm^2·s$^{1/2}$ to 10.7 ± 2.0 mg/cm^2·s$^{1/2}$) respect to *N_CAL* (from 12.6 ± 1.8 mg/cm^2·s$^{1/2}$ to 10.6 ± 1.2 mg/cm^2·s$^{1/2}$).

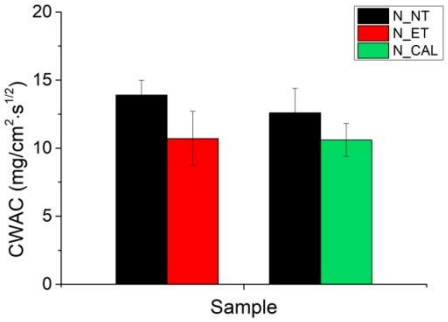

Figure 3.61 *- Comparison of capillary water absorption coefficient (CWAC) between treated and untreated samples.*

Results regarding the drying behaviour (**Fig. 3.62**) show that for both treatments the time required to reach a drying state is a bit higher respect to untreated samples.

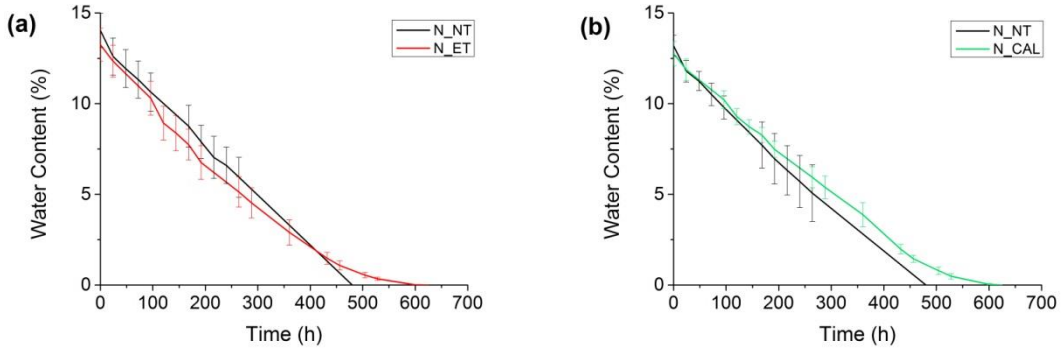

Figure 3.62 *- Comparison of drying curves between treated and untreated samples:* ***(a)*** *N_ET and* ***(b)*** *N_CAL.*

Water vapour permeability test (**Fig 3.63**) confirms water absorption test showing a decrease in water vapour permeability for both treatments, with an excessive reduction for *N_ET* (from 156.74 ± 9.77 g/m^2·s to 90.93 ± 1.01 g/m^2·s).

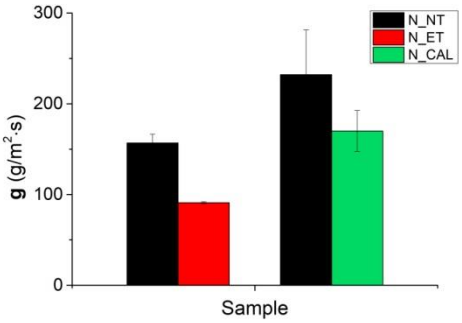

Figure 3.63 *- Water vapour permeability test results expressed as water vapour permeability coefficient (g) and reported as comparison before and after treatment.*

Changes in total open porosity and cumulative volume due to the applied treatments calculated by MIP are reported in **Tab. 3.13**. The results indicate that both treatments lead to a reduction of porosity value similar to not-aged sample (30.3 ± 0.9% as reported in paragraph 3.3.2).

Table 3.13 *- Porosity data obtained by MIP measurements, reported as comparison between treated and untreated samples.*

Sample code	Total open porosity (%)	Total cumulative volume (mm^3/g)
N_NT	34.5 ± 2.6	173.4 ± 0.9
N_ET	30.1 ± 1.9	172.1 ± 0.9
N_CAL	28.9 ± 0.8	166.3 ± 5.6

Variation in pores radius dimension after treatments are reported in **Fig. 3.64**; the results show that both treatments lead to a decrease of average pores radius.

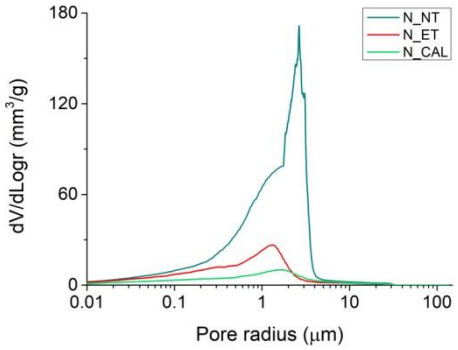

Figure 3.64 *- Pore size distribution curves expressed as log differential intruded volume vs. pore radius of untreated and treated samples.*

Porosity distribution and cumulative volume reported as function of pore radius are graphically shown in **Fig. 3.65**. As reported in **Tab. 3.8**, both treatments cause a change in porosity and cumulative volume distribution, with a major reduction for pores with radius between 2-4 μm. In particular, *ET* leads to a decrease of pores with radius between 2-10 μm, and an increase of pores with radius between 1-2 μm (**Fig. 3.65 (b)**).

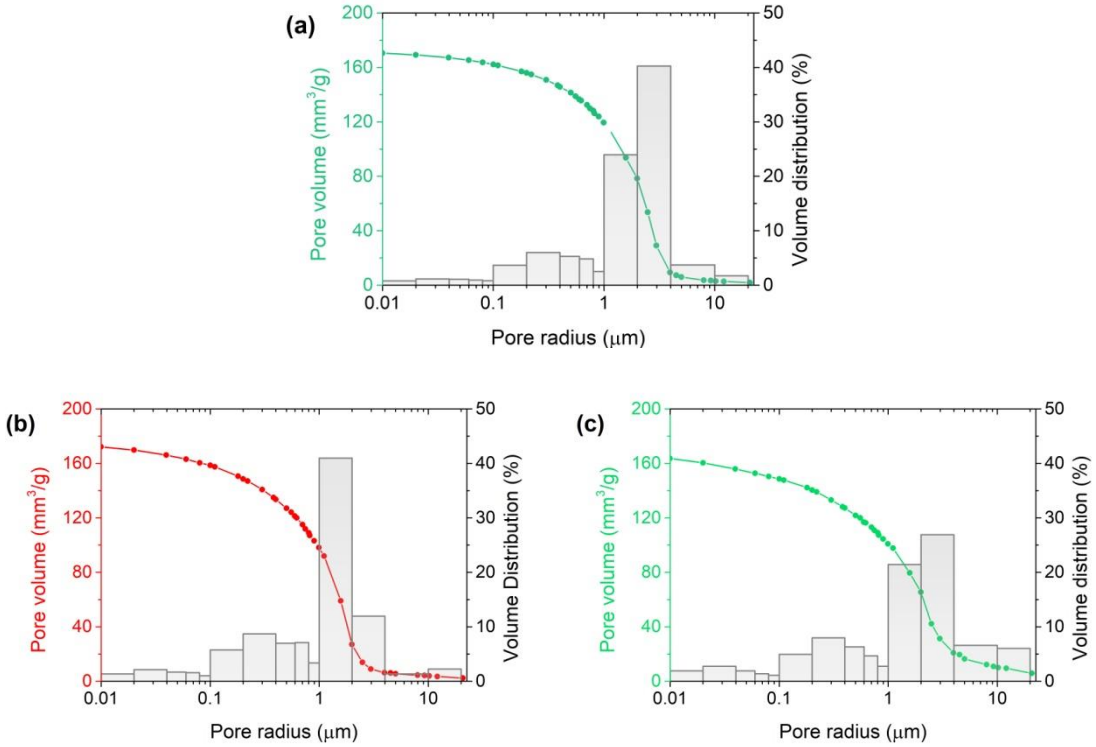

Figure 3.65 *- Cumulative pore volume and volume distribution versus pore radius:* ***(a)*** *N_NT,* ***(b)*** *N_ET and* ***(c)*** *N_CAL.*

While, *N_CAL* show a decrease of pores with radius between 1-4 μm, but a bit increase for pores with radius greater than 4 μm (**Fig. 3.65 (c)**).

Looking at NMR results (**Fig. 3.66**) T2 distribution functions of treated samples are qualitatively different respect to untreated ones for both treatments. In particular, bigger changes are visible for pores of higher dimensions (T > 10 ms), as reported also for MIP measurements.

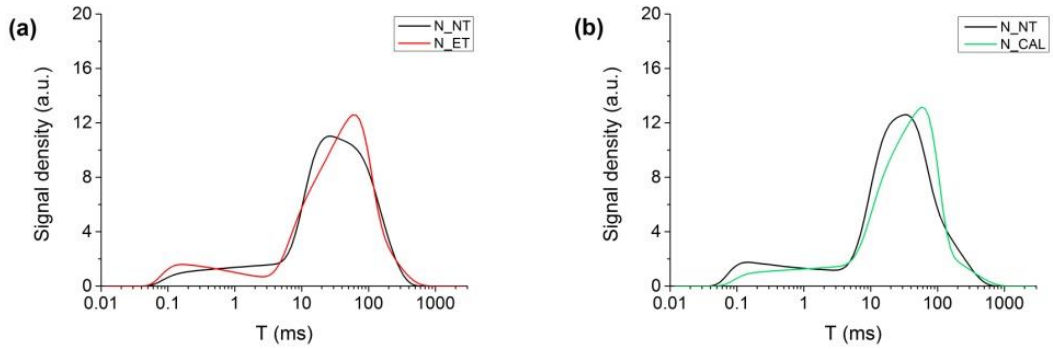

Figure 3.66 *- Comparison of T2 distribution functions between treated and untreated samples:* ***(a)*** *N_ET and* ***(b)*** *N_CAL.*

As discussed for Noto samples treated by brush till saturation, also with a pre-set number of brush strokes, only surface treated with *ET* shows no visible difference with untreated surface, while *N_CAL* presents a superficial layer on the surface (**Fig. 3.67**).

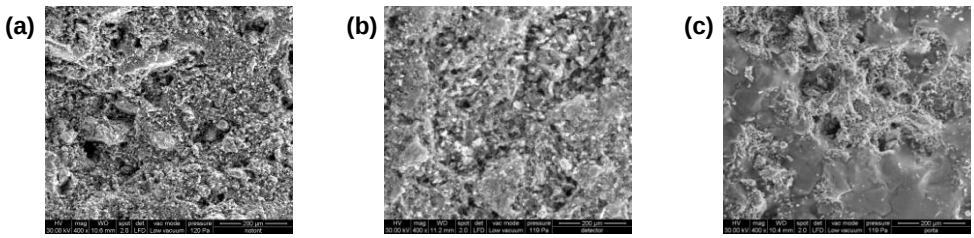

Figure 3.67 *- Surface observation with SEM:* ***(a)*** *N_NT,* ***(b)*** *N_ET and* ***(c)*** *N_CAL*

For this type of application procedure, ultrasonic pulse velocity and drilling resistance measurement system were not performed.

In conclusion, even if the amount of product retained is lower than application by brush till saturation, the several analyses show how both *ET* and *CAL* applied with a controlled number of brush strokes produce a similar porosity variation and they are compatible with the treated support leading to a variation of water transport properties and porosity value in a acceptable range. Therefore, as the results between two applications procedures are comparable and since a controlled number of brush strokes prevents a colour change of the

surface, it can be considered a better application procedure than brush till saturation. However, analysis regarding the ability of both treatments to penetrate inside the stone are fundamental to have a complete picture of their effectiveness as consolidating products.

3.3.2.3 Application procedure: by absorption through capillarity

Regarding this application procedure, treated and untreated samples were analysed only with ultrasonic pulse velocity and drilling resistance measurement system to understand if this different type of application can produce a different penetration of treatments. Colorimetric measurements were carried out to evaluate chromatic effect due to the treatments. The analysed samples are the same for the three analyses. **Tab. 3.14** reports data regarding the quantity of product retained after one month from the application.

Table 3.14 *- Application by absorption through capillarity: amount of product retained after one month from the application.*

Product	Quantity of product retained (kg/m²)
ET	0.107
NBUT	0.235
2BUT	0.478
CAL	0.138

By comparing this type of application procedure with the others, in this casa a bigger amount of product was retained from the treated samples.

The fringe reached by the products during the proof are reported in **Tab. C.9** in **Appendix C**.

Despite a better penetration of *CAL (***Tab. C.9**, **Appendix C)**, UPV results show that only *NBUT* causes an increase of UPV velocity with a penetration till 35 mm from the treated surface; *2BUT* shows a small increase of UPV in the first 20 mm from the surface, while profiles related to *N_CAL* and *N_ET* are similar before and after treatment (**Fig 3.68**). Despite, a bigger amount of retained product respect to application by brush till saturation, also in this case, only *NBUT* causes an increase of UPV values. More details about UPV values before and after treatments for all products are reported in **Tab. C.10** (**Appendix C**).

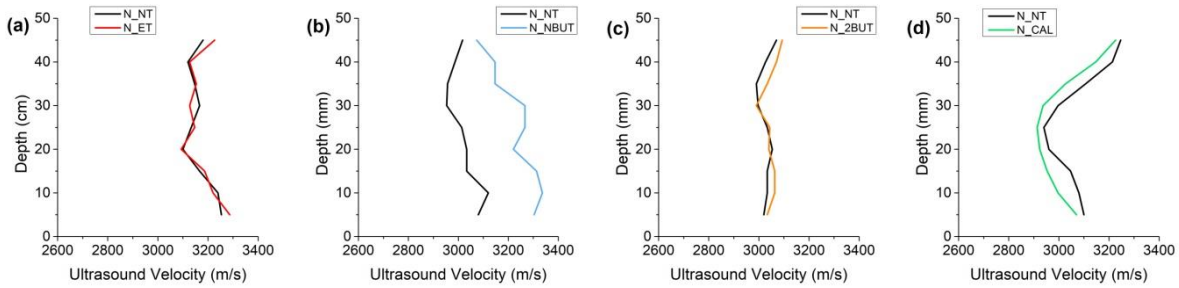

Figure 3.68 *- Ultrasonic profile before and after treatment:* ***(a)*** *N_ET,* ***(b)*** *N_NBUT,* ***(c)*** *N_2BUT and* ***(d)*** *N_CAL.*

Drilling measurements (**Fig. 3.69**) confirm UPV results showing an increase of stone resistance for *N_NBUT* from 2,2 N to 3 N in the first 10 mm (**Fig. 3.69 (b)**).

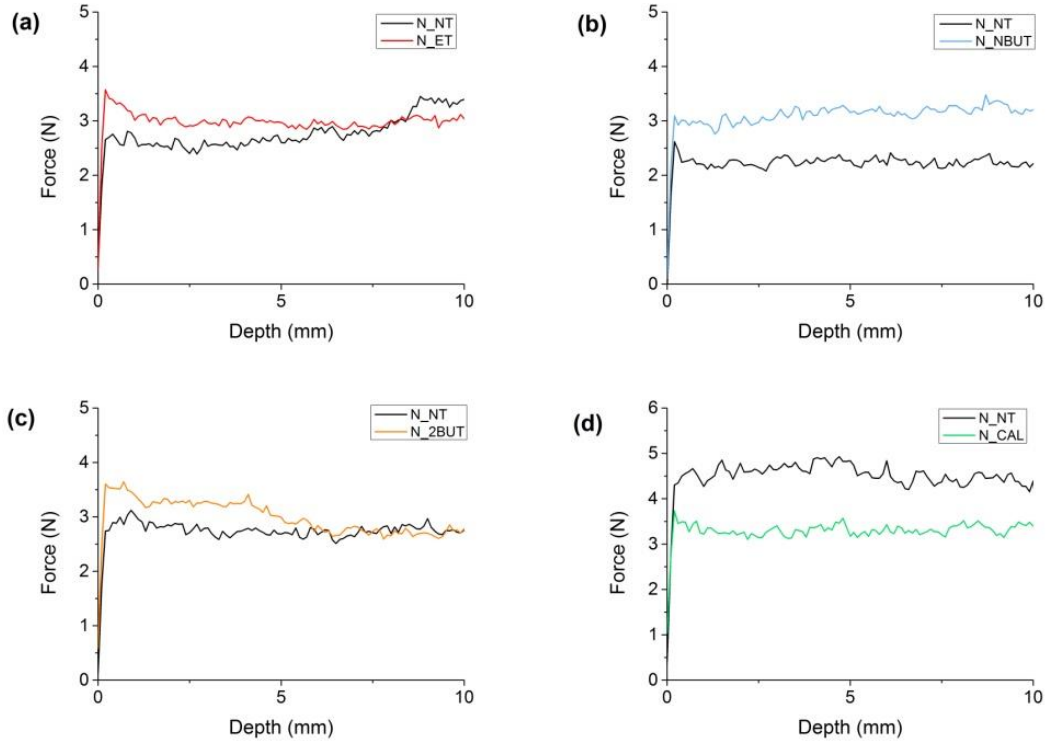

Figure 3.69 *- Drilling profiles before and after treatment:* ***(a)*** *N_ET,* ***(b)*** *N_NBUT,* ***(c)*** *N_2BUT and* ***(d)*** *N_CAL.*

While DRMS related to *N_ET* and *N_2BUT* shows a small increase of stone resistance in the first 5 mm below the treated surface. These data cannot be confirmed by UPV, because data acquired by this measurement starts 5 mm below the surface. Furthermore, the difference in stone resistance registered for *N_CAL* with DRMS is probably due to the heterogeneity of the specimen between treated and untreated faces, rather than the treatment. In fact, also UPV measurements show two different velocities between 5-25 cm and 25-45 cm from the

treated surface, with a higher UPV in the second part which correspond to the not-treated one analysed with DRMS.

Regarding the colour change of the surface, also with this type of application procedure, all treatments lead to ΔE^* value higher than the acceptable limit (**Fig 3.70**).

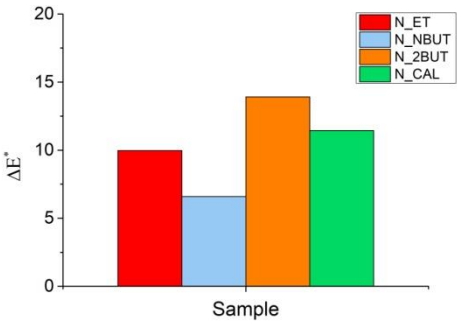

Figure 3.70 *- Colour variation ⊿E* generated by four consolidating products.*

Making a comparison between results obtained with UPV and DRSM between applications by brush till saturation and by absorption through capillarity, both techniques agree that the best consolidating agent for Noto stone is calcium ethoxide nanosuspension diluted in n-butylacetate. In fact, both an increase of UPV and stone resistance is obtained, indicating a consolidating effect produced by this treatment. Despite *2BUT* is the most retained product, it did not led to a consolidating effect, probably because the treatment remained most of all on the surface; therefore, no UPV increase is registered with a penetration higher than 5 mm.

3.3.3 Vicenza Stone

This organogenic limestone is characterized by the presence of 95.6% of calcium carbonate determined on the base of mass loss of 41.5% between 600-800 cm^{-1}, as shown by TG-DSC analysis (**Fig. 3.71 (a)**).

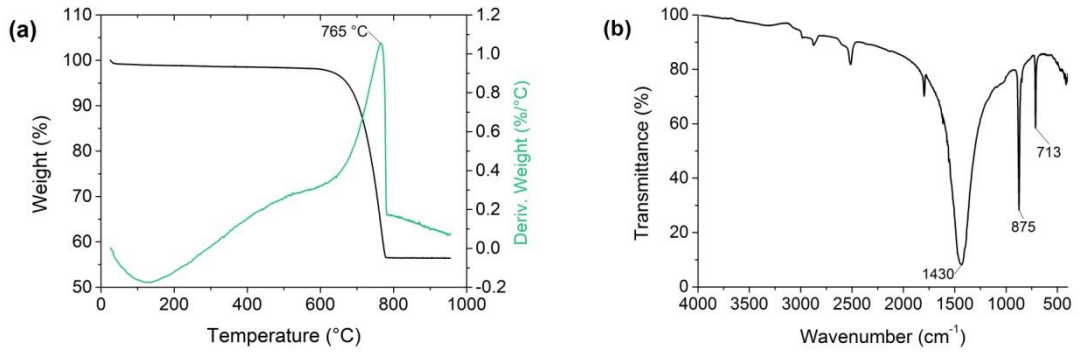

Figure 3.71 *- Chemical characterization of Vicenza stone by* ***(a)*** *TG-DSC and* ***(b)*** *FT-IR analyses.*

FT-IR analysis agrees with TG-DSC result showing the characteristic vibrational peaks of calcite (1430, 875 and 713 cm^{-1}) (**Fig. 3.71 (b)**). Furthermore, a small shoulder between 1014 and 1120 cm^{-1} is associated to asymmetric stretching vibration of silicon-oxygen group (Si-O). Therefore, a silicate component is present.

The effect of ageing test for this type of stone - evaluated with MIP analysis - is particular because instead of an increase of porosity, this process led to a decrease of this value moving from an initial porosity value of 31.2 ± 1.9% to a final one of 28.3 ± 0.8% (**Fig. 3.72**). In accordance with this value, also the cumulative volume changed from a higher value of 149.9 ± 12.7 mm^3/g to a lower value of 131.5 ± 4.1 mm^3/g. This result may be related to an internal stress induced by the ageing process, which led to the clogging of internal open porosity. This ageing process caused a decrease of pores with radius between 0.2-0.4 μm, and an increase of pores between 0.1-0.2 μm and bigger than 10 μm.

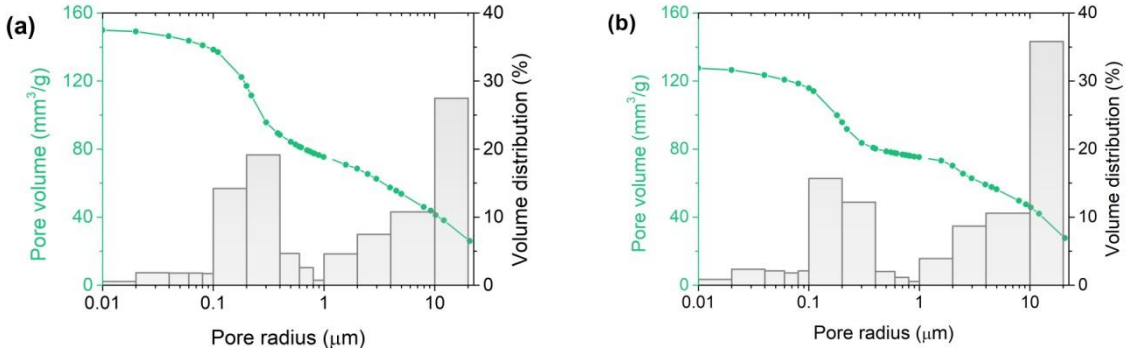

Figure 3.72 *- Cumulative pore volume and volume distribution versus pore radius of* ***(a)*** *not aged and* ***(b)*** *aged Vicenza stone.*

In the following paragraphs, results regarding the efficacy of four products as consolidating agents for Vicenza stone, applied with different application procedures, will be discussed.

3.3.3.1 Application procedure: by brush till saturation

In this section, results regarding the several analyses performed to test the efficacy of the four products applied by brush till saturation are reported. **Tab. 3.15** reports data regarding the quantity of product retained after one month from the application. The results are reported as a range of value between the minimum and the maximum quantity for each type of product. Differences among quantity of product retained for samples treated with the same product are probably due to the different shape of mock-ups (in accordance to the different analyses,

mock-ups of different dimensions were necessary). More details of product retained in relation to the different analyses and material tests are shown in **Tab. C.11** in **Appendix C**.

Table 3.15 *- Application by brush till saturation: range of amount of product retained after one month from the application.*

Product	Quantity of product retained (kg/m²)
ET	0.011 – 0.060
NBUT	0.028 – 0.058
2BUT	0.012 – 0.051
CAL	0.027 – 0.210

Regarding the quantity of retained product, the range of value are similar for all type of treatments. Only *CAL* leads to a major quantity of product retained, in particular for samples treated for UPV and DRMS analyses.

Water transport properties were evaluated with three types of tests as for other carbonate stones. All the treatments, included the reference one (CaLoSil), reduce the water absorption in the first 45 minutes of the test and the capillary water absorption coefficient, whit a too high change for *V_ET* (from 17.9 ± 1.2 mg/cm^2·s$^{1/2}$ to 11.3 ± 1.4 mg/cm^2·s$^{1/2}$) and *V_CAL* (from 18.8 ± 0.5 mg/cm^2·s$^{1/2}$ to 13.3 ± 2.7 mg/cm^2·s$^{1/2}$) (**Fig. 3.73** and **Fig. 3.74**). Despite *V_CAL* presents a major quantity of retained product, the effect of this treatment and *ET* is comparable. This behaviour could be related to a non homogeneous distribution of *CAL* inside the sample.

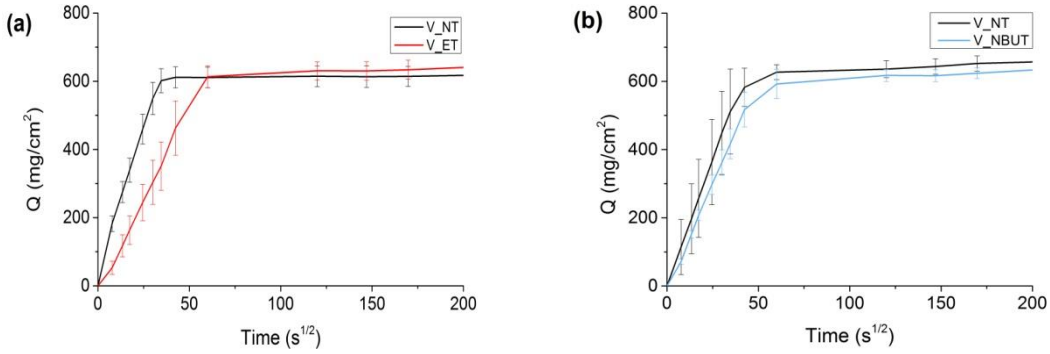

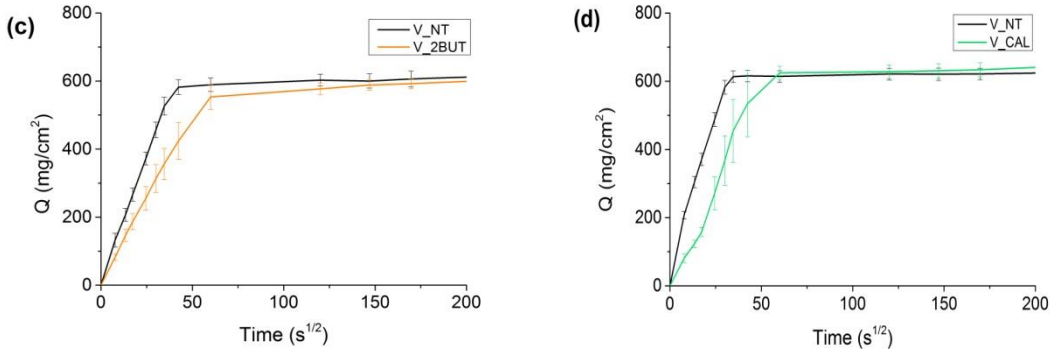

Figure 3.73 *- Quantity of water absorbed by capillarity, comparison before and after treatment:* ***(a)*** *V_ET,* ***(b)*** *V_NBUT,* ***(c)*** *V_2BUT and* ***(d)*** *V_CAL.*

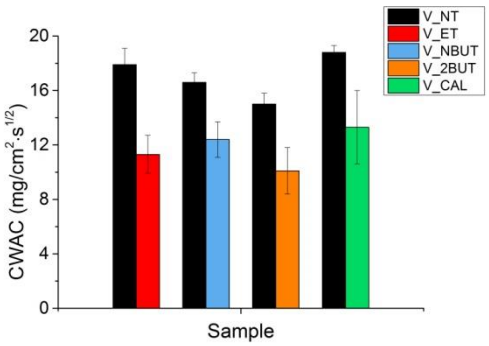

Figure 3.74 *- Comparison capillary water absorption coefficient (CWAC) before and after treatment.*

By comparing the drying rate, *V_ET, V_2BUT, V_CAL* show a similar behaviour between treated and untreated samples, while *V_NBUT* shows a slower drying particularly from the half of the test (**Fig. 3.75**).

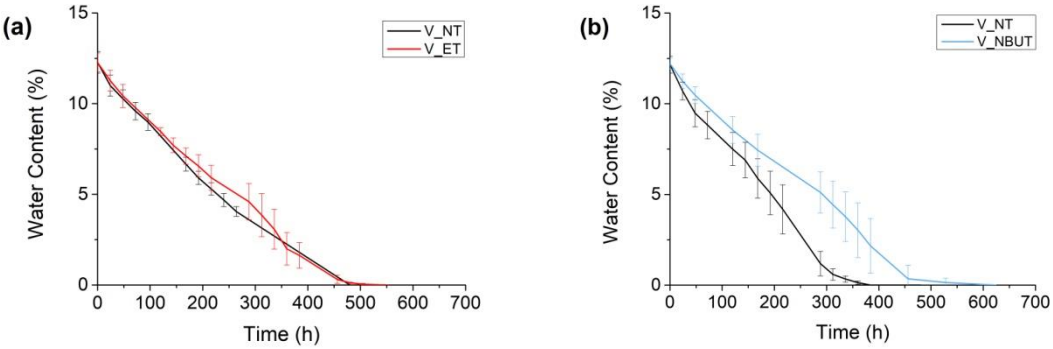

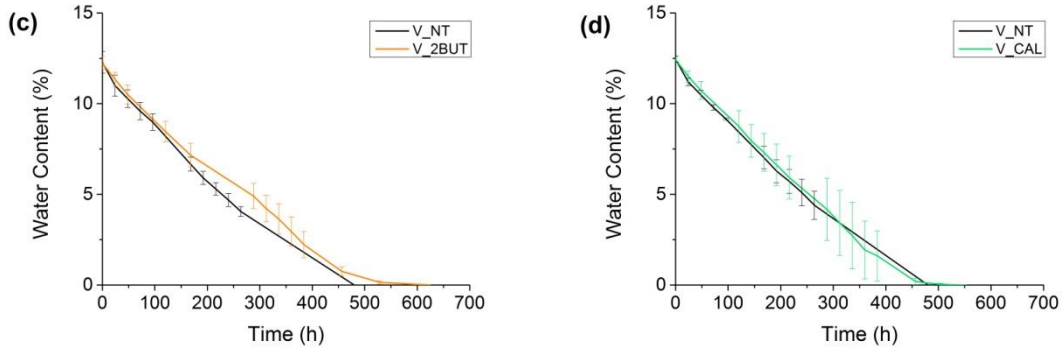

Figure 3.75 *- Comparison of drying curves before and after treatment:* ***(a)*** *V_ET,* ***(b)*** *V_NBUT,* ***(c)*** *V_2BUT and* ***(d)*** *V_CAL.*

Regarding the water vapour permeability test, all treatments based on calcium ethoxide cause a reduction of water vapour permeability to an acceptable limit (**Fig. 3.76**).

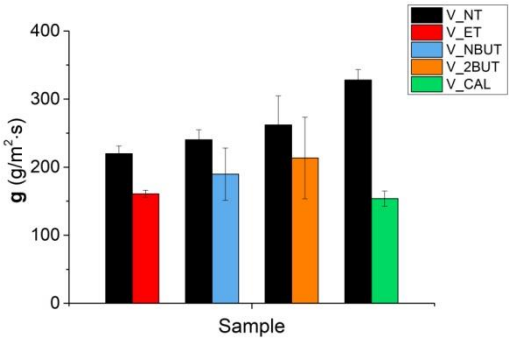

Figure 3.76 *- Water vapour permeability test results expressed as water vapour permeability coefficient (g) and reported as comparison before and after treatment.*

On the contrary, *V_CAL* presents an excessive g reduction respect to untreated stone (from 328.19 ± 15.26 g/m²·s to 153.89 ± 11.06 g/m²·s), causing an unacceptable change of water vapour properties [37].

Total open porosity and total cumulative volume for untreated and treated stone are reported in **Tab. 3.16**. Treatments which are effective in reducing the total open porosity are those based on $Ca(OEt)_2$ nanosuspension.

Table 3.16 *- Porosity data obtained by MIP measurements, reported as comparison between treated and untreated samples.*

Sample code	Total open porosity (%)	Total cumulative volume (mm^3/g)
V_NT	28.3 ± 0.8	131.5 ± 4.1
V_ET	24.9 ± 0.4	113.1 ± 4.2
V_NBUT	24.4 ± 0.9	149.0 ± 2.2
V_2BUT	24.5 ± 1.1	123.8 ± 3.8
V_CAL	28.1 ± 1.4	139.8 ± 3.2

All the products maintain constant the bimodal pores size distribution of untreated stone (**Fig. 3.77** and **Fig. 3.78**). Respect to untreated samples, *ET* causes a small reduction of pores with radius between 2-4 μm; *NBUT* leads to a decrease of pores with radius between 0.1-0.4 μm and 2-10 μm; *2BUT* reduces pores with radius greater than 10 μm but increase those ones between 0.2-0.4 μm and 2-10 μm; finally, *N_CAL* show a decrease in pores higher than 10 μm, with an increase of those ones between 0.2-0.4 μm.

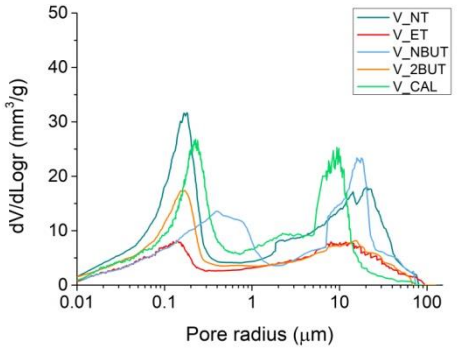

Figure 3.77 *- Pore size distribution curves expressed as log differential intruded volume vs. pore radius of untreated and treated samples.*

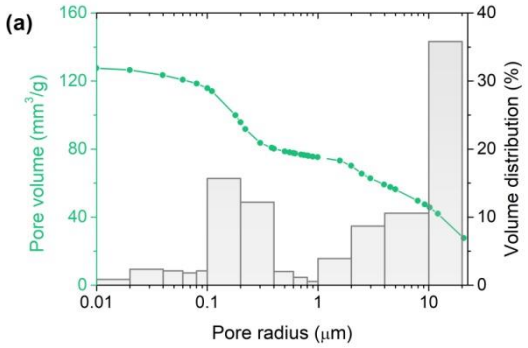

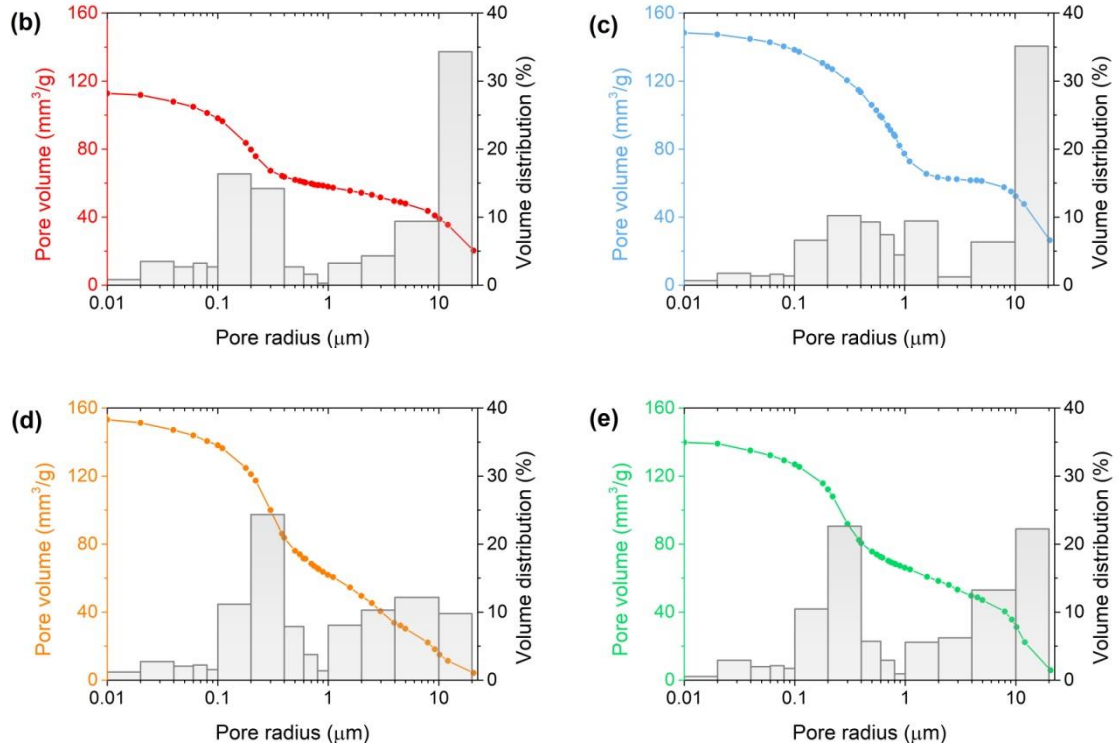

Figure 3.78 *- Cumulative pore volume and volume distribution versus pore radius:* ***(a)*** *V_NT,* ***(b)*** *V_ET,* ***(c)*** *V_NBUT,* ***(d)*** *V_2BUT and* ***(d)*** *V_CAL.*

In this case, NMR results (**Fig. 3.79**) are not always consistent with MIP analysis. In fact, a qualitative analysis of T2 distribution functions shows that *ET* causes a change only for pores of smaller dimensions, an effect not visible for MIP analysis for which only a change in pores of bigger dimension is evident (**Fig. 3.78 (a)**). *NBUT* leads to a change in pores of smaller dimension, as detected also for MIP analysis, but evident changes for pore of higher dimensions are not present, differently from MIP analysis (**Fig 3.78 (b)**). *2BUT* causes a variation for pores of bigger dimensions (**Fig. 3.78 (c)**), while *CAL* leads to a change for both pores of smaller and bigger dimensions (**Fig. 3.78 (d)**), as detected by MIP.

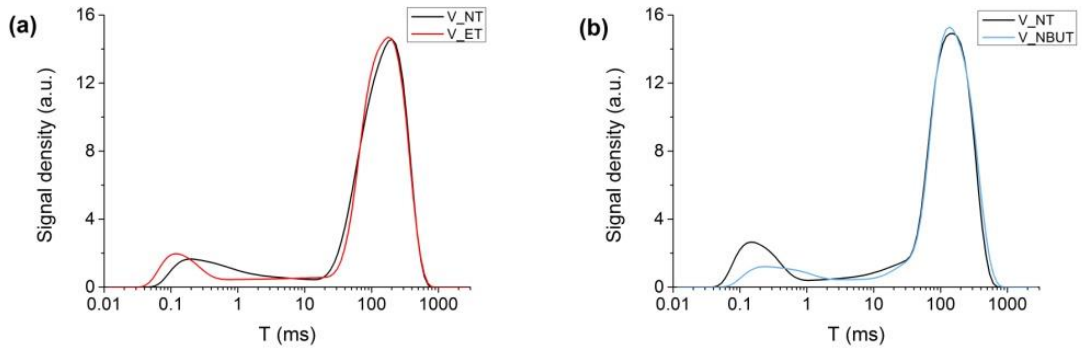

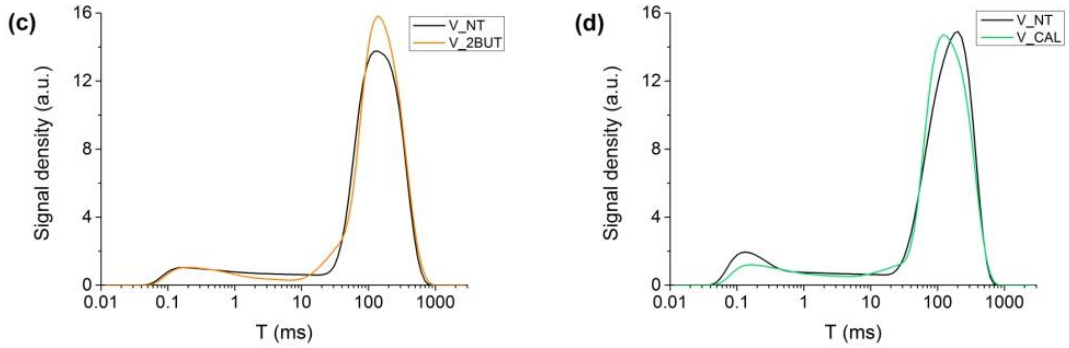

Figure 3.79 *- Comparison of T2 distribution functions before and after treatment:* ***(a)*** *V_ET,* ***(b)*** *V_NBUT,* ***(c)*** *V_2BUT and* ***(d)*** *V_CAL.*

Differently from the carbonate stones seen previously - Lecce and Noto stones - in this case only *2BUT* causes a not acceptable variation of surface colour ($\Delta E^*>5$) (**Fig. 3.80**).

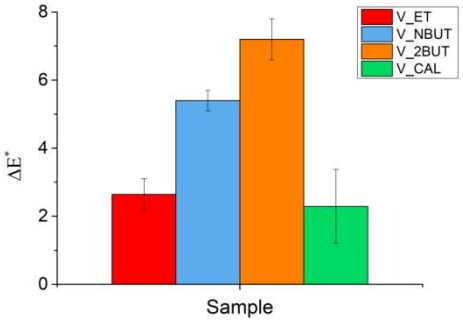

Figure 3.80 *- Colour variation ⊿E* generated by four consolidating products.*

As for the previous carbonate stone, by observing the treated surface with SEM, products based on calcium ethoxide nanosuspension seem to not alter the surface of the stone, while *CAL* creates a superficial layer on the treated surface (**Fig. 3.81**).

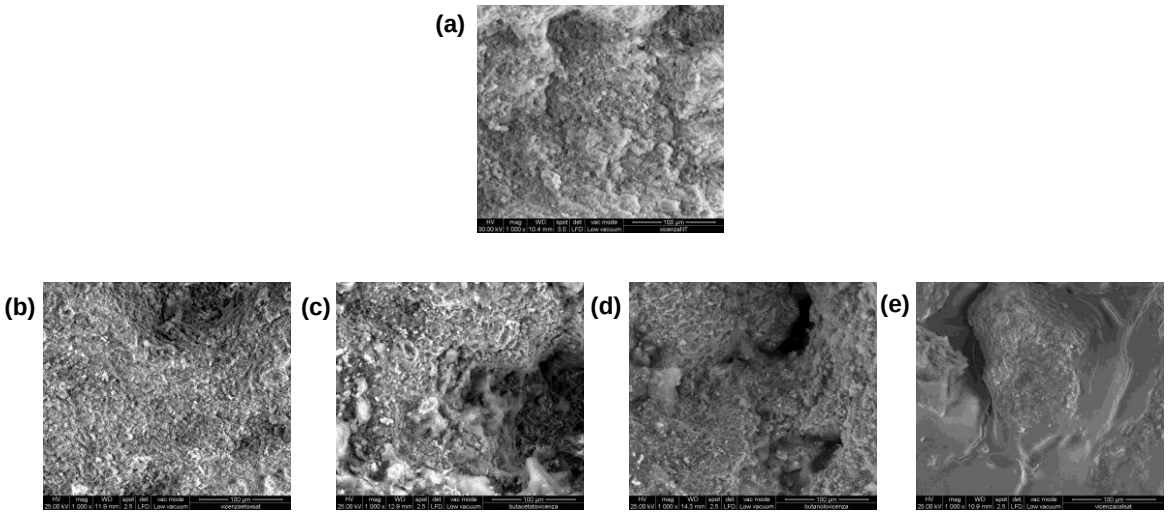

Figure 3.81 *- Surface observation with SEM:* ***(a)*** *V_NT,* ***(b)*** *V_ET,* ***(c)*** *V_NBUT,* ***d)*** *V_2BUT and* ***e)*** *V_CAL.*

Ultrasound pulse velocity were obtained and reported in the same way of previous carbonate stones. The graphs in **Fig. 3.82** show that all treatments cause a small increase of stone resistance in the first millimetres from the treated surface, except for *V_CAL* - even if *CAL* corresponds to the product most retained during this analysis. More details about UPV values before and after treatments for all products are reported in **Tab. C.12** (**Appendix C**).

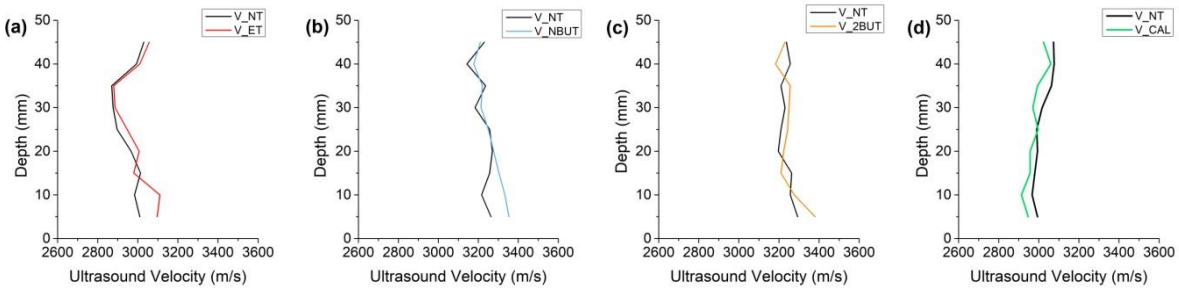

Figure 3.82 *- Ultrasonic profile before and after treatment:* ***(a)*** *V_ET,* ***(b)*** *V_NBUT,* ***(c)*** *V_2BUT and* ***(d)*** *V_CAL.*

UPV are only partly confirmed by drilling test; in fact, DRMS shows how for *V_2BUT* an increase of stone resistance only in the first mm below the surface is evident, while starting from 5 mm no meaningful change between treated and untreated profiles are visible, differently from UPV for which a decrease of stone porosity is registered also between 5-10 mm from the treated surface (**Fig. 3.83 (c)**). Also the increase of UPV for *V_ET* between 5-10 mm are not confirmed by DRMS.

Only *V_NBUT* presents a small increase of stone resistance few mm from the treated surface, as shown by UPV results. Probably this effect could be related to the higher boiling point of the solvent which by delaying the beginning of the carbonation process can lead to a higher penetration of the product.

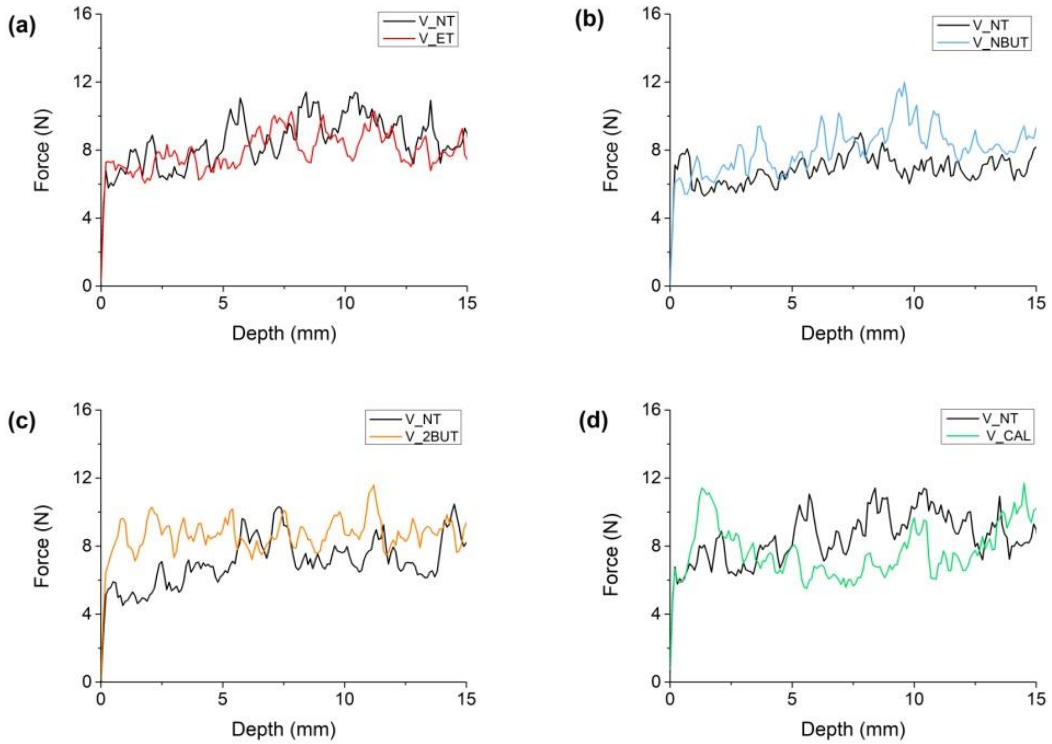

Figure 3.83 *- Drilling profiles before and after treatment:* ***(a)*** *V_ET,* ***(b)*** *V_NBUT,* ***(c)*** *V_2BUT and* ***(d)*** *V_CAL.*

Looking at the overall results, treatments based on calcium ethoxide nanosuspension present better results respect to the reference product. Considering the analyses regarding water transport properties inside the stone, *2BUT* and *NBUT* show a better performance, reducing the water absorption coefficient and the water vapour permeability but remaining in an acceptable range of variation respect to untreated stone, differently from *V_ET*. Furthermore, both *2BUT* and *NBUT* lead to a variation of stone porosity after treatment, but both of them change considerably the colour of the treated surface. UPV and DRMS measurements show that *2BUT* can penetrate inside the stone for 5 mm, while *NBUT* causes a small variation of stone resistance.

3.3.3.2 Application procedure: by brush with pre-set number of brush strokes

This application procedure was performed only for calcium ethoxide diluted in ethanol and the reference product. The number of applications for Vicenza stone, decided on the basis of the colorimetric measurements performed after each brush stroke, was 11. Colour change of the surface (ΔE^*) was 2.0 ± 0.3 for *V_ET* and 1.8 ± 0.6 for *V_CAL*. **Tab. 3.17** reports data regarding the quantity of product retained after one month from the application. The results are reported as a range of value between the minimum and the maximum quantity for each product. Small differences among quantity of product retained for samples treated with the same product are probably due to the different shape of mock-ups (in accordance to the different analyses, mock-ups of different dimensions were necessary). More details of product retained in relation to the different analyses are shown in **Tab. C.13** in **Appendix C**.

Table 3.17 *- Application by brush with pre-set number of brush strokes: range of amount of product retained after one month from the application.*

Product	Quantity of product retained (kg/m²)
ET	0.019 – 0.053
CAL	0.014 – 0.062

Results regarding water absorption through capillarity are reported in **Fig. 3.84** and **Fig. 3.85**. The graphs indicate that both treatments lead to a reduction of water absorbed in an acceptable way.

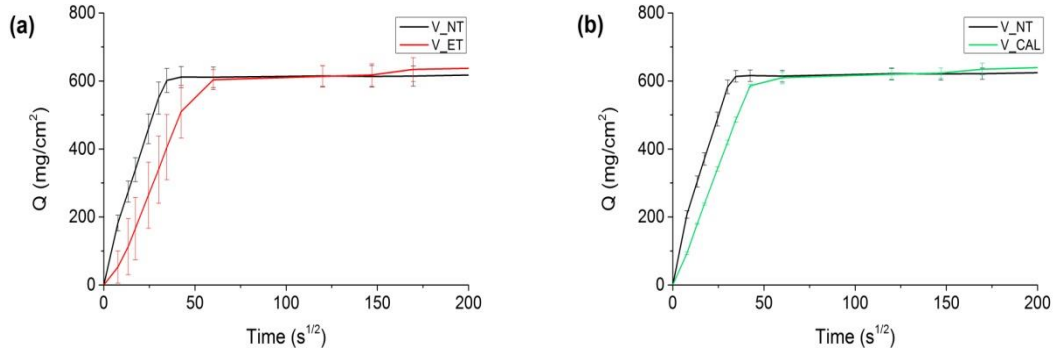

Figure 3.84 *- Quantity of water absorbed by capillarity, comparison before and after treatment:* ***(a)*** *V_ET and* ***(b)*** *V_CAL.*

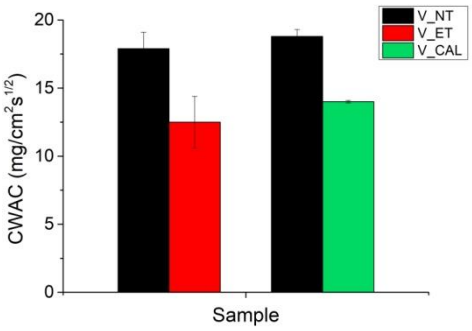

Figure 3.85 *- Comparison of capillary water absorption coefficient (CWAC) before and after treatment.*

By analyzing the drying behaviour of the stone, both treatments do not alter significantly the drying rate of the stone (**Fig. 3.86**). However, *ET* slows down the process of water evaporation.

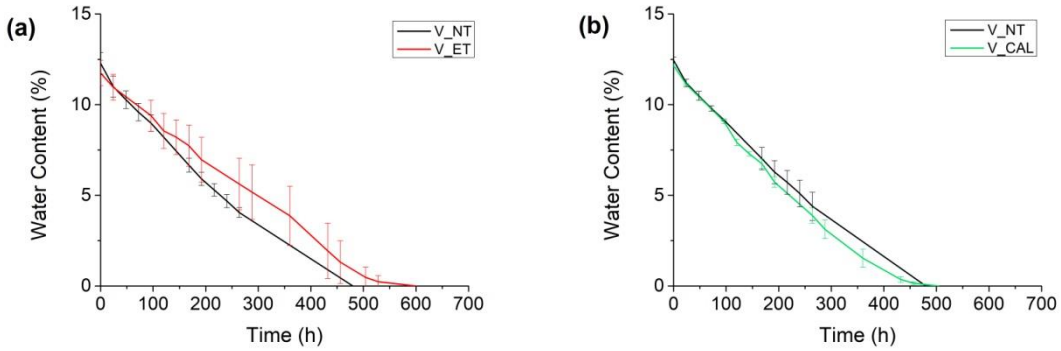

Figure 3.86 *- Comparison of drying curves before and after treatment:* ***(a)*** *V_ET and* ***(b)*** *V_CAL.*

Both treatments reduce the water vapour permeability with respect to untreated samples, with a reduction of g value higher than 25% for *V_CAL* (from 328.13 ± 15.26 g/m^2·s to 193.22 ± 19.39 g/m^2·s), the maximum value for an acceptable change [37] (**Fig. 3.87**).

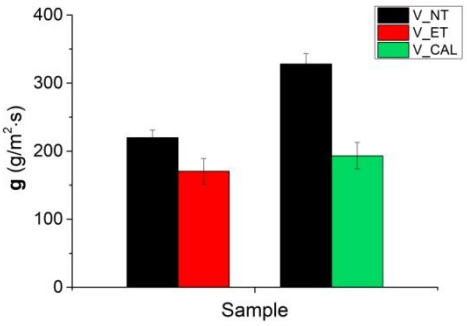

Figure 3.87 *- Water vapour permeability test results expressed as water vapour permeability coefficient (g) and reported as comparison before and after treatment.*

Changes in total open porosity and cumulative volume due to the applied treatments calculated by mercury intrusion porosimetry are reported in **Tab 3.18**; while, **Fig. 3.88** shows how both treatments maintain a bimodal pore radius distribution. *ET* leads to a reduction of pores with radius >10 μm and increase those ones between 4-10 μm (**Fig. 3.89 (b)**); while *CAL* reduces pores with radius > 2 μm and slightly increase pore with radius between 0.2-0.4 μm (**Fig. 3.89 (c)**).

Table 3.18 *- Porosity data obtained by MIP measurements, reported as comparison between treated and untreated samples.*

Sample code	Total open porosity (%)	Total cumulative volume (mm^3/g)
V_NT	28.3 ± 0.8	131.5 ± 4.1
V_ET	24.5 ± 1.1	121.9 ± 10.4
V_CAL	24.1 ± 1.2	130.3 ± 1.6

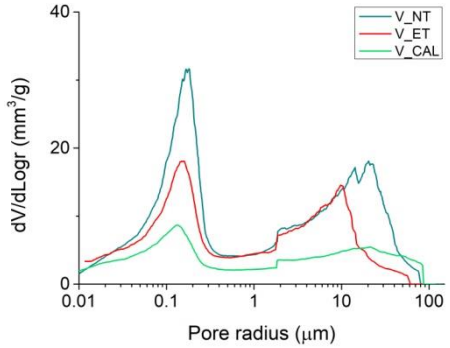

Figure 3.88 *- Pore size distribution curves expressed as log differential intruded volume vs. pore radius of untreated and treated samples.*

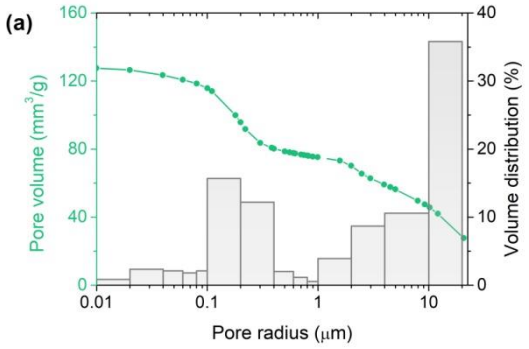

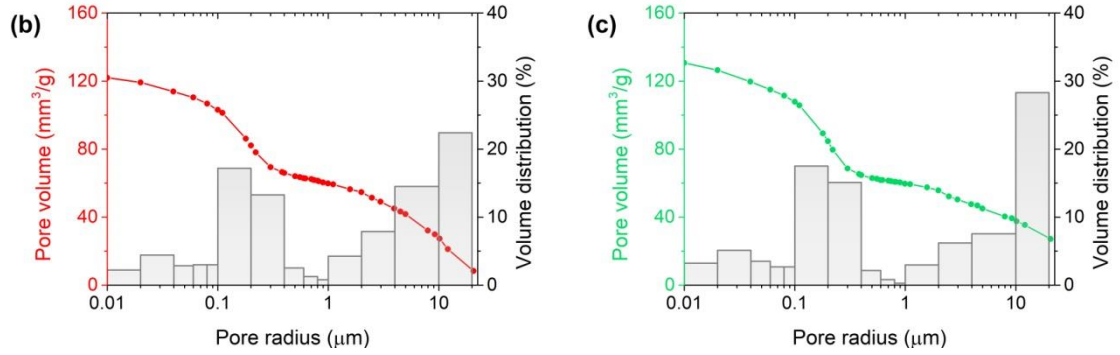

Figure 3.89 *- Cumulative pore volume and volume distribution versus pore radius:* ***(a)*** *V_NT,* ***(b)*** *V_ET and* ***(c)*** *V_CAL.*

NMR relaxometry referred to *V_ET* is not consistent with MIP analysis; in fact, no visible change in T2 curves before and after treatments are visible (**Fig. 3.90 (a)**). Instead, for *V_CAL,* NMR results agree with MIP, by showing a modification of the curve for both pores of smaller (T< 1 ms) and greater dimension (T>10 ms) (**Fig. 3.90 (b)**).

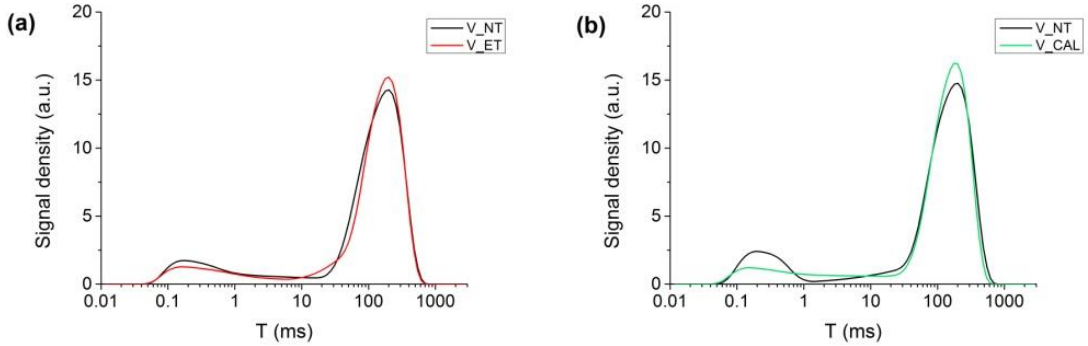

Figure 3.90 *- Comparison of T2 distribution functions before and after treatment:* ***(a)*** *V_ET and* ***(b)*** *V_CAL.*

By observing the surface of support before and after the application of treatments, it can be seen that *CAL* forms a superficial layer on the surface, differently from *ET* (**Fig. 3.91**).

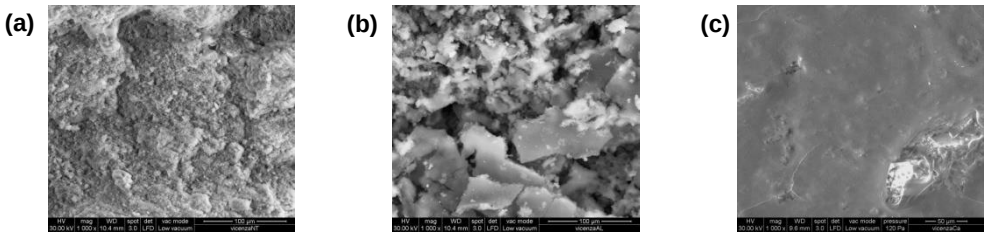

Figure 3.91 *- Surface observation with SEM:* ***(a)*** *V_NT,* ***(b)*** *V_ET and* ***(c)*** *V_CAL.*

For this type of application procedure, results about ultrasonic pulse velocity and drilling measurement system were not performed. Therefore, consideration about the capacity of the consolidating treatments to penetrate inside the stone with this type of application procedure cannot be discussed. Regarding the compatibility between products and stone support, results show that both *ET* and *CAL* change water transport properties and total open porosity compared to untreated stone in a comparable way; but, *CAL* reduces to much the value of water vapour permeability of the stone (from 328.1 to 193.2 g/(m^2·s)) and forms a superficial layer on the treated surface.

3.3.3.3 Application procedure: by absorption through capillarity

Regarding this application procedure, treated and untreated samples were analysed only with ultrasonic pulse velocity and drilling resistance measurement system to acquire information about the penetration of products with a different type of application. Also colorimetric analysis was performed on the same samples. **Tab. 3.19** reports data regarding the quantity of product retained and, with respect to the application by brush till saturation, a higher amount of consolidating agent is retained by the stone treated with calcium ethoxide nanosuspension based treatments; while for *CAL* the situation is different, in fact the quantity of product retained by absorption through capillarity is lower.

Table 3.19 *- Application by absorption through capillarity: amount of product retained after one month from the application.*

Product	Quantity of product retained (kg/m^2)
ET	0.230
NBUT	0.463
2BUT	0.357
CAL	0.154

The fringe reached by the product during the proof are reported in **Tab. C.14** in **Appendix C**.

Fig. 3.92 reports UPV measurements and, looking at the graphs, all treatments based on $Ca(OEt)_2$ nanosuspension seem to penetrate several cm inside the stone (**Fig 3.92 (a)**, **(b)**, **(c)**) in accordance with the fringe reached by these products respect than *CAL* (**Tab. C.14, Appendix C)**.

More details about UPV values before and after treatments for all products are reported in **Tab. C.15** (**Appendix C**).

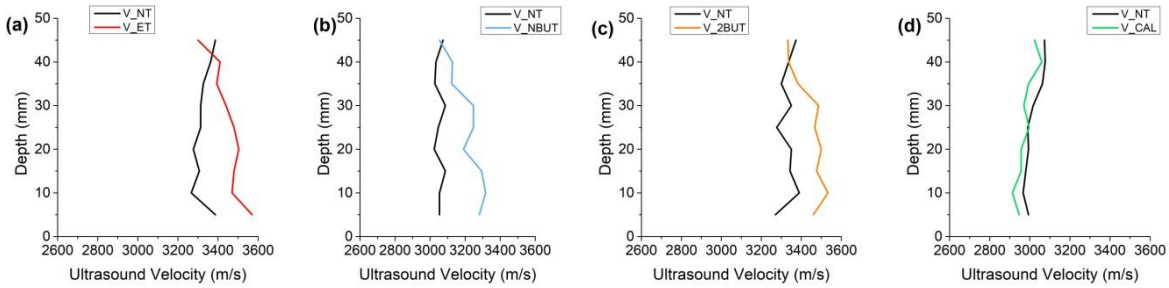

Figure 3.92 *- Ultrasonic profile before and after treatment:* ***(a)*** *V_ET,* ***(b)*** *V_NBUT,* ***(c)*** *V_2BUT and* ***(d)*** *V_CAL.*

DRMS results partially agree with UPV measurements, in fact only *NBUT* shows a good penetration inside the stone in the first 8 mm leading to an increase in stone resistance from 7,3 N to 9,7 N (**Fig. 3.93 (b)**).

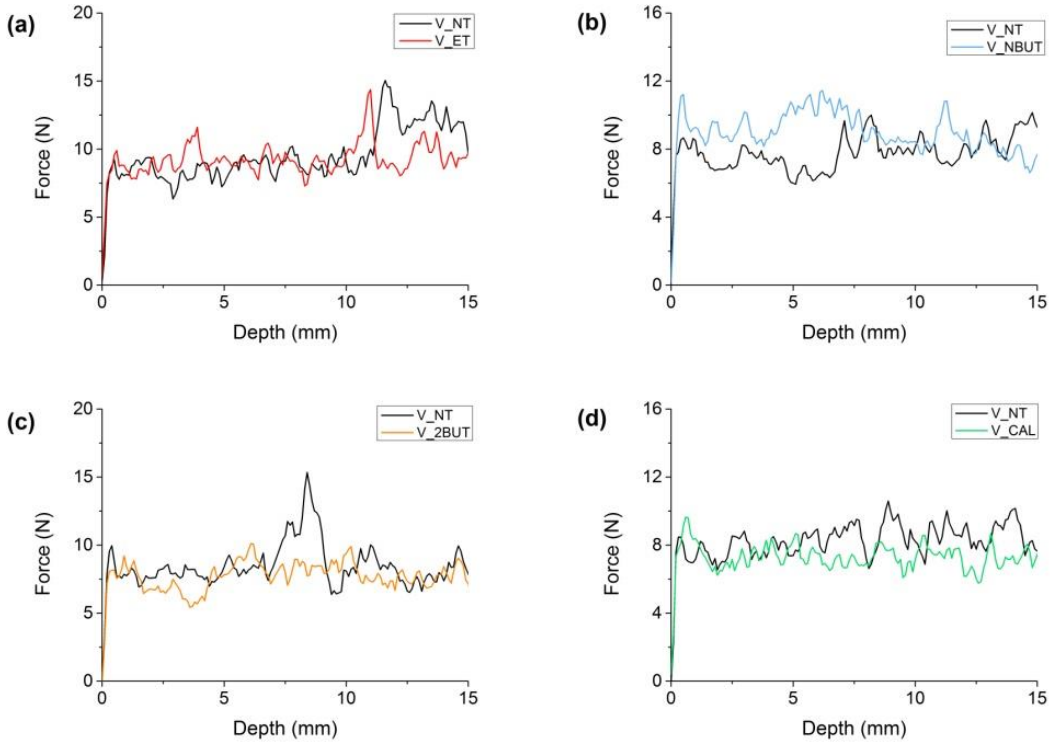

Figure 3.93 *- Drilling profiles before and after treatment:* ***(a)*** *V_ET,* ***(b)*** *V_NBUT,* ***(c)*** *V_2BUT and* ***(d)*** *V_CAL.*

The discordance between UPV and DRMS for samples *V_ET* and *V_2BUT*, can be ascribed to a lower consolidation effect which does not correspond to a stone resistance increase detectable with DRMS.

Looking at the colour measurements, in this case only the reference product lead to a ΔE^* value higher than 5. All treatments based on $Ca(OEt)_2$ nanosuspension remained in an acceptable range (**Fig. 3.94**).

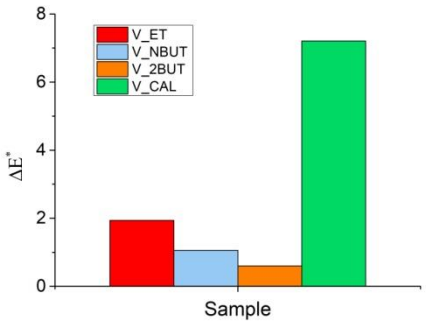

Figure 3.94 *- Colour variation ⊿E* generated by four consolidating products.*

By comparing this type of application procedure with brush till saturation, results about UPV and DRMS are comparable. In fact, both application procedures show how only *NBUT* leads to an increase of UPV together with an increase of stone resistance, while *CAL* does not cause any change for both the analyses. By evaluating what happens with other consolidating treatments based on calcium ethoxide, the lack of a consolidating effect registered with DRMS may be ascribed to a low increase of stone resistance due to the treatments, not detectable with this technique.

3.3.4 Carrara Marble

TG-DSC analysis (**Fig. 3.95 (a)**) shows that this stone is composed mainly of calcium carbonate due to the mass loss of 43.2% around 600-800 °C [26]. This technique allows to make a quantitative analysis of calcium carbonate which results of 99.7%. FT-IR analysis confirms the presence of calcite with characteristic peaks at 1420-1460, 875 and 713 cm^{-1} (**Fig. 3.95 (b)**).

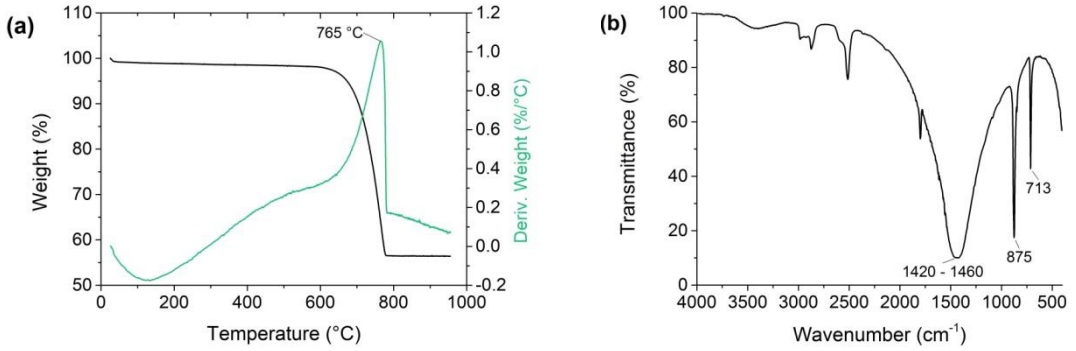

Figure 3.95 *- Chemical characterization of Carrara marble by* ***(a)*** *TG-DSC and* ***(b)*** *FT-IR analyses.*

Marble samples were subjected to the artificial ageing and **Fig. 3.96** shows the results of MIP measurements before and after the process. The initial porosity of 1.2 ± 0.1% and cumulative volume of mercury intruded of 4.4 ± 0.4 mm^3/g do not change significantly; in fact, after the test, they became 1.3 ± 0.1% and 4.8 ± 0.6 mm^3/g. Therefore, this ageing process was not successful for this type of stone.

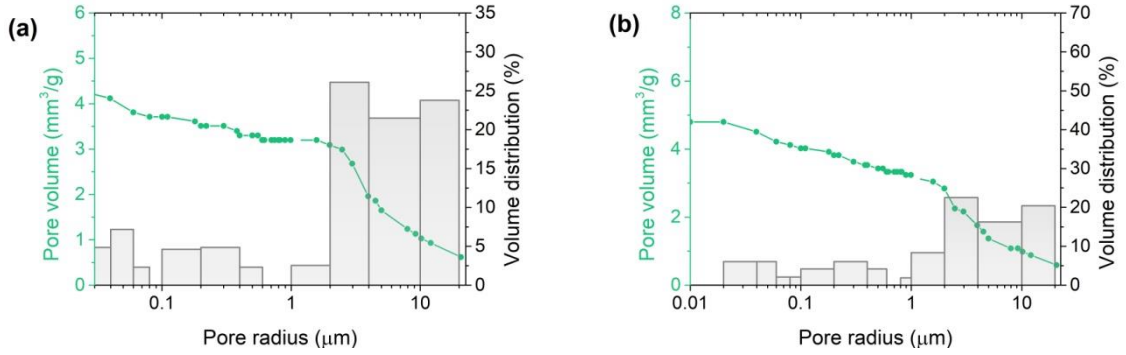

Figure 3.96 *- Pore-size distribution curves by means of MIP for* ***(a)*** *not aged and* ***(b)*** *aged Carrara marble.*

Despite the ageing test was not successful, in the following sections, results about application of consolidating treatments on Carrara marble will be reported for completeness. The discussed application procedures will be only: brush till saturation and brush with pre-set number of brush strokes.

3.3.4.1 Application procedure: by brush till saturation

Tab. 3.20 reports results regarding the quantity of product retained after one month from the application. The results are reported as a range of value between the minimum and the maximum quantity for each type of product. Small differences among quantity of product retained for samples treated with the same product are probably due to the different shape of

mock-ups (in accordance to the different analyses, mock-ups of different dimensions were necessary). More details of product retained in relation to the different analyses are shown in **Tab. C.16** in **Appendix C**. Carrara marble has a low value of porosity, thus it was difficult to perform capillary absorption test and to evaluate the drying rate. Therefore, the only data about water transport properties inside the material are referred to water vapour permeability test.

Table 3.20 *- Application by brush till saturation: range of amount of product retained after one month from the application.*

Product	Quantity of product retained (kg/m²)
ET	0.002 – 0.005
NBUT	0.010 – 0.044
2BUT	0.009 – 0.030
CAL	0.003 – 0.041

Carrara marble presents a very low permeability to water vapour and all treatments based on $Ca(OEt)_2$ cause a reduction of the initial values (**Fig. 3.97**). The only exception is due to *M_CAL* for which the water vapour permeability value increase after treatment; this different behaviour could be related to different atmospheric conditions present during the water vapour permeability proof for treated and untreated sample. In fact, the used formula, involves also atmospheric pressure, which varies in relation to the atmospheric conditions.

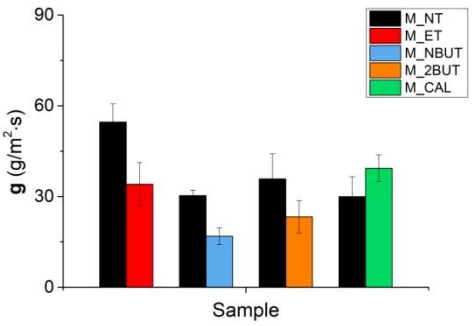

Figure 3.97 *- Water vapour permeability test results expressed as water vapour permeability coefficient (g) and reported as comparison before and after treatment.*

A summary of MIP results for each type of applied treatment is given in **Tab. 3.21.** Due to the low initial porosity, all the applied treatments do not show any significant change respect to untreated support by maintaining the variation in a very small range, ascribable to the

measurement rather to a real effect due to the treatment. Therefore, the decrease of g value seen for treated samples can be explained with the formation of a superficial layer on the treated surface which does not have a consolidating effect but influences the water vapour transmission between treated and untreated faces.

Table 3.21 *- Porosity data obtained by MIP measurements, reported as comparison between treated and untreated samples.*

Sample code	Total open porosity (%)	Total cumulative volume (mm^3/g)
M_NT	1.3 ± 0.1	4.8 ± 0.6
M_ET	1.1 ± 0.1	4.1 ± 0.7
M_NBUT	1.9 ± 0.1	7.6 ± 0.6
M_2BUT	1.3 ± 0.1	5.1 ± 2.1
M_CAL	1.6 ± 0.5	6.0 ± 0.8

In this case, pore size distribution curves expressed as log differential intruded volume versus pore radius are difficult to read, being the average pore radius very small (**Fig. C.1** in **Appendix C**).

Also results about NMR relaxometry are difficult to interpret due to the small value of porosity of marble; furthermore, data regarding *M_CAL* was not possible to acquire, probably due to the impossibility of water to penetrate inside the sample during the water absorption under vacuum - the procedure preliminary to NMR analysis (**Fig. C.2** in **Appendix C**).

Colour measurement shows that all treatments do not cause a significant colour variation, being all the ΔE^* values < 5 (**Fig. 3.98**). Since the treatments producing calcium carbonate usually induce a whitening of the surface, this effect is more difficult to be detected in a white stone like Carrara marble.

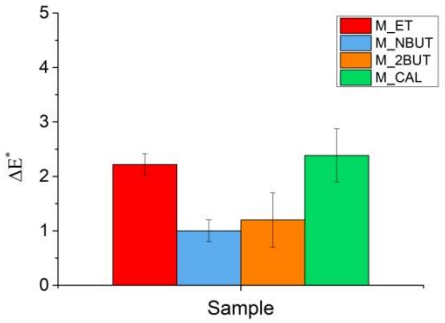

Figure 3.98 *- Colour variation ⊿E* generated by four consolidating products.*

The formation of a superficial layer due to application of *CAL* is present also for Carrara marble, differently from products based on calcium ethoxide nanosuspension (**Fig. 3.99**).

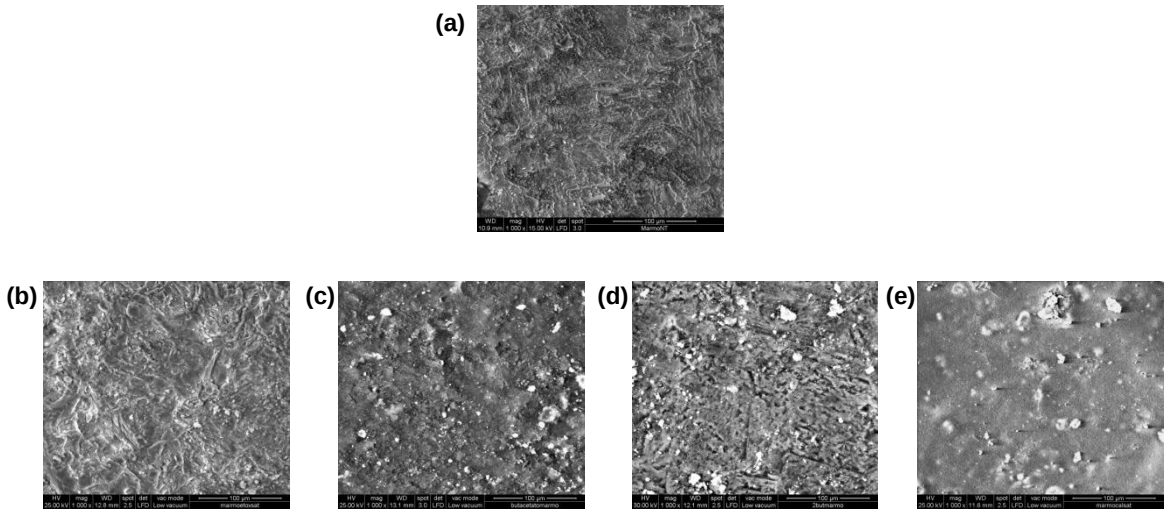

Figure 3.99 *- Surface observation with SEM:* ***(a)*** *M_NT,* ***(b)*** *M_ET,* ***(c)*** *M_NBUT,* ***d)*** *M_2BUT and* ***e)*** *M_CAL.*

3.3.4.2 Application procedure: by brush with pre-set number of brush strokes

This application procedure was performed only for calcium ethoxide diluted in ethanol and the reference product. The number of applications for Carrara marble, decided on the basis of the colorimetric measurements performed after each brush stroke, was 10. ΔE^* results calculated after 10 applications were: 3.5 ± 0.3 for *M_ET* and 2.1 ± 0.1 for *M_CAL*.

As for the application by brush till saturation, also in this case it was not possible to acquire information about water transport properties with capillarity water absorption test and drying rate. **Tab. 3.22** reports data regarding the quantity of product retained after one month from the application. The results are reported as a range of value between the minimum and the maximum quantity for each type of product. Small differences among quantity of product retained for samples treated with the same product are probably due to the different shape of mock-ups (in accordance to the different analyses, mock-ups of different dimensions were necessary). More details of product retained in relation to the different analyses are shown in **Tab. C.17** in **Appendix C**.

Table 3.22 *- Application by brush with pre-set number of brush strokes: range of amount of product retained after one month from the application.*

Product	Quantity of product retained (kg/m²)
ET	0.006 – 0.020
CAL	0.007 – 0.015

Also in this case, the only test which can give information about water transport properties is water vapour permeability and it shows that both treatments *ET* and *CAL* reduce water vapour permeability respect to untreated samples, with a bit higher change for *M_CAL* (**Fig. 3.100**).

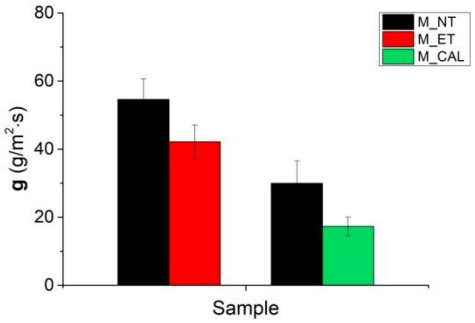

Figure 3.100 *- Water vapour permeability test results expressed as water vapour permeability coefficient (g) and reported as comparison before and after treatment.*

Looking at the porosity data obtained with mercury intrusion porosimetry (**Tab. 3.23**), both treatments do not cause any significant change in stone porosity, as for the application by brush till saturation; indeed, as for application by brush till saturation, the variation of water vapour permeability may be related to the formation on a superficial layer of the product on the treated surface due to the impossibility of the products to penetrate more inside the stone. Graphs regarding cumulative pore volume and volume distribution versus pore radius do not show significant change between treated and untreated samples (**Fig. C.3** in **Appendix C**).

Table 3.23 *- Porosity data obtained by MIP measurements, reported as comparison between treated and untreated samples.*

Sample code	Total open porosity (%)	Total cumulative volume (mm^3/g)
M_NT	1.3 ± 0.1	4.8 ± 0.6
M_ET	1.6 ± 0.1	6.7 ± 1.5
M_CAL	1.1 ± 0.1	4.2 ± 0.5

Also NMR relaxometry presents results difficult to interpret due to the very small value of porosity of marble (**Fig. C.4** in **Appendix C**).

Looking at SEM images, also for this type of application procedures, *CAL* forms a superficial layer on the treated surface, differently from *ET* which maintains a morphology similar to untreated support (**Fig. 3.101**).

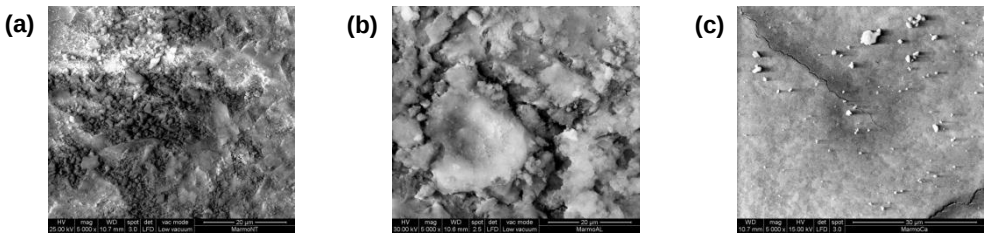

Figure 3.101 *- Surface observation with SEM:* ***(a)*** *M_NT,* ***(b)*** *M_ET and* ***(c)*** *M_CAL.*

For this type of application procedure, results about ultrasonic pulse velocity and drilling measurement system were not performed.

3.4 Bibliography

[1] H. H. Adler and P. F. Kerr, "Infrared absorption frequency trends for anhydrous normal carbonates," *Am. Mineral.*, vol. 48, pp. 124–137, 1963.

[2] R. M. Hazen, R. T. Downs, A. P. Jones, and L. Kah, "Carbon Mineralogy and Crystal Chemistry," *Rev. Mineral. Geochemistry*, vol. 75, no. 1, pp. 7–46, 2013.

[3] H. Essabir, M. O. Bensalah, D. Rodrigue, R. Bouhfid, and A. el kacem Qaiss, "A comparison between bio and mineral calcium carbonate on the properties of polypropylene composites," *Constr. Build. Mater.*, vol. 134, pp. 549–555, 2017.

[4] H. Wei, Q. Shen, Y. Zhao, D. Wang, and D. Xu, "Influence of polyvinylpyrrolidone on the precipitation of calcium carbonate and on the transformation of vaterite to calcite," *J. Cryst. Growth*, vol. 250, pp. 516–524, 2003.

[5] O. E. Meiron, E. Bar-david, E. D. Aflalo, A. Shechter, D. Stepensky, A. Berman, and A. Sagi, "Solubility and Bioavailability of Stabilized Amorphous Calcium Carbonate," *J. Bone Miner. Res.*, vol. 26, no. 2, pp. 364–372, 2011.

[6] F. A. Andersen and L. Brečević, "Infrared Spectra of Amorphous and Crystalline Calcium Carbonate," *Acta Chem. Scand.*, vol. 45, pp. 1018–1024, 1991.

[7] J. D. Rodriguez-Blanco, S. Shaw, and L. G. Benning, "The kinetics and mechanisms of amorphous calcium carbonate (ACC) crystallization to calcite, via vaterite," *Nanoscale*, vol. 3, pp. 265–271, 2011.

[8] C. Rodriguez-Navarro, A. Suzuki, and E. Ruiz-Agudo, "Alcohol Dispersions of Calcium Hydroxide Nanoparticles for Stone Conservation," *Langmuir*, vol. 29, pp. 11457–11470, 2013.

[9] V. Cumaran Arunasalam, I. Baxter, J. A. Darr, S. R. Drake, M. B. Hursthouse, A. M. K.M., and D. M. P. Mingos, "Insertion reactions of small molecules into group 2 metal alkoxides; structural characterization of $[Mg_9(\mu_5\text{-}CO_3)(O_2COMe)_8(\mu_3OMe)_8(MeOH)_{13}]\cdot MeOH\cdot C_7H_8$," *Polyhedron*, vol. 17, no. 5–6, pp. 641–657, 1998.

[10] M. Favaro, P. Tomasin, F. Ossola, and P. A. Vigato, "A novel approach to consolidation of historical limestone: the calcium alkoxides," *Appl.Organometal.Chem.*, vol. 22, pp. 698–704, 2008.

[11] Z. Zhao, Y. Xia, J. Xue, and Q. Wu, "Role of E. coli-Secretion and Melamine in

Selective Formation of $CaC_2O_4 \cdot H_2O$ and $CaC_2O_4 \cdot 2H_2O$ Crystals," *Cryst. Growth Des.*, vol. 14, pp. 450–458, 2014.

[12] F. Ossola, P. Tomasin, C. De Zorzi, N. El Habra, M. Chiurato, and M. Favaro, "New Calcium Alkoxides for Consolidation of Carbonate Rocks. Influence of Precursors' characteristics on morphology, crystalline phase and consolidation effects," *New J. Chem.*, vol. 36, pp. 2618–2624, 2012.

[13] X. Zhang, F. P. Glasser, and K. L. Scrivener, "Reaction kinetics of dolomite and portlandite," *Cem. Concr. Res.*, vol. 66, pp. 11–18, 2014.

[14] J. Chang, Y. Li, M. Cao, and Y. Fang, "Influence of magnesium hydroxide content and fineness on the carbonation of calcium hydroxide," *Constr. Build. Mater.*, vol. 55, pp. 82–88, 2014.

[15] J. Chen and L. Xiang, "Controllable synthesis of calcium carbonate polymorphs at different temperatures," *Powder Technol.*, vol. 189, no. 1, pp. 64–69, 2010.

[16] Z. Nan, X. Chen, Q. Yang, X. Wang, Z. Shi, and W. Hou, "Structure transition from aragonite to vaterite and calcite by the assistance of SDBS," *J. Colloid Interface Sci.*, vol. 325, pp. 331–336, 2008.

[17] C. G. Kontoyannis and N. V Vagenas, "Calcium carbonate phase analysis using XRD and FT-Raman spectroscopy," *R. Soc. Chem.*, vol. 125, pp. 251–255, 2000.

[18] S. F. Chen, S. H. Yu, J. Hang, F. Li, and Y. Liu, "Polymorph discrimination of $CaCO_3$ mineral in an ethanol/water solution: formation of complex vaterite superstructures and aragonite rods," *Chem. Mater.*, vol. 18, no. 1, pp. 115–122, 2006.

[19] T. Ogino, T. Suzuki, and K. Sawada, "The formation and transformation mechanism of calcium carbonate in water," *Geochim. Cosmochim. Acta*, vol. 51, no. 10, pp. 2757–2767, 1987.

[20] F. Manoli and E. Dalas, "Spontaneous precipitation of calcium carbonate in the presence of ethanol, isopropanol and diethylene glycol," *J. Cryst. Growth*, vol. 218, pp. 359–364, 2000.

[21] A. J. Easton and D. Claugher, "Variations in a growth form of synthetic vaterite," *Mineral. Mag.*, vol. 50, pp. 332–336, 1986.

[22] S. R. Dickinson, G. E. Henderson, and K. M. McGrath, "Controlling the kinetic versus

thermodynamic crystallisation of calcium carbonate," *J. Cryst. Growth*, vol. 244, no. 3–4, pp. 369–378, 2002.

[23] P. López-arce, L. S. Gómez-villalba, S. Martínez-ramírez, M. Alvarez de Buergo, and R. Fort, "Influence of relative humidity on the carbonation of calcium hydroxide nanoparticles and the formation of calcium carbonate polymorphs," *Powder Technol.*, vol. 205, pp. 263–269, 2011.

[24] S. Gopi, V. K. Subramanian, and K. Palanisamy, "Aragonite – calcite – vaterite: A temperature influenced sequential polymorphic transformation of $CaCO_3$ in the presence of DTPA," *Mater. Res. Bull.*, vol. 48, no. 5, pp. 1906–1912, 2013.

[25] C. Gabrielli, R. Jaouhari, S. Joiret, and G. Maurin, "In situ Raman spectroscopy applied to electrochemical scaling. Determination of the structure of vaterite," *J. Raman Spectrosc.*, vol. 31, no. 6, pp. 497–501, 2000.

[26] X. G. Li, Y. Lv, B. G. Ma, W. Q. Wang, and S. W. Jian, "Decomposition kinetic characteristics of calcium carbonate containing organic acids by TGA," *Arab. J. Chem.*, vol. 10, pp. S2534–S2538, 2017.

[27] Z. B. Bundur, A. Amiri, Y. C. Ersan, N. Boon, and N. De Belie, "Impact of air entraining admixtures on biogenic calcium carbonate precipitation and bacterial viability," *Cem. Concr. Res.*, vol. 98, pp. 44–49, 2017.

[28] S. Kirboga and M. Öner, "Investigating the effect of ultrasonic irradiation on synthesis of calcium carbonate using Box-Behnken experimental design," *Powder Technol.*, vol. 308, pp. 442–450, 2017.

[29] N. V. Vagenas, A. Gatsouli, and C. G. Kontoyannis, "Quantitative analysis of synthetic calcium carbonate polymorphs using FT-IR spectroscopy," *Talanta*, vol. 59, pp. 831–836, 2003.

[30] M. Singh, S. Vinodh Kumar, S. A. Waghmare, and P. D. Sabale, "Aragonite – vaterite – calcite: Polymorphs of $CaCO_3$ in 7th century CE lime plasters of Alampur group of temples, India," *Constr. Build. Mater.*, vol. 112, pp. 386–397, 2016.

[31] F. Bosch Reig, J. V. Gimeno Adelantado, and M. C. M. Moya Moreno, "FTIR quantitative analysis of calcium carbonate (calcite) and silica (quartz) mixtures using the constant ratio method. Application to geological samples," *Talanta*, vol. 58, pp. 811–821, 2002.

[32] G. Yuan, X. Chen, X. Li, Q. Liang, G. Miao, and B. Yuan, "The synthesis of calcium carbonate microparticles with multiple morphologies through self-assembly method," *Powder Technol.*, vol. 284, pp. 253–256, 2015.

[33] B. J. Saikia, G. Parthasarathy, and N. C. Sarmah, "Fourier transform infrared spectroscopic estimation of crystallinity in SiO_2 based rocks," *Bull. Mater. Sci.*, vol. 31, no. 5, pp. 775–779, 2008.

[34] E. Finocchio, G. Busca, S. Rossini, U. Cornaro, V. Piccoli, and R. Miglio, "FT-IR characterization of silicated aluminas, active olefin skeletal isomerization catalysts," *Catal. Today*, vol. 33, pp. 335–352, 1997.

[35] F. Bosch-Reig, J. V. Gimeno-Adelantado, F. Bosch-Mossi, and A. Doménech-Carbó, "Quantification of minerals from ATR-FTIR spectra with spectral interferences using the MRC method," *Spectrochim. Acta - Part A Mol. Biomol. Spectrosc.*, vol. 181, pp. 7–12, 2017.

[36] N. Kovač, "Chemical Characterization of stromatolitic 'petola' layer (sečovlje salt-pans, Slovenia) using FT-IR spectroscopy," *Ann. Ser. hist. nat*, vol. 19, pp. 3–10, 2009.

[37] J. Delgado Rodrigues and A. Grossi, "Indicators and ratings for the compatibility assessment of conservation actions," *J. Cult. Herit.*, vol. 8, no. 1, pp. 32–43, 2007.

[38] H. S. Sasse and R. Snethlage, "Methods for the evaluation of stone conservation treatments," in *Report of Dahlem Workshop on Saving our Architectural Heritage, Berlin*, N.S. Baer, R. Snethlage (Eds.), 1996, p. 225.

[39] G. Borsoi, B. Lubelli, R. van Hees, R. Veiga, A. S. Silva, L. Colla, L. Fedele, and P. Tomasin, "Effect of solvent on nanolime transport within limestone: How to improve in-depth deposition," *Colloids Surfaces A Physicochem. Eng. Asp.*, vol. 497, pp. 171–181, 2016.

CHAPTER 4

Conclusion and future perspectives

During this research work a new product based on calcium ethoxide was studied and applied on carbonate stones with different total open porosity to understand its compatibility and efficacy as consolidating agent. The initial calcium ethoxide nanosuspension was diluted in three organic solvents (ethanol, 2-butanol and n-butylacetate); therefore, three different products to test were obtained and compared with a reference one, CaLoSil E50 (calcium hydroxide nanoparticles dispersed in ethanol).

Calcium ethoxide leads to the formation of calcium carbonate inside the porous structure of the material by reacting with moisture and carbon dioxide of the atmosphere; therefore, the first part of the project concerned the analysis of the kinetic and reaction pathway of this carbonation process. Furthermore, an evaluation of the mineralogical phases formed in products' coatings deposited on glass surface and maintained at different relative humidity conditions (RH) and controlled room temperature for two weeks, one months and three months was carried out; the aim of this second analysis was to investigate the effects of solvents and different relative humidity conditions on carbonate phase formation.

Regarding the kinetic process, n-butylacetate resulted the solvent which mostly delayed the conversion of calcium ethoxide to calcium carbonate, probably because of the higher boiling point of this solvent with respect to the others. In fact, by μFT-IR analysis, peaks related to calcium carbonate were registered after two minutes for product in ethanol and 2-butanol and six minutes for product in n-butylacetate, from the beginning of the carbonation reaction. Therefore, the type of solvent plays effectively an important role in the control of carbonation rate: lower vapour pressure (slow evaporation rate) leads to slower carbonation.

Concerning the reaction pathway, two possible mechanisms can be followed: (i) insertion of a CO_2 molecule within the Ca-O bond followed by hydrolysis and alcohol elimination, and (ii) hydrolysis reaction of the ethoxide with the formation of calcium hydroxide as intermediate which subsequently carbonates. Also in this case a different behaviour was registered between the alcohols and n-butylacetate; in fact, while alcohols followed both reaction pathways, for n-butylacetate only the first mechanism occurred. Probably this is due to the lower quantity of water in n-butylacetate and therefore of available OH groups.

Coating analysis highlighted the complexity of carbonation process, which always led to the formation of vaterite, the most kinetically favoured, in all relative humidity conditions. It is very interesting to underline how in presence of a major quantity of water - higher relative humidity condition - vaterite can partially transform to calcite, most thermodynamically stable. In fact, for all the analysed products, vaterite formed for both relative humidity conditions (50-90%), while calcite is found only at 90% RH. This difference may be related to the process of dissolution of vaterite and subsequent recrystallization to calcite in presence of water (90% RH). In the case of products diluted in ethanol and 2-butanol, the prevalence of only vaterite at 50% RH, can be ascribed to the presence of alcohols, which influence the morphology of the vaterite stabilizing this phase and preventing the transformation to the thermodynamically stable calcite as observed by Manoli et al[1]. In the case of n-butyalcetate, the presence at 50% RH of an amorphous phase after two weeks and subsequently of vaterite after one month and three months may be related to the higher boiling point of the solvent which delays the carbonation process and, therefore, the formation of a crystalline phase. By comparing the coating analysis of $Ca(OEt)_2$ based products with the reference one (CaLoSil E50), the presence of calcite is confirmed only for the value of 90% RH. **Tab. 4.1**. reports the global results regarding the mineralogical phases formed for all products in both relative humidity conditions and for all the considered periods.

Table 4.1 - *Summary of coating results regarding calcium carbonate polymorphs, obtained with XRD and μFT-IR analyses, for all the analysed products after two weeks, one month and three months. ACC - amorphous calcium carbonate.*

	2 weeks		**1 month**		**3 months**	
Product	**50% RH**	**90% RH**	**50% RH**	**90% RH**	**50% RH**	**90% RH**
ET	vaterite	vaterite calcite	vaterite	vaterite calcite	vaterite	vaterite calcite
2BUT	vaterite	vaterite calcite	vaterite	vaterite calcite	vaterite	vaterite calcite
NBUT	ACC	vaterite calcite	ACC	vaterite	vaterite	vaterite
CAL	aragonite	vaterite calcite	aragonite	vaterite calcite	aragonite	vaterite calcite

[1] F. Manoli and E. Dalas, "Spontaneous precipitation of calcium carbonate in the presence of ethanol, isopropanol and diethylene glycol," *J. Cryst. Growth*, vol. 218, pp. 359–364, 2000.

In the second part of the research, the proposed new products were applied on carbonate stones with different total open porosity - Lecce stone, Noto stone, Vicenza stone and Carrara marble. Three different types of application procedures (by brush till saturation, by brush with a pre-set number of brush strokes in order to avoid a colour change of the treated surface and by absorption through capillarity) and a multi-technique approach was used for the assessment of products' effectiveness and compatibility as consolidating agents. In particular, Mercury Intrusion Porosimetry and Nuclear Magnetic Resonance Relaxometry were used to determine the variation of cumulative volume and pore size distribution; variation of water transport properties was evaluated by observing the water absorption through capillarity, drying rate and water vapour permeability; Scanning Electron Microscopy (SEM) and spectrophotometric measurements were used to assess morphological and aesthetical variation of the surface with, respectively; finally the penetration reached by the products was identified by using Ultrasonic Pulse Velocity (UPV) and Drilling Resistance Measurement System (DRMS).

Before the application of treatments, all stones were subjected to an artificial ageing process based on thermal cycles, which led to different results in accordance with the type of substrate. This process resulted successful for Lecce and Noto stones and ineffective for Carrara Marble due to its low initial porosity. Vicenza stone presented a decrease of the porosity, probably because the ageing process led to an internal stress which brought to the clogging of the pores.

Results showed that the major differences in terms of effectiveness among all treatments are mainly connected to type of used solvent rather than the type of application procedure. Moreover, the results are not always related to the quantity of retained product, both in terms of chromatic variation and consolidating effect.

For all types of stone, products based on $Ca(OEt)_2$ nanosuspension resulted able in reducing the total open porosity and changed the water transport properties of the stones in an acceptable way. Exceptions were registered for $Ca(OEt)_2$ diluted in ethanol and applied on Noto stone by brush with pre-set number of brush strokes and on Vicenza stone by brush till saturation.

Instead, in some cases, the reference product did not reduce the porosity of samples (as for Lecce stone and Vicenza stone treated with brush till saturation). CaLoSil E50 led to the formation of a superficial layer on the treated surface and it showed a low compatibility by inducing a too high change of water transport properties, especially for Vicenza stone treated with both types of brush procedures.

However, low aesthetical compatibility is registered when products are applied by brush till saturation and absorption through capillarity, mostly for Lecce stone but also for Noto stone, in a minor way; for Vicenza stone the chromatic variations range within acceptable limits.

The penetration depth reached by the treatments was evaluated with UPV and DRMS for the two application procedures by brush. The most promising product for Lecce stone resulted *NBUT* for both types of application procedures; while for Noto stone good results were obtained mostly with *NBUT* applied by brush till saturation and also with *ET* and *2BUT* for the application through capillarity absorption. Finally, a better penetration for Vicenza stone was reached by *2BUT* and *NBUT* applied by brush till saturation and only by *NBUT* for the application through capillarity absorption. Therefore, the higher boiling point of the solvent seems to be an important parameter to permit a better penetration of the treatments based on $Ca(OEt)_2$ nanosuspension. This behaviour agrees with a study described by Borsoi et al.[2] which highlights that to improve the penetration depth and the effectiveness of a lime nanosuspension in stones with different porosity, a compromise between the stability of the nanosuspension and the evaporation rate of the used solvent must be reached. Calcium ethoxide may have a similar behaviour, even if the carbonation process is more complex.

Different results were achieved by applying the consolidating agents on Carrara marble. In fact, the ageing process was not appropriate to damage this lithotype, therefore no significant change regard compatibility and effectiveness of the treatments was recorded.

In conclusion, by considering the overall analyses, best results in terms of compatibility and effectiveness are obtained by diluting the product in n-butylacetate, the solvents with the highest boiling point.

Some integrations of previous results will involve a study regarding the interaction between the calcium ethoxide applied on carbonate stone and environmental conditions and the acquisition of information about the penetration depth reached by the treatments applied with pre-set number of brush strokes. Moreover, to complete the data regarding this type of application procedure, also *2BUT* and *NBUT* will be applied on carbonate supports and the evaluation of their efficacy and compatibility as consolidating agents will be performed.

Future perspectives concern the application of the analysed products on real case studies involving the same carbonate stones, to understand how environmental conditions can influence the obtained results. The efficacy evaluation of the applied products will be performed with non-

[2] G. Borsoi, B. Lubelli, R. van Hees, R. Veiga, A. S. Silva, L. Colla, L. Fedele, and P. Tomasin, "Effect of solvent on nanolime transport within limestone: How to improve in-depth deposition," *Colloids Surfaces A Physicochem. Eng. Asp.*, vol. 497, pp. 171–181, 2016.

destructive techniques and compared with commercial treatments usually applied for the consolidation of carbonate stones. Furthermore, an evaluation of durability of the considered products will be carried out.

APPENDIX A - Kinetic of carbonation process and reaction pathway

- **Calcium ethoxide in ethanol**

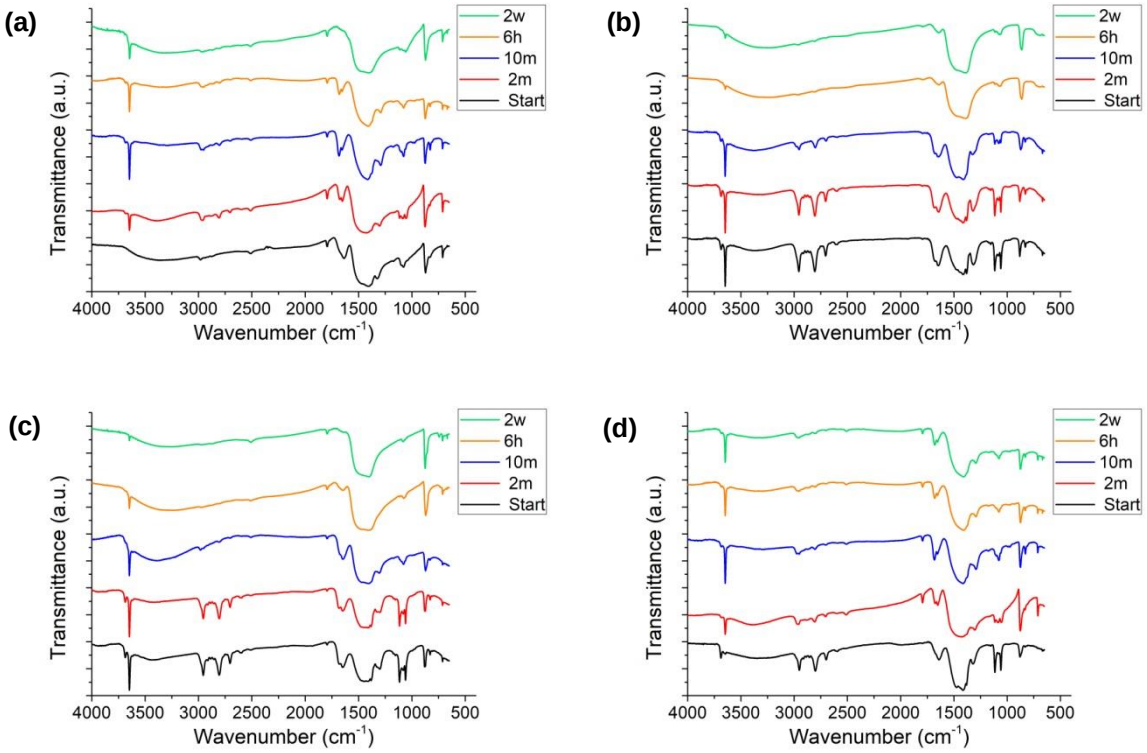

Figure A.1 *- μFT-IR spectra showing kinetic process and reaction pathway of calcium ethoxide diluted in ethanol mixed with powered carbonate stones:* ***(a)*** *Lecce stone,* ***(b)*** *Noto stone* ***(c)*** *Vicenza stone and* ***(d)*** *Carrara marble. Time intervals: start, beginning of the reaction; 2m, two minutes; 10m, ten minutes; 6h, six hours; 2w, two weeks.*

- **Calcium ethoxide in 2-buthanol**

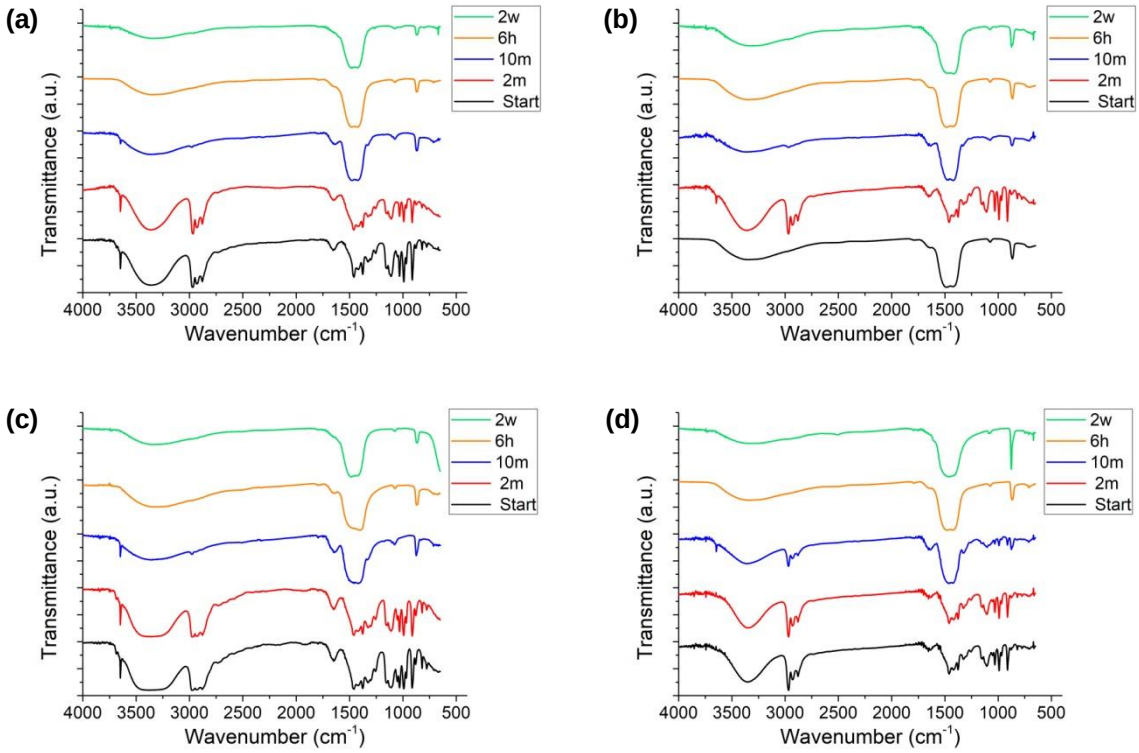

Figure A.2 *- μFT-IR spectra showing kinetic process and reaction pathway of calcium ethoxide diluted in 2-buthanol mixed with powered carbonate stones:* ***(a)*** *Lecce stone,* ***(b)*** *Noto stone* ***(c)*** *Vicenza stone and* ***(d)*** *Carrara marble. Time intervals: start, beginning of the reaction; 2m, two minutes; 10m, ten minutes; 6h, six hours; 2w, two weeks.*

- **Calcium ethoxide in n-butylacetate**

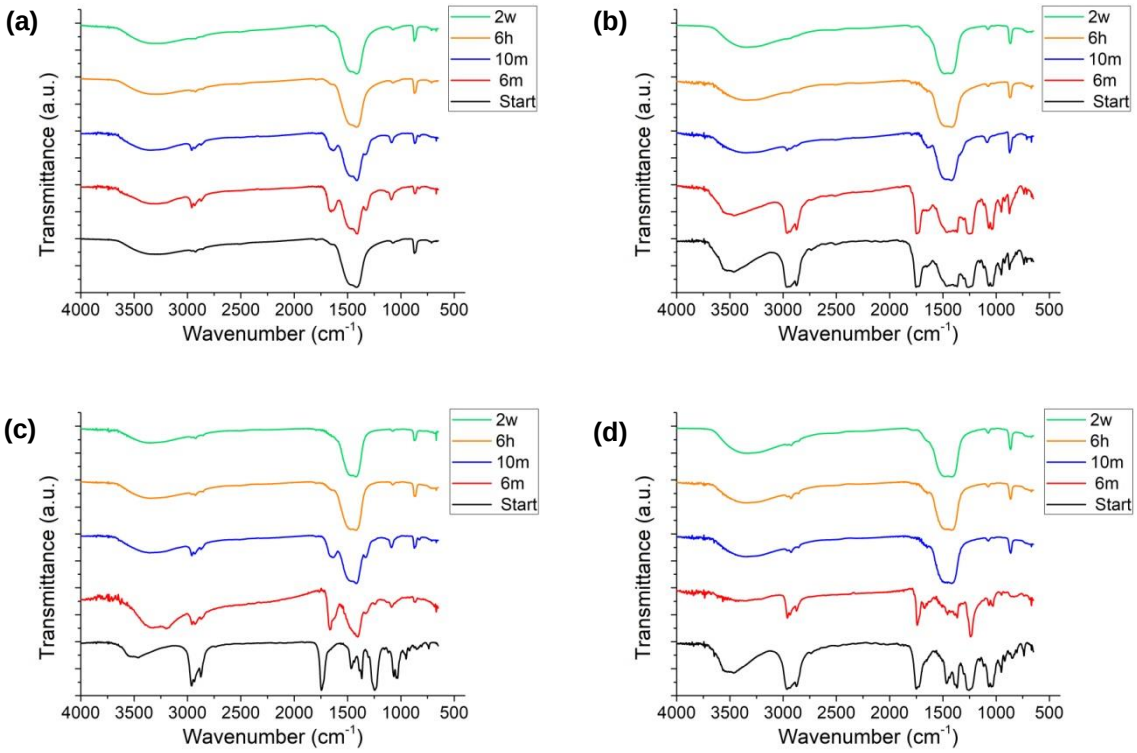

Figure A.3 *- μFT-IR spectra showing kinetic process and reaction pathway of calcium ethoxide diluted in n-butylacetate mixed with powered carbonate stones:* ***(a)*** *Lecce stone,* ***(b)*** *Noto stone* ***(c)*** *Vicenza stone and* ***(d)*** *Carrara marble. Time intervals: start, beginning of the reaction; 6m, six minutes; 10m, ten minutes; 6h, six hours; 2w, two weeks.*

APPENDIX B - Coating analysis

- **Calcium ethoxide in 2-buthanol**

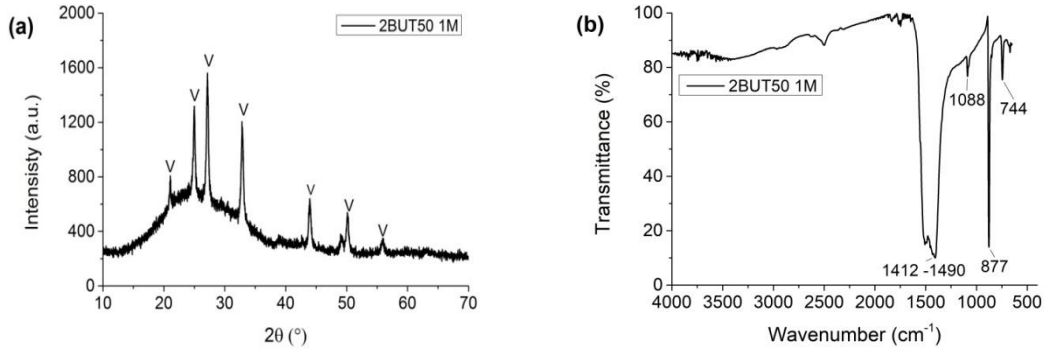

Figure B.1 *- 2BUT50 after one month:* ***(a)*** *XRD pattern and* ***(b)*** *μFT-IR spectrum. XRD peak assignments: V, vaterite.*

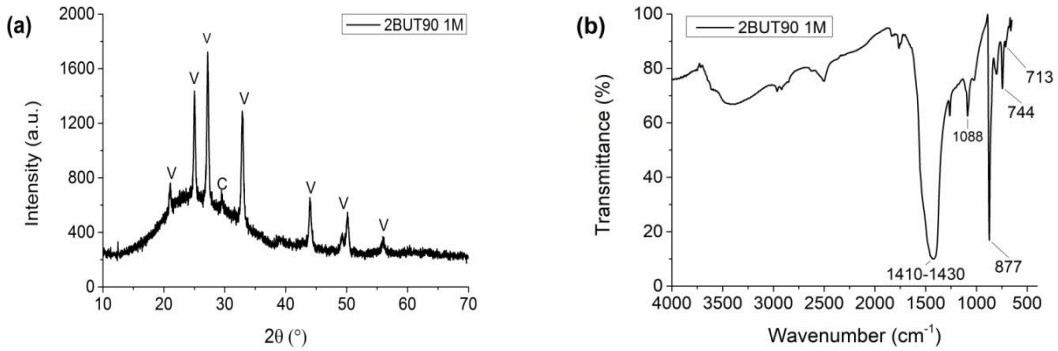

Figure B.2 *- 2BUT90 after one month:* ***(a)*** *XRD pattern and* ***(b)*** *μFT-IR spectrum. XRD peak assignments: C, calcite; V, vaterite.*

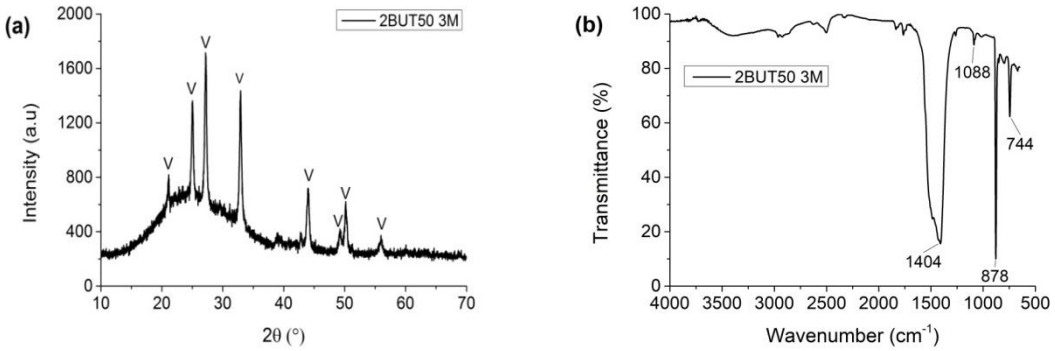

Figure B.3 *- 2BUT50 after three months:* ***(a)*** *XRD pattern and* ***(b)*** *μFT-IR spectrum. XRD peak assignments: V, vaterite.*

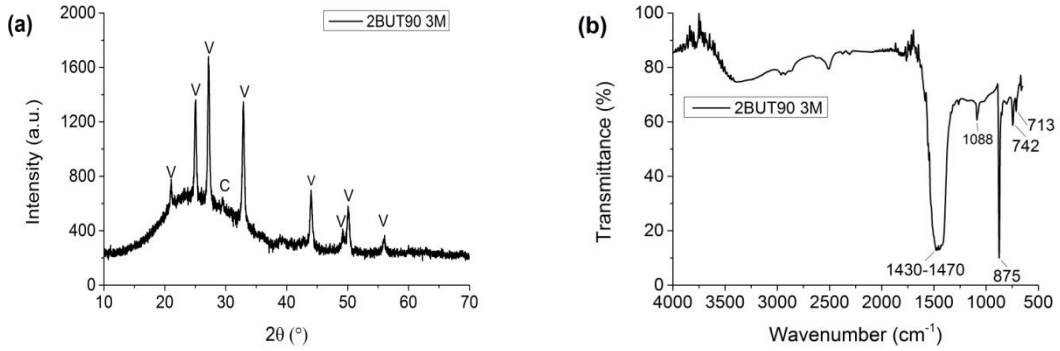

Figure B.4 *- 2BUT90 after three months:* ***(a)*** *XRD pattern and* ***(b)*** *μFT-IR spectrum. XRD peak assignments: C, calcite; V, vaterite.*

- **CaLoSil**

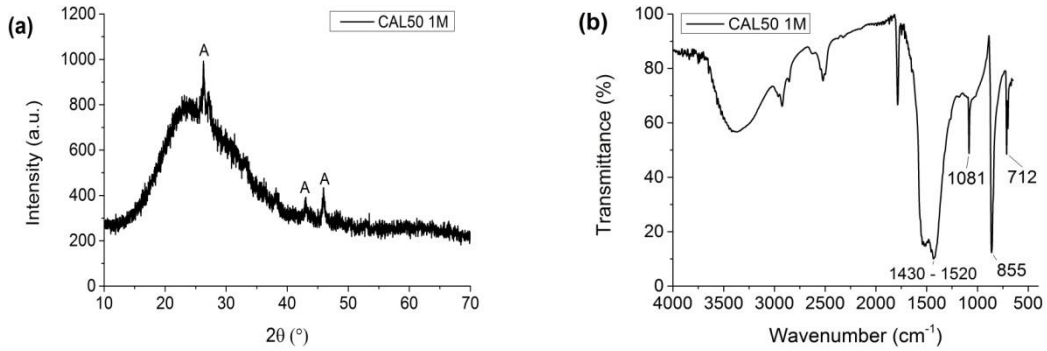

Figure B.5 *- CAL50 after one month:* ***(a)*** *XRD pattern and* ***(b)*** *μFT-IR spectrum. XRD peak assignments: A, aragonite.*

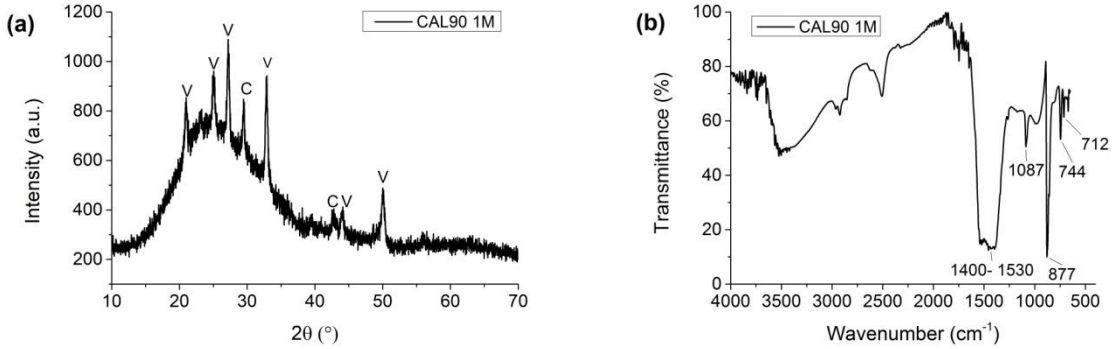

Figure B.6 *- CAL90 after one month:* ***(a)*** *XRD pattern and* ***(b)*** *μFT-IR spectrum. XRD peak assignments: C, calcite; V, vaterite.*

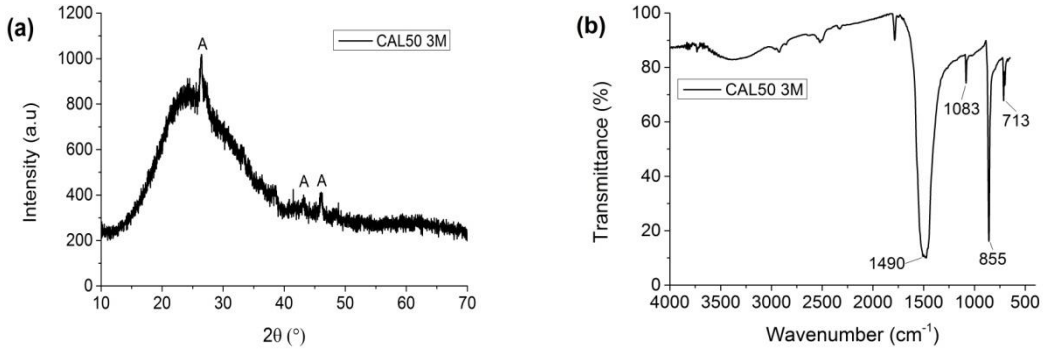

Figure B.7 *- CAL50 after three months:* ***(a)*** *XRD pattern and* ***(b)*** *μFT-IR spectrum. XRD peak assignments: A, aragonite.*

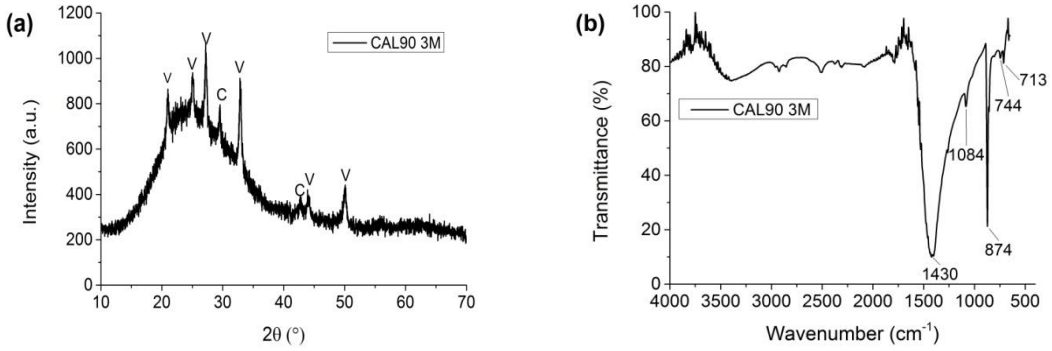

Figure B.8 *- CAL90 after three months:* ***(a)*** *XRD pattern and* ***(b)*** *μFT-IR spectrum. XRD peak assignments: C, calcite; V, vaterite.*

APPENDIX C - Characterization and analysis of treated samples

- **LECCE STONE**

Table C.1 *- Lecce stone, application by brush till saturation: amount of product retained according to different type of analysis.*

Sample	Analysis	Quantity of product retained (Kg/m²)
L_ET	Water absorption by capillarity Drying Rate	0.115 ± 0.016
L_NBUT		0.108 ± 0.010
L_2BUT		0.165 ± 0.068
L_CAL		0.097 ± 0.021
L_ET	Water vapour permeability	0.026 ± 0.002
L_NBUT		0.044 ± 0.001
L_2BUT		0.044 ± 0.005
L_CAL		0.028 ± 0.008
L_ET	MIP	0.016 ± 0.011
L_NBUT		0.012 ± 0.003
L_2BUT		0.018 ± 0.007
L_CAL		0.063 ± 0.008
L_ET	NMR Colorimetric measurement	0.026 ± 0.002
L_NBUT		0.016 ± 0.003
L_2BUT		0.017 ±0.006
L_CAL		0.047 ± 0.005
L_ET	UPV DRMS	0.065 ± 0.002
L_NBUT		0.081 ± 0.004
L_2BUT		0.051 ± 0.005
L_CAL		0.012 ± 0.002

Table C.2 *- Lecce stone, application by brush till saturation: values of ultrasound pulse velocity before and after treatment for all products. The depth profile is expressed from not treated (5 mm) to treated surface (45mm).*

	UPV (m/s)							
Depth (mm)	*L_ET NT*	*L_ET T*	*L_NBUT NT*	*L_NBUT T*	*L_2BUT NT*	*L_2BUT T*	*L_CAL NT*	*L_CAL T*
5	3213	3220	3613	3710	3703	3723	3246	3196
10	3193	3246	3546	3700	3576	3653	3223	3253
15	3200	3206	3590	3673	3553	3690	3236	3290
20	3233	3226	3563	3683	3550	3603	3190	3250
25	3233.	3186	3546	3646.	3583	3636	3210	3280
30	3246	3240	3580	3636	3593	3620	3190	3250
35	3213	3220	3546	3580	3560	3560	3190	3230
40	3240	3213	3570	3543	3560	3606	3210	3223
45	3233	3160	3590	3616	3613	3620	3170	3203

Table C.3 *- Lecce stone, application by brush with pre-set number of brush strokes: amount of product retained according to different type of analysis.*

Sample	**Analysis**	**Quantity of product retained (kg/m^2)**
L_ET	Water absorption by capillarity Drying Rate	0.114 ± 0.027
L_CAL		0.010 ± 0.003
L_ET	Water vapour permeability	0.019 ± 0.001
L_CAL		0.012 ± 0.000
L_ET	MIP	0.025 ±0.001
L_CAL		0.022 ± 0.006
L_ET	NMR	0.023 ± 0.005
L_CAL		0.014 ± 0.003

Table C.4 - *Lecce stone, application by absorption through capillarity: fringe reached by the products during the application.*

Product	Fringe (mm)
ET	4
NBUT	10
2BUT	5
CAL	7

Table C.5 *- Lecce stone, application by absorption through capillarity: values of ultrasound pulse velocity before and after treatment for all products. The depth profile is expressed from not treated (5 mm) to treated surface (45mm).*

	UPV (m/s)							
Depth (mm)	*L_ET NT*	*L_ET T*	*L_NBUT NT*	*L_NBUT T*	*L_2BUT NT*	*L_2BUT T*	*L_CAL NT*	*L_CAL T*
5	3726	3716	3636	3693	3756	3720	3166	3166
10	3560	3670	3713	3706	3703	3683	3163	3113
15	3623	3700	3633	3713	3673	3710	3216	3123
20	3603	3696	3670	3786	3633	3613	3196	3210
25	3630	3626	3643	3723	3646	3646	3210	3183
30	3646	3673	3626	3676	3766	3700	3223	3170
35	3666	3636	3643	3720	3600	3630	3223	3166
40	3700	3690	3633	3706	3650	3653	3216	3173
45	3603	3636	3713	3780	3633	3730	3210	3133

- **NOTO STONE**

Table C.6 *- Noto stone, application by brush till saturation: amount of product retained according to different type of analysis.*

Sample	Analysis	Quantity of product retained (kg/m^2)
N_ET	Water absorption by capillarity Drying Rate	0.101 ± 0.009
N_NBUT		0.077 ± 0.008
N_2BUT		0.113 ± 0.045
N_CAL		0.122 ± 0.026
N_ET	Water vapour permeability	0.028 ± 0.002
N_NBUT		0.032 ± 0.024
N_2BUT		0.047 ± 0.001
N_CAL		0.017 ± 0.001
N_ET	MIP	0.208 ± 0.005
N_NBUT		0.020 ± 0.013
N_2BUT		0.019 ± 0.008
N_CAL		0.047 ± 0.013
N_ET	NMR Colorimetric measurement	0.028 ± 0.003
N_NBUT		0.010 ± 0.001
N_2BUT		0.020 ± 0.005
N_CAL		0.057 ± 0.013
N_ET	UPV DRMS	0.044 ± 0.035
N_NBUT		0.072 ± 0.064
N_2BUT		< 0.010 *
N_CAL		0.084 ± 0.019

** For this sample, the quantity of product was very low to be measured with the available scale.*

Table C.7 *- Noto stone, application by brush till saturation: values of ultrasound pulse velocity before and after treatment for all products. The depth profile is expressed from not treated (5 mm) to treated surface (45mm).*

	UPV (m/s)							
Depth (mm)	*N_ET NT*	*N_ET T*	*N_NBUT NT*	*N_NBUT T*	*N_2BUT NT*	*N_2BUT T*	*N_CAL NT*	*N_CAL T*
5	2993	2996	3016	3033	2896	2983	2950	2903
10	3003	3010	2980	3043	2786	2890	2933	2910
15	2983	2996	2950	2953	2823	2853	2956	2926
20	2966	2990	2906	3026	2836	2833	2980	2973
25	2930	2956	2900	2940	2856	2876	2996	2970
30	3033	3030	2906	2963	2926	2953	2990	2976
35	3173	3186	2936	2980	2970	3003	2996	2986
40	3200	3193	2936	2990	2986	3036	3003	2996
45	3160	3160	2920	2980	3023	3046	3006	2956

Table C.8 *- Noto stone, application by brush with pre-set number of brush strokes: amount of product retained according to different type of analysis.*

Sample	**Analysis**	**Quantity of product retained (Kg/m^2)**
N_ET	Water absorption by capillarity Drying Rate	0.051 ± 0.019
N_CAL		0.013 ± 0.002
N_ET	Water vapour permeability	0.017 ± 0.001
N_CAL		0.010 ± 0.000
N_ET	MIP	0.033 ± 0.002
N_CAL		0.025 ± 0.001
N_ET	NMR	0.031 ± 0.003
N_CAL		0.019 ± 0.003

Table C.9 *Noto stone, application by absorption through capillarity: fringe reached by the products during the application.*

Product	Fringe (mm)
ET	14
NBUT	13
2BUT	7
CAL	27

Table C.10 *- Noto stone, application by absorption through capillarity: values of ultrasound pulse velocity before and after treatment for all products. The depth profile is expressed from not treated (5 mm) to treated surface (45mm).*

	UPV (m/s)							
Depth (mm)	*N_ET NT*	*N_ET T*	*N_NBUT NT*	*N_NBUT T*	*N_2BUT NT*	*N_2BUT T*	*N_CAL NT*	*N_CAL T*
5	3253	3286	3080	3303	3020	3033	3100	3070
10	3240	3220	3120	3336	3033	3063	3080	2996
15	3166	3186	3033	3313	3033	3063	3046	2953
20	3100	3093	3033	3220	3053	3040	2960	2923
25	3133	3146	3013	3266	3033	3043	2940	2913
30	3166	3126	2953	3266	2996	2990	2996	2936
35	3146	3153	2956	3146	2990	3033	3106	3026
40	3120	3126	2986	3146	3026	3070	3213	3146
45	3180	3226	3016	3073	3070	3093	3246	3226

- **VICENZA STONE**

Table C.11 *- Vicenza stone, application by brush till saturation: amount of product retained according to different type of analysis.*

Sample	Analysis	Quantity of product retained (kg/m^2)
V_ET	Water absorption by capillarity Drying Rate	0.060 ± 0.010
V_NBUT		0.028 ± 0.002
V_2BUT		0.012 ± 0.001
V_CAL		0.108 ± 0.008
V_ET	Water vapour permeability	0.011 ± 0.002
V_NBUT		0.058 ± 0.005
V_2BUT		0.045 ± 0.001
V_CAL		0.027 ± 0.007
V_ET	MIP	0.039 ± 0.001
V_NBUT		0.076 ± 0.004
V_2BUT		0.040 ± 0.005
V_CAL		0.038 ± 0.030
V_ET	NMR Colorimetric measurement	0.014 ± 0.003
V_NBUT		0.034 ± 0.002
V_2BUT		0.028 ± 0.002
V_CAL		0.113 ± 0.025
V_ET	UPV DRMS	0.012 ± 0.002
V_NBUT		0.076 ± 0.014
V_2BUT		0.051 ± 0.017
V_CAL		0.210 ± 0.030

Table C.12 *- Vicenza stone, application by brush till saturation: values of ultrasound pulse velocity before and after treatment for all products. The depth profile is expressed from not treated (5 mm) to treated surface (45mm).*

	UPV (m/s)							
Depth (mm)	*V_ET NT*	*V_ET T*	*V_NBUT NT*	*V_NBUT T*	*V_2BUT NT*	*V_2BUT T*	*V_CAL NT*	*V_CAL T*
5	3010	3096	3263	3353	3293	3380	2950	2903
10	2983	3110	3216	3333	3256	3276	2933	2910
15	3013	2980	3256	3303	3263	3210	2956	2926
20	2966	3006	3270	3276	3196	3223	2980	2973
25	2896	2946.	3256	3250	3210	3243	2996	2970
30	2876	2886	3183	3213	3230	3250	2990	2976
35	2870	2880	3236	3220	3210	3256	2996	2986
40	2993	3010	3143	3176	3256	3183	3003	2996
45	3030	3056	3230	3210	3236	3230	3006	2956

Table C.13 *- Vicenza stone, application by brush with pre-set number of brush strokes: amount of product retained according to different type of analysis.*

Sample	**Analysis**	**Quantity of product retained (kg/m²)**
V_ET	Water absorption by capillarity Drying Rate	0.025 ± 0.009
V_CAL		0.040 ± 0.001
V_ET	Water vapour permeability	0.019 ± 0.001
V_CAL		0.014 ± 0.001
V_ET	MIP	0.053 ± 0.006
V_CAL		0.062 ± 0.001
V_ET	NMR	0.035 ± 0.003
V_CAL		0.022 ± 0.003

Table C.14 *- Vicenza stone, application by absorption through capillarity: fringe reached by the products during the application.*

Product	Fringe (mm)
ET	35
NBUT	45
2BUT	35
CAL	24

Table C.15 *- Vicenza stone, application by absorption through capillarity: values of ultrasound pulse velocity before and after treatment for all products. The depth profile is expressed from not treated (5 mm) to treated surface (45mm).*

	UPV (m/s)							
Depth (mm)	*V_ET NT*	*V_ET T*	*V_NBUT NT*	*V_NBUT T*	*V_2BUT NT*	*V_2BUT T*	*V_CAL NT*	*V_CAL T*
5	3386	3570	3053	3280	3270	3460	2993	2946
10	3266	3470	3053	3316	3390	3533	2966	2913
15	3306	3480	3086	3293	3343	3476	2980	2956
20	3276	3503	3023	3190	3350	3500	2993	2956
25	3313	3480	3046	3246	3276	3466	2990	2996
30	3313	3440	3086	3246	3350	3486	3016	2970
35	3326	3393	3026	3123	3300	3383	3063	2993
40	3363	3410	3033	3126	3336	3336	3076	3060
45	3386	3300	3073	3053	3373	3333	3073	3023

- **CARRARA MARBLE**

Table C.16 *- Carrara marble, application by brush till saturation: amount of product retained according to different type of analysis.*

Sample	Analysis	Quantity of product retained (kg/m^2)
M_ET	Water vapour permeability	0.002 ± 0.001
M_NBUT		0.044 ± 0.001
M_2BUT		0.030 ± 0.024
M_CAL		0.041 ± 0.023
M_ET	MIP	0.005 ± 0.003
M_NBUT		0.012 ± 0.003
M_2BUT		0.010 ± 0.005
M_CAL		0.012 ± 0.004
M_ET	NMR Colorimetric measurement	0.003 ± 0.001
M_NBUT		0.010 ± 0.001
M_2BUT		0.009 ± 0.001
M_CAL		0.003 ± 0.003

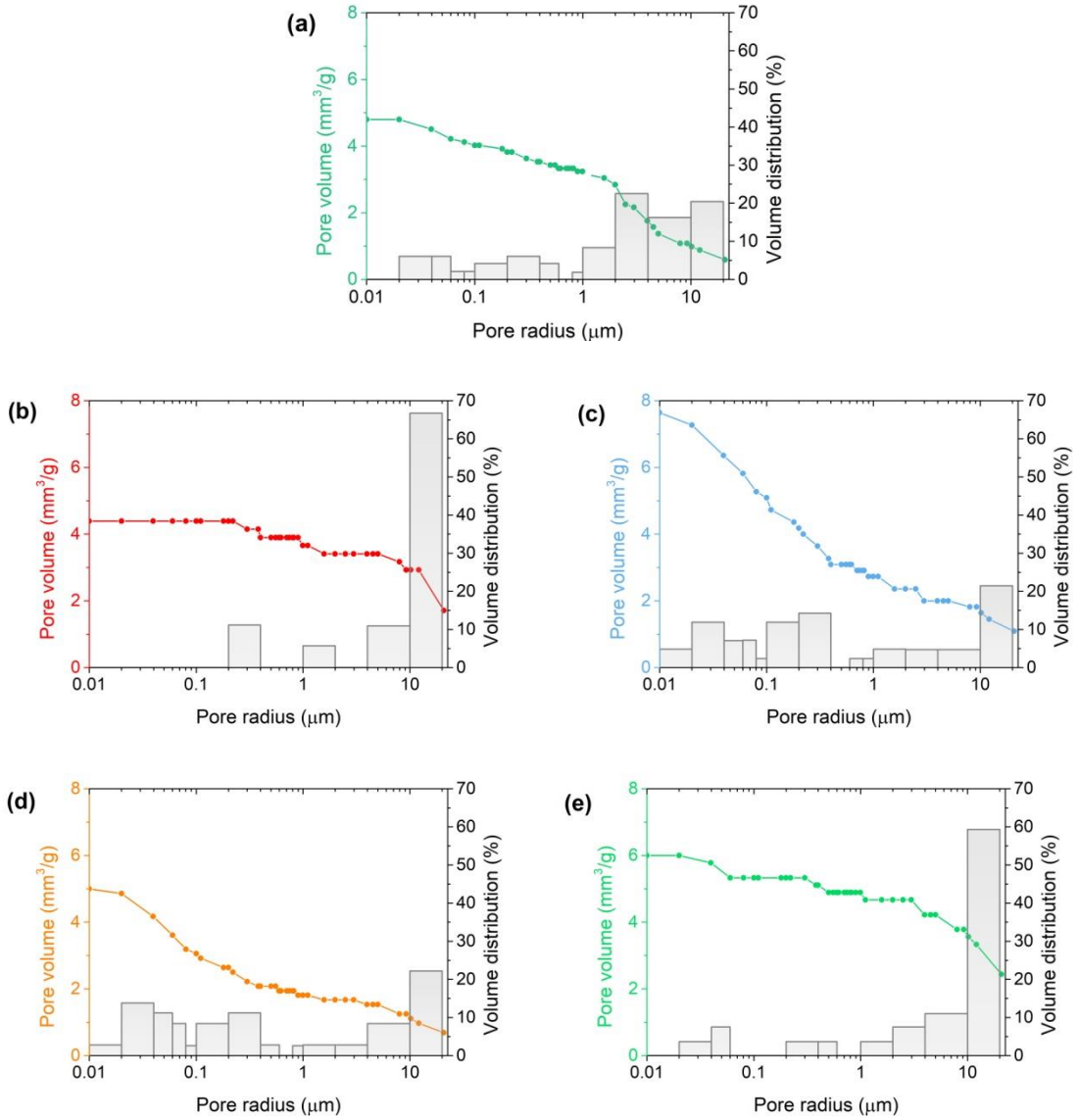

Figure C.1 *- Carrara marble, application by brush till saturation. Cumulative pore volume and volume distribution versus pore radius of:* ***(a)*** *M_NT,* ***(b)*** *M_ET,* ***(c)*** *M_NBUT,* ***(d)*** *M_2BUT and* ***(d)*** *M_CAL.*

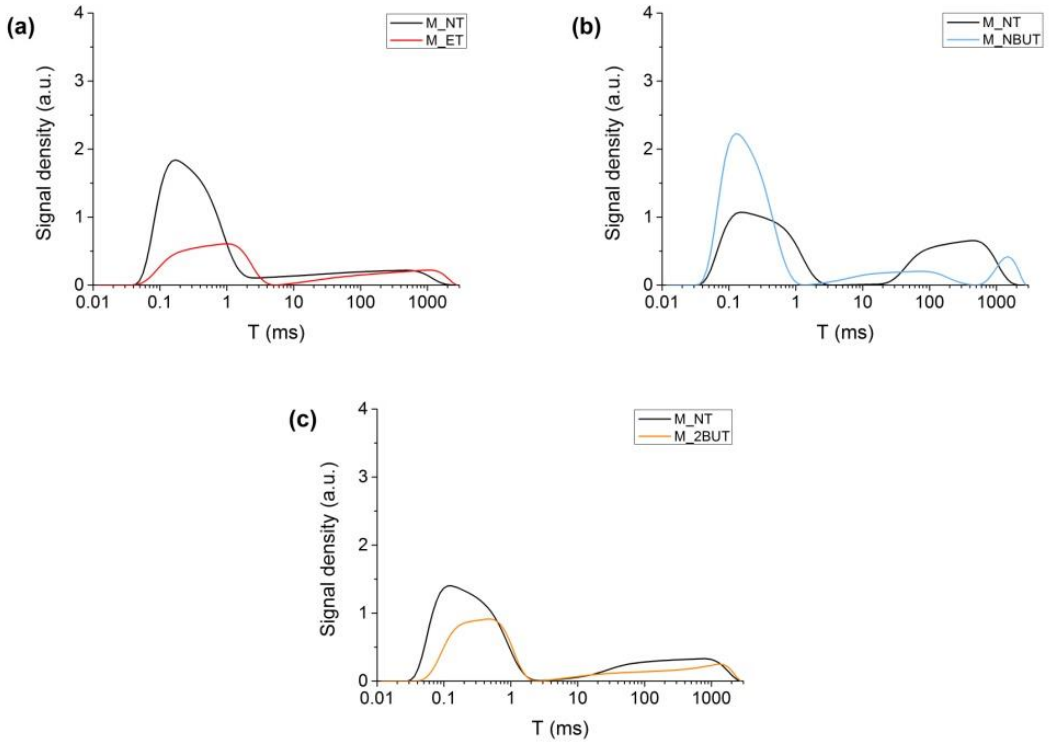

Figure C.2 *- Carrara marble, application by brush till saturation. Comparison of T2 distribution functions between treated and not treated supports:* ***(a)*** *M_ET,* ***(b)*** *M_NBUT and* ***(c)*** *M_2BUT.*

Table C.17 *- Carrara marble, application by brush with pre-set number of brush strokes: amount of product retained according to different type of analysis.*

Sample	Analysis	Quantity of product retained (kg/m²)
M_ET	Water vapour permeability	0.006 ± 0.000
M_CAL		0.007 ± 0.001
M_ET	MIP	0.020 ± 0.001
M_CAL		0.013 ± 0.001
M_ET	NMR	0.009 ± 0.001
M_CAL		0.015 ± 0.003

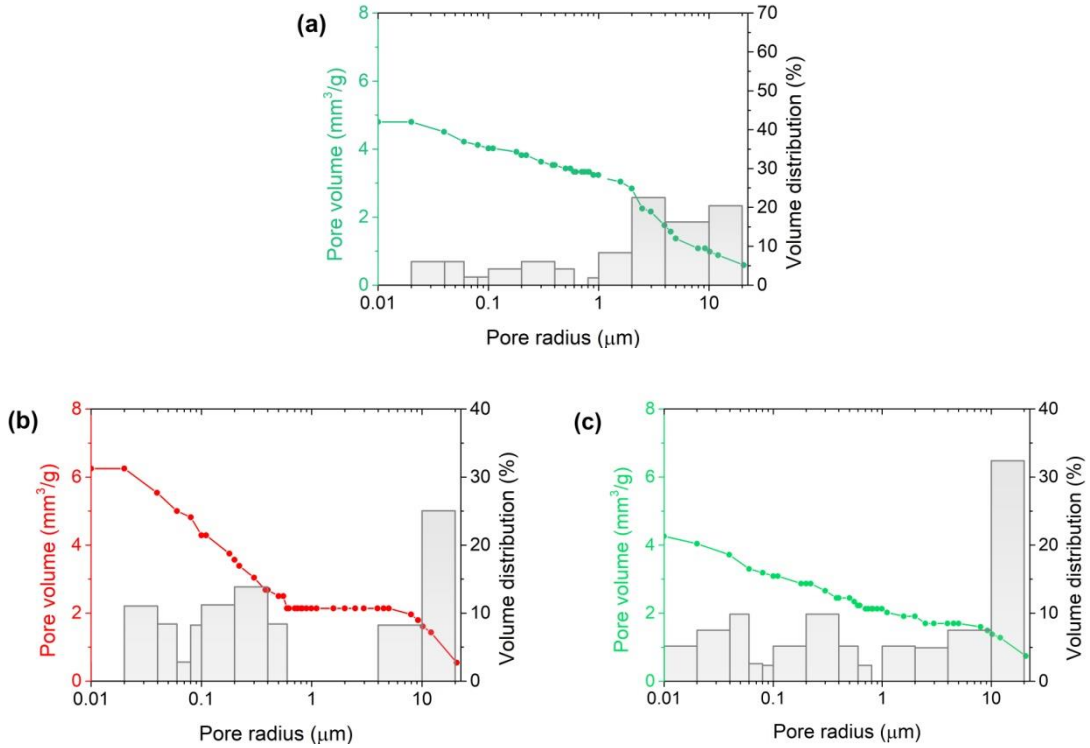

Figure C.3 *- Carrara marble, application by brush with pre-set number of brush strokes. Cumulative pore volume and volume distribution versus pore radius of:* ***(a)*** *M_NT,* ***(b)*** *M_ET and* ***(c)*** *M_CAL.*

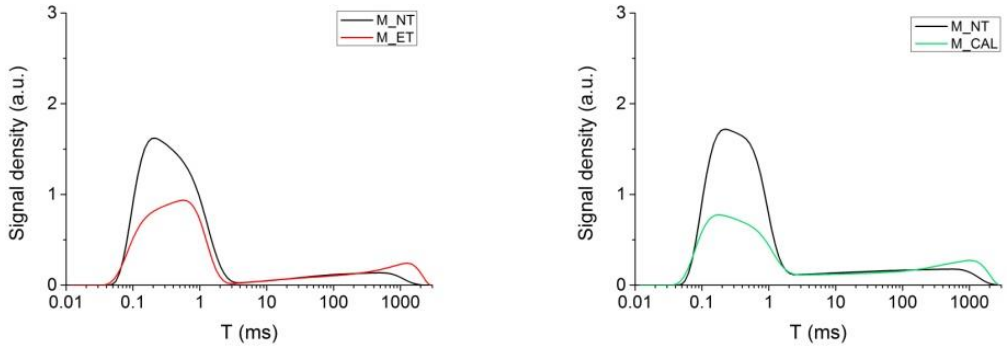

Figure C.4 *- Carrara marble, application by brush with pre-set number of brush strokes. Comparison of T2 distribution functions between treated and not treated supports:* ***(a)*** *M_ET and* ***(b)*** *M_CAL.*

GLOSSARY

$Ca(OEt)_2$: calcium ethoxide nanosuspension a 1:3 solution (v/v%) of ethanol and tetrahydrofuran, with an initial calcium concentration of 46,5 g/L and average particles' dimension of 295 nm.

EtOH: ethanol.

THF: tetrahydrofuran.

REL: Recommended Exposure Limits, terms adopted from the US legislation and referred to the concentration of solvent not to be exceed for a safety region, mediated in a 40-hour working week.

ET: calcium ethoxide nanosuspension diluted in ethanol to reach a calcium concentration of 20 g/L.

2BUT: calcium ethoxide nanosuspension diluted in 2-buthanol to reach a calcium concentration of 20 g/L.

NBUT: calcium ethoxide nanosuspension diluted in n-butylacetate to reach a calcium concentration of 20 g/L.

CAL: Calosil E50 diluted in ethanol to reach a calcium concentration of 20 g/L.

ACC: amorphous calcium carbonate.

KBr: potassium bromide used to prepare pellets for FT-IR analysis.

$Ca(NO_3)_2$: calcium nitrate used to reach and maintain a relative humidity condition of 50% inside a drier.

KNO_3: potassium nitrate used to reach and maintain a relative humidity condition of 90% inside a drier.

ETD: everhart-thornley detector for secondary electrons, SEM analysis.

LTD: large field detector for secondary electrons, SEM analysis.

ACKNOWLEDGMENTS

First of all, I would like to express my gratitude to my advisor Prof. Elisabetta Zendri for her supervision, suggestions, guidance and encouragement throughout this research. She has always a right answer and empathy to solve problems.

I am also grateful to my co-tutors Dr. Patrizia Tomasin, for her precious support and invaluable contributions to my thesis and Dr. Loretta Storaro for her advices and availability.

Sincere thanks to Prof. Maria Brai, from the University of Palermo and all her collaborators, Maurizio Marrale, Anna Longo, Salvo Gallo, Luigi Tranchina and Dorotea Fontana for introducing me in the world of nuclear magnetic resonance and for their help and availability during my stay in Palermo. A special thank goes to Francesca Alberghina and Salvatore Schiavone, firstly dear friends and also after, precious colleagues.

Many thanks to Doria Costa, João Mimoso, José Delgado Rodriguez and all the people met at LNEC in Lisbon, for their hospitality and competences shown during my PhD period abroad. I love this city also for your kindness and hilarity. Thank you for sharing with me your skills and Portuguese culture and anecdotes.

A huge thanks to Dr. Francesca Becherini from the national research centre of Padua who dedicated time and energy to explain me the difficult world of statistics.

I also would like to thank Dr. Naida El Habram from the national research centre of Padua and Prof. Pietro Riello and his group from the University of Venice for their facilities availability.

Great thank to my research group and all the guys in ViaTorino for giving me support, encouragement, friendship and for sharing all the lunches and laughs.

I would thank all the people I have met in these three years, with whom I shared schools, courses, experiences, in Italy and abroad, which contributed to my personal and professional growth with their fruitful advices and comparisons.

A lovely thank to my friends, close and far way, thank you for all the wonderful experience, the good mood, the right advice and the constant support and encouragement in work but, mostly, in the daily life.

Thanks to my closest friends, so far away from me but always by my side and to my Venetian Family, I am so glad to have you as "Fratellis".

A special thank to a wonderful new person which encouraged me and shared with me the most smiling and nicest moments in this last year.

At last but not the least, the greatest thank goes to mum and dad, always my biggest fans with blind and endless confidence, thank you for being my reference point wherever I go and wherever I live.